ETH

Eidgenössische Technische Hochschule Zürich
Swiss Federal Institute of Technology Zurich

Reactive Oxygen Species (ROS) Measurements in Laboratory and Ambient Studies

Jun Zhou

DISS. ETH NO. 24835

DISS. ETH NO. 24835

Reactive Oxygen Species (ROS) Measurements in Laboratory and Ambient Studies

A thesis submitted to attain the degree of

DOCTOR OF SCIENCES of ETH ZURICH

(Dr. sc. ETH Zurich)

presented by

JUN ZHOU

MSc in Environmental Science, Zhengzhou University

born on 07.02.1987

citizen of China

accepted on the recommendation of

Prof. Dr. Urs Baltensperger (examiner)
Prof. Dr. Kristopher McNeill (co-examiner)
Dr. Josef Dommen (co-examiner)
Prof. Dr. Markus Kalberer (co-examiner)

2018

Table of Contents

Summary

Breathing pristine clean air, a fundamental human right ever since the world was created, is threatened now and then on the road of human society development. To create the environment that supports our life in a sustainable way, we must solve the air pollution problem and at the same time continue our technologically based civilization. Although air pollution has attracted attention for centuries, the air-cleaning task is still arduous and needs long-term efforts to be settled. Understanding the composition of the atmospheric air, what causes the air pollution and its adverse health effects to human beings, is of highest importance to make decisions in preventing air pollution.

The chemical composition of ambient air, including both the gas and the particle phase, is changing due to human activities. Aerosol particles are defined as the tiny particles suspended in a gas, where particulate matter (PM) with an aerodynamic diameter $d < 10$ μm (PM_{10}) often represents the aerosol particles of interest in atmospheric studies. Exposure to $PM_{2.5}$ (PM with $d < 2.5$ μm) was linked to 3.15 million premature deaths worldwide in 2010. Our study focused on the tropospheric aerosols, which are the major factors in climate change and health effects. One of the most important pathways of particulate PM leading to deleterious impacts on health is believed to be the induced oxidative stress by the generation of reactive oxygen species (ROS) from the inhaled PM in vivo (endogenous ROS), or by the transportation of particle-bound ROS (PB-ROS) into the lungs (exogenous ROS). Therefore the understanding of the ROS formation and decay in PM is of utmost importance for mitigating their impact on health. In our work, to enable a rapid screening of the ROS content of PM, we have developed and characterized a highly sensitive ROS analyzer using a 2',7'-dichlorofluorescin (DCFH) based assay, which can be used either online or offline. The online ROS analyzer greatly improved the quality of the real-time ROS monitoring, and provided a reliable ROS quantification by reducing the losses of the short-lived ROS. This instrument was used in laboratory studies to measure PB-ROS in the exhaust of different emission sources, including the primary emissions and secondary formation of wood and coal combustion, as well as secondary formation from α-pinene oxidation. To study this secondary formation, two atmospheric aging simulators, a smog chamber (SC) and a potential aerosol mass reactor (PAM) chamber, were employed. Further, the PB-ROS content in ambient aerosols was quantified in-situ at two contrasting places: Beijing and Bern. The ROS data were complemented by data from an aerosol mass spectrometer (AMS) in most of our studies, and advanced source apportionment approaches (positive matrix factorization and multilinear engine) were used to identify the major sources of the organic fraction in the ambient studies. The combination of PB-ROS measurements on ambient aerosols and different emission sources revealed the main PB-ROS contributors in the ambient aerosol. The aims of this thesis were:

1) Build a robust and reliable fast online ROS analyzer and characterize its performance. Quantify the PB-ROS contributions from different emission sources including wood combustion, coal combustion as well as in the photooxidation of α-pinene.
2) Investigate the influence of aging conditions on PB-ROS formation of different emission sources by simulating the atmospheric aging process.
3) Confirm the main acellular sources of PB-ROS in ambient air by combining in-situ ambient measurements with laboratory studies.

During the course of this study, it was demonstrated that the online ROS analyzer is sufficiently sensitive and robust to be applied to routine analysis of ROS emissions in both laboratory and ambient studies. A characterization of the instrument with tested model organic compounds showed that only peracetic acid were quantitatively measured, while large organic peroxides or those with bulky functional groups (i.e., tert-butyl and phenyl) showed a strongly reduced fluorescence response of the DCFH assay. Potential interferences from gas-phase O_3 and NO_2 were not observed and matrix effects of particulate SO_4^{2-} and NO_3^- were not statistically significant. No interference of Fe^{3+} was detected, while high concentrations of soluble Fe^{2+} reduced the ROS signal. The comparison of online and offline ROS measurement demonstrated the degradation of the highly reactive ROS fraction, and the offline method generally underestimated the ROS concentration, on average by 60 ± 20 %, suggesting that the fast online method presented in this study is advantageous. However, the ROS signal from ambient aerosols may be below or around the instrument detection limit at cleaner sites (such as in Bern). In such cases a versatile aerosol concentration enrichment system (VACES) was successfully used to enhance the sensitivity.

PB-ROS from wood combustion emissions varied for different combustion devices and technologies, different fuel types, operation methods, combustion regimes, combustion phases and aging conditions. For all tested eight combustion devices (within different technologies), primary PB-ROS emissions substantially increased upon aging. The primary and secondary PB-ROS emission factors (EF_{ROS}) were dominated by the combustion devices (within different combustion technologies) and by the combustion regimes (expressed as the air to fuel ratio lambda). EF_{ROS} from automatically operated combustion devices were on average one order of magnitude lower than those from manually operated appliances, indicating that automatic combustion devices operated at optimum conditions to achieve near-complete combustion, is most effective to minimize PB-ROS emissions. The variability of EF_{ROS} within one device was much higher than the variability from different manual devices. In general, an increase of aged EF_{ROS} was observed from optimal to high lambda values, with ~2-80 times higher aged EF_{ROS} values under bad combustion conditions than under optimum combustion conditions. The PB-ROS content in the secondary organic aerosol (SOA) (represented as $f_{ROS-SOA}$), increased with the SOA oxidation state, which increased with OH exposure and decreased with the additional partitioning of semi-volatile components with lower PB-ROS content at higher OA concentrations, while further aging seemed to result in a decay of PB-ROS.

Further, the PB-ROS concentrations of five types of coal used in residential heating in different regions in China were investigated, including three types of bituminous

coal and two types of anthracite coal. The primary EF_{ROS} of the three bituminous coals were not statistically different. Primary EF_{ROS} of the two types of anthracite coal were not detectable. The EF_{ROS} of the bituminous coals further increased upon aging, and their secondary EF_{ROS} were ~ 7 times higher than of the anthracite coal, indicating the importance of the type of coal used for the combustion. The primary EF_{ROS} from the wood combustion were significantly higher than those of the bituminous coal, while the aged EF_{ROS} from wood combustion were on average comparable to those from bituminous coal. The $f_{ROS-SOA}$ initially increased upon aging, and decreased with even higher OH exposure. For all three types of bituminous coal, variable $f_{ROS-SOA}$ were observed under the same OH exposure, which was dominated by the OA loading: $f_{ROS-SOA}$ was higher at lower SOA loading for each individual type of coal.

Atmospheric aerosol measurements at the two contrasting locations Beijing (China) and Bern (Switzerland) showed large predominance of SOA to PB-ROS activity in fine aerosol. During the campaign in Beijing (from January to February 2015), the main OA composition was a mixture of hydrocarbon-like OA and coal combustion OA (HOA+CCOA), cooking emissions OA (COA), biomass burning OA (BBOA), as well as of oxygenated OA (OOA). In Bern, the main OA sources were HOA, COA, BBOA and OOA in November, 2014. The combination of these source apportionment results with observed PB-ROS by a multiple linear regression model (MLRM) revealed that the main parameter affecting the ROS concentration was OOA at both locations. In Bern, OOA contributed on average to more than 52 % of the explained ROS by MLRM, followed by HOA (19 %), BBOA (24 %) and COA (5 %). In Beijing, OOA explained 77% of the observed PB-ROS, while the contribution of primary OA sources to PB-ROS activity could not be retrieved within our uncertainties, when these sources were considered individually or lumped together. The PB-ROS content in the OOA derived from the ambient measurements was comparable to those from the direct source emissions obtained from the laboratory studies, where the PB-ROS contents in SOA emissions are about 4 to 25 times higher than those in the corresponding primary samples, confirming the importance of the secondary organic aerosol for the PB-ROS level in the ambient atmosphere. The source-to-source variation of the PB-ROS content in SOA from laboratory studies could be explained by the different SOA precursors.

This study describes a much improved state-of-the-art estimate of the PB-ROS, a large fraction of which is labile. By coupling the PB-ROS with the revealed dominant sources and components of fine particles, the result clearly suggests the SOA, which is formed from precursors of different anthropogenic and biogenic emissions, plays a predominant role to PB-ROS activity in fine aerosol. The findings and special data analysis may provide a guideline for future ROS analyses and facilitate further toxicological and epidemiological studies in related fields.

Résumé

L'accès à un air pur, une nécessité pour les organismes vivants, est de plus en plus incompatible avec le développement de la société humaine. Afin d'améliorer la durabilité de l'environnement, il est important de s'atteler aux problèmes causés par la pollution atmosphérique sans toutefois freiner le développement technologique mondial. Bien que la pollution de l'air ait attiré l'attention depuis des siècles, l'amélioration de la qualité de l'air reste une tâche ardue nécessitant une forte implication et des efforts à long terme. En vue de comprendre la composition de l'air atmosphérique, les causes et conséquences de la pollution, notamment sur la santé, il est important de prendre des décisions majeures pour prévenir la pollution de l'air.

La composition de l'air ambiant (gaz et phase particulaire) est en train de changer en raison des activités humaines. Les aérosols sont définis comme de très petites particules en suspension dans une phase gazeuse et comprennent les particules fines (particulate matter : PM) qui possèdent un diamètre aérodynamique $d < 10\mu m$, particulièrement étudiées dans les recherches sur la pollution atmosphériques. L'exposition aux particules fines $PM_{2.5}$ (PM dont $d < 2,5\ \mu m$) aurait été responsable de 3.15 millions de décès prématurés dans le monde sur l'année 2010. Notre étude porte sur les aérosols troposphériques qui sont considérés comme les acteurs les plus importants dans le changement climatique et les effets sur la santé. Le stress oxydant, provoqué soit par la production *in vivo* d'espèces réactives de l'oxygène (reactive oxygen species : ROS, endogènes) après inhalation de PM soit par transport de ROS contenus dans les particules jusqu'aux poumons (PB-ROS ou particle bound ROS), est considéré comme une des voies principales de la toxicité des particules fines. Il est donc de la plus haute importance de comprendre les mécanismes de formation et de dégradation des ROS au sein des particules fines afin de comprendre leur impact sur la santé. Dans ce travail, afin de permettre un suivi rapide du contenu en ROS des PM, nous avons développé et caractérisé une méthode d'analyse des ROS utilisant la 2',7'-dichlorofluoresceine (DCFH), opérationnelle en ligne ou hors ligne. Cet analyseur de ROS en ligne améliore fortement la qualité du suivi en temps réel des ROS et permet d'obtenir une quantification fiable en réduisant les pertes dues aux espèces de courte durée de vie. Cet instrument a été utilisé lors d'études en laboratoire mesurant les PB-ROS dans les gaz d'échappement de différentes sources d'émission, comprenant les émissions primaires et secondaires de combustion de bois et de charbon, ainsi que les émissions secondaires dues à l'oxydation d'α-pinène. Afin d'étudier ces formations secondaires, deux simulateurs de vieillissement atmosphérique, une chambre à smog

(SC) et une chambre à potential aerosol mass (PAM) chambre ont été utilisées. De plus, la teneur en ROS des aérosols ambiants a été quantifiée *in situ* dans deux lieux géographiques présentant de forts contrastes : Beijing et Berne. Ces données obtenues pour les ROS ont été couplées aux données d'un spectromètre de masse d'aérosol (AMS) pour la majorité des études, ainsi qu'à des approches améliorées de répartition des sources d'aérosols (factorisation matricielle positive et moteur multilinéaire) dans le but d'identifier les principales sources de la fraction organique dans les études sur l'air ambiant. La combinaison de mesures de PB-ROS des aérosols ambiants et de différentes sources d'émissions a permis de révéler les principales sources qui contribuent aux ROS.

Les objectifs de cette thèse sont:

1) Construire un analyseur en ligne de ROS robuste, fiable et rapide et caractériser ses performances.

2) Quantifier les émissions de PB-ROS provenant de différentes sources d'émissions incluant la combustion du bois, la combustion du charbon et la photo-oxydation de l'α-pinène.

3) Étudier l'influence des conditions de vieillissement sur la formation de PB-ROS de différentes sources d'émission par simulation du processus réel de vieillissement atmosphérique.

4) Confirmer les principales sources acellulaires de PB-ROS dans l'air ambiant en combinant des mesures ambiantes *in situ* avec des études en laboratoire.

Au cours de cette étude, il a été démontré que l'analyseur en ligne de ROS est suffisamment sensible et robuste pour être appliqué à l'analyse de routine des émissions de ROS dans les études en laboratoire et de l'air ambiant. La caractérisation de l'instrument a montré qu'avec des composés organiques modèles testés, seul l'acide péracétique était mesuré quantitativement, tandis que les peroxydes organiques volumineux ou ceux avec des groupes fonctionnels volumineux (par exemple : *tert*-butyle et phényle) présentaient une réponse de fluorescence réduite au test DCFH. Les interférences potentielles liés à O_3 et NO_2 de la phase gazeuse n'ont pas été observées et les effets matriciels des particules SO_4^{2-} et NO_3^- n'étaient pas statistiquement significatifs. Aucune interférence n'a été observée avec le Fe^{3+} alors que des concentrations élevées en Fe^{2+} soluble présentes réduisent le signal des ROS. La comparaison des mesures en ligne et hors ligne des ROS a démontré une dégradation de la fraction des ROS fortement réactifs avec en général une sous-estimation de 60 ± 20% de la concentration en ROS lors des mesures par la méthode hors ligne, confirmant l'intérêt d'une méthode de mesure en ligne. Cependant, la teneur en ROS dans les aérosols peut également être inférieure ou proche de la limite de détection de l'instrument lors des mesures ambiantes *in situ*, notamment lors des mesures de l'air ambiant à Berne dans cette étude. Dans de tels cas, nous avons

utilisé un système polyvalent d'enrichissement de la concentration en aérosols (VACES) fut utilisé avec succès pour améliorer la sensibilité.

Les PB-ROS liés aux particules des émissions de combustion du bois varient selon les différents dispositifs de combustion, les technologies de combustion, les types de combustibles, les méthodes d'exploitation, les régimes de combustion, les phases de combustion et les conditions de vieillissement. Pour les huit appareils de combustion testés (utilisant différentes technologies), les émissions primaires de PB-ROS augmentent considérablement avec le vieillissement. Le niveau des facteurs d'émission de PB-ROS (EF_{ROS}) primaires et secondaires est dominé par les dispositifs de combustion (parmi différentes technologies de combustion) et par les régimes de combustion (exprimé par le ratio air/combustible lambda). Les EF_{ROS} obtenus pour les dispositifs de combustion automatiques sont en moyenne d'un ordre de grandeur inférieur à ceux des appareils manuels, ceci indiquant que les appareils de combustion automatique opérant dans des conditions optimales et réalisant une combustion quasi-complète sont plus efficaces pour réduire les émissions de PB-ROS. La variabilité du EF_{ROS} intra appareil est plus importante que la variabilité inter appareil, ce qui peut s'expliquer par les conditions de combustion. De façon générale, une augmentation du EF_{ROS} vieilli est observée pour une valeur optimale à haute du lambda, avec des valeurs d' EF_{ROS} vieilli 2 à 80 fois plus hautes au cours de mauvaises conditions de combustion comparé aux conditions optimales. La teneur en PB-ROS des aérosols organique secondaire (SOA)(représenté par $f_{ROS-SOA}$) augmente avec l'état d'oxydation des SOA, qui lui-même augmente avec l'exposition a OH et diminue avec la partition supplémentaire des composants semi-volatils ayant une plus faible teneur en PB-ROS à des concentrations d'OA plus élevées, tandis que le vieillissement supplémentaire semble entraîner la dégradation des PB-ROS.

En parallèle, les concentrations en PB-ROS liés aux particules de cinq types de charbon utilisés pour le chauffage résidentiel dans différentes régions Chine a été étudié, ces charbons incluant trois types de charbon bitumineux chinois et deux types de charbon anthracite chinois. Les EF_{ROS} primaires des trois charbons bitumineux ne sont pas statistiquement différents. Les EF_{ROS} primaires des deux types de charbon anthracite n'ont pu être détectés. Les EF_{ROS} des charbons bitumeux augmentent d'autant plus avec le vieillissement et leurs EF_{ROS} secondaires sont environs 7 fois plus élevés que pour les charbons anthracite indiquant l'importance du type de charbon utilisé pour la combustion. Les EF_{ROS} primaires de la combustion du bois sont également significativement plus élevés que ceux des charbons bitumeux alors que les EF_{ROS} vieillis de la combustion du bois et du charbon bitumeux sont comparables en général. Le $f_{ROS-SOA}$ augmente initialement avec le vieillissement et diminue pour une exposition plus élevée a OH. Pour les trois types de charbon bitumeux, des $f_{ROS-SOA}$ variables sont observés pour une même exposition a OH, ce qui est dominé par la charge en OA : $f_{ROS-SOA}$ étant plus élevé pour une plus faible charge en SOA pour chaque type de charbon.

Les mesures d'aérosols atmosphériques sur les deux sites fortement différents de Beijing (Chine) et Bern (Suisse) montrent une large prédominance des SOA dans l'activité des PB-ROS des particules fines. Au cours de la période de mesure à Beijing (janvier à février 2015), la composition principale en OA était un mélange : d'OA de type hydrocarbures et d'OA de combustion du charbon (HOA + CCOA), d'OA d'émissions de cuisine (COA), d'OA de combustion de bois (BBOA) et d'OA oxygéné (OOA). À Berne, les principales sources d'OA sont HOA, COA, BBOA et OOA (novembre 2014). La combinaison de ces résultats de répartition de source avec les PB-ROS observés par un modèle de régression linéaire multiple (MLRM) a révélé que les principaux paramètres affectant la formation de PB-ROS étaient les OOA pour les deux sites. À Berne, les OOA contribuent en moyenne à plus de 52 % des ROS expliquées par MLRM, suivi par HOA (19 %), BBOA (24 %) et COA (5 %). À Beijing, les OOA contribuent à 77% des PB-ROS, alors que la contribution des sources primaires d'OA à l'activité des PB-ROS n'a pu être établie dans notre marge d'erreur que ces sources soient considérées individuellement ou regroupées. Le contenu en PB-ROS dans les OOA dérivés des mesures ambiantes est comparable à ceux obtenus par des mesures directes de sources d'émissions réalisées en laboratoires avec des valeurs en PB-ROS des émissions de SOA 4 à 25 fois plus importants que leurs équivalents dans les échantillons primaires. Ceci confirme l'importance des aérosols organiques secondaires vis-à-vis de la concentration en PB-ROS dans l'atmosphère ambiante. La variabilité inter source des taux de PB-ROS dans les SOA, observée en laboratoire, peut s'expliquer par la différence entre les précurseurs de SOA utilisés.

Cette étude décrit une estimation de pointe des PB-ROS dont une large fraction est labile. En couplant les PB-ROS avec les sources dominantes obtenues et les composants des particules fines, les résultats suggèrent distinctement que les SOA, formés à partir de précurseurs provenant de différentes émissions anthropogéniques et biogéniques, jouent un rôle prédominant dans l'activité des PB-ROS des particules fines. Les conclusions et l'analyse spécialisée des données peuvent ainsi fournir de nouvelles lignes directrices pour les analyses des ROS et faciliter les études toxicologiques et épidémiologiques dans les domaines connexes.

1

Introduction

1.1 Atmospheric aerosol

1.1.1 Atmospheric aerosol characteristics

*An aerosol is technically defined as a suspension of solid or liquid particles in a gas, common usage refers to the aerosol as the particulate component only. Atmospheric aerosols consist of particles ranging in size from a few tens of angstroms (Å) to several hundred micrometers (μm). PMx is usually used to indicate the particulate matter (PM) with an aerodynamic diameter smaller than x micrometers. The total surface area of all particles in the atmosphere is ~1 × 10^{14} m^2; which is roughly equivalent to the total surface area of the Earth, ~1.25 × 10^{14} m^2. Particles with a diameter smaller than 1 μm generally have atmospheric concentrations in the range from around ten to several thousand per cm^3; those exceeding 1 μm diameter are usually found at concentrations of < 1 cm^{-3}. PM is classified into different size modes, and each size mode has its distinctive chemical and optical properties, transformation mechanisms, and deposition pathw*ays (the Italic part is adapted from: Seinfeld and Pandis, 2016). Fig. 1.1 depicts the size distribution of aerosol particles for various parameters in an idealized atmospheric sample, together with illustrations of their formation mechanisms (Buseck and Adachi, 2008). The uppermost solid line in Fig. 1.1 presents the number size distribution of aerosol particles in an idealized volume of the atmosphere. It includes the following modes:

·Nucleation mode: The nucleation mode particles are usually fresh aerosols created in-situ from the gas phase by nucleation (Seinfeld and Pandis, 2016), it has the smallest size range by particles smaller than 0.01 μm but by far the largest number, its surface to volume ratio is high but the total surface area and volume are small compared to the other modes (Buseck and Adachi, 2008). Most nucleation-mode particles consist of sulfates, nitrates, elemental carbon, trace metals and low-volatility organic compounds in the atmosphere (Lagzi et al., 2013). Nucleation mode particles coagulate with larger particles.
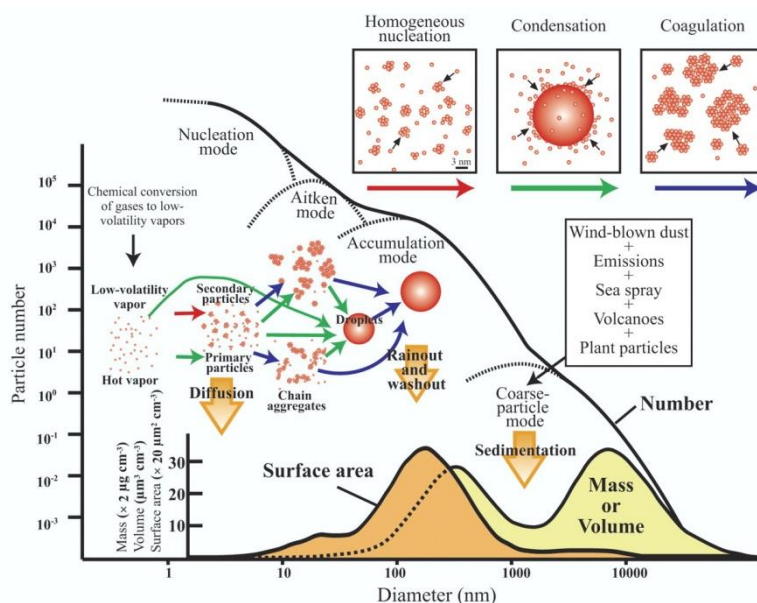
Figure 1.1 The size distribution of aerosol particles for various parameters, including: number, N; mass, M; volume, V; surface area, S, in an idealized atmospheric sample, as well as the illustrations of their formation mechanisms. The N, S, V, and M distributions, as well as the principal modes, sources, and particle formation and removal mechanisms, are adapted from Whitby (1978) (Buseck and Adachi, 2008).

·Aitken-mode: The Aitken mode has a larger size than the nucleation mode, and is between 0.01 μm and 0.1 μm. It is formed by coagulation of nucleation mode particles as well as condensation. Together with the particles of the nucleation mode, they are called "ultrafine particles" or "nanoparticles", however, these terms are rather loosely defined (Judith, 2005).

·Accumulation mode: Particles with diameters between 0.1 and 2.5 μm, resulting from primary emissions or secondary formation and growth by coagulation and condensation processes. This mode usually accounts for most of the aerosol surface area and a substantial part of the aerosol mass. The removal efficiency is the least in this mode and occurs mainly by precipitation (Lagzi et al., 2013; Seinfeld and Pandis, 2016; Buseck and Adachi, 2008).

·Coarse mode: Particles with a diameter greater than 2.5 μm, produced mainly from mechanical processes including particles from natural sources (e.g. windblown dust, natural biomass burning, sea spray, volcanic eruptions, rock abrasion, biological emissions, etc.) and anthropogenic sources (e.g.

resuspension of dust, break wear, etc). They can be removed through dry deposition due to their gravity or through precipitation.

1.1.2 The chemical composition of ambient aerosol

Although the term "atmospheric aerosol" includes both the tropospheric aerosol (suspended in the lowest ~ 10 km of the atmosphere) and the stratospheric aerosol (suspended in the stratosphere above the troposphere, mainly composed of aqueous sulfuric acid), we usually mean the tropospheric aerosol. The atmospheric aerosol is mainly composed of sulfate, ammonium, sodium, chloride, trace metals, carbonaceous material, crustal elements, and water (Lagzi et al., 2013). It can be further classified as primary aerosol which directly emitted into the atmosphere and secondary aerosol which is formed by nucleation of molecules that have undergone photochemical reaction processes. Distinctions are commonly made between anthropogenic and natural nanoparticles, both of which are subdivided into primary PM and secondary PM. The primary natural sources include soil dust (mineral aerosol, e.g. Fe, Si, Ca, Mg), sea salt, volcanic dust and biological debris (e.g. pollen and spores), the primary anthropogenic sources include the industrial dust, soot, etc. (Buseck and Pósfai, 1999; Hari and Liisa, 2008); the secondary natural sources include sulfates from biogenic gases, the sulfates from volcanic SO_2, the organic matter from biogenic volatile organic compounds (VOC), nitrates from NOx, the anthropogenic secondary sources include the sulfates from SO_2, the biomass burning, the nitrates from NO_x, the organics from anthropogenic VOC, etc. (Seinfeld and Pandis, 2016).

Aerosol chemical composition affects its properties such as hygroscopicity (Gysel et al., 2007) and toxicity (Reiss et al., 2007; Schlesinger and Cassee, 2003). Therefore, a good knowledge on the properties of the aerosols is needed to estimate their influence on climate change and the health. The chemical composition of the aerosol is often measured by bulk analysis using the Aerodyne aerosol mass spectrometer (AMS), which was developed for on-line analysis of the non-refractory PM_1 (other studies) or $PM_{2.5}$ (this study) (Jayne et al., 2000; Allan et al., 2003; Jimenez et al., 2003). A detailed description of AMS can be found in Chapter 2. The chemical composition of PM_1 measured by AMS on a global scale in the Northern Hemisphere is shown in Fig. 1.2 (Jimenez et al., 2009), including organic aerosol (OA), sulfate (SO_4^{2-}), nitrate (NO_3^-), ammonium (NH_4^+) and chloride (Cl^-). The remaining parts of the atmospheric aerosol, which cannot be measured by the AMS, are the light-absorbing carbonaceous aerosol (black carbon, BC) and different kinds of elements (S, K, Ca, Ti, Mn, Fe, Cu, As, Zn, Br, Sr, Ba, Pb, etc.), which are usually quantified by e.g. an aethalometer and X-ray fluorescence (XRF), respectively.

OA determined by the AMS can usually be further attributed to different types of OA due to different emission sources or processes by applying factor analysis to the AMS data (FA-AMS). Examples are: commonly identified hydrocarbon-like OA (HOA) which originates from fossil fuel combustion or traffic emissions and other urban sources, biomass burning OA (BBOA), and the oxygenated OA (OOA) related to the formation of the secondary organic aerosol (SOA) (Lanz et al., 2007; Jimenez et al., 2009). Recent studies also identified cooking emissions OA (COA) (Mohr et al., 2012; Crippa et al., 2013a) and the coal combustion OA (Dall'Osto et al., 2013; Sun et al., 2014; Elser et al., 2016). FA-AMS discriminated OOA further into low-volatility OOA (LV-OOA) and semi-volatile

OOA (SV-OOA). The inset in Fig. 1.2 shows the O:C ratio of HOA, LV-OOA and SV-OOA (or alternatively total OOA), and other OA. HOA has an O:C below 0.1, while the SV-OOA is between 0.2 and 0.4 and LV-OOA and total OOA have an O:C larger than 0.5 (Jimenez et al., 2009) indicating their strong ageing.
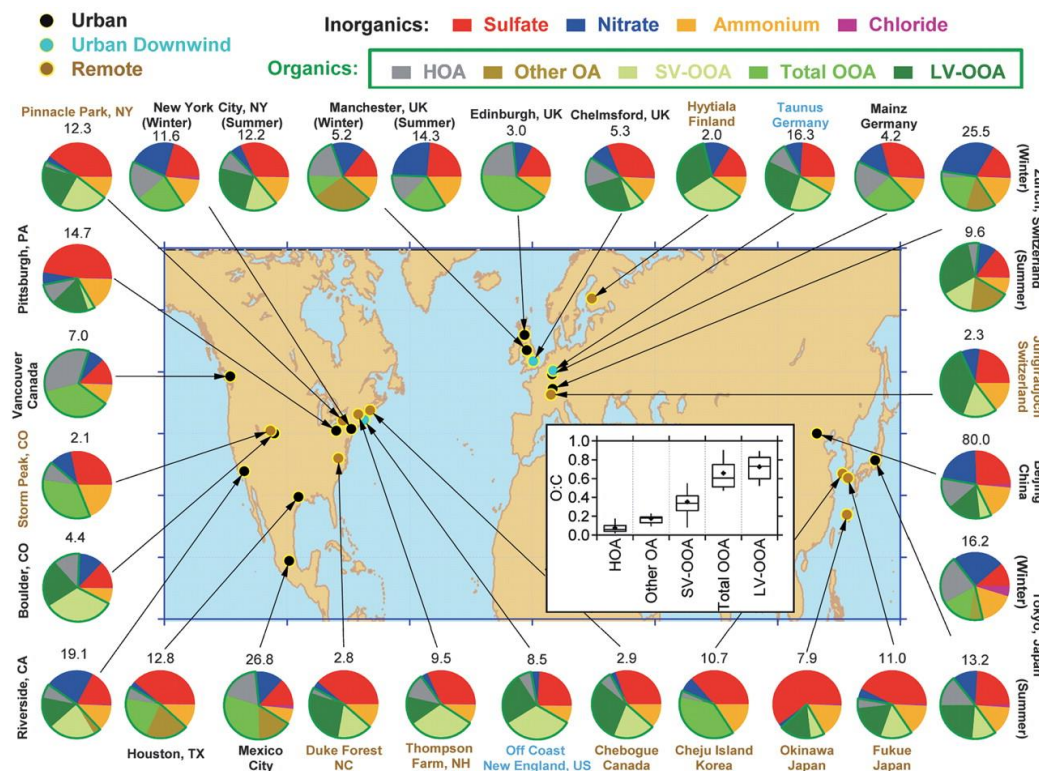
Figure 1.2 Total mass concentration ($\mu g\ m^{-3}$) and mass fractions of non-refractory inorganic species and organic components in submicrometer aerosols measured with the AMS at multiple surface locations in the Northern Hemisphere, O:C ratios of the organic components are shown in the white box. From Jimenez et al. (2009).

1.1.3 *The aging of organic aerosol*

High-volatility compounds are mainly in the gas phase and the very low volatility compounds are in the aerosol phase. The intermediate volatility compounds can either be in the gas phase or in the aerosol phase, largely depending on conditional variety of parameters, such as temperature, OA mass and the volatility (Robinson et al., 2007). The "volatility basis set" (VBS) was proposed to describe the partitioning of the semi-volatile organic compounds (SVOC) by Donahue et al. (2006). Basically, according to the measured saturation vapor pressure C^*, the SVOCs can be separated into 9 bins, whereby each bin contains the C^* range of one order of magnitude (Hallquist et al., 2009). Due to the total OA loading, the partitioning coefficient ξ for a compound i with an effective saturation concentration C_i^* can be calculated as:

$$\xi_i = \left(1 + \frac{C_i^*}{c_{OA}}\right)^{-1} \tag{1.1}$$

i.e., if C_{OA}=1 $\mu g\ m^{-3}$, and i has a C^* of 1 $\mu g\ m^{-3}$, then ξ_i will be 0.5, which means 50 % of the mass of i will condense on the particle phase and the rest will remain in the gas phase. As the dilution ratio of

the emissions from different kinds of sources is an important factor it would be far more revealing to represent results in terms of the ultimate particulate organic mass C_{OA} achieved at the end (Donahue et al., 2006). Two examples of ambient concentrations and fresh emissions, as well as the effects of dilution are shown in Fig. 1.3.
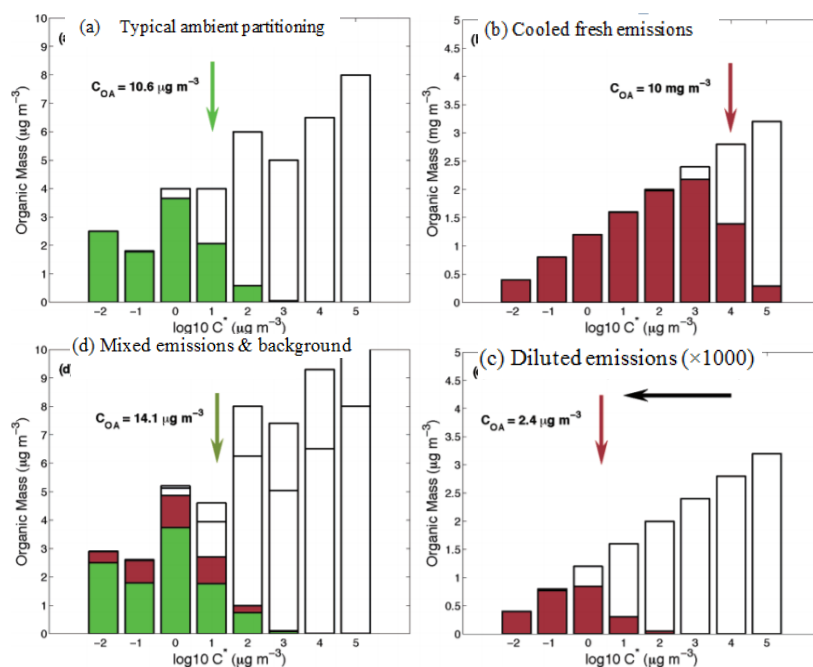

Figure 1.3 a) Partitioning of a collection of semi-volatile compounds, with total loadings (µg m^{-3}) shown in full bars and the condensed-phase portion with filled green bars. At C_{OA}=10.6 µg m^{-3}, the bin of C*=10 µg m^{-3} is evenly split between the vapor and the condensed-phase. b) Partitioning of semi-volatile emissions from a plausible primary source such as a gasoline or diesel engine, before it is diluted into the background atmosphere. The concentration shown in this figure is 1000 times greater than the ambient case shown in a, and is representative of the highly concentrated conditions occurring near the emission point of a heavily emitting source. The high loading leads to the portioning well into the high C* end of the distribution (shown in brown). c) Partitioning of the emissions depicted in Figure 1.3b after dilution by a factor of 1000 using pure air. The aerosol mass actually decreased by a factor of 4000 instead of 1000, due to the repartitioning into the vapor phase. d) The mixture of the background organic material (green) and the fresh emissions after dilution (brown). The separated white bars represent the vapor portions of the background and the fresh emissions (Donahue et al., 2006).

Jimenez et al. (2009) presented the ambient aerosol in a 2D-VBS frame work for OA, lumping all species with C*< ~10^7 µg m^{-3} into bins that are spaced evenly in a C* and O:C space (Fig. 1.4a), each bin includes many organic compounds. Only species with C* < 10 µg m^{-3} (log10 C* = 1) typically partition substantially into the aerosol (Hallquist et al., 2009) at moderate ambient concentrations. The OOA factors, including LV-OOA, SV-OOA, as well as the volatile α-pinene are located in different parts of the 2D-VBS scheme as shown in Fig. 1.4 a. In the ambient atmosphere, most OA is a mixture of low-volatility oxygenated OA (LV-OOA) and semi-volatile oxygenated OA (SV-OOA), with an O:C ratio between 0.25 and 1. Most primary emissions lie in the lower range of O:C, with various C*, while photochemical aging causes them to evolve in the 2D space. Functionalization and fragmentation occur upon oxidation, which is shown using α-pinene (brown pentagon in Fig. 1.4a) as an example. The

evolution of the condensed O:C versus approximate OH exposure for simulated aging is shown in Fig. 1.4b. The oxidation can occur in the gas or condensed phase, form three categories: fragmentations (carbon number decreases, generate more volatile species), functionalization (carbon number stays the same, reduce volatility considerably), or oligomerization (carbon number increases) (Fig. 1.4c), the 2D-VBS described here simulates photochemical aging using a functionalization kernel and a fragmentation kernel, a branching ratio between these two pathways, and a simple representation of differing homogeneous and heterogeneous oxidation by OH (Jimenez et al., 2009).
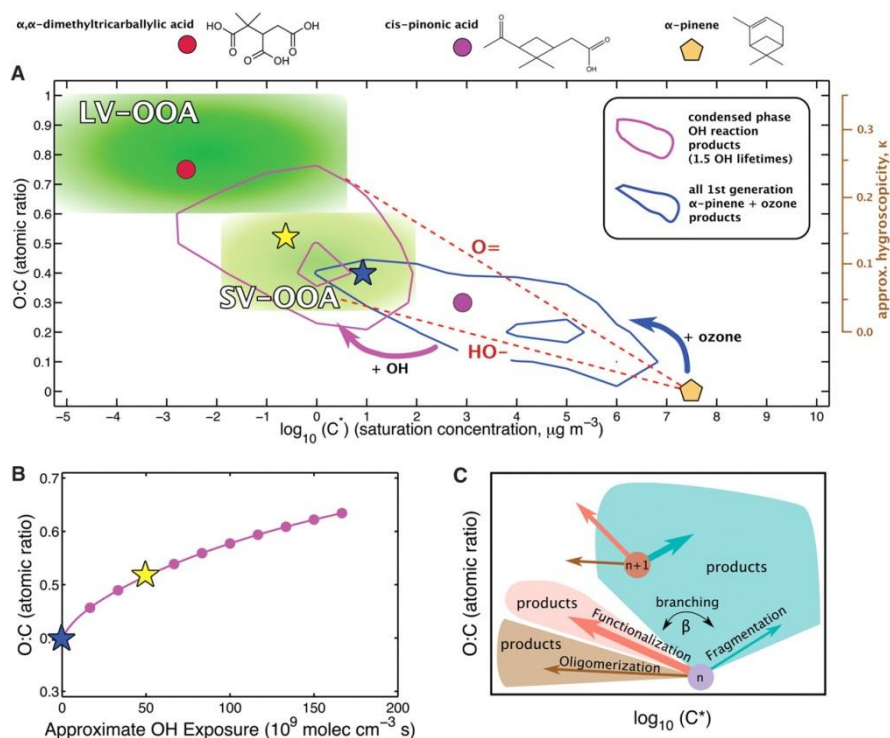

Figure 1.4 a) 2D framework for OA aging, where the x-axis represents volatility ($\log_{10}$ of C^* at 298 K), the y-axis oxidation state, approximated by the O:C ratio, the secondary y-axis shows the approximate hygroscopicity parameter κ of α-pinene SOA. All products from the α-pinene + ozone reaction, modeled explicitly, are distributed according to the blue contours, the material at low C^* and high O:C forms SOA (with mean properties indicated by the blue star). The subsequent aging reactions of α-pinene SOA with OH was modelled within 2D-VBS, and a representative secondary generation product, a C8 triacid is shown in the LV-OOA range with a crimson dot, the modelled condense-phase products after 1.5 lifetimes of OH oxidation are shown with purple contours, the mass-weighted average is indicated by the yellow star. The shift between the blue and yellow stars indicates the simulation reproduces a substantial shift toward ambient OOA characteristics. b) Evolution of condensed-phase O:C ratio versus approximate OH exposure for simulated aging, where the blue and yellow stars for organic aerosol represent the same as in a; c) The processes during aging (Jimenez et al., 2009).

1.1.4 The VOC degradation

The degradation of gaseous VOCs in the atmosphere is initiated either by reaction with hydroxyl radicals (OH is the main atmospheric oxidant with concentrations between 10^6 - 10^7 cm^{-3} depending on the pollution level, Hausmann et al., 1997), nitrate radicals (NO$_3$, an oxidant reacting with some specific compounds during night) or ozone (O$_3$, oxidizing alkenes during both day and night). Chlorine atoms (Cl), e.g. from sea salt aerosols, may also initiate the oxidation of VOCs under certain conditions (Wang

et al., 2005; Fantechi et al., 1998). Atmospheric reactions may also occur by photolysis; due to the absorption of the short wavelengths of the solar spectrum by stratospheric ozone and molecular oxygen, the photochemistry in the atmospheric is driven by the radiation with the wavelengths between 300 and 600 nm (Seinfeld and Pandis, 2016).
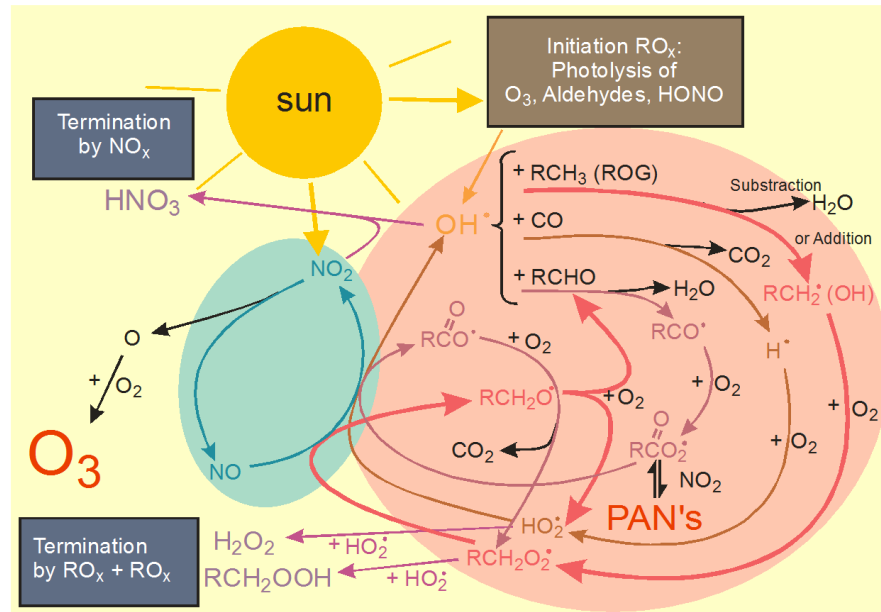
Figure 1.5 Schematic overview of photochemistry in the polluted planetary boundary layer (Staehelin et al., 2000).

A variety of reactions takes place in the gas phase as outlined in Fig. 1.5, but they can be classified into mainly three types of reactions (Vanda et al., 2010):

1) Initiation reactions: Photolysis of certain molecules (ozone, HCHO, HONO, NO_2), producing an OH radical as indicated in Eq. 1.2, Eq. 1.3, Eq. 1.4, Eq. 1.5, respectively, which then reacts with most gaseous compounds and is regarded as "cleaning agent" in the troposphere.

$$\left\{ \begin{array}{l} O_3 \xrightarrow{hr} (^1O) + O_2 \\ ^1O + H_2O \rightarrow 2 \cdot OH \end{array} \right. \tag{1.2}$$

$$\left\{ \begin{array}{l} HCHO \xrightarrow{hr} H \cdot + HCO \\ H \cdot + O_2 \rightarrow HO_2 \\ HCO \cdot + O_2 \rightarrow HO_2 \cdot + CO \\ HO_2 \cdot + NO \rightarrow \cdot OH + NO_2; \; HO_2 \cdot + O_3 \rightarrow \cdot OH + 2O_2 \tag{1.3} \\ HONO \xrightarrow{hr} \cdot OH + NO \tag{1.4} \end{array} \right.$$

$$\left\{ \begin{array}{l} H_2O_2 \xrightarrow{hr} \cdot OH + \cdot OH \\ ROOH \xrightarrow{hr} RO \cdot + \cdot OH \end{array} \right. \tag{1.5}$$
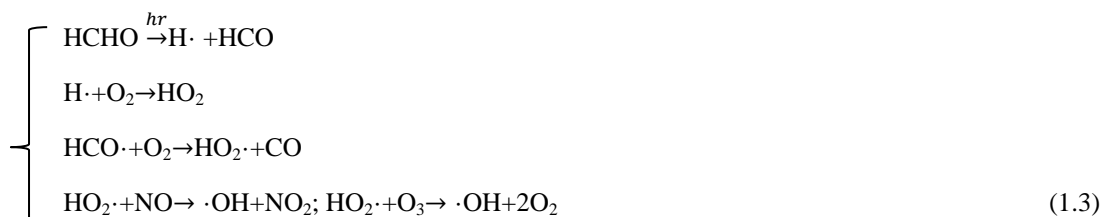
There are also reactions that lead to OH without sunlight:

$$\left\{ \begin{array}{l} O_3 + C_2H_4 \rightarrow (\cdot CH_2OO \cdot)^* + HCHO \end{array} \right.$$

$$(\cdot CH_2OO\cdot)^* \rightarrow HO_2\cdot+CO+\cdot OH \tag{1.6}$$
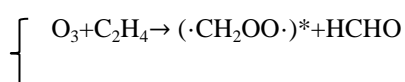
2) Propagation or radical chain: OH produced by the initiation reaction can react with most molecules, causing sequences of radical reactions in which some radicals are formed again, leading to a radical chain. There are mainly two types of radical chains in tropospheric chemistry:

a. the NO_x radical chain

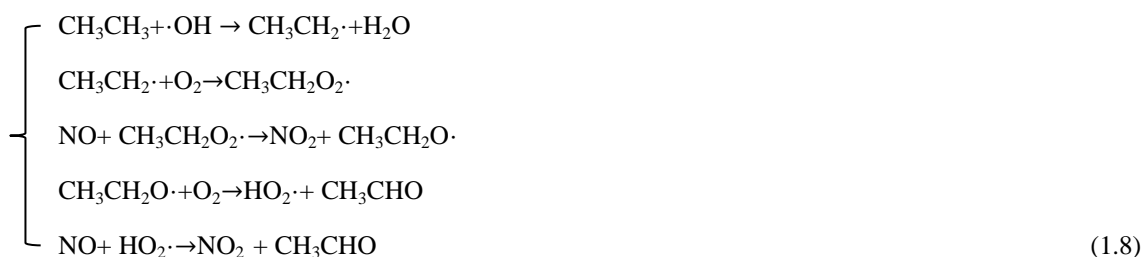$$\begin{cases} NO_2 \overset{hr}{\rightarrow} NO+O\cdot \\ O\cdot+O_2\,(+M) \rightarrow O_3\,(+M) \\ NO+O_3 \rightarrow NO_2+O_2 \end{cases} \tag{1.7}$$

b. the RO_x/HO_x radical chain.

$$\begin{cases} CH_3CH_3+\cdot OH \rightarrow CH_3CH_2\cdot+H_2O \\ CH_3CH_2\cdot+O_2 \rightarrow CH_3CH_2O_2\cdot \\ NO+ CH_3CH_2O_2\cdot \rightarrow NO_2+ CH_3CH_2O\cdot \\ CH_3CH_2O\cdot+O_2 \rightarrow HO_2\cdot+ CH_3CHO \\ NO+ HO_2\cdot \rightarrow NO_2 + CH_3CHO \end{cases} \tag{1.8}$$

These two radical chains are connected by the reactions

$$\begin{cases} NO+HO_2 \rightarrow NO_2+OH\cdot \\ NO+RO_2\cdot+O_2 \rightarrow NO_2+HO_2\cdot+\text{secondary VOC} \end{cases} \tag{1.9}$$

3) Termination: If two radicals react with each other and form less reactive species, these reactions stop the radical chain, including: RO_2 and/or HO_2 radicals (forming peroxides, shown in Eq. 1.10), or OH and NO_2 (forming HNO_3, shown in Eq. 1.11).

$$\begin{cases} HO_2+HO_2\,(+H_2O) \rightarrow H_2O_2+O_2\,(+H_2O) \\ RCH_2\text{-}O_2+HO_2 \rightarrow RCH_2\text{-}OOH + O_2 \tag{1.10} \\ OH+NO_2 \rightarrow HNO_3 \tag{1.11} \end{cases}$$

In strongly polluted areas the termination reaction of OH with NO_2 is dominant, while in less polluted areas the formation of peroxides is more important.

1.1.5 Atmospheric aerosol effects on climate

Scientific evidence for warming of the climate system is unequivocal (IPCC, 2007). The current warming trend is specially significant because most of it is extremely likely (>95% probability) to be the result of human activity since the mid-20th century and proceeds at an unprecedented rate over decades to millennia (IPCC Fifth Assessment Report, 2014). The causative links between human activity and the climate change can be explained by the "radiative forcing" of the anthropogenic emissions. The term "radiative forcing (RF)" has been employed in the IPCC assessments for evaluating and comparing the strength of the various mechanisms affecting the Earth's radiation balance and thus causing climate change (IPCC, 2013), i.e. RF quantifies the change in the Earth's energy budget caused by changes in natural and anthropogenic substances and processes for today relative to 1750. Fig. 1.6 shows the

estimation of the RF by the various components. CO_2 is the dominant cause for the positive RF, followed by other greenhouse gases, including CH_4, N_2O and halocarbons. O_3 shows a positive effect in the troposphere and a slightly negative effect in the stratosphere. Stratospheric water vapor from CH_4 exhibits a positive RF. The surface albedo, defined as the ratio of irradiance reflected to the irradiance received by a surface shows a negative forcing due to the changes in land use, and a positive RF due to black carbon on snow. Contrails and contrail induced cirrus cause a slightly positive RF. Aerosol-radiation interactions referring to the scatting and absorption of short-wavelength solar radiation by aerosol particles have a negative RF, and aerosol-cloud interactions, which relate to the influence of aerosol particles on the cloud cover, reflectance and lifetime, have also a negative RF. On a global scale, aerosols have a negative RF. The total anthropogenic RF is positive, with a large uncertainty. The solar irradiance has a small RF positive as well.
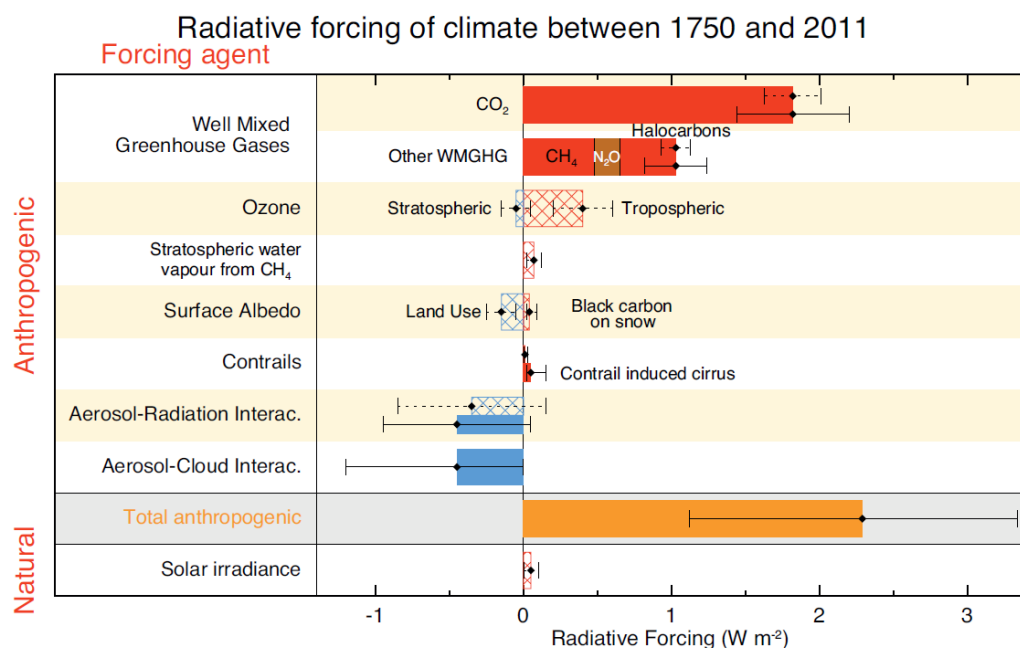

Figure 1.6 Global average radiative forcing estimates between 1750 and 2011 (IPCC 2013). Error bars represent the estimated uncertainties.

1.1.6 *Atmospheric aerosol effects on health*

Particle penetration

Human exposure to PM occurs by inhalation (respiratory tract), ingestion (gastrointestinal), dermal (skin), and injection of engineered nanomaterials (blood circulation) (Oberdorster et al., 2005), of which inhalation is the utmost important pathway as we breathe all the time throughout our life. The deposition of inhaled particles under conditions of nose breathing during rest in the human lung is shown in Fig. 1.7 (Oberdorster et al., 2005). The inhaled PM of different sizes can settle down in all three regions of the respiratory tract of humans, including the nasopharyngeal/head airways/nasal cavity area, the bronchia area and the alveoli area, as indicated in blue, green and red in Fig. 1.7, respectively. The diameters of the respiratory tracts of the nasal cavity, bronchi and alveoli are 4.6, 1 and 0.02 cm, respectively (Ochs et al., 2004). The behavior of the particles within the human respiratory system is determined largely by

their size, a crude distinction is that $PM_{2.5}$ penetrate to the alveoli and terminal bronchioles, larger particles (within diameters up to 10 μm) will deposit primarily in the primary bronchi, much larger particles (within diameters up to 100 μm) will deposit in the nasopharynx (Kelly and Fussell, 2012). The PM with a diameter of 0.1 μm or less by far possesses the greatest number and presents a particular health threat as their small size allows the greatest lung penetration and onward passage across the air-blood barrier (Kelly and Fussell, 2012). To keep the mucosal surfaces free from cell debris and particles deposited by inhalation, the defense mechanisms exist throughout the respiratory tract, the clearance of deposited particles are basically due to two processes (Oberdorster et al., 2005):

a) physical translocation of particles by different mechanisms, including mucociliary movement (nasal, tracheobronchial), macrophage phagocytosis (tracheobronchial, alveolar), epithelial endocytosis (nasal, tracheobronchial, alveolar), interstitial translocation (tracheobronchial, alveolar), lymphatic drainage (tracheobronchial), blood circulation (tracheobronchial, alveolar), sensory neurons (nasal, tracheobronchial).

b) chemical clearance processes, including dissolution (all three regions); leaching (all three regions), protein binding (all three regions).
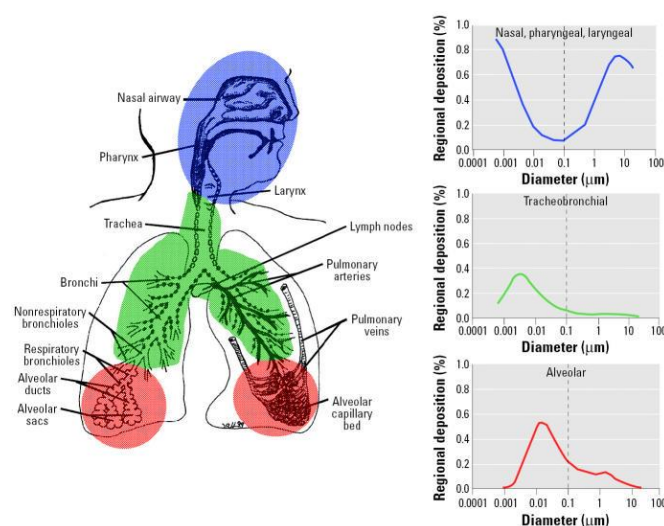

Figure 1.7 Predicted fractional deposition of inhaled particles in the nasopharyngeal, tracheobronchial, and alveolar region of the human respiratory tract during nose breathing. Based on data from the International Commission on Radiological Protection (ICRP, 1994). Drawing courtesy of J. Harkema (Oberdorster et al., 2005).

Health impacts

Although humans were exposed to PM throughout the evolutionary stages, such exposure increased dramatically in recent centuries, due to the anthropogenic activities with the advent of the industrial revolution (Oberdorster et al., 2005). In the majority of the regions of the world, annual median concentrations of $PM_{2.5}$ are higher than the World Health Organization (WHO) guideline levels of 10 μg m^{-3}, with 93 % of the world population exposed to $PM_{2.5}$ levels that exceed WHO limits. Exposures are particularly high in the Eastern Mediterranean, South-east Asian and Western Pacific Regions (WHO, 2016). Epidemiological and toxicological studies have demonstrated a link between exposure to airborne

particulate matter (PM) and adverse health effects and observed statistically significant and robust associations between air pollution and mortality. Dockery et al. (1993) found in six cities (including Portage (P), Topeka (T), Watertown (W), St. Louis (L), Harriman (H) and Steubenville (S)) in America that the adjusted mortality-rate ratios are almost linearly correlated with the pollution levels (represented as fine particle concentrations), as shown in Fig. 1.8a. The mortality rates in the 9 largest U.S. cities were found to rise on average by 0.5 % with each 10 μg m^{-3} increase in fine PM (Kaiser et al., 2000). In an acute fatal incident in the London smog of December 1952, the daily death count highly correlated with the concentration of the smog (as shown in Fig. 1.8b).

The study of Beelen et al. (2013) from 22 European cohorts revealed that long-term exposure to fine particulate matter air pollution was associated with natural-cause mortality. According to the air pollution study of He et al. (2016) in China, an increase of 10 μg m^{-3} in PM_{10} and $PM_{2.5}$ was associated with a 0.53 % and 0.57 % increase of daily death counts, respectively. Wheeler et al. (2006) reported increases in heart rate variability (HRV) amongst chronic obstructive pulmonary disease (COPD) sufferers, but a decrease in HRV amongst the people with recent myocardial infarctions. A study investigating the effects of ambient air pollution on pulmonary function among school children showed that the ambient traffic-related pollution had chronic adverse effects on pulmonary function in schoolchildren, especially for boys (Lee et al., 2011). Adam et al. (2015) showed an adverse association of ambient air pollution with lung function in adults at very low levels in Europe. Hwang et al. (2015) revealed long-term exposure to $PM_{2.5}$ and O_3 may have a detrimental effect on the development of lung function in children.

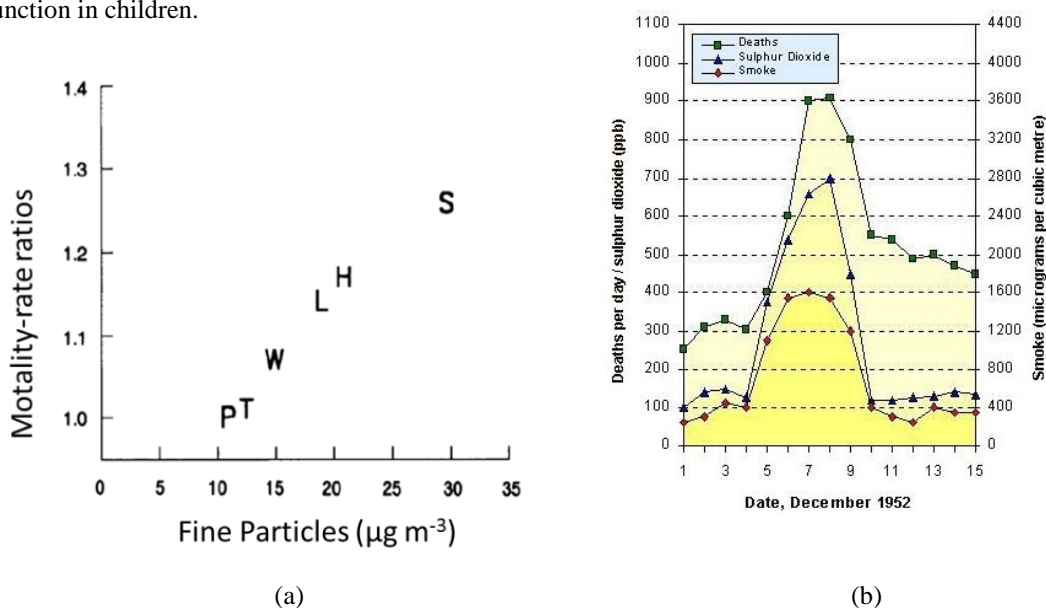(a)   (b)

Figure 1.8 (a) Estimated adjusted mortality-rate ratios and pollution levels in the Six Cities study. P denotes Portage, Wisconsin; T Topeka, Kansas; W Watertown, Massachusetts; L St. Louis; H Harriman, Tennessee; and S Steubenville, Ohio (adapted from Dockery et al., 1993). (b) Deaths due to the great smog in London in 1952 (source for image: it is originally drawn by Wilkins, E. T. (1954), the figure here is taken from http://www.air-quality.org.uk/03.php, last accessed: 1st November 2017).

Although epidemiological studies consistently show an association between adverse health effects and the PM concentrations as listed above, the mechanisms by which PM affects human health remain unclear. Thus controlled toxicological studies are essential for a better understanding of the links

between them. Toxicological investigations have demonstrated substantial pulmonary toxicity of model and real environmental particles, and have postulated particle size, surface area, and composition as potential parameters and components relevant to the observed health effects (Donaldson et al., 2002).

Toxicity of different emissions sources

The characteristics of the atmospheric aerosol have changed dramatically over the past century. More detailed analyses revealed associations between health effects and specific sources of particulate matter, such as wildfires, traffic, shipping, construction dust, metals sources, coal and residual oil combustion (Lippmann et al., 2013; Liu et al., 2017; Os; Adam et al., 2015), thus it is important to understand the contributions of different sources to the aerosol. The report of the World Health Organization (WHO, 2011) stated that the largest contributors to urban outdoor air pollution are motor transport, small-scale manufactures and other industries, burning of biomass and coal for cooking and heating, as well as coal-fired power plants. Residential wood and coal burning for space heating is an important contributor to air pollution, especially in rural areas during cold periods. Each year 61000 premature deaths are attributable to ambient air pollution from residential heating with wood and coal in Europe, with an additional 10000 attributable deaths in North America (WHO, 2015).

Traffic is a major source of $PM_{2.5}$. Studies found vehicles contributing up to one-third of ambient $PM_{2.5}$ in urban areas in the US (Hammond et al., 2008; Lee et al., 2008). In summary the available epidemiological literatures finds strong evidence for a causative role of traffic-related air pollution on mortality, particularly from cardiovascular events (HEI, 2009). Traffic-related air pollutants may have adverse effects on birth weight (Slama et al., 2007). An in-vitro study showed that even a single, short-term exposure to atmospherically aged gasoline exhaust particles increases necrotic cell death in a dose-dependent manner in normal and in compromised respiratory epithelia and decreases cytokine release in cystic fibrosis epithelia (Künzi et al., 2015).

Wood-burning stoves and fireplaces as well as wildland and agricultural fires emit significant quantities of known health-damaging pollutants (Naeher et al., 2007). Chemical characterization reveals that residential wood combustion can contribute 5–44 % to the total ambient $PM_{2.5}$, depending on the environment (Zhang et al., 2010; Canada, 2005; USEPA, 2000; EEA, 2013; Barregard et al., 2006). Barregard et al. (2006) found that exposure to wood smoke particles affects inflammation, coagulation, and possibly lipid peroxidation. Short-term exposure to wildfire-specific $PM_{2.5}$ was associated with risk of respiratory diseases in the elderly population in the Western United States during severe smoke days (Liu et al., 2017). Toxicological studies revealed that exposure to wood combustion particles may cause moderate inflammatory activity, cell death and DNA damage, and adverse effects to airway epithelia (Krapf et al., 2017; Tapanainen et al., 2012; Muala et al., 2015; Ruusunen et al., 2011).

Coal is widely used in power plants or residential stoves. It primarily consists of carbon but also contains sulfur, oxygen, nitrogen, and hydrogen. When coal is used for residential heating it can also result in emissions of sulfur and other toxic contaminants found in some types of coal; even with good combustion, these contaminants are not destroyed (WHO, 2015). $PM_{2.5}$ emitted from coal combustion

can decrease cell viability, increase global DNA methylation, and cause oxidative DNA damage in human umbilical vein endothelial cells (Wang et al., 2016).

Biogenic emissions are the predominant sources of volatile organic compounds, which lead to fine particle formation and the formation of ozone near the ground. Ground-level ozone is a known pulmonary irritant which affects the respiratory mucous membranes, other lung tissues, and respiratory function (Ebi and McGregor, 2009). Ren et al. (2017) found that both urban green spaces and rural forests play important roles in threatening human health. Decreased phagocytic activity was found in human macrophages exposed to SOA from α-pinene (Gaschen et al., 2010).

1.2 Reactive oxygen species (ROS)

The mechanisms of adverse health effects of PM have been widely studied. The generation of reactive oxygen species (ROS) and pulmonary and systemic oxidative stress in the initial and process of dysfunction associated with PM exposures is believed to be a main contributor to these health issues (Gurgueira et al., 2002; Nel et al., 1998; Tao et al., 2003; Li et al., 2003). Reactive oxygen species (ROS) denote chemically reactive molecules containing oxygen, e.g., OH radicals, $O_2\cdot^-$, H_2O_2, organic peroxides (S. J. Fuller et al., 2014; Sagai et al., 1993; Halliwell and Cross, 1994). ROS play a dual role as both toxic and beneficial compounds. The delicate balance between their two antagonistic effects is very important. At low or moderate levels, ROS exert beneficial effects on cellular responses and immune function. At high concentrations, they generate oxidative stress (Pham-Huy et al., 2008). Mild oxidative stress often induces antioxidant defense enzymes, but severe stress can cause oxidative damage to lipids, proteins, and DNA within cells (Halliwell and Cross, 1994).

It is important to assess the ROS content in PM. In the ambient air, both gas-phase and particle-bound ROS (PB-ROS) can be generated through combustion and atmospheric chemical processes. Atmospheric exposure to ROS can occur either through the gas or particle phase. Gas phase ROS are most likely removed in the upper mucus membranes, while PB-ROS in inhaled air could easily be carried by small particles, penetrate into the lungs and deposit in the alveolar region (Kao and Wang, 2002; Friedlander and Yeh, 1998). Other studies indicate that particles could efficiently enter the cells, be internalized within cells and then release high levels of toxic ions by a "Trojan-horse type mechanism" (Hsiao et al., 2015). The oxidative stress provoked by particles containing cobalt or manganese can be up to eight times higher than the reference cultures exposed to aqueous solutions of cobalt or manganese (Limbach et al., 2007). Hydrogen peroxide (H_2O_2) is an important species in photochemical smog as a chain terminator. H_2O_2 is not expected to be a large fraction of typical ambient aerosol but H_2O_2 concentrations of 0.5-5 ppb have been observed in the gas phase (Khurshid et al., 2014; Hung and Wang, 2001; Jackson and Hewitt, 1999). We estimated that Henry's law predicts only ~0.0002 % of H_2O_2 in the particle phase by assuming: 1 ppb H_2O_2 in the gas phase, RH = 90 %, hygroscopic growth factor = 1.5, Henry's law coefficient K_h (M atm^{-1}) = 1.0×10^5 at T = 298.15 K; pH = 7.2. However, studies have observed that urban hydroperoxide levels within aerosols greatly exceed the concentrations predicted by Henry's law (Arellanes et al., 2006; Dusek et al., 2006; Hasson and Paulson, 2003), which might be due to other compounds contributing to the oxidation potential of particles, or

because the Henry's law constant in aerosols may be different from that in liquid water (Hasson and Paulson, 2003). This further emphasizes the importance of assessing the PB-ROS.

PB-ROS inside the human body can be classified as endogenous (generated by the inhaled particulate matter (PM) in vivo) and exogenous (transported into the lungs in respirable particles) (Zhao and Hopke, 2012). The hypotheses that ROS present in particles could cause the same kind of systemic dysfunction as endogenously generated ROS (Venkatachari et al., 2007) and that exposure to an exogenous source of ROS can influence endogenous production of ROS thereby influencing the disease process (Khurshid et al., 2014) have merit and require further investigation (Venkatachari et al., 2007; Khurshid et al., 2014). Li et al. (2003) demonstrated that UFPs are more potent than fine < 2.5 μm) or coarse (2.5–10 μm) particles toward inducing oxidative stress. Endogenous ROS was shown to be generated through the interaction of ultrafine particles with organic hydrocarbons, such as polycyclic aromatic hydrocarbons and quinones, as well as transition metal ions (Squadrito et al., 2001; Lakey et al., 2016). These processes usually take place at the site of infection; e.g., the epithelial lining fluid (ELF) has been suggested as the site (compartment) of antimicrobial activity against lung infections caused by extracellular pathogens (Rodvold et al., 2011), which contains a range of antioxidants like ascorbate, uric acid (UA), glutathione (GSH), α-tocopherol, as well as surfactants (Mudway and Kelly, 2000; Van der Vliet et al., 1999). The ELF extends from the nasal cavity to the pulmonary alveoli with a film thickness that decreases from several micrometers in the upper airways to dozens of nanometers in the lungs, and can be regarded as an interface between atmospheric and physiological chemistry (Mudway and Kelly, 2000). The surface areas of the ELF comprise 180, 4500 and 885000 cm^2 in the nasal cavity, bronchi and alveoli, respectively (Cross et al., 1998). A simplified mechanism of the ROS produced by inhaled PM in the epithelial lining fluid is shown in Fig. 1.9 (Lakey et al., 2016). In case of endogenous ROS formation the initial step is the antioxidant's transfer of electrons to transition metal ions, or quinones forming reduced metal ions or semiquinones, respectively. The redox-active transition metal ions and quinones are regenerated by reaction with O_2 forming O_2^- radicals which are further converted into hydrogen peroxide, which plays a central role in radical reaction cycles and causes the oxidative stress in the respiratory tract (Winterbourn, 2008). Via a Fenton (with Fe^{2+}) or Fenton-like (with Cu^{2+}) reaction, the formation of the most reactive form of ROS --- OH radicals is possible (Charrier et al., 2011; Lakey et al., 2016).
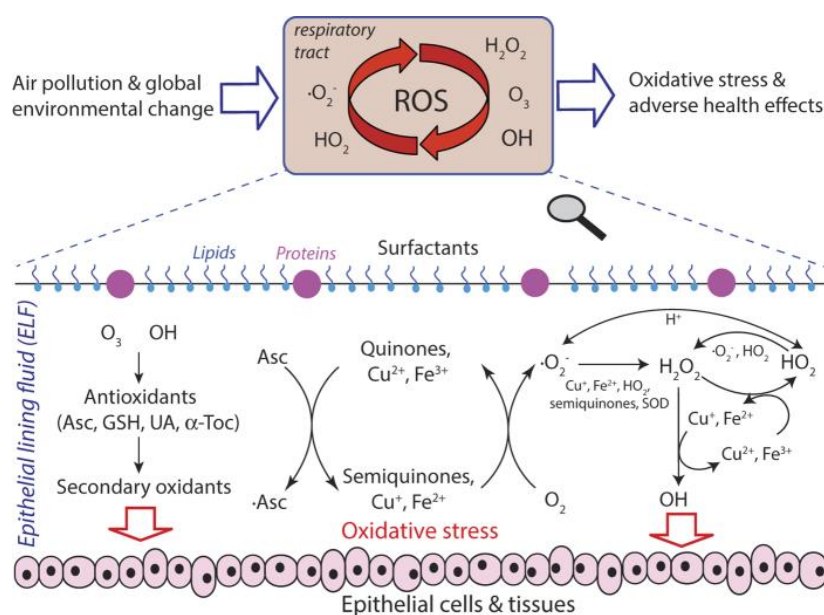
Figure 1.9 Interaction of air pollutants and reactive oxygen species (ROS) in the epithelial lining fluid (ELF) of the human respiratory tract (Lakey et al., 2016). Atmospheric ozone and OH radicals react with surfactants and antioxidants (ascorbate, uric acid, reduced glutathione, α-tocopherol) forming secondary organic oxidants. Redox-active components of fine particulate matter, including quinones, iron and copper ions, can trigger and sustain catalytic reaction cycles generating ROS and oxidative stress (Lakey et al., 2016). A similar mechanism of quinoid redox cycling of $PM_{2.5}$ was also found by (Squadrito et al., 2001), where reducing equivalents like nicotinamide adenine dinucleotide phosphate (NAD(P)H) or ascorbate can provide the electrons to reduce the quinones and sustain the cycle, continuously reducing oxygen and producing hydrogen peroxide, and the superoxide and hydroxyl radicals.

Based on the link between the PM-induced oxidative potential (OP) and the adverse human health effects, numerous studies have been initiated which focus on the quantification of the PM-induced OP or the particle-bound components act as ROS (PB-ROS). These include both cellular assays and acellular assays. The cellular assays mainly detect the response of the cells when exposed to aerosols as for instance; the macrophage ROS generation (Landreman et al., 2008), the cytokine activation (Wilson et al., 2010), the induction of heme oxygenase-1(HO-1) and other stress protein expressions (Li et al., 2003). Other acellular chemical assays include the mimic of the loss of antioxidants, such as the oxidation of dithiothreitol (DTT) (Fang et al., 2015), glutathione(GSH) (Godri et al., 2011), ascorbic acid (AA) (DiStefano et al., 2009), and 2,7-dichlorofluorescin (DCFH) (Hung and Wang, 2001; King and Weber, 2013; S. J. Fuller et al., 2014; Huang et al., 2016; Antonini et al., 1998; Zhou et al., 2018a). To make a quick and reliable estimation of the toxicity of the PM, the online measurements of the PB-ROS using a 2', 7'-dichlorofluorescin (DCFH) assay were applied in this study. The direct acellular PB-ROS measurements by the DCFH assay was adapted from intracellular ROS measurement (Hung and Wang, 2001). The DCFH assay has been shown to be non-selective toward a full range of ROS, and possesses a fast response rate and linear response to varying ROS concentrations, making it suitable to evaluate the overall oxidative activity of PM (Zhou et al., 1997; Venkatachari and Hopke, 2008; King and Weber, 2013; Zhou et al., 2017a).

1.3   Study motivation and thesis outline

A better characterization of the PB-ROS concentration in ambient aerosol as well as their sources and formation mechanism is meaningful to make better estimations of various health effects of air pollution. The aim of the thesis is to elucidate the PB-ROS sources and its formation pathways upon atmospheric aging of PM. By quantifying the PB-ROS content and characterizing the chemical composition of primary and secondary emissions of both anthropogenic and biogenic sources in laboratory studies, we were able to better understand the ambient in-situ measurements. The secondary aerosol formation was accomplished by employing two commonly used atmospheric simulation facilities: a smog chamber (SC) and a potential aerosol mass (PAM) chamber, where experiments were conducted under well-determined conditions for different emission sources, including wood and coal combustion as well as α-pinene ozonolysis. The different parameters that control ROS formation upon the aging of wood and coal combustion emissions were investigated. Further, we performed in-situ ambient studies at two contrasting urban locations: Beijing (China) and Bern (Switzerland). For the characterization and quantification of the PB-ROS and other chemical compositions of the PM, a modified ROS analyzer and an aerosol mass spectrometer (AMS), respectively, were deployed. Further, the equivalent black carbon (eBC) was determined by an aethalometer. An improved identification and quantification of OA sources compared to conventional positive matrix factorization (PMF) analysis was accomplished with the multi-linear engine tool (ME-2). The source apportionment results were then coupled with the measured PB-ROS by a multiple linear regression model (MLRM) to identify the different emission sources of PB-ROS.

Chapter 2 provides an overview of the methodologies applied in this study. This includes the setups of all campaigns performed (Sect. 2.1), the aging tools (Sect. 2.2), the instrumentation (Sect. 2.3), the versatile aerosol concentration enrichment system (2.4) and the source apportionment techniques (Sect. 2.5).

Chapter 3 describes the development and characterization of the online and offline ROS analyzer used in this study. The removing efficiency of interfering oxidizing trace gases like O_3 and NO_2 was tested, and the matrix effects of particulate SO_4^{2-} and NO_3^-, as well as transition metals were assessed. Results from the application of this online and offline methodology to laboratory measurements of wood combustion emissions and ambient measurements at an urban site in Bern (Switzerland) are presented. To assess the stability of ROS, online in-situ and laboratory measurements were compared with offline measurements.

Chapter 4 is dedicated to PB-ROS emissions during wood combustion. The PB-ROS generation potential from different combustion devices and technologies, different fuel types, operation types, combustion regimes and combustion phases, as well as aging conditions were investigated. The aging tools included both smog chamber (SC) and potential aerosol mass reactor (PAM). Primary and secondary PB-ROS emissions were quantified, and the dominating factors of PB-ROS emissions were elaborated. The combination and comparison of the results of SC and PAM aging indicates the key parameters that influence PB-ROS formation upon aging.

Chapter 5 investigates the evolution of PB-ROS emissions in the primary and secondary organic aerosols emitted from five types of coal (three types of bituminous coal and two types of anthracite coal) used for residential heating in different regions of China. The PB-ROS content in primary and aged aerosol emissions from coal combustion was investigated by using an atmospheric aging simulator, called the Paul Scherrer Institute Mobile Smog Chamber (PSI-MSC). An inter-comparison of the EF_{ROS} of the different types of coal was done, as well as its association with the OA loading. We also investigated the influence of the different aging conditions to the PB-ROS formation upon aging. Further, the EF_{ROS} from coal combustion were compared with wood combustion. These results provide the first investigation of the PB-ROS emissions of the residential coal used in China and can be used to guide the policy and following toxicological studies of residential coal combustion emissions.

The focus of chapter 6 lies on the analysis of PB-ROS and the characterization of the variable chemical nature of ambient particulate matter (PM) at two contrasting locations, Beijing (China) and Bern (Switzerland). Additionally, primary and secondary aerosol emissions generated from different biogenic and anthropogenic sources were evaluated in laboratory studies. A novel positive matrix factorization procedure was applied to apportion the sources of organic aerosols in Beijing and Bern. Together with a multiple linear regression model the observed PB-ROS was attributed to different sources. The main parameters affecting PB-ROS formation in both locations were revealed. The ROS content of different emission sources obtained from the model were then compared with that of laboratory-characterized sources. Results of this study may provide reliable evidence to infer the adverse health impacts of aerosols at different ambient locations.

Chapter 7 summarizes the major findings obtained from this study and the applicability of the results presented in this thesis to toxicological studies, and provides perspectives in terms of methodology.

2

Methodology

2.1 Laboratory and field campaigns

In total six campaigns were performed in this study, including four laboratory studies and two field campaigns. The laboratory measurements including the characterization of the primary and secondary wood combustion, coal combustion emissions, as well as α-pinene ozonolysis were performed at Paul Scherrer Institute (PSI), Villigen, Switzerland and Lucerne University of Applied Sciences and Arts, Horw, Switzerland. The atmospheric aging simulation was achieved by using a smog chamber (SC) and the potential aerosol mass (PAM) chamber as the aging tools. In-situ ambient measurements were performed at two contrasting locations: National Center for Nanoscience and Technology, Beijing, China and Institute of Anatomy, University of Bern, Bern, Switzerland.

Fig. 2.1 shows the schematic of the studies performed in the smog chambers (SC), where the wood/coal combustion emissions were injected into the SC by using an ejection diluter. After filling the chamber, secondary organic aerosol (SOA) formation was induced by turning the UV lights on. For the α-pinene ozonolysis, α-pinene and O_3 (~ 500 ppb) were injected into the SC, and the O_3 was used as the oxidant which enabled the rapid formation of SOA. The evolution of the gas and particle phase species was done in parallel which serves to understand how atmospheric transformation changes the properties of the primary particles with respect to their particle bound components act as reactive oxygen species (ROS). More details on the laboratory experimental setup can be found in Chapter 4, 5 and 6 for different emission sources.
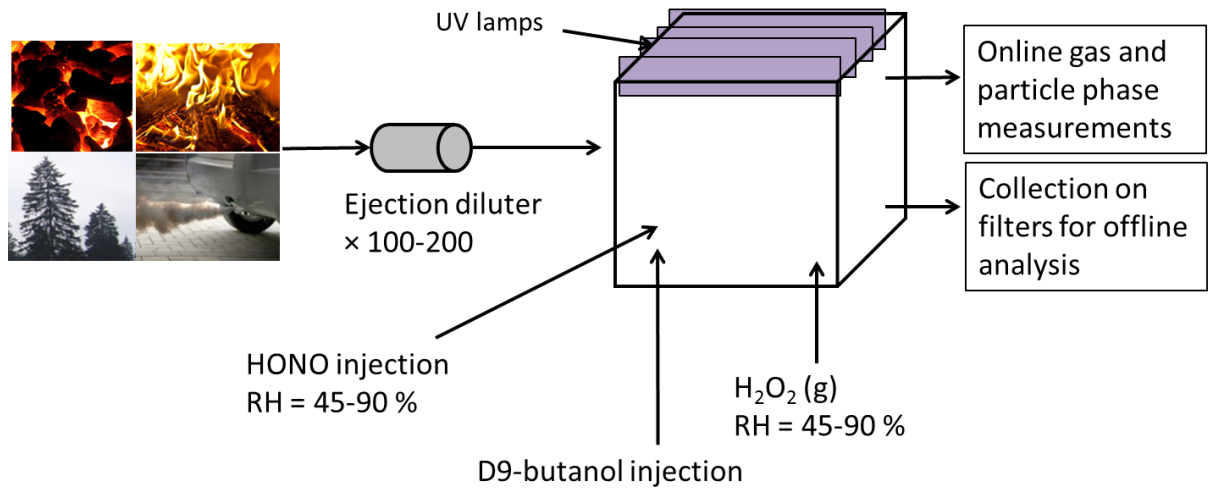
Figure 2.1 Schematic of the studies performed in smog chambers.

The experimental setup of the studies performed with the potential aerosol mass (PAM) chamber is shown in Fig. 2.2. Wood combustion emissions from eight burning devices were tested in this setup. The wood combustion emissions were sampled through a heated line (473 K), diluted by a factor of ~100-150 using two ejector diluters in series (VKL 10, Palas GmbH), and then injected into the PAM chamber flanked by two UV lamps (more information is shown in Chapter 3 and 4).
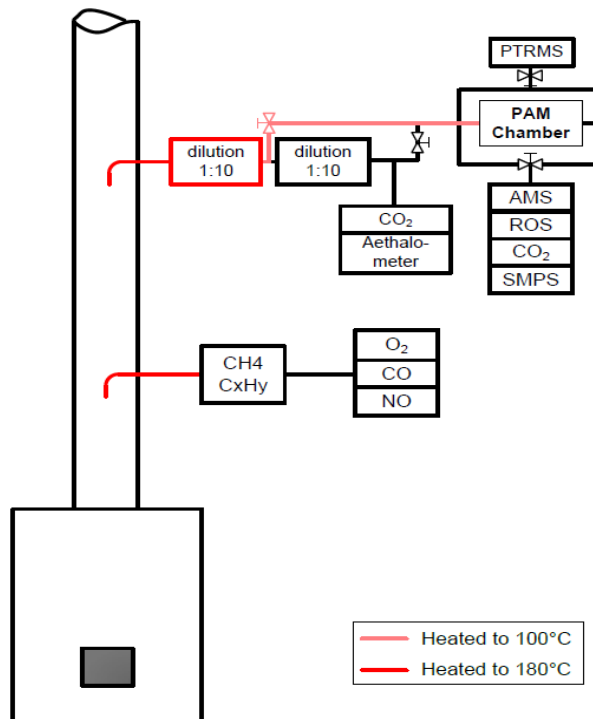
Figure 2.2 Schematic of the studies performed with the PAM chamber.

Fig. 2.3 and Fig. 2.4 show the schematic and the locations of the field campaigns, respectively. The in-situ ambient measurements were performed at two environmentally contrasting locations, i.e., Bern,

Switzerland and Beijing, China. The first campaign was conducted in November 2014 at the campus of the Institute of Anatomy at University of Bern, Switzerland, to enrich the Bern ambient aerosol thus increase the particle-bound reactive oxygen species (PB-ROS) concentration above the instrument detection limit, the versatile aerosol concentration enrichment system (VACES) was employed during the campaign. A schematic of the VACES and more details can be found in Sect. 2.4. The second ambient campaign took place from January to February 2015 at the National Center for Nanoscience and Technology, Beijing, China. Ambient air was sampled through a $PM_{2.5}$ inlet. The instruments used in the different campaigns are listed in Table 2.1.
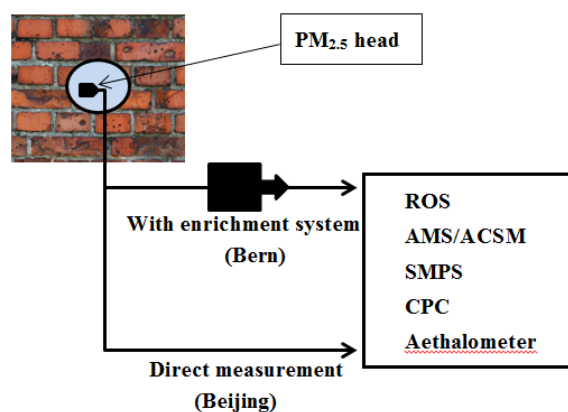
Figure 2.3 The schematic of the field campaigns.
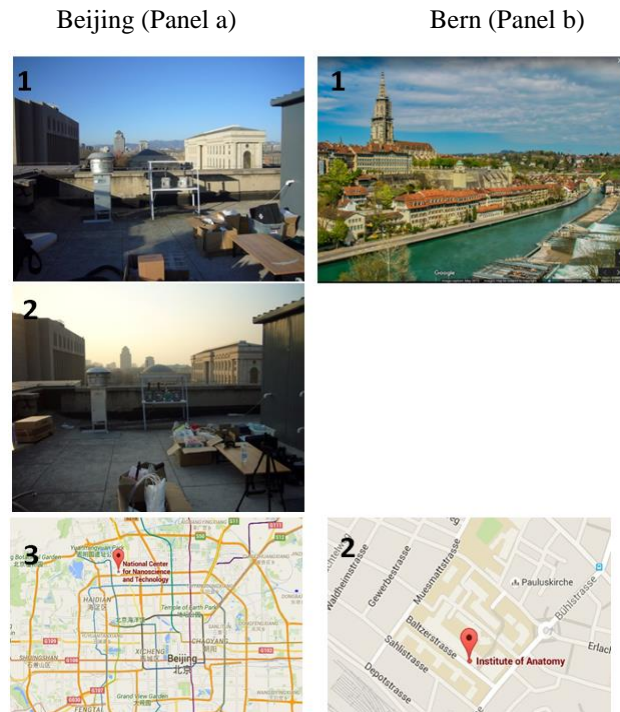
Figure 2.4 In-situ ambient measurements at two contrasting locations: Beijing, China (Panel a) and Bern Switzerland (Panel b). Figures in Panel a represent the reference episodes (labeled as NO. 1), the haze episodes (labeled as No. 2), as well as the location of the measurement campaign (labeled as NO.3) in Beijing, respectively; Figures in Panel b represent the city of Bern (labeled as NO. 1) and the location of the measurement campaign (labeled as NO. 2), respectively.

2.2 Aging tools

2.2.1 Paul Scherrer Institut Smog chambers

To gain a better understanding of atmospheric environmental reactions, the simulation of the atmospheric aging is indispensable. The smog chamber is one of the commonly used tools in current studies to investigate the oxidation reactions of anthropogenic and biogenic gaseous precursors. In this study, two of the Paul Scherrer Institute Atmospheric Chemistry Simulation Chambers were used, including a 27 m^3 (3×3×3 m) stationary chamber and a 7 m^3 (2.7×1.6×1.7 m, L×W×H) mobile chamber, both of them have the air-conditioned at 10 to 30 ^{o}C. The 27 m^3 chamber is called the Paul Scherrer Institute Stationary Smog Chamber (PSI-SSC), which is a flexible bag made of fluorinated ethylene propylene (FEP) suspended in a temperature-controlled enclosure. The walls and ceiling of the enclosure are covered with reflective aluminum foil to maximize the light intensity and increase light diffusion (Paulsen et al., 2005), as the aluminum foil has greater than 80 % reflection for spectra greater than 300 nm. The housing floor is covered with less reflective but more durable aluminum sheets. Four xenon arc lamps (4 kW rated power, 1.55 × 105 lumens each, XBO 4000 W/HS, OSRAM) placed at four corners of the housing are used to simulate the solar light spectrum and to mimic natural photochemistry (Fig. 2.5a). Particle samples are taken from the center of the chamber using stainless steel lines while gas samples are taken between the center and the edge of the chamber using Teflon lines. High concentrations of ozone (> 2 ppm) and humidified pure air are flushed into the chamber for at least 1 hour to clean the bag walls with lights on, followed by flushing with dry, pure air for at least 10 h (Bruns et al., 2015). The plan view and the photograph of the PSI-SSC are shown in Fig. 2.5a and Fig. 2.5b, respectively. The 7 m^3 chamber is called the Paul Scherrer Institute Mobile Smog Chamber (PSI-MSC). The schematic and the cleaning procedure are similar to the PSI-SSC. The PSI-MSC is located inside a temperature-controlled housing to maintain a constant temperature during aging and flanked by 4 sets of 10 UV-lights (90–100 W, Cleo Performance, Philips). In SC studies, OH exposure was formed from the photolysis of HONO, which was evaluated by the decay of d9-butanol. The gas- and particle-phase primary products that were injected in the chambers were first thoroughly studied. Photochemical gas-phase reactions were then initiated by turning on the lights in the smog chambers. These reactions can lead to condensable species, which can condense homogeneously or heterogeneously to form particles and then partition between the gas and particle phases.
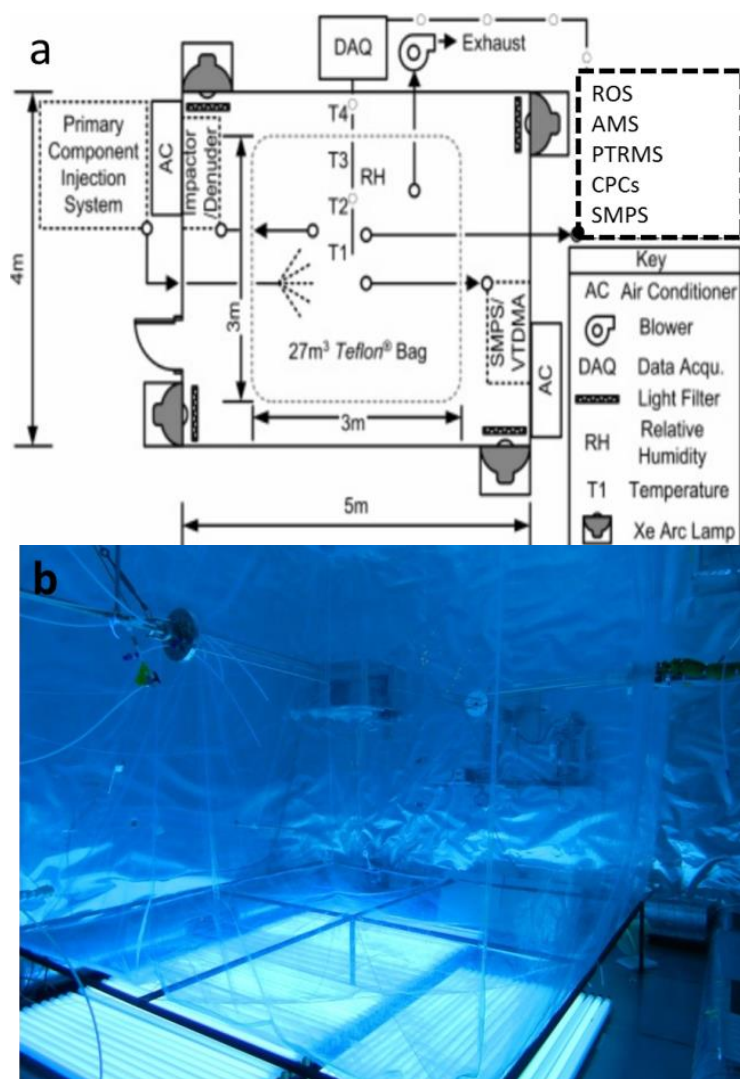
Figure 2.5 a) Plan view of the SC and enclosure, adapted from Paulsen et al., (2005). b) the 27 m³ PSI-SC during UV irradiation

2.2.2 Potential aerosol mass (PAM) chamber

Another commonly used atmospheric aging simulator is the potential aerosol mass (PAM) chamber. The original concept of the PAM is described in detail by Kang et al. (2007) and Bruns et al. (2015). Briefly, the PAM is a single, 0.015 m³ cylindrical glass chamber, flanked by two UVC lamps (185 and 254 nm emission lines, BHK Inc.). The plan view and a photograph of the PAM are shown in Fig. 2.6a and Fig. 2.6b. Prior to entering the PAM, humidified pure air (1.6 L min⁻¹, Nafion membrane, Perma Pure LLC) used as an OH precursor and a stream of diluted d9-butanol (98 %, Cambridge Isotope Laboratories) were merged with the incoming reactant flow. The OH exposure during aging was defined as the integral of the OH concentration over the reaction time, where the OH concentration was calculated from the decay of the d9-butanol, measured by a proton transfer reaction–mass spectrometer (PTR-MS 8000, Ionicon Analytik GmbH) (Barmet et al., 2012). Unlike in smog chambers, the OH exposure is not originated from HONO, but through the photolysis of O_3 with humidified air in the PAM ($O_2 + h\nu\ (185\ nm) \rightarrow O + O(^1D); O(^1D) + O_2 \rightarrow O_3; O_3 + h\nu \rightarrow O_2 + O(^1D); O(^1D) + H_2O \rightarrow 2OH$).
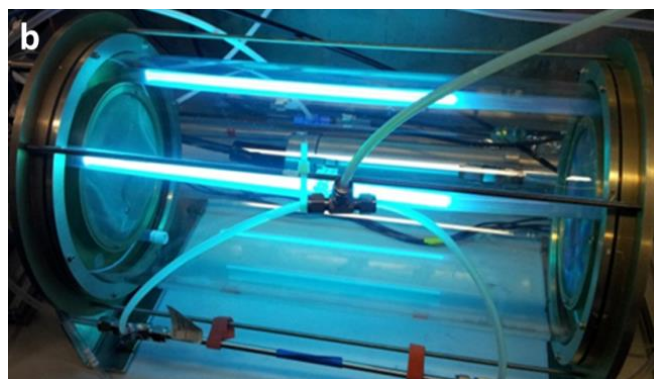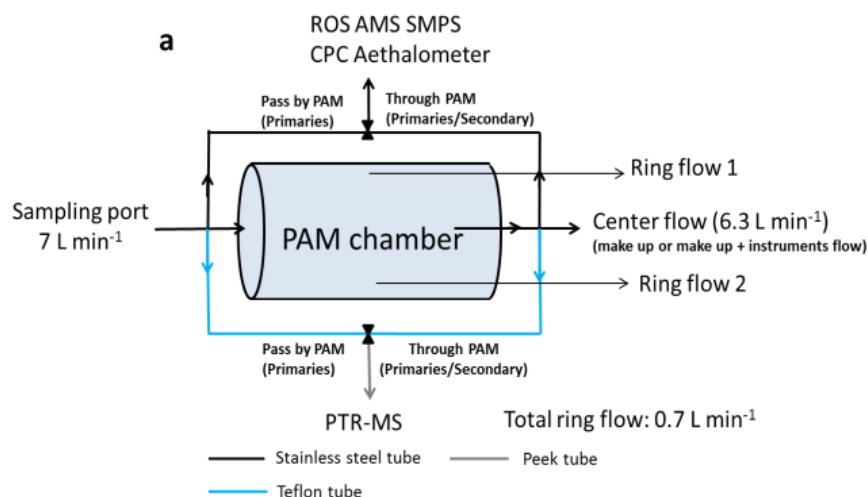
Figure 2.6 a) Plan view of the PAM b) the photograph of the PAM during UV irradiation (without the wrapped aluminum foil).

2.3 Instrumentation

A suite of online instrumentation were deployed to characterize the chemical and physical properties of gas and particle phase emissions in all the above mentioned campaigns, including a reactive oxygen species analyser (ROS), a high resolution time of flight aerosol mass spectrometer (HR-ToF-AMS), an aethalometer, a proton transfer reaction-mass spectrometer (PTR-MS), and other gas phase monitors, the scanning mobility particle sizer (SMPS), condensation particle counter (CPC), Aethalometer, etc. Further, in Bern, ambient air was sampled through the versatile aerosol concentration enrichment system (VACES) to enrich the concentration of ambient $PM_{2.5}$. A description of all the instruments follows. The instrumentations deployed in all the campaigns as well as the measured aspects and time resolutions are listed in Table 2.1. A description of all the instruments follows.

2.3.1 Reactive oxygen species analyzer (ROS analyzer)

An on-line ROS analyzer based on the 2',7'-dichlorofluorescin (DCFH) assay was used for the monitoring of the water-soluble particle bound components to act as ROS (PB-ROS) of PM. A detailed description of the ROS analyzer is given in Zhou et al. (2018a) and Chapter 3. Particles were collected

using an aerosol collector, of which the main part is the mist chamber. Before the aerosol collector, a honeycomb charcoal denuder was installed in a stainless steel tube to remove the gasphase. The collected aerosol was mixed with oxygen-free ultra-pure water (OF-OPW), which was continuously sprayed into the mist chamber and incorporated the aerosol particles into the water droplets. The sample extracts were then mixed with the working solution (the DCFH solution) for analysis. The measurement of the ROS is continuous and the ROS content in the particulate matter were calculated as H_2O_2 equivalents.

2.3.2 Aerosol mass spectrometer (AMS)

A field-deployable high-resolution time-of-flight aerosol mass spectrometer (HR-ToF-AMS) was used for the monitoring of non-refractory inorganic and organic species in Beijing. A detailed description of the instrument and its operation can be found elsewhere (DeCarlo et al., 2006). In short, ambient air was sampled through a critical orifice into an aerodynamic lens that determines the size cut-off of the instrument. In this work we also used a recently developed aerodynamic lens that efficiently transmitted particles between 80 nm and up to at least 3 µm (Williams et al., 2013) for the Beijing campaign and smog chamber studies. At the exit of the lens the particle beam was accelerated into the sizing region. A chopper wheel of AMS can either alternately block and unblock the beam (MS mode) or modulate it (PToF mode). While the MS mode yields the mass spectrum of the bulk aerosol, the PToF mode allows to determine the particle size by measuring flight time across a fixed distance. In both modes, particles are flash-vaporized by impaction on a resistively heated surface (~ 600 $^{\circ}$C) and ionized by electron ionization (70 eV). The mass-to-charge ratios (m/z) of the resulting fragments are finally determined by a ToF mass spectrometer (Fig. 2.7).

Table 2.1 Instrumentation, measured aspects, time resolutions in different campaigns.

Campaigns	Number of experiments	Instruments	Measured aspects	Time resolution
1) Wood combustion PSI-MSC (~7 m^3) aging	5	ROS analyzer	PB-ROS	8 min
		HR-ToF-AMS	Chemical composition of NR-PM$_{2.5}$	1 min (25 sec V-mode, 25 sec W-mode, 10 sec switch)
		Aethalometer	eBC (7 wavelengths)	1 sec
		NDIR analyzer	CO_2	1 sec
2) PSI-SSC (27 m^3) aging	3 (2 α-pinene Ozonolysis & 1 wood combustion emissions aging)	ROS analyzer	PB-ROS	8 min
		HR-ToF-AMS	Chemical composition of NR-PM$_{2.5}$	1 min (25 sec V-mode, 25 sec W-mode, 10 sec switch)
		Aethalometer	eBC (7 wavelengths)	1 sec
		NDIR analyzer	CO_2	1 sec
3) Wood combustion PAM aging	200 wood combustion emissions	ROS analyzer	PB-ROS	8 min
		HR-ToF-AMS	Chemical composition of NR-PM$_{2.5}$	1 min (25 sec V-mode, 25 sec W-mode, 10 sec switch)
		Aethalometer	eBC (7 wavelengths)	1 sec
		PTR-MS	NMVOCs	100 ms
		NDIR analyzer	CO_2	1 sec
		FID	THC	1 sec
4) Coal combustion PSI-MSC (9 m^3) aging	15 Coal combustion emissions	ROS analyzer	PB-ROS	8 min
		HR-ToF-AMS	Chemical composition of NR-PM$_{2.5}$	1 min (25 sec V-mode, 25 sec W-mode, 10 sec switch)
		Aethalometer	eBC (7 wavelengths)	1 sec
		Licor	CO_2	1 sec
		FID	THC	1 sec
5) In-situ Bern ambient measurements	November 2014	ROS analyzer	PB-ROS	8 min
		ACSM	Chemical composition of NR-PM$_1$	10 min
		Aethalometer	eBC (7 wavelengths)	1sec
6) In-situ Beijing ambient measurements	January-February 2015	ROS analyzer	PB-ROS	8 min
		HR-ToF-AMS	Chemical composition of NR-PM$_{2.5}$	1 min (25 sec V-mode, 25 sec W-mode, 10 sec switch)
		Aethalometer	eBC (7 wavelengths)	1 sec

PB-ROS: particle bounded ROS; FID: Flame ionization detector; NDIR: Non-dispersive infrared; THC: total hydrocarbon;
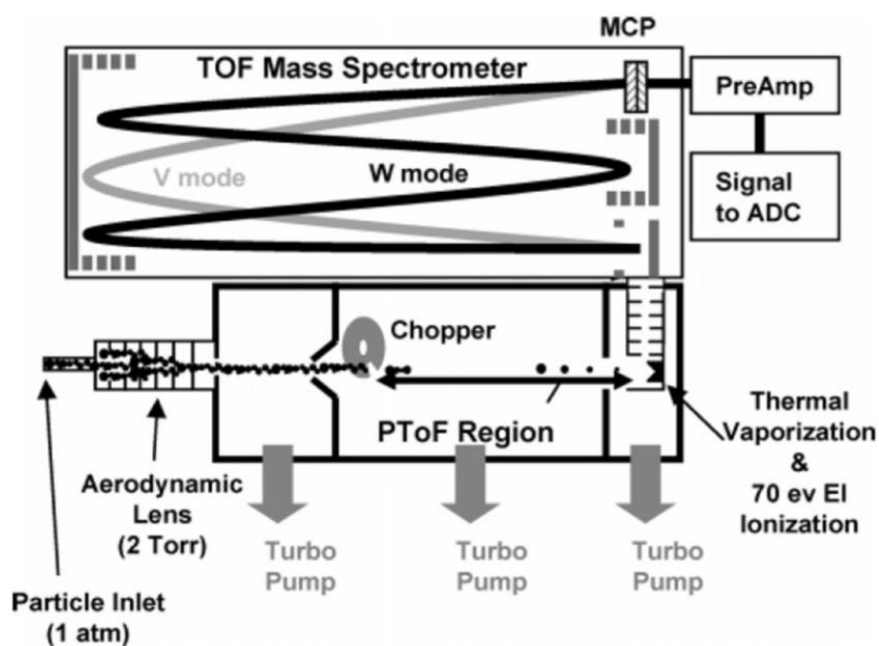
Figure 2.7 Schematic of the HR-ToF-AMS showing its two ion optical modes, adapted from DeCarlo et al. (2006).

2.3.3 Aerosol chemical speciation monitor (ACSM)

A quadrupole aerosol chemical speciation monitor (Q-ACSM, Aerodyne Research Inc.) was employed for monitoring of the composition and mass concentration of non-refractory submicron PM in Bern (Ng et al., 2011b). The Q-ACSM is built upon the same sampling and detection technology as the AMS described above, but with reduced complexity (e.g. no particle size measurement), resolution and performance (Fröhlich et al., 2013). But compared to AMS, the ACSM is simpler to operate and capable to long time period route analysis.

2.3.4 Aethalometer

A real-time measurement of the optical absorption (b_{abs}) was performed by a "next generation" Aethalometer (AE33, Magee Scientific, Berkeley, CA, USA) at 7 different wavelengths, which performs an online correction for possible scattering artefacts (Drinovec et al., 2015). The b_{abs} is then converted to the equivalent black carbon (eBC) using the mass absorption cross section (MAC). Mostly nominal MAC values from literature (Bond and Bergstrom, 2006; Gundel et al., 1984) or the instrument manufacturer (Hansen et al., 1984, Drinovec, et al., 2014) are used, but in some studies MAC is also empirically derived (Zotter et al., 2017, Zanatta et al., 2016). The data output is expressed in units of eBC mass per volume sampled air, for example, ng m^{-3}.

2.3.5 *Scanning mobility particle sizer (SMPS) and condensation particle counter (CPC)*

The scanning mobility particle sizer (SMPS) is deployed to make routinely accurate size measurements of particles. The SMPS consists of a custom built differential mobility analyzer (DMA) with a length of 0.44 cm and measures the size distribution from 2 nm to 1 μm. The separation of the particles occurs in an electric field and is fundamentally related to particle size. A condensation particle counter (CPC, 3022, TSI) subsequently counts the mobility selected particles via light scattering after condensation growth. Usually the total particle number concentration was additionally counted by another CPC.

2.3.6 *Gas phase instrumentation*

In the wood combustion PAM chamber experiments, total volatile organic compounds and CH_4 were measured with a flame ionization detector (FID) with a non-methane cutter (model 109A, J.U.M Engineering), CO and NO with a non-dispersive infrared analyzer (Ultramat 23 Siemens), O_2 with a paramagnetic oxygen analyzer (Ultramat 23 Siemens) and CO_2 with a non-dispersive infrared (NDIR) analyzer (model LI-820, LI-COR®). In the smog chamber (SC) aging experiments CO, CO_2, and CH_4 were measured with a cavity ring-down spectrometer (G2401, Picarro, Inc.). In all experiments, the composition of VOCs was determined by a proton transfer reaction–mass spectrometer (PTR-MS 8000, Ionicon Analytik GmbH).

2.4 The versatile aerosol concentration enrichment system (VACES)

We enriched the Bern ambient aerosol to increase the reactive oxygen species (ROS) concentration above the instrument detection limit. A schematic of the VACES and more details can be found in Künzi et al. (2015), as shown in Fig. 2.8. Aerosols were drawn into the VACES at a flow rate of ~100 L min^{-1} into a tank with water heated up to ~ 30 °C. The water vapour saturated air stream was then cooled down in a condenser (-2 °C) and water droplets (diameter $d > 2$ μm) form on the aerosol particles. The droplets were then drawn through a virtual impactor and enriched in concentration. The concentration enriched droplets were then dried by passing a diffusion dryer to remove the water and return the aerosols to their original size (Wang et al., 2012). The concentration enrichment factor CE was calculated by Eq. 2.1:

$$E = Q_{tot}/q_{min}(1 - WL) \times \eta_{vi}$$
(2.1)

where Q_{tot} and q_{min} are the intake and minor output flows of the impactor, respectively, η_{vi} and WL are the collection efficiency and fractional loss of the impactor , respectively (Sioutas et al., 1999).
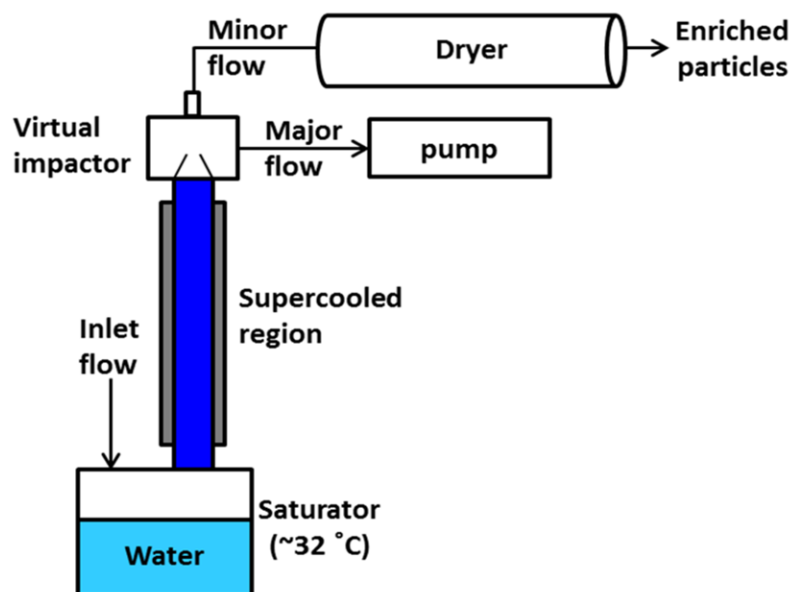
Figure 2.8 Schematic of the versatile aerosol concentration enrichment system (VACES) (Künzi et al., 2015)

2.5 Source apportionment techniques

Efforts have been made to relate measured concentrations of airborne constituents to their origins for more than 50 years (Hopke et al., 2016). Scientists are teasing out which emissions contribute most to the OA as well as the black carbon in ambient aerosols. Receptor models including the positive matrix factorization (PMF) and the multilinear engine (ME-2; Paatero, 1997) and controlled via the interface SoFi coded in Igor Wavemetrics (Source Finder; Canonaco et al., 2013) are used for the source apportionment (SA) of ambient atmospheric aerosols. Further, the Aethalometer model was employed to investigate the sources of black carbon (BC).

2.5.1 Positive matrix factorization

PMF was developed by Paatero and Tapper (Paatero and Tapper, 1993, 1994) as a receptor model to apportion the sources on the basis of observations (internal correlations) at the receptor site alone (Viana et al., 2008), as represented by Eq. 2.2.

$$x_{ij} = \sum_{k=1}^{p}(g_{ki} \times f_{ki}) + e_{ij} \tag{2.2}$$

Here x_{ij}, g_{ik}, f_{ki} and e_{ij} are matrix elements of the measurements, factor profiles, factor time series, and residual matrices, respectively, where $f_{ik} \geq 0$, $g_{ik} \geq 0$. The subject i, j, k conrrespond to time, m/z and a discrete factor, respectively. p denote the number of factor in the PMF solution determined by the user. The factor profiles remains static, their contributions to the matrix elements of the measurements are allowed to vary with time (concentration time series). In PMF, an "objective function" Q as defined in Eq. 2.3, is iteratively minimized:

$$Q(E) = \sum_{i=1}^{m} \sum_{j=1}^{n} \left[\frac{e_{ij}}{s_{ij}}\right]^2 \tag{2.3}$$

In this equation, e_{ij} is the residual in the ith variable measured in the jth sample. s_{ij} represents the corresponding "uncertainty" of e_{ij}. The main theoretical limitations of PMF are: 1) Source interpretation is relatively subjective. 2) Inability to clearly separate covariant sources (Viana et al., 2008) with similar chemical composition, e.g. cooking and traffic, advanced factor analysis models are needed.

2.5.2   Multilinear engine (ME-2)

ME-2 provides a more flexible framework for controlling the solutions of the factor analysis in that it permits the imposition of explicit external constraints (Ramadan et al., 2003). Within the a-value approach *a priori* information (factor profiles or factor time series) of one or more sources can be used as an additional input in the model, using the scalar *a* to regulate the strength of the constraints:

$$f_{j,solution} = f_j \pm a \times f_j \tag{2.4}$$

$$g_{i,solution} = g_i \pm a \times g_i \tag{2.5}$$

Here $0 \leq a \leq 1$, and f_j, g_i are the input profile and the time series, which can either entirely or partially be constrained by *a*.

2.5.3   Aethalometer model

The Aethalometer-based source apportionment model developed by Sandradewi et al. (2008) was used to separate the contributions of traffic (TR) and wood burning (WB) to the measured eBC in Bern. The equation used for the model is:

$$b_{abs,total}(\lambda) = b_{abs,tr}(\lambda) + b_{abs,wb}(\lambda \tag{2.6}$$

Using the power law of the spectral dependence of the absorption, the measured b_{abs} at two different wavelengths, and Eq. 6.6, TR and WB can be apportioned in the following way (Zotter et al., 2017):

$$\frac{b_{abs,TR(\lambda_1)}}{b_{abs,TR(\lambda_2)}} = \left(\frac{\lambda_1}{\lambda_2}\right)^{-\alpha TR} \tag{2.7}$$

$$\frac{b_{abs,WB(\lambda_1)}}{b_{abs,WB(\lambda_2)}} = \left(\frac{\lambda_1}{\lambda_2}\right)^{-\alpha WB} \tag{2.8}$$

$$b_{abs,WB(\lambda_2)} = \frac{b_{abs}\lambda_1 - b_{abs}\lambda_2 \times \left(\frac{\lambda_1}{\lambda_2}\right)^{-\alpha TR}}{\left(\frac{\lambda_1}{\lambda_2}\right)^{-\alpha WB} - \frac{\lambda_1}{\lambda_2}^{-\alpha TR}} \tag{2.9}$$

$$b_{abs,TR(\lambda_2)} = \frac{b_{abs}\lambda_1 - b_{abs}\lambda_2 \times \left(\frac{\lambda_1}{\lambda_2}\right)^{-\alpha WB}}{\left(\frac{\lambda_1}{\lambda_2}\right)^{-\alpha TR} - \frac{\lambda_1}{\lambda_2}^{-\alpha WB}} \tag{2.10}$$

In the Eq. 2.7-10, α is the absorption Ångström exponent for traffic and wood combustion emissions (α_{TR} and α_{WB}, respectively) which have to be assumed a priori. For the strong broadband absorber BC, α ~ 1, which is close to the α_{TR}, but smaller than the α_{WB}. The b_{abs} attributed to each source were then converted to eBC using a MAC (as described above). This model has been validated using ^{14}C analyses for Switzerland and other Alpine regions in Europe, especially in winter, where the contributions of other combustion emissions are negligible (Zotter et al., 2017). In other regions of the world, for example, Beijing and Poland, the contribution of coal combustion emissions are clear and quantifiable

(Liu et al., 2016; Elser et al., 2016; Pyka and Wierzchowski, 2016), thus making it impossible for such locations to perform BC source apportionment using this model, due to the still large uncertainty of optical properties of eBC emitted from coal combustion.

2.6 Multiple linear regression model

The multiple linear regression model (MLRM) in this study aimed to identify the dependence of variable ROS on the different organic aerosol (OA) sources. The model follows Eq. 2.11 (modified from http://www.stat.yale.edu/Courses/1997-98/101/linmult.htm; last access: 10 November 2017):

$$y = \beta_0 + \beta_1 x_1 + \ldots + \beta_p x_p + \xi \tag{2.11}$$

Generally and technically, the MLRM specifies the relation between response y and given p predictors $xi,\ i=1\text{-}p$. The expression part "$\beta_0 + \beta_1 x_1 + \ldots + \beta_p x_p$" is the fit term, β_0 is the intercept and the remaining parameters $\beta_1, \ldots, \beta_p$ are the regression coefficients of different parameters. ξ is the residual term and represents the deviation of the observed y from their means μ_y, which are normally distributed with mean 0 and variance σ.

3

Development, characterization and first deployment of an improved online reactive oxygen species analyzer

J. Zhou[1], E. A. Bruns[1], P. Zotter[2], G. Stefenelli[1], A. S. H. Prévôt[1], U. Baltensperger[1], I. El-Haddad[1], and J. Dommen[1]

[1] Paul Scherrer Institute, Laboratory of Atmospheric Chemistry, 5232 Villigen PSI, Switzerland

[2] Lucerne University of Applied Sciences and Arts, School of Engineering and Architecture, CC Thermal Energy Systems & Technology, Bioenergy Research, 6048 Horw, Switzerland

Abstract. Inhalation of atmospheric particles is linked to human diseases. Reactive oxygen species (ROS) present in these atmospheric aerosols may play an important role. However, the ROS content in aerosols and their formation pathways are still largely unknown. Here, we have developed an online and offline ROS analyzer using a 2',7'-dichlorofluorescin (DCFH) based assay. The ROS analyzer was calibrated with H_2O_2 and its sensitivity was characterized using a suite of model organic compounds. The instrument detection limit determined as 3 times the noise is 1.3 nmol L^{-1} for offline analysis and 2 nmol m^{-3} of sampled air when the instrument is operated online at a fluorescence response time of approximately 8 min, while the offline method detection limit is 18 nmol L^{-1}. Potential interferences from gas-phase O_3 and NO_2 as well as matrix effects of particulate SO_4^{2-} and NO_3^{-} were tested, but not observed. Fe^{3+} had no influence on the ROS signal while soluble Fe^{2+} reduced it if present at high concentrations in the extracts. Both online and offline methods were applied to identify the ROS content of different aerosol types, i.e., ambient aerosols as well as fresh and aged aerosols from wood combustion emissions. The stability of the ROS was assessed by comparing the ROS concentration measured by the same instrumentation online in situ with offline measurements. We also analyzed the evolution of ROS in specific samples by conducting the analysis after storage times of up to 4 months. The ROS were observed to decay with increasing storage duration. From their decay behavior, ROS in secondary organic aerosol (SOA) can be separated into short- and long-lived fractions. The half-life of the short-lived fraction was 1.7 ± 0.4 h, while the half-life of the long-lived fraction could not be determined with our uncertainties. All these measurements showed consistently that on average 60 ± 20 % of the ROS were very reactive and disappeared during the filter storage time. This demonstrates the importance of a fast online measurement of ROS.

3.1 Introduction

Aerosol particles have negative effects on human health (Pope and Dockery, 2006), with an estimated 3 % of cardiopulmonary and 5 % of lung cancer deaths attributable to particulate matter (PM) globally (WHO, 2013). One of the important pathways leading to deleterious impacts on health is believed to be induced oxidative stress by the generation of reactive oxygen species (ROS), through the interaction of particulate matter with the human lung (Donaldson et al., 2002). Reactive oxygen species denote chemically reactive molecules containing oxygen (e.g., radicals, oxygen ions and peroxides including the OH radicals, O_2^{-} radical, H_2O_2 or organic peroxides) (S. J. Fuller et al., 2014; Sagai et al., 1993). As one of the main free radical sources generated in our body by various endogenous systems, ROS can adversely alter lipids, proteins and DNA structures, potentially leading to aging and numerous human diseases (Devasagayam et al., 2004). ROS exist both in the gas phase and in PM. ROS are either produced inside the human body through generation by the inhaled PM (i.e., by transition metals) in vivo (endogenous ROS) or by transportation into the lungs on respirable particles (exogenous ROS) (Zhao and Hopke, 2012). While gas-phase ROS are most likely removed in the upper mucus membranes through diffusion (Kao and Wang, 2002), ROS associated with fine particles can penetrate deeply into the lungs, causing oxidative stress and cell damage. Understanding the mechanisms by which ROS are

formed, evolve and decay in the atmosphere is therefore of utmost importance for mitigating their influence on human health (Khurshid et al., 2014).

Currently, many acellular assays exist for the determination of ROS quantities in particles, including dithiothreitol (DTT) (Fang et al., 2015) and 2',7'-dichlorofluorescin (DCFH) (S. J. Fuller et al., 2014; King and Weber, 2013; Wang et al., 2011a). The DCFH assay is one of the most commonly used assays today. Accurate ROS quantification remains challenging because some ROS are highly reactive and are likely at least partially degraded prior to measurement when using offline techniques, which typically have delays of hours, days or weeks. Therefore, online techniques (through direct sampling into the liquid phase and measurement within a few minutes) are necessary for reliable ROS quantification (Wragg et al., 2016).

In this work, we developed and characterized a highly sensitive ROS analyzer which can be used either online or offline. The removing efficiency of interfering oxidizing trace gases of O_3 and NO_2 was tested, and the matrix effects of particulate SO_4^{2-} and NO_3^- as well as transition metals were assessed. Results from the application of this online and offline methodology to laboratory measurements of wood combustion emissions and ambient measurements at an urban site in Bern (Switzerland) are presented. To assess the stability of ROS, online in situ measurements were compared with offline measurements using the same instrumentation, and the evolution of ROS on specific samples was evaluated by conducting the analysis after storage times of up to 4 months. The results are put into perspective for future ROS measurement strategies.

3.2 Methods

3.2.1 ROS analyzer

In our experiments, ROS were measured using a DCFH assay, which is commonly used for examining ROS generation at a cellular level but has also been used for determining the oxidation potential of PM as an acellular assay (S. J. Fuller et al., 2014; King and Weber, 2013; Perrone et al., 2016; Sauvain et al., 2013; Venkatachari et al., 2007; Venkatachari et al., 2005). In this assay, the presence of oxidizing species is assessed from the rapid oxidation of DCFH to the fluorescent compound dichlorofluorescein (DCF) in the presence of horseradish peroxidase (HRP). The chemical reaction mechanism is shown in Fig. A.1.
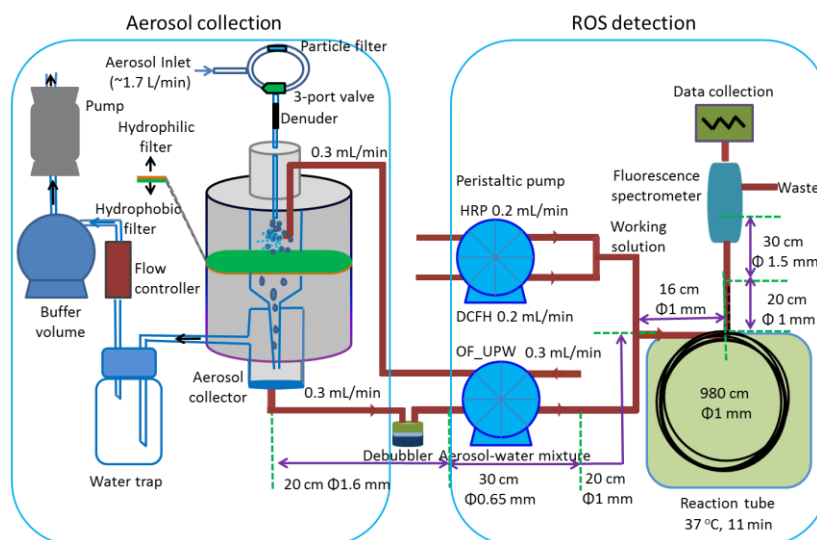
Figure 3.1 An overview of the online ROS analyzer. OF-UPW refers to oxygen-free ultra-pure water. The same setup without the aerosol collector was used for the offline analysis (shown in Fig. A. 2).

A schematic of the online aerosol ROS analyzer is shown in Fig. 3.1. The analyzer is composed of three components: the aerosol collector, the reaction chamber and the fluorescence analyzer. The same setup without the aerosol collector was used for offline analysis (Fig. A. 2).

3.2.2 Aerosol collection

Particles were collected at a flow rate of ~1.7 L min^{-1}, using an aerosol collector, of which the main part is the mist chamber (Takeuchi et al., 2005). Before the aerosol collector, a honeycomb charcoal denuder of 10 cm length with 7 mm outer diameter (36 % open area; 450 µm channel width) was installed inside a stainless steel tube to remove O_3, NO_2 and organic vapors. The denuder was regenerated for at least 24 h at 250 $^{\circ}$C under a stream of 99.999 % N_2 before each experiment. By using at least two denuders, we were able to switch between them and to perform the experiments continuously. The Plexiglas aerosol collector had an approximate volume of 13.5 cm^3. It consisted of an air inlet, a nebulizing nozzle inlet port for pure water injection, a mist chamber, a 2.5 cm diameter hydrophilic cellulose filter (Grade 497 circles, Schleicher & Schuell Rundfilter) supported by a 5.0 µm pore size hydrophobic membrane filter (Isopore membrane filters, TMTP series, Merck Millipore) to prevent the loss of the sample solution, an outlet to the vacuum pump and an exit for the water extracts (Fig. 3.1). The collection efficiency for water-soluble particles was determined by Takeuchi et al. (2005) to be 80 % for 100 nm particles and higher than 97.7 % for particles > 280 nm. Between the vacuum pump and the mist chamber, a flow controller protected by a water trap was installed. To stabilize the air sampling flow, an additional gas buffer volume was introduced before the pump. The 1.7 L min^{-1} air stream was mixed with oxygen-free ultra-pure water (OF-UPW), which was continuously sprayed into the mist chamber with a flow rate of 0.3 mL min^{-1}, where the aerosol particles were incorporated into the water droplets. The liquid containing the water-soluble fraction of the aerosol was continuously collected at the bottom of the aerosol collector at a flow rate of 0.3 mL min^{-1} and then mixed with the working solution at a flow rate of 0.4 mL min^{-1} for analysis. This resulted in a total flow rate of 0.7 mL min^{-1}. Therefore, the

measurement of ROS is continuous, which provides real-time measurement of ROS. OF-UPW was prepared by bubbling 99.999 % N_2 for ~ 20 min through Milli-Q water (18.2 MΩ cm at 25 °C, total organic carbon < 3 ppb) to reduce the dissolved oxygen. The use of oxygen-free water reduced the instrument background by a factor of ~2 compared to normal ultra-pure water.

In most studies using the DCFH assay, aerosol samples were extracted either in a DCFH–HRP (King and Weber, 2013b) or an HRP solution (S. J. Fuller et al., 2014). We tested the auto-oxidation of the working solution containing both HRP and DCFH. By mixing only OF-UPW with the HRP–DCFH working solution the signal, which is actually the background, increased with a rate of 0.9% h^{-1}. This means that there is a slow reaction with the dissolved oxygen consuming the DCFH consequently shortening the lifespan of the HRP–DCFH solution. When the sample is extracted online with the HRP solution as in S. J. Fuller et al. (2014), the HRP needs to go through the aerosol collector, where contaminants adsorbed on the hydrophilic and hydrophobic filters or the oxygen in the mist chamber might react with HRP and then oxidize DCFH as described by Berglund et al. (2002) and modified by S. J. Fuller et al. (2014). Therefore, we used only OF-UPW to extract the aerosol samples. The DCFH and HRP reagents were kept separate and were only mixed together right before the aerosol aqueous extract was added.

3.2.2.1 ROS detection

The aerosol aqueous extract collected from the aerosol collector was sampled by a peristaltic pump through a "TRACE TRAP bubble trap" debubbler (TRACE Analytics GmbH, Germany), which effectively removed gas bubbles in the sample liquid without introducing a large dead liquid volume and signal broadening. At the same time, the two reagent solutions DCFH and HRP were drawn by another peristaltic pump and mixed to form the WS. The aerosol aqueous extract was then mixed with the WS and pumped through a reaction coil consisting of polyetheretherketone (PEEK) tubing (9.8 m length 1.6 mm OD, 1.0 mm ID, Kinesis GmbH) in an air-ventilated temperature controlled housing held at 37 °C. The obtained solution was then analyzed using a spectrofluorometer with excitation and emission wavelengths of 470 nm and 520 nm, respectively. All transparent parts of the system were wrapped with aluminum foil to avoid the photooxidation of the DCFH.

3.2.2.2 Offline analysis

The instrument was also used for offline analysis of filters (Fig. A.2). In general, we extracted a filter punch of 14 mm Ø of the filter area in 10 mL of OF-UPW for 15 min at 30 °C. However, the filter area and/or the volume of the OF-UPW was sometimes adjusted to keep the extracted ROS concentration in the measurement range of the instrument. The vial was then vortexed (Vortex Genie 2, Bender& Holbein AG, Switzerland) for 1 min to ensure homogeneity and filtered through a 0.45 μm nylon membrane syringe filter (Infochroma, Switzerland). The extract was then injected into the ROS analyzer in the same way as the online method with a flow rate of 0.3 mL min^{-1} and mixed with the working solution at a rate of 0.4 mL min^{-1} for analysis. Thus, the mixture of the flows was the same for online and offline analysis.

Often filters are extracted in an ultrasonic bath. However, recent studies suggest that sonication of pure water with dissolved air may create hydroxyl radicals due to the high temperature and pressure created by the collapse of bubbles formed by cavitation, which then form H_2O_2 or react with sample species (Mark et al., 1998; Miljevic et al., 2014). This was also demonstrated by S. J. Fuller et al. (2014), who showed the formation of 0.08 nmol m^{-3} ROS by the sonication of pure water. These effects have also been confirmed in our laboratory by analyzing filters collected at an urban site in Milan extracted with and without sonication (Perrone et al., 2016). Therefore, sonication was not used for filter extraction during offline measurements.

3.2.2.3   Working solution

The stability of the WS is an important factor. Since HRP can catalyze the reaction of DCFH with dissolved oxygen in the phosphate buffer (Berglund et al., 2002; Huang et al., 2016; Rota et al., 1999a; Rota et al., 1999b), the phosphate buffer solution (PBS, 1 M, Sigma-Aldrich, USA) was degassed with 99.999 % N_2 for ~20 min. Furthermore, the two reagents DCFH and HRP were prepared separately as follows:

For the DCFH reagent, 2′,7′-dichlorofluorescin diacetate (DCFH-DA) (0.61 mL, Sigma-Aldrich, USA) stock solution (0.001 M) was mixed with NaOH (10 mL, 0.001M, Sigma-Aldrich, USA) for 30 min under dark conditions to initiate a deacetylation at room temperature. Then PBS (25 mL) was added to set the solution pH at 7.2 and neutralize any remaining NaOH. This produces the fluorescent probe DCFH, referred to as WS-A hereafter.

For the HRP reagent, horseradish peroxidase (0.44 mg, HRP, type II, Sigma-Aldrich, USA) was dissolved in PBS (35.6 mL) to generate a stock solution of 2 units mL^{-1}, which is referred to as WS-B afterwards.

WS-A and WS-B were then degassed for 20 min and only mixed together during the analysis at a 1:1 ratio. The final WS was 17.6 μM of DCFH and 1 unit mL^{-1} of HRP. This WS and the applied procedures provided the following advantages compared to previous analyzers using the same assay:

(1) The pH of the WS was maintained constant at 7.2, which resulted in a stable background.

(2) HRP and DCFH were prepared separately and mixed together only right before the combination with the sample solution. This reduced auto-oxidation and decreased the instrument background signal.

(3) Both working solutions were stored at ~ 4 $^\circ$C and could be used for up to 1 week, while a mixed DCFH–HRP is not stable for more than 1 day.

3.2.2.4   Calibration

The instrument was calibrated with known concentrations of H_2O_2 solutions. Standards were prepared from a concentrated solution of hydrogen peroxide (H_2O_2; Sigma-Aldrich, solution, 3 wt. % in water, Sigma-Aldrich). Calibration solutions of different concentrations were generated by diluting different amounts of a stock solution with OF-UPW. The blank values were obtained by measuring OF-UPW alone.

For the online operation mode, H_2O_2 equivalent particulate ROS concentrations were determined as follows:

$$c(\frac{nmol}{m^3}) = (\frac{I-b}{a})(\frac{V_i}{Q_c}) \tag{3.1}$$

Where I is the fluorescence signal (volt), b is the calibration intercept from the linear regression fit, a is the calibration slope from the linear regression fit (Volt nM^{-1}), V_i is the OF-UPW flow into the mist chamber (mL min^{-1}) and Q_c is the air volume drawn through the aerosol collector (L min^{-1}, at ambient temperature and pressure). For the offline operation mode, particulate ROS concentrations c in air were determined as follows:

$$c(\frac{nmol}{m^3}) = (\frac{I-b}{a})(\frac{V_i}{Q_c})(\frac{A_{filter}}{A_{punch}}) \tag{3.2}$$

where V_i: volume of OF-UPW for filter extraction (mL), Q_c is the total air flow through the filter (L, at ambient temperature and pressure) and $\frac{A_{filter}}{A_{punch}}$ is the ratio of the area of the entire filter to the area of the filter punch.

The instrument background of the online operation mode was always higher than that of the offline operation mode, which may be due to the uptake of oxygen in the mist chamber in the online system.

3.2.3 Instrument maintenance and portability

The instrument can be easily disassembled and rebuilt to be used in both laboratory and field campaigns. The instrument is not yet fully automatized. The following manual operations are required: 1) calibration; 2) replacing the hydrophilic and hydrophobic filters in the aerosol collector and the denuder every 2-3 days during ambient measurements – while in laboratory experiments, we exchanged the denuder for each laboratory experiment (~ 5 h) to be on the safe side; 3) regularly switching the air inlet channel to the particle-free mode (ROS blank) and checking the air flow during the measurement (before the experiment, during the experiment and after the experiment) to insure that the air sample flow was constant at 1.7 L min^{-1}; 4) cleaning of the ROS analyzer with 1 M H_2SO_4 for ~ 12 hours every 2 weeks to remove contaminations in the system; 5) replacing all the tubes used in the system every 6 months.

3.2.4 Instrument testing

In order to assess the performance of the ROS analyzer several tests were performed, including the following:

1) The influence of the reaction time and the instrument detection limit, repeatability and reproducibility (Sect. 3.3.1.1 and 3.3.1.2).

2) Response of the DCFH assay to selected components with expected capability to act as reactive oxygen species (Sect. 3.3.1.2 and 3.3.3).

3) Assessment of the interference from selected abundant gas-phase and PM constituents (Sect. 3.3.2 and 3.3.3) on the ROS signals.

4) Verification of the instrument performance using genuine aerosol samples. Measurement of the ROS content in ambient aerosols was performed offline using filter samples collected in Milan (Italy), San Vittore (Switzerland) and Bern (Switzerland) and online using the developed ROS analyzer in Bern (Switzerland) (Sect. 3.3.1.3, 3.3.4.1 and 3.3.4.2). These samples include total suspended particulate matter (TSP), $PM_{2.5}$ and PM_{10} (particulate matter with a diameter smaller than 2.5 µm and 10 µm, respectively). Laboratory samples were also measured, including online and offline ROS measurements of fresh and aged aerosols from wood combustion emissions, by using two different aging tools, a potential aerosol mass (PAM) chamber and a smog chamber (SC). Tests aimed at the verification of the instrument linearity, the assessment of matrix effects, the comparison of online and offline ROS measurements and the examination of the ROS degradation.

3.3 Results

3.3.1 Instrument performance

3.3.1.1 Reaction time and detection limit

The reaction time between the WS and the aerosol sample is an important parameter. Here, reaction times of 11 and 22 min were investigated by using different reaction tube lengths in the reaction chamber and followed by measurement of the fluorescence intensity resulting from the reaction of H_2O_2 (Fig. 3.2a) and 2-hydroperoxy-2-(2-hydroperoxybutan-2-ylperoxy)butane (Fig. 3.2b) with the WS. The 22 min reaction time resulted in a 35% higher instrumental background signal than the 11 min reaction time. However, the same incremental increase in fluorescence intensity was found for the sample solutions of both H_2O_2 and the organic peroxide at the two reaction times, resulting in the same detection sensitivity. Here the detection sensitivity (V nM^{-1}) is defined as the ratio between the change in the output signal (in volt) to the corresponding change in the peroxide concentration (in nM). This suggest that the fluorescence response is unaffected by the reaction time in the investigated range, even for compounds protected by *tert-butyl* groups. Therefore, a reaction of 11 min seems to be sufficient to reduce all peroxides that can react with DCFH and we consequently used this reaction time for the further experiments. The residence and response time of the sample in the instrument were measured to be approximately 19 min and 8 min, respectively. The former was determined as the time from the injection of an H_2O_2 solution to the time the fluorescence signal started to increase, while the response time corresponds to the rise time of the fluorescence signal from 10 % to 90 % of the full signal.
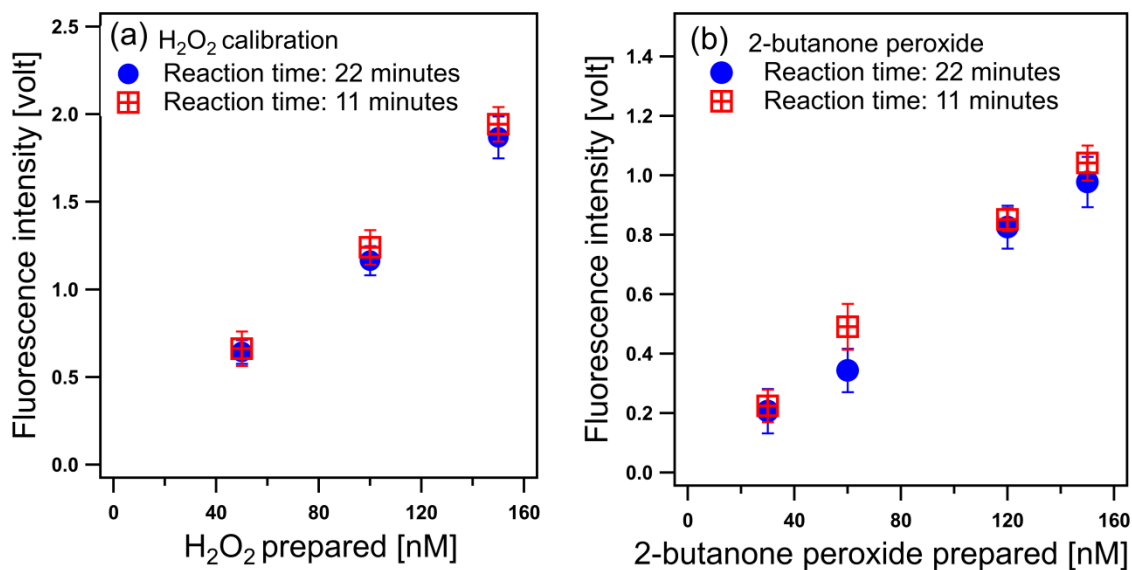
Figure 3.2 Fluorescence responses to (a) H_2O_2 and (b) 2-butanone (2-hydroperoxy-2-(2-hydroperoxybutan-2-ylperoxy)butane) peroxide under different reaction times. Error bars represent the propagation of the uncertainty ($\delta = \sqrt{\delta_1^2 + \delta_2^2}$, with δ_1 representing the standard deviation of the instrument background signal of that experiment day, and δ_2 the standard deviation of the sample signal.)

Under normal instrument operation conditions, an instrument limit of detection (LOD) of 2 nmol m^{-3} of sampled ambient air was determined for the online methodology. This was obtained as 3 times the standard deviation when a particle filter was placed in the sampling line upstream of the analyzer (Long and Winefordner, 1983). For the offline methodology, which is used for the instrument testing, it is important to define two different parameters: the instrument LOD and the method LOD. The instrument LOD was 1.3 nmol L^{-1}, determined as 3 times the standard deviation of the background when OF-UPW was injected into the sampling line. The method LOD was determined based on the reproducibility of the instrument background and the filter blanks. The reproducibility of the background was assessed by injecting different batches of OF-UPW several times. The value of 9 nmol L^{-1}, equivalent to 3 times the standard deviation of the resulting signals, was then used as a measure of this reproducibility and the offline method LOD. A similar LOD value was obtained as 3 times the standard deviation of the measurements of extracts of fractions of four different blank filters (2.2 cm^2) and was equal to 13 nmol L^{-1}(for both quartz and Teflon filters). We note that the average signal of these blanks was 25 nmol L^{-1}, which was subtracted from the signals measured when extracts of aerosol samples (with equivalent filter area) were injected.

3.3.1.2 Repeatability, reproducibility and response to selected model compounds
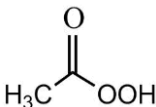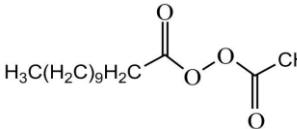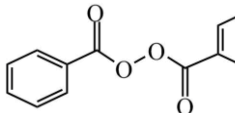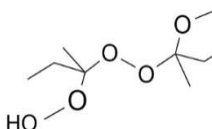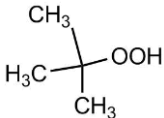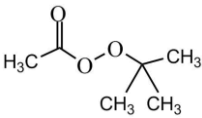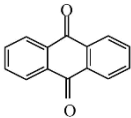
We assessed the instrument performance based on three repeated calibrations with 0, 30, 50, 100 and 150 nM H_2O_2 (Fig. A. 3). The instrument accuracy in determining the ROS concentration was found to be 3 % (n=15), based on the standard deviation of the slope of the linear fit. The precision (repeatability) of the preparation of the H_2O_2 solution used for the calibration, estimated at different H_2O_2 concentrations based on the fit prediction interval, was 25 %, 10 % and 5 %, at 30 nM, 70 nM and 150

nM, respectively. Based on this, the uncertainty of H_2O_2 at extremely low concentrations would be 18 nM. This is larger than the method LOD determined above from the OF-UPW and blank filters. We consider the largest of these uncertainties (i.e.,18 nM) as our final method LOD.

The instrument reproducibility was assessed based on the variation in the instrument sensitivity (in V nM^{-1}). In practice, we calculated the standard deviation of the response of 10 repeated measurements of known concentrations of H_2O_2 at different days using different WS. This reproducibility was found to be ~40 % (1 σ), which is much higher than the instrument precision, possibly due to the solution preparation and instrument operation conditions. Consequently, a calibration was always carried out at the beginning or at the end of each measurement series.

While the characterization tests discussed above were carried out using the offline mode, we obtained similar results when the instrument was used in the online mode. Fig. 3.3 shows that a similar linear relationship was obtained between the instrument response and the H_2O_2 concentration for the online (blue stars) and offline (red triangles) modes, resulting in statistically similar sensitivities (*t* test, *p* value = 0.93). This provides confidence in using the calibration and tests performed offline to predict online concentrations.

Table 3.1 Model organic peroxides used in this study.

Peracetic acid (PAA)	Lauroyl peroxide (LP)	Benzoyl peroxide (BenP)	2-Butanone peroxide (2-BP)
tert-Butyl hydroperoxide (tBuOOH)	tert-Butyl peracetate (tBuPA)	Anthraquinone (AQ)	

We also tested the response of the instrument to components expected to exhibit the capability to act as reactive oxygen species, including peracetic acid (PAA; Sigma-Aldrich, ~39 % in acetic acid, $\leq$ 6 % H_2O_2, Sigma-Aldrich), tert-butyl hydroperoxide (tBuOOH; Luperox® TBH70X, 70 wt. % in water, Sigma-Aldrich), benzoyl peroxide (BenP; Aldrich, Luperox® A75, 75 %, remainder water, Sigma-Aldrich), lauroyl peroxide (LP; Luperox® LP, 97 %, Sigma-Aldrich), tert-butyl peracetate (tBuPA; Luperox® 7M50, 50 wt. % in aliphatic hydrocarbons, Sigma-Aldrich), anthraquinone (AQ; 97 %, Sigma-Aldrich,) and 2-butanone peroxide (2-BP, Luperox® DHD-9, 32 wt. %, Sigma-Aldrich). Table 3.1 provides an overview of the chemical structures of these compounds. The water-soluble peroxides, i.e., PAA, tBuOOH and tBuPA, were dissolved in OF-UPW. The water insoluble compounds, i.e.,

BenP, LP and AQ, were dissolved in ethyl acetate (99.8 %, Sigma-Aldrich) and then diluted (by a factor of ~10 000) using OF-UPW.

Response curves of the selected compounds with an expected capability to act as reactive oxygen species compared to H_2O_2 are shown in Fig. 3.3. PAA showed a linear fluorescence intensity response similar to H_2O_2 (relative sensitivity $s = 93$ %). In contrast, AQ and organic peroxides like tBuPA barely reacted. Low responses were observed for tBuOOH ($s = 25$ %), BenP ($s = 16$ %) and LP ($s = 15$ %), as well as for 2-BP, which includes three O-O- function groups ($s = 21$ %). The hydroperoxide groups in tBuPA, tBuOOH, BenP, LP and 2-BP are heavily protected by *tert*-butyl, phenyl and alkyl groups, which likely suppresses the reaction with DCFH. Less protected peroxides might be more reactive but such compounds are also less stable and therefore not usually commercially available. This indicates that, using a DCFH assay, the signal intensity of peroxides varies significantly depending on the peroxide molecular structure and that sterically hindered peroxides may contribute much less to the DCFH signal. Thus, we regard the ROS signal measured by the DCFH assay as a lower limit for the effective ROS content. Additionally, components known to induce redox cycling (e.g., metal ions and anthraquinone) do not seem to react with DCFH. Thus, we conclude that DCFH measures the capability of particle-borne compounds to act as reactive oxygen species rather than the potential of species to mediate ROS formation.
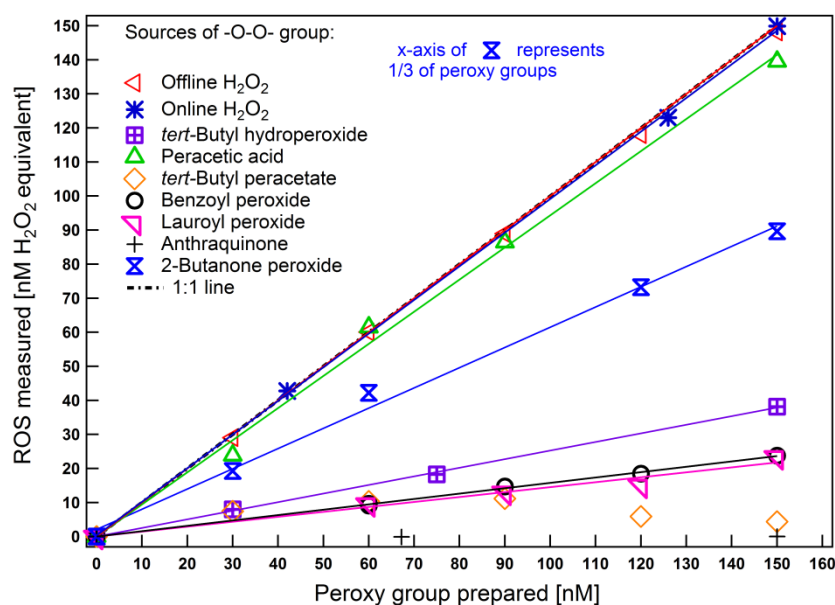
Figure 3.3 Calibration curves of H_2O_2 and response of selected compounds (with the instrument used in the offline mode unless indicated otherwise). Linear fits are shown for different peroxides and other compounds of interest in the concentration range of 0 to 150 nM. The correlation coefficients R^2 were 0.99, except for lauroyl peroxide ($R^2 = 0.91$).

3.3.1.3 Instrument performance in ambient and smog chamber measurements

In order to evaluate the performance of the ROS analyzer in the field, two sets of experiments were conducted. In the first set, the instrument was operated in the offline mode using filter samples collected at two different sites: a) a site influenced by traffic emissions in Milan (northern Italy), where quartz filters were sampled during October 2013 (Perrone et al., 2016); and b) a rural site in San Vittore

(southern Switzerland in an Alpine valley) influenced by biomass burning, where samples were collected during January 2013 (Daellenbach et al., 2017; Zotter et al., 2014). More details on the analysis of the samples can be found in the cited references. The samples from both sites were stored in the freezer at -20 ^{o}C for 2 years before ROS analysis. A filter punch was dissolved in water and several sample solutions were prepared by consecutive dilutions. Fig. 3.4 shows a linear relationship of the fluorescence response with decreasing particle mass concentration (based on the mass on the filter punch and assuming 100 % water solubility) for both samples, where equivalent H_2O_2 concentrations span a wide range, which confirms the instrument linearity. The different slopes between these two data sets might be due to the different emission sources (traffic in Milan and wood combustion in San Vittore) at these two locations (see Perrone et al., 2016; Zotter et al., 2014).
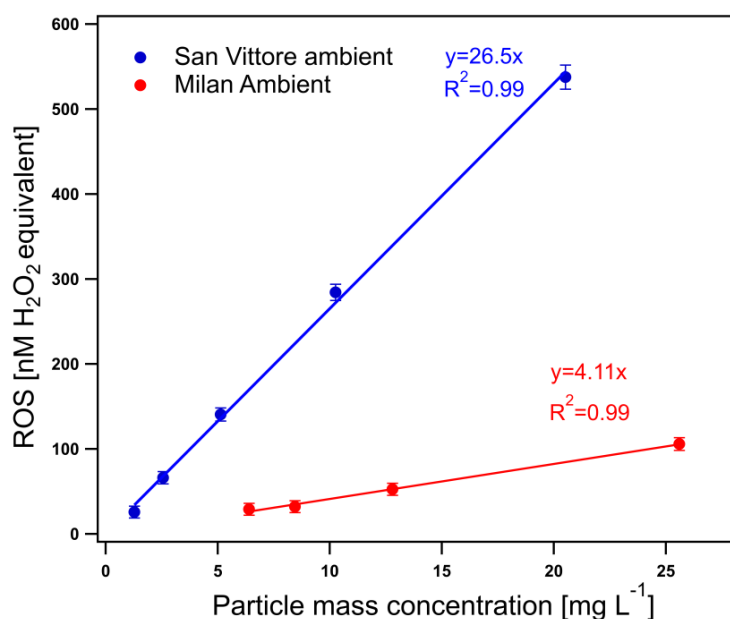
Figure 3.4 ROS content vs. dissolved particle mass concentration. Blue symbols represent PM$_{10}$ samples from San Vittore in winter (Switzerland), and red symbols represent TSP samples from Milan in autumn (Italy). The error bars represent the instrument precision (see Sect. 3.3.1.2).

The second set of experiments was performed at the PSI smog chamber. Beechwood logs were combusted in a residential wood burner (Avant, 2009, Attika), following the procedure described in Bruns et al. (2016, 2017). The resulting emissions were sampled from the chimney through a heated line (473 K), diluted by a factor of ~8-10 using an ejector diluter (473 K; DI-1000, Dekati Ltd.), and injected into the smog chamber. Emissions were only sampled during the stable flaming phase for 11-21 min and the total dilution factors ranged from ~100 to 200. Experiments were conducted at -10 ^{o}C or 15 ^{o}C and at a relative humidity of ~50 %. After the characterization of the primary emissions, d9-butanol (D9, 98 %, Cambridge Isotope Laboratories) was injected into the chamber to determine the OH exposure from its decay (Barmet et al., 2012). A continuous injection of nitrous acid (2.3-2.6 L min^{-1}) was used to create OH by photolysis. The chamber was then irradiated with UV light (40 lights, 90-100 W, Cleo Performance, Philips) for 4.5-6 h (Platt et al., 2013). Real-time characterization of the aerosols from the smog chamber was carried out throughout the experiment with the online ROS analyzer and a high-resolution time-of-flight aerosol mass spectrometer (HR-ToF-AMS, Aerodyne Research Inc.).

The evolution of ROS measured by the online method is shown in Fig. 3.5 for one exemplary smog chamber aging experiment. Injection of the wood combustion emissions led to a primary organic aerosol (POA) concentration of 25 μg m^{-3} and 26 nmol m^{-3} of particulate ROS in the smog chamber. After the lights were switched on (referred to as "lights on"), secondary organic aerosol (SOA) was produced and total organic aerosol (OA) measured by AMS reached a maximum concentration 1 h later, but then decreased because of higher wall loss than the SOA production rate. The ROS concentration increased concurrently with the increasing OA, indicating the formation of ROS by photochemical reactions induced by OH radicals, but then decreased faster than OA. When we sampled through a particle filter inserted upstream of the ROS online analyzer (pink areas), the ROS signal went to almost zero, which was considered as a measurement baseline during aging (Fig. 3.5, Panel a).

To investigate the influence of aging on ROS formation, SOA and secondary ROS (ROS formed during aging, ROSs) were calculated by subtracting POA and primary ROS from the total OA and total ROS measured during lights on (Fig. 3.5, panel b), respectively. Here the POA and primary ROS calculation was based on the assumption that they were not further oxidized after lights on and the wall loss rate was the same as for the inert tracer black carbon (BC). The content of secondary ROS in SOA (represented by ROSs/SOA) was in the range of 0.4-1.26 nmol μg^{-1} within the oxidant OH exposure range of 0-30×10^6 molec m^{-3} h. Initially, aging resulted in a high ROS content in SOA, which then decreased strongly with increasing OH exposure (Fig. 3.5, Panel c). This decrease could be due to further oxidation or decay of particulate ROS, indicating that first generation products from the volatile organic compounds (VOCs) oxidation might play a more important role in ROS formation than later-generation molecules.
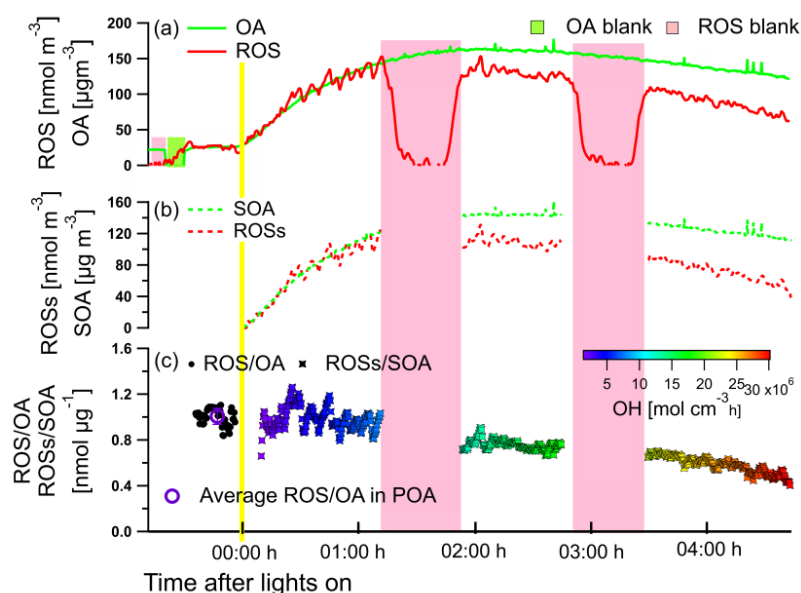
Figure 3.5 Evolution of the concentrations of OA mass and ROS during an online wood combustion smog chamber aging experiment. a) Total OA and ROS, b) SOA and ROS, c) ROS content in the OA (before lights on) and ROS content in the SOA (after lights on) as a function of the OH dose.

3.3.2 Gas-phase interference test

We tested the potential interference of trace gases and aerosol components on the DCFH signal. In principle, at the applied sample flow rate, 99 % of the trace gases should get removed by the denuder. Specifically, we assessed the removal efficiency of the denuder with respect to the most abundant oxidizing trace gases O_3 and NO_2. After exposing the denuder to 464 ppb ozone for ~5 h, no increase in the background signal was observed (Table 2). An amount of 500 ppb NO_2 showed no increase in the background signal even without the denuder. The results in Table 2 indicate that a newly regenerated denuder completely removes O_3, making the denuder suitable for both smog chamber (usually ~5 h aging per experiment) and ambient measurements (1 day/denuder replacement interval). Based on these results we assume that gaseous H_2O_2 is also completely removed. Further, we regularly checked the ROS blank by measuring particle-free air by switching a three-port valve and sampling through a particle filter (disposable filter units, Balston, UK) installed in another line.

Table 3.2 Effects of the potential interferences in the gas and aerosol phase on the DCFH signal.

Species tested		Concentration applied		Measured concentration (H_2O_2_eq.)	
	without denuder	without denuder	with denuder	without denuder	with denuder
Gas phase	O_3	464 ppb	464 ppb[*]	150 nM	0 nM
	NO_2	500 ppb	-	0 nM	-
Particle phase	SO_4^{2-}	23.5 μg m^{-3}	-	-4.8 nM	-
	NO_3^-	228 μg m^{-3}	-	-3.5 nM	-
	SO_4^{2-}+H_2O_2	23.5 μg m^{-3}+ 115 nM	-	105 nM	-
	NO_3^-+H_2O_2	228 μg m^{-3}+ 115 nM	-	110 nM	-
	SO_4^{2-}+2-BP	23.5 μg m^{-3}+ 272.5 nM	-	272.5 nM	-

* Denuder was exposed for ~ 5 h

3.3.3 Particle-phase matrix effects

3.3.3.1 Particulate $SO4^{2-}$ and NO_3^-

Previous measurements of filters from Milan showed a clear correlation of ROS with the particulate SO_4^{2-} and NO_3^- concentration (Perrone et al., 2016). During the investigated period, the average SO_4^{2-} and NO_3^- concentrations in Milan were 4 μg m^{-3} and ~5-10 μg m^{-3}, respectively. Here, we investigate whether SO_4^{2-} and NO_3^- exhibit a response in the DCFH assay. Therefore, we tested the fluorescence response to ~ 1.38 μM SO_4^{2-} and ~20 μM NO_3^- solutions prepared from $(NH_4)_2SO_4$ and NH_4NO_3, respectively. Such concentrations would typically be observed after collection of 23.5 μg m^{-3} of SO_4^{2-} and 228 μg m^{-3} of NO_3^- with the online instrument. This is equivalent to ~ 5 and ~ 30 times higher concentrations than observed in Milan (Perrone et al., 2016). These measurements are then compared to cross-sensitivity tests of ~1.38 μM SO_4^{2-} and ~20 μM NO_3^- with 115 nM H_2O_2 and 272.5 nM 2-BP (Table 3.2).

Results show that the signals generated by injecting $(NH_4)_2SO_4$ and NH_4NO_3 were on average lower than the instrument background by -4.8 and -3.5 nM (H_2O_2_e.q.), respectively. According to the

reproducibility of the instrument background discussed in Sect. 3.1.1, these differences are not statistically significant. For the cross-sensitivity test, the fluorescence response of the SO_4^{2-}–H_2O_2 mixture (23.5 μg m^{-3} SO_4^{2-} + 115 nM H_2O_2) and the NO_3^-–H_2O_2 mixture (228 μg m^{-3} NO_3^- + 115 nM H_2O_2) corresponded on average to 105 nM and 110 nM H_2O_2 equivalent, respectively. These deviations from the value measured for H_2O_2 alone (115 nM) are not statistically different from zero (z score test, p value ~0.7 for SO_4^{2-} and NO_3^-), within our measurement precision (Sect. 3.1.2). The SO_4^{2-}–2-BP mixture (23.5 μg m^{-3} SO_4^{2-} + 272.5 nM 2-BP) also showed a similar result. We conclude from these tests that particulate SO_4^{2-} and NO_3^-, the most abundant single particulate components, neither show any ROS signals nor influence the H_2O_2 and 2-BP measurements and that the observed relationship between the secondary species and the ROS signals in ambient air is rather a correlation and not based on causation.

3.3.3.2 Transition metals

Transition metals may induce a response through redox cycling. Iron is one of the most abundant transition metals in the aerosol (Valko et al., 2005; Dall'Osto et al., 2016). However, potential iron-catalyzed ROS formation in an oxygen-rich environment has not yet been examined using a DCFH assay. In order to investigate the effect of metals on the ROS signal we conducted two experiments: 1) the analysis of the H_2O_2 reaction with DCFH in the presence of $FeCl_2$ (anhydrous, 99.998%, Sigma-Aldrich, USA) and $FeCl_3$ ($FeCl_3 \cdot 6H_2O$, Sigma-Aldrich, USA) and 2) the analysis of the H_2O_2 signal in the presence of ambient aerosols extracted from filter samples.

In the first set of experiments (shown in Fig. 3.6) the signal of H_2O_2 measured alone was compared with that of a mixed $FeCl_2$–H_2O_2 solution. At a concentration of 1 nM soluble Fe^{2+} in water, no influence on the ROS signal was observed within a standard deviation. The same procedure was then applied to H_2O_2 (226 nM) combined with significantly higher Fe^{2+} concentrations (182.5 nM). The fluorescence signals of the Fe^{2+}–H_2O_2 mixture, both with and without the presence of dissolved O_2, were significantly lower than the signal when measuring H_2O_2 alone. This might be due to the consumption of a substantial amount of H_2O_2 by Fe^{2+}, for the production of HO ($Fe^{2+} + H_2O_2 \rightarrow Fe^{3+} + OH^- + HO$), which will further react with H_2O_2 and result in further reduction of the H_2O_2 concentration ($HO + H_2O_2 \rightarrow H_2O + HO_2$; $HO_2 + H_2O_2 \rightarrow O_2 + H_2O + HO$) (Kolthoff and Medalia, 1949). This indicates that concentrations of soluble $Fe^{2+} \leq 1$ nM, which were obtained at ambient concentrations of ≤ 10 ng m^{-3} soluble Fe^{2+} in the online instrument, will not influence the ROS measurement. However, in cases of high ambient soluble Fe^{2+} concentrations the ROS signal might be reduced, whereby this also depends on the H_2O_2 equivalent concentration. Measured ambient iron concentrations were found to be in the range of tens to several thousands of ng m^{-3} (Perrone et al., 2016; Oakes et al., 2012; Visser et al., 2015). Oakes et al. (2012) reported that water-soluble Fe (II) constitutes between 2.5 and 32 % of total iron, resulting in a water-soluble Fe (II) concentration up to 30 ng m^{-3}, which would be equivalent to ~ 2 nM in our online instrument. According to our first pair of experiments in Fig. 3.6 (1 nM Fe^{2+} mixed with 113 nM H_2O_2 solution) this would not suppress the ROS signal. Meanwhile, the H_2O_2–Fe^{3+} mixture signal was observed to be almost the same as the H_2O_2 signal alone with and without the presence of O_2, which is in agreement with the findings of LeBel et al. (1992) and Keenan et al. (2009). These findings

were further evaluated below by examining the influence of genuine atmospheric particulate metals on the H_2O_2 signal.
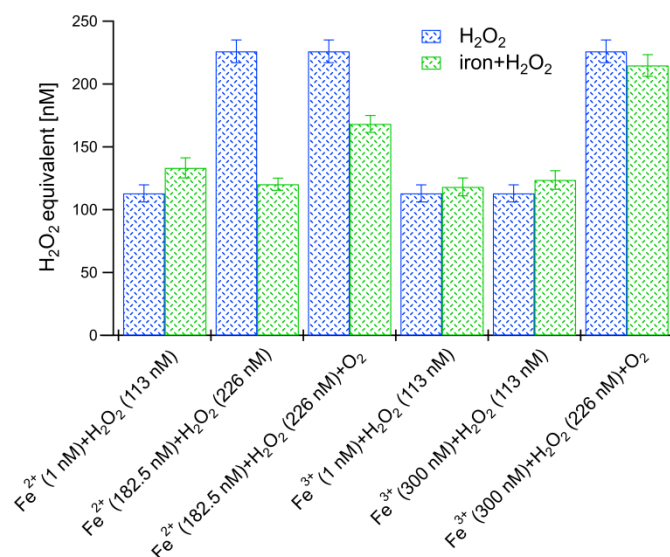
Figure 3.6 The relative fluorescence intensity during Fe^{2+} and Fe^{3+} cross-sensitivity tests with H_2O_2. The blue bars represent the premixed H_2O_2 concentrations, and the green bars represent the [iron+H_2O_2] mixture concentrations. The error bars were calculated based on the instrument precision (see Sect. 3.3.1.2).
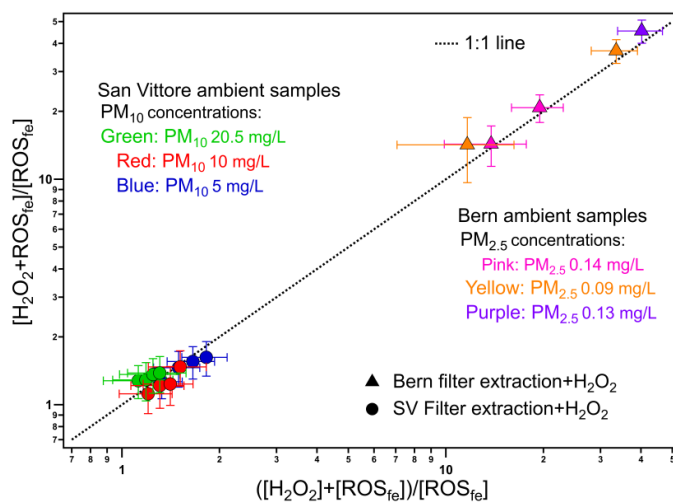

Figure 3.7 Comparison of the filter extract (fe)–H_2O_2 mixture with the sum of the separately measured filter extract and H_2O_2 response, both normalized to the filter extract signal. [H_2O_2+ROS_{fe}] represents the fluorescence response of the filter-extract–H_2O_2 mixture; [H_2O_2] and [ROS_{fe}] represent the fluorescence response of H_2O_2 and the filter extracts alone. The symbols represent different locations of the samples collected. The colors represent different PM concentrations based on the mass on the filter punch and assuming 100 % water solubility. H_2O_2 concentrations mixed together with each PM concentration ranged from 56.5 to 113 nM and from 40 to 100 nM in Bern and San Vittore, respectively, which are also indicated indirectly on the x and y axes. Error bars represent the propagated uncertainty from the measurements of [H_2O_2+ROS_{fe}], [ROS_{fe}] and [H_2O_2].

We then investigated whether the complex matrix of ambient particles, which also include different forms of iron together with other metals, has an influence on ROS measurements. For this second set of experiments, ambient filter samples from a rural site in San Vittore (Switzerland) collected in January 2013 and an urban site located in Bern (Switzerland) collected in November 2014 were extracted and

cross tested with H_2O_2. In San Vittore, three concentrations of PM_{10} from one filter punch were prepared, while in Bern three concentrations of $PM_{2.5}$ from three different filters were prepared. Fig. 3.7 compares the fluorescence response of the filter-extract–H_2O_2 mixture with the sum of the separately measured signals of the filter extract and of the H_2O_2. To account for the large differences in PM concentrations the signals were normalized to the signal of the filter extract. Results from both San Vittore and Bern lie on the 1:1 line within our errors. This indicates that at concentrations relevant for the ambient atmosphere the complex matrix of ambient particles has no influence on ROS signals.

3.3.4 Assessment of ROS stability

3.3.4.1 Comparison of online and offline measurements

A direct intercomparison of online in situ and offline filter sample measurements of the ROS content from different emission sources was performed. These aerosol samples included fresh and aged aerosols from wood combustion emissions from a smog chamber, as well as ambient aerosols collected in Bern (Switzerland).

The smog chamber experiments and the online performance were described in Sect. 3.1.3. In addition to the online measurements, the particles from the chamber were collected on quartz filters (47 mm, Pall Corporation) at a flow rate of 26 L min^{-1} for 30-32 min behind a charcoal denuder to remove organic vapors. Primary particles were collected after injection of the emissions into the smog chamber and before the lights were turned on. Aged particles were collected after around 1 and 4 h of aging. The filters were immediately stored at 253 K and analyzed ~ 2 years after the smog chamber experiments.

Ambient measurements were performed at an urban site located at the Institute of Anatomy of the University of Bern. A stainless steel cyclone (URG-2000-30ET, URG Corporation) was operated at a constant flow rate of ~ 100 L min^{-1} to select particulate matter with an aerodynamic diameter <2.5 µm. After size selection, particles were enriched using a versatile aerosol concentration enrichment system (VACES) (Kim, et al., 2001) and dried by passing through a diffusion dryer. Organic vapors were removed from the airstream using a charcoal denuder. The physicochemical properties of the aerosols were characterized using the online ROS analyzer, a scanning mobility particle sizer (SMPS, custom built) and a quadrupole aerosol chemical speciation monitor (ACSM, Aerodyne Research Inc.) for the measurement of the non-refractory aerosol composition. Particle-bound ROS were always measured downstream of the VACES due to the low ambient aerosol concentration while the other instruments measured ambient air most of the time. For offline quantification of particle-bound ROS, particles were periodically collected either up- or downstream of the VACES on Teflon filters (47 mm Fluoropore membrane, 3.0 µm pore size, Millipore, Molsheim, France) for at least 2 hours. Prior to deposition on the filter, the sample flow was passed through a charcoal denuder removing oxidizing and organic gases. Sampling time was 3 h and filters were immediately stored at -20 ^{o}C. Filter punches were then extracted as described in Sect. 2.1.3 and analyzed for the ROS content ~1 year after sampling.

The ROS concentrations measured by the online and offline method from the wood combustion experiments and ambient air in Bern are compared in Fig. 3.8. We did not observe a systematic

difference between ROS concentrations on filters taken before and after the VACES compared with the online measurements. The ROS concentrations measured offline are on average 31 % lower than the online data in the Bern ambient measurements and on average 67 % and 61 % lower than the online data for primary and secondary wood combustion samples, respectively. For the ambient measurements in Bern, a small number of measurements show agreement between the two methods indicating no ROS decay. A more detailed analysis is given in the following section to further explain the discrepancies of offline and online measurements.
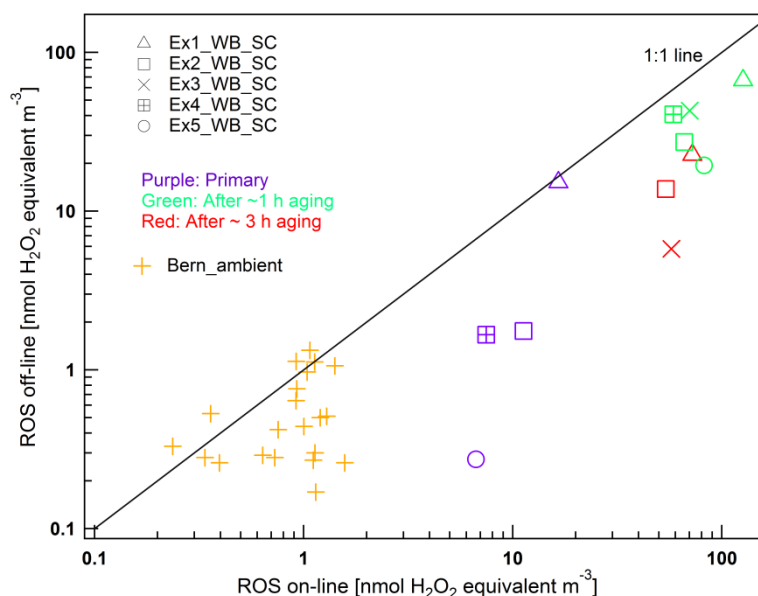
Figure 3.8 Comparison of online and offline measured ROS concentrations in the city of Bern in winter and during wood combustion smog chamber experiments (Ex*n*_WB_SC), including primary aerosol samples (purple) and secondary aerosol samples after aging for ~1 h (green) and ~4 h (red). A deviation from the 1:1 line indicates a discrepancy between the online and offline method. Filters from the wood combustion experiments were analyzed 2 years after sampling, and those from ambient measurements were measured 1 year later.

3.3.4.2   ROS degradation

As ROS decay with time, we investigated the evolution of the particle-bound ROS over time by measuring ROS from filter samples taken during additional biomass combustion laboratory experiments. The temperature of the filter samples was maintained at -20 ^{o}C, except during transport which lasted ~3 h where the samples were packed at 0 ^{o}C using ice packs. As this might have an additional effect on the results, ROS lifetimes determined at -20 ^{o}C should be considered as the lowest estimates.

A pellet boiler was operated under two different conditions: high excess of combustion air (λ^{++}) and lack of combustion air (λ^-) (see Table 3.3). The emissions from the pellet boiler were sampled from the chimney through a heated line (473 K), and diluted by a factor of ~100-150 using two ejector diluters in series (VKL10, Palas GmbH). The emissions were then aged in a PAM chamber to simulate photochemical aging of the emissions and assess the potential of secondary organic aerosol (SOA) formation. The design and the use of the PAM chamber is described by Kang et al. (2007) and Bruns et

al. (2015). Gas-phase O_2 and CO (using a paramagnetic oxygen analyzer for O_2 and a non-dispersive infrared, NDIR, analyzer for CO; Ultramat 23, Siemens), CO_2 (NDIR analyzer, model LI-820, LI-COR®), as well as total volatile organic compounds, and CH_4 (using a flame ionization detector, with a non-methane cutter; model 109A, J.U.M Engineering) were monitored in the hot, undiluted flue gas. In addition, non-methane volatile organic compounds (NMVOCs) as well as the OA, nitrate, ammonium and sulfate were measured after dilution using a proton transfer reaction mass spectrometer (PTR-MS, Ionicon) and a HR-ToF-AMS. Aerosol filter samples were taken for ~ 30 min on Teflon filters (47 mm Fluoropore membrane, 3.0 μm pore size, Millipore) after the PAM chamber for ROS offline analyses. The filters were stored in the freezer from hours up to 4 months before the measurements of the ROS activity using the offline ROS setup (see Sect. 3.2.1.3).

Table 3.3 Short-lived and long-lived ROS fractions and parameters from the different experiments (Ex*n* denotes the number of the experiment).

Filter	Ex1	Ex2	Ex3	Ex4	Ex5	Ex6
λ^1	1.31 (λ^-)	3.25 (λ^{++})	3.33 (λ^{++})	3.18 (λ^{++})	3.16 (λ^{++})	3.36 (λ^{++})
MCE[6]	0.99	0.98	0.97	0.98	0.98	0.96
T (Chamber, °C)	37.9	37.9	37.9	39.8	39.8	39.8
RH (Chamber, %)	18.6	24	24.5	20.9	20.9	20.9
OA[2] $[\mu g\ m^{-3}]^2$	43.0	39.1	29.0	4.5	9.9	16.5
CH_4[4,5] (ppmv, norm)	0.017	0.16	0.16	0.027	0.087	0.13
CO[4,5] (ppmv, norm)	2.2	11.0	11.5	4.5	6.3	8.6
CO_2[3,4,5] (ppmv, norm)	375.5	391.5	381.1	210.8	212.13	203.0
NMVOCs[4,5,7] (ppm, norm)	0.04	0.74	0.78	0.13	0.45	0.6
Long-lived fraction (A_2)	29.3±2.5 %	58.4±10.6%	59.3±12.6 %	24.5±3.7 %	100±17.6%	90.8±3.6%

[1]air fuel equivalence ratio (λ). $\lambda = O_{2,amb}[\%]/(O_{2,amb}[\%] - O_{2,exh}[\%])$ where $O_{2,amb}$ and $O_{2,exh}$ are the oxygen contents in ambient air ($O_{2,amb}$= 21 %) and the one measured in the flue gas, respectively.[2]OA = primary OA + secondary OA. [3] background corrected values. [4]all the concentrations of gas and particle phase compounds are after the PAM. [5]norm indicates that concentrations are reported at 0 °C and 1013 mbar and normalized to a reference O_2 content of 13 %, x_{norm} = [species x] × $\lambda_{actual}/\lambda_{reference}$. [6]MCE = $[CO_2]/([CO_2] + [CO])$ (Ward and Radke, 1993). [7]Non-methane VOCs (NMVOCs) = VOC-CH_4

The measured ROS concentrations in SOA from the different wood combustion experiments exhibit a clear decrease with increasing filter storage duration (Fig. 3.9). In addition, this decay seems to follow a double exponential function. This indicates the presence of a short-lived fraction A_1 with a decay constant $\pi_1 = \ln(2)/T_1$ and a long-lived fraction A_2 with a decay constant $\pi_2 = \ln(2)/T_2$, where T_i represents the half-life. A biexponential decay function was applied to fit the experimental values, whereby the two decay constants are considered to be the same for all experiments:

$$ROS_{norm}(t) = A_1 * EXP(-\pi_1 * (t - t_1)) + A_2 * EXP(-\pi_2 * (t - t_1)) \tag{3.3}$$

Here $A_{2,i}$ = 1-$A_{1,i}$, $0 \leq A_{1,i}$, $A_{2,i} \leq 1$, where i refers to an experiment number; t is the time after sampling and t_1 is the time when the first offline measurement was performed. $ROS_{norm}(t)$ is the ROS measured

at time t normalized to the ROS measured at time t_1. The model parameters and their respective uncertainties are shown in Table 3. Measured and modeled values are compared in Fig. 3.9.

The results show that the two ROS fractions have highly different reactivity. The final modeling yields $\pi_1 = 9.68 \pm 2.56$ and $\pi_2 = 0.0016 \pm 0.0019$. The second fraction (long lived) appears to be not reactive within our uncertainties and experimental timescales, as the associated reaction rate, π_2, is not statistically different from 0. The first fraction (short lived) is highly reactive, with a half-life $T_1 \approx 1.7 \pm 0.4$ h, similar reaction timescales and extents were observed for SOA from α-pinene ozonolysis (Krapf et al., 2016). The uncertainty analysis suggests that we are capable of determining the reaction rate of reactive ROS, but not that of the long-lived ROS. The fraction of the long-lived ROS ($A_{2,i}$) could be determined with acceptable errors of 20 %. The main aim of the model is to show that the fraction of unstable ROS may vary significantly between experiments but could be as high as 75 %, which highlights the need for an online ROS measurement technique. This variability in the contribution of the unstable ROS fraction could be related to the burning conditions in this study (shown in Fig. A.5).

The model considers ROS to be composed of two components with different decay rates. However, we do expect that the OA contains the spectrum of ROS with a wide range of reactivities. The model is thus a simplification of the ROS in the aerosol. Another simplification is that the decay rates of these two ROS components are considered to be the same between experiments. This may explain the reasons behind the high uncertainties in determining the rates, but does not have a significant effect on the determination of the contributions of the two fractions, $A_{1,i}$ and $A_{2,i}$. We also note that the decay rates and the ROS fractions determined from our results are specific for biomass burning SOA and cannot be extrapolated to other systems.
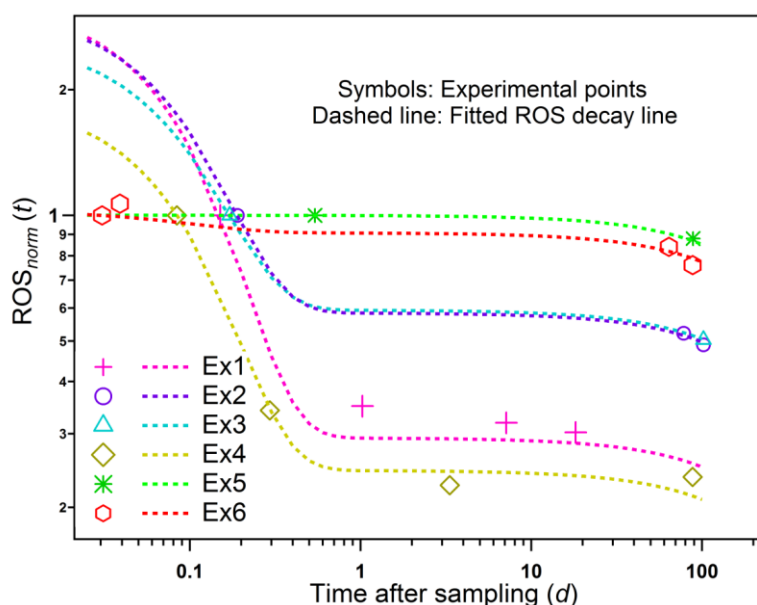
Figure 3.9 Measured and modeled ROS decays in SOA from wood combustion emissions with increasing sample storage duration for six experiments (Exn). The symbols and dashed lines represent measured and modeled values, respectively. $ROS_{norm}(t)$ is the ROS measured at time t normalized to the ROS measured when the first offline measurement was performed at time t_1. More information about the experiments can be found in Table 3. The very good agreement between measured and modeled ROS can be seen in Fig. A. 4.

To understand the variability in the contributions of the long-lived and unstable ROS fractions of different experiments, the long-lived fraction of ROS was compared with various wood combustion parameters. No correlation was found with λ, CO, CO_2 and NMVOCs (defined in Table 3.3), nor with specific gas-phase families, e.g., polycyclic aromatic hydrocarbons, furans, oxygenated aromatics, and N-containing or O-containing compounds. However, as shown in Fig. A.5 the fraction of long-lived ROS seems to be negatively correlated with the modified combustion efficiency (MCE) and the total OA mass present in the chamber (with Ex4 as an exception). These results might indicate that the composition of ROS formed from photo-oxidation of wood combustion emissions depends on the combustion conditions. As semivolatile organic compounds have a higher chance to condense to the particle phase with increasing OA concentration, the anticorrelation of the long-lived fraction of ROS with OA concentration suggests that the more oxidized and low-volatility ROS tend to have longer lifetimes than the less oxidized and higher volatility ROS. However, this would be in contradiction to Krapf et al. (2016), who concluded the highly oxygenated compounds to be unstable. The results presented here are preliminary and need to be further evaluated by more experiments.

Estimations of ROS lifetimes were done previously. ROS measured in oxidized oleic acid particles were separated into short- and long-lived species with a half-life of a few minutes and hours to days, respectively (S. J. Fuller et al., 2014). Chen et al. (2011) determined a ROS half-life of 6.5 h in oxidized organic aerosols. Krapf et al. (2016) showed that more than 60 % of peroxides contained in SOA from α-pinene ozonolysis decayed with a short half-life of 45 min.

To compare the ROS online measurement with immediate offline measurements, 2,6-dimethoxyphenol was used as a precursor and aged in the PAM chamber. SOA was then sampled on a Teflon filter (47 mm Fluoropore membrane, 3.0 μm pore size, Millipore), at a flow rate of 1.7 L min⁻¹ for ~1 hour after passing through a similar charcoal denuder as applied for the online measurements. The filter was then measured directly after sampling. Results showed that the offline measurement was 40 % lower than the online measurement, indicating that already without significant sample storage duration the short-lived ROS fraction was lost in the offline methodology. This is in agreement with S. J. Fuller et al. (2014) and Krapf et al. (2016), who showed that a larger fraction of ROS in fresh SOA decays within tens of minutes.

As a summary of the ROS decay behavior in aerosols from Bern ambient and wood combustion experiments, a normalized frequency distribution of the ROS decay percentage of different sources is plotted in Fig. A. 6. The decay percentage of ROS was calculated as follows:

$$ROS_{decay\ percentage} = [\frac{ROS_{online}-ROS_{offline}}{ROS_{online}}]\times100\ \% \tag{3.4}$$

The normalized frequency of a specified ROS decay percentage was then calculated as the ratio of the number of experiments yielding a certain decay percentage normalized to the number of total experiments. From Fig. A. 6 we conclude that the most frequently occurring ROS decay percentages were 40-80 % in wood combustion experiments, whereby aging in the smog chamber and PAM chamber yielded similar results. Similarly, around 60 % of ROS decayed in the majority of all the 27 ambient

samples collected in Bern. Overall, the offline method underestimates the ROS content due to the degradation of short-lived ROS prior to filter analysis. The comparison of online and offline ROS measurements from ambient and wood combustion smog chamber experiments indicates that on average 60 ± 20 % of ROS decayed during filter storage and handling, highlighting the importance of online measurements.

3.4 Conclusions

In this study, a modified online and offline ROS analyzer was presented and characterized. The major improvements compared to previous studies (S. J. Fuller et al., 2014; Huang et al., 2016; Wang et al., 2011a; King et al., 2013) to optimize the analysis were as follows: (1) degassing of the water and PBS to prepare the working solutions; (2) separation of DCFH and peroxidase working solutions, which were then mixed just before reaction with the sample solution; and (3) no ultrasonic filter extraction for offline analysis. All these efforts resulted in an instrument LOD of 2 nmol m^{-3} and 1.3 nmol L^{-1} for online and offline analysis, respectively. The method LOD of the offline analysis was 18 nmol L^{-1} based on the variability of the filter blanks and preparation of the solutions, respectively. The online instrument accuracy in determining the ROS concentration was found to be 3 %, and the instrument precision (repeatability) was 25 %, 10 % and 5 % at 30 nM, 70 nM and 150 nM, respectively. The reproducibility of the instrument sensitivity was ~40 % due to solution preparation and instrument operation; thus, a calibration is needed for each experiment and new batch of WS.

As shown with model organic compounds only peracetic acid was quantitatively measured, while large organic peroxides or those with bulky functional groups (i.e., *tert*-butyl and phenyl) strongly reduced the fluorescence response of the DCFH assay. Potential interferences from gas-phase O_3 and NO_2 were not observed and matrix effects of particulate SO_4^{2-} and NO_3^- were not statistically significant. While Fe^{3+} does not show a detectable interference, high soluble Fe^{2+} concentrations present in ambient aerosol could reduce the ROS signal.

Both online and offline measurements with the analyzer were performed in field and laboratory experiments. ROS concentrations from offline field measurements showed a linear relationship with increasing ambient particle concentrations. Smog chamber aging experiments of wood combustion emissions revealed a high initial ROS content in SOA, which then strongly decreased with OH exposure. Generally, ROS decayed with increasing filter storage duration. Due to the degradation of the highly reactive ROS fraction, the offline method generally underestimates the ROS concentration on average by 60 ± 20 %. From the decay behavior, ROS in SOA can be separated into two categories: a short-lived or highly reactive fraction with a half-life of ~1.7 h and long-lived or less reactive species. Consequently, to obtain a better estimate of the real ROS concentration in the ambient air or in simulation chamber experiments, a fast online method as presented in this study is advantageous.

Data related to this chapter are available online at https://zenodo.org/record/1118968#WjkuTk2WxmM. The Supplement related to this chapter is available online at https://doi.org/10.5194/amt-11-65-2018-supplement.

Acknowledgements

4

Particle-bound reactive oxygen species (PB-ROS) emissions and formation pathways in residential wood smoke under different combustion and aging conditions

J. Zhou[1], P. Zotter[2], E. A. Bruns[1], G. Stefenelli[1], D. Bhattu[1], S. Brown[1,3], A. Bertrand[4], N. Marchand[4], H. Lamkaddam[1], J. G. Slowik[1], A. S. H. Prévôt[1], U. Baltensperger[1], T. Nussbaumer[2], I. El-Haddad[1], and J. Dommen[1]

[1]Laboratory of Atmospheric Chemistry, Paul Scherrer Institute, 5232 Villigen PSI, Switzerland

[2]Lucerne University of Applied Sciences and Arts, Engineering and Architecture, Bioenergy Research, 6048 Horw, Switzerland

[3]Institute for Atmospheric and Climate Science, ETH, Zurich, Switzerland

[4]Aix Marseille Univ, CNRS, LCE, Marseille, France

Abstract. Wood combustion emissions can induce oxidative stress in the human respiratory tract by reactive oxygen species (ROS) in the aerosol particles, which are emitted either directly or formed through oxidation in the atmosphere. To improve our understanding of the particle-bound ROS (PB-ROS) generation potential of wood combustion emissions, a suite of smog chamber (SC) and potential aerosol mass (PAM) chamber experiments were conducted under well-determined conditions for different combustion devices and technologies, different fuel types, operation methods, combustion regimes, combustion phases and aging conditions. The PB-ROS content as well as the chemical properties of the aerosols were quantified by a novel ROS analyzer using the DCFH (2',7'-dichlorofluorescin) assay and a high resolution time of flight aerosol mass spectrometer (HR-ToF-AMS). For all eight combustion devices tested, primary PB-ROS concentrations substantially increased upon aging. The level of primary and aged PB-ROS emission factors (EF_{ROS}) were dominated by the combustion device (within different combustion technologies) and to a greater extent by the combustion regimes: the variability within one device was much higher than the variability of EF_{ROS} from different devices. Aged EF_{ROS} under bad combustion conditions were ~2-80 times higher than under optimum combustion conditions. EF_{ROS} from automatically operated combustion devices were on average 1 order of magnitude lower than those from manually operated devices, which indicates that automatic combustion devices operated at optimum conditions to achieve near-complete combustion should be employed to minimize PB-ROS emissions. The use of an electrostatic precipitator decreased the primary and aged ROS emissions by a factor of ~1.5 which is however still within the burn-to-burn variability. The parameters controlling the PB-ROS formation in secondary organic aerosol were investigated by employing a regression model, including the fractions of the mass-to-charge ratios m/z 44 and 43 in secondary organic aerosol (SOA; $f_{44\text{-SOA}}$ and $f_{43\text{-SOA}}$), the OH exposure, and the total organic aerosol mass. The regression model results of the SC and PAM chamber aging experiments indicate that the PB-ROS content in SOA seems to increase with the SOA oxidation state, which initially increases with OH exposure and decreases with the additional partitioning of semi-volatile components with lower PB-ROS content at higher OA concentrations, while further aging seems to result in a decay of PB-ROS. The results and the special data analysis methods deployed in this study could provide a model for PB-ROS analysis of further wood or other combustion studies investigating different combustion conditions and aging methods.

4.1 Introduction

Numerous studies worldwide have shown a link between exposure to airborne particulate matter (PM) and morbidity and mortality (Beelen et al., 2013; Dockery et al., 1993; He et al., 2016), and a strong correlation of airborne PM with lung function (Lee et al., 2011; Pope et al., 2002; Adam et al., 2015; Hwang et al., 2015). The adverse health effects of PM are related to the aerosol chemical composition (Kelly and Fussell, 2012; Baltensperger et al., 2008). Residential wood combustion can contribute to 5–44 % of the total ambient $PM_{2.5}$ (particulate matter with a diameter smaller than 2.5 μm), depending on the environment (Zhang et al., 2010; Germain 2005; EPBE, 2005; USEPA, 2000; EEA, 2013a; Ciarelli et al., 2017). In addition to PM, wood combustion emits a wide range of gaseous pollutants, including

volatile organic compounds, upon which oxidation can form secondary organic aerosol (SOA). Although wood is considered to be a climate neutral source of energy, epidemiological studies suggest that wood smoke may contribute significantly to premature mortality (Boman et al., 2003; Johnston et al., 2012), because of its association with respiratory disease, cerebrovascular diseases and impaired lung function (Liu et al., 2017; Yap, 2008; Fullerton et al., 2011). Liu et al. (2017) found a 7.2 % increase in the risk of respiratory hospital admissions during days with high wildfire-specific $PM_{2.5}$ compared to non-wildfire smoke event days. Exposure to wood combustion particles may cause moderate inflammatory activity, cell death and DNA damage, and adverse effects to airway epithelia (Krapf et al., 2017; Tapanainen et al., 2012; Muala et al., 2015; Marabini et al., 2017). These adverse effects may be related to oxidative stress caused by free radicals induced by inhaled PM, which overwhelms the antioxidants in the body (Lobo et al., 2010).

This may happen via two pathways. 1) particles may contain reactive oxygen species (particle-bound reactive oxygen species, PB-ROS, exogenous), which act as oxidants in the biological system; 2) particles may contain transition metals or organic compounds like quinones, which generate reactive oxygen species by interaction with physiological species undergoing Fenton reactions and redox cycling. For the measurement of the latter property several assays have been introduced, where the loss of reductants like dithiothreitol (DTT), glutathione (GSH) or ascorbic acid (AA) is measured (Cho et al., 2005; Verma et al., 2012; Charrier and Anastasio, 2012; Verma et al., 2015; Fang et al., 2016; Weber et al., 2018; Mudway et al., 2004; Li et al., 2003; Fang et al., 2016). Also cellular tests with an ROS probe have been developed to measure ROS induced by aerosols in a biological system (Landreman et al., 2008; Zhang et al., 2016; Tuet et al., 2017). The DCFH (2',7'-dichlorofluorescin) assay has been shown to be sensitive to a broad range of organic peroxides, alkyl peroxide radicals, and hypochlorite, but not to components that are known to induce redox cycling (i.e., metal ions and quinones; Venkatachari and Hopke, 2008; Wang et al., 2011b; King and Weber, 2013; S. J. Fuller et al., 2014; Zhou et al., 2018a). The DCFH assay has fast response rates and a linear response to varying ROS concentrations, for which reason it was applied as a suitable measure for the PB-ROS concentration (Zhou et al., 1997; Venkatachari and Hopke, 2008; King and Weber, 2013, Zhou et al., 2018a).

Several studies tried to establish links between such measurements and specific inflammatory biomarkers of oxidative stress in cell cultures or human subjects. For example Delfino et al. (2010; 2013) found that macrophage ROS generation from $PM_{2.5}$ was significantly positively associated with nitric oxide exhaled from elderly subjects and school children with persistent asthma. Janssen et al. (2015) reported a significant association between exhaled nitric oxide and increases in interleukin-6 in nasal lavage and the ROS generation measured by DTT and AA. Others found correlations between DTT activity and emergency department visits for asthma/wheezing and congestive heart failure (Bates et al., 2015; Fang et al., 2016). We are not aware of a study that relates measurements of ambient PB-ROS by DCFH with inflammatory biomarkers. However, it was shown that fresh SOA can release OH and H_2O_2 when dissolved in water (Wang et al., 2011b; Tong et al. 2016). This phenomenon was attributed to labile peroxides contained in SOA, which were shown do decay with a rather short lifetime of less than 1 h (Krapf et al., 2016). Lakey et al. (2016) modeled the ROS produced in the human respiratory tract upon inhalation of PM and showed that the OH production rate from SOA can be as high as the H_2O_2

production rate from trace metals. This indicates that PB-ROS might also lead to oxidative stress. Obviously, further research is needed to establish a link between PB-ROS and health effects.

Based on these considerations we performed a study with a DCFH assay to focus on exogenous PB-ROS formed by wood combustion exhaust and during its atmospheric aging. For this purpose, a suite of smog chamber (SC) and potential aerosol mass (PAM) experiments were conducted. As different types of wood, combustion devices and combustion conditions result in varying levels of emissions (Johansson et al., 2004; Schmidl et al., 2011; Fitzpatrick et al., 2007; Heringa et al, 2011), eight wood combustion devices with variable combustion conditions were tested. Primary and aged biomass smoke generated under different combustion and aging conditions were characterized by an online ROS analyzer based on the DCFH assay coupled with an aerosol collector. Observations from this study provide more detailed evidence of the influence of combustion technology on the PB-ROS of the emitted PM compared to a previous similar study (Miljevic et al., 2010). We also show the variation of the PB-ROS content from primary and aged aerosols under different operation conditions. Further, the contribution of reactive oxygen species to aged organic aerosol generated with different aging tools was investigated to clarify the PB-ROS formation potential upon photo-oxidation. Results from these experiments may be directly compared with ambient measurements.

4.2 Experimental setup and methodology

We performed two sets of measurement campaigns, utilizing several wood combustion devices with different combustion conditions and two aging tools. First we present the different devices, then give a description of the PAM chamber and the Paul Scherrer Institute (PSI) mobile smog chamber (PSI-MSC, ~ 7 m^3) and the PSI stationary smog chamber (PSI-SSC, 27 m^3) (Platt et al., 2013, 2014; Paulsen et al., 2005), including the experimental procedures, and finally discuss the combustion conditions and measurement strategy. An experimental schematic is shown in Figure S1. The combustion devices, experiment aging tools, and the test aspects are listed in Table 1.

4.2.1 Combustion devices

Eight combustion devices with different technologies were tested, including a pellet boiler (PB, automatic), a moving grate boiler equipped with electrostatic precipitator (MGB, automatic), a updraft combustion pellet stove (PS, automatic), a two-stage combustion downdraft log wood boiler (LWB, manual), two advanced two-stage combustion log wood stoves (LWS1, manual, updraft; LWS2, manual, updraft combustion when cold and downdraft combustion when hot), and two conventional single-stage combustion log wood stoves (LWS3, manual, and LWS4, manual). In the following, we describe the different combustion devices.

PB. Automatically operated pellet boiler, with two-stage updraft combustion and a nominal heat output of 15 kW, using wood pellets (EN certified, moisture content 7 %) as the combustion fuel. Under optimum combustion conditions, the ideal air-to-fuel ratio (λ) is achieved leading to near-complete combustion and, consequently, the particle emissions are dominated by inorganic components which are

contained in the pellets. The PB was also altered to enable the variation of the air-to-fuel ratio to investigate the influence of this parameter on the emissions. In this way, different combustion regimes could be achieved with this device; details are described in Sect. 4.2.2.

MGB. Automatically operated industrial moving grate boiler with nominal heat output of 150 kW, operated with wood chips (30 % moisture content). The grate has several zones where primary and secondary combustion air can be regulated.

PS, LWB, LWS1, LWS2, LWS3 and LWS4. LWB, LWS1 and LWS2 are advanced stoves/boilers with two-stage combustion technology, while in LWS3 and LWS4 conventional single-stage updraft combustion is applied. PS is an automatically operated pellet stove with a nominal heat output of 6 kW under full load. It possesses a ventilator for the injection of the combustion air. However, due to a relatively simple air control, the PS is operated at high λ. We also investigated partial-load conditions at 3 kW. LWB, LWS1, LWS2, LWS3, and LWS4 are manually operated devices, with the nominal heat outputs of 30, 8, 4.6, 8, and 4.5 kW, respectively. Further, the LWS1 is equipped with a storage container for logs, which slide on the grate due to gravity. For all four two-stage combustion devices (PS, LWB, LWS1, and LWS2) and one single-stage combustion device (LWS3), PB-ROS emissions from starting, flaming, and burn-out phases were investigated (details of the combustion phases are described in Sect. 2.3). In the case of the LWS4, only the flue gas from the flaming phase was injected into the smog chamber, where the EF_{ROS} under different aging temperatures of -10 ^{o}C and 15 ^{o}C were tested. In three of the log wood operated devices (LWS1, LWS2, and LWS3) dry (13–16 % moisture content) and wet logs (24–42 % moisture content) were investigated. In the PS, wheat pellets (manufactured from milling residues, moisture content 9 %) were tested in addition to conventional wood pellets (EN certified, moisture content of 7 %). In the LWS4, beech wood logs with a moisture content of 19 ± 2 % were used.

Table 4.1 Overview of combustion devices and test aspects.

Aging conditions	Combustion devices	Test aspects
	pellet boiler (PB)	EF_{ROS} of different burning regimes* (λ^{++}, λ^{-}, λ^{opt})
	moving grate boiler (MGB)	EF_{ROS} of full/part load; with/without electrostatic precipitator (ESP)
	pellet stove (PS)	EF_{ROS} of different burning phases*
PAM chamber (T = ~38 °C, RH = 20 – 25 %)	log wood boiler (LWB)	EF_{ROS} of different burning phases*
	log wood stove 1 (LWS1)	EF_{ROS} of different burning phases*
	log wood stove 2 (LWS2)	EF_{ROS} of different burning phases*
	log wood stove 3 (LWS3)	EF_{ROS} of different burning phases* secondary ROS formation
PSI-MSC (~7 m^3) T = -10 or 15°C, RH = 50 %	log wood stove 4 (LWS4)	flaming phase, aging temperature; secondary ROS formation
PSI-SSC (~ 27 m^3) Ambient T (22.5 °C), RH = 50 %	log wood stove 4 (LWS4)	flaming phase; secondary ROS formation

* The definitions of the burning regimes and burning phases are described in sect. 4.2.2.

4.2.2 Combustion conditions

Two parameters are used to describe the combustion conditions, namely, the combustion regimes and the combustion phases. Combustion regimes are defined by the air fuel equivalence ratio (λ) (Nussbaumer et al., 2000).

$$\lambda = \frac{O_{2,amb}[\%]}{O_{2,amb}[\%] - O_{2,flue\ gas}[\%]} \tag{4.1}$$

where $O_{2,amb}$ and $O_{2,flue\ gas}$ are the oxygen contents in ambient air ($O_{2,amb} = 21$) and in the flue gas, respectively. Depending mainly on the level of excess air three combustion regimes are distinguished: lack of oxygen (λ^-), optimum combustion conditions (λ^{opt}), and (high) excess of oxygen (λ^{++}). Each of these is characterized by a different type of combustion particles, i.e., comprising mostly soot, salts, and condensable organic compounds, respectively (Nussbaumer and Lauber, 2010). It should be noted that in wood combustion λ is always > 1. Consequently, λ^- and λ^{++} only describe λ values which are clearly (for λ^{++} at least 1.5-fold or higher) below or above λ^{opt}.

The three combustion regimes were achieved by changing the air-to-fuel ratio in the pellet boiler (PB). Optimum combustion conditions (λ^{opt}) were easily achieved by operating the PB under the designed optimum operation mode. High excess of oxygen (λ^{++}) compared to λ^{opt} was obtained by additionally blowing air into the combustion chamber via the ignition tube. The lack of oxygen (λ^-) regime was obtained by manually closing the secondary combustion air inlet. It should be noted that in real life operation λ^{++} and λ^- conditions only occur with severe mal-operation. These conditions were investigated since they result in distinct emission characteristics (high non-methane volatile organic compound emissions during λ^{++} and high soot emissions during λ^- (Nussbaumer and Lauber, 2010).

In the MGB, partial-load (50 kW) and full-load (150 kW) conditions, and the influence of an electrostatic precipitator (ESP) installed downstream of the combustion unit, were tested. ESPs are widely used in both large- and small-scale wood combustion devices to reduce PM emissions (Bologa et al., 2011; Nussbaumer and Lauber, 2010).

Combustion phases in the log wood stoves, log wood boiler and pellet stove were classified using the modified combustion efficiency (MCE), defined as the molar ratio of the emitted CO_2 divided by CO plus CO_2 ($CO_2/(CO+CO_2)$), in the flue gas after wood combustion (Ward and Radke, 1993). Each full combustion cycle includes three combustion phases: start phase (beginning of the burning cycle before MCE reaches 0.974), flaming phase (between start and burn-out phase, with MCE > 0.974), and burn-out phase (after flaming phase, with MCE < 0.974). As mentioned in Sect. 2.1, all three phases were obtained in the PS, LWB, LWS1, LWS2, and LWS3. In the PS, LWB, and LWS1, experiments started with a cold start, followed by a flaming phase and burn out. In the LWS2 and LWS3, after the first complete combustion cycle starting with a cold start, several full combustion cycles followed by adding new logs into the combustion chamber after the burn-out was finished (warm start). In devices where the

combustion phases were rapidly changing, the ROS analyzer was not able to separate these combustion phases due to a slow response time (~ 8 min). Consequently, the single combustion phases, including the start, flaming, and burn-out, and the combined combustion phases start + flaming or flaming + burn-out were used for the PB-ROS analysis. In the LWS4, with which the experiments were conducted in the PSI-MSC (at temperatures of 263 K and 288 K), and the PSI-SSC (at a temperature of 288 K), only emissions from the flaming phase were sampled.

4.2.3 Experimental procedures and aging tools

4.2.3.1   PAM chamber

Seven combustion devices (except LWS 4) were tested using the PAM chamber as an aging tool. The emissions were sampled through a heated line (473 K), diluted by a factor of ~100-150 using two ejector diluters in series (VKL 10, Palas GmbH), and then injected into the PAM chamber (see Figure S1 in the Supporting Information). The original concept of the PAM chamber is described by (Kang et al., 2007). Briefly, the PAM chamber is a single 0.015 m^3 cylindrical glass chamber, flanked by two UV lamps. Prior to entering the PAM chamber, pure air (1.6 L min^{-1}, humidified with a Nafion membrane, Perma Pure LLC) used as an OH precursor and a stream of diluted d9-butanol (98%, Cambridge Isotope Laboratories) were merged with the incoming reactant flow. The OH exposure during aging was defined as the integral of the OH concentration over the reaction time, and was calculated from the decay of the d9-butanol, measured by a proton transfer reaction–mass spectrometer (PTR-MS 8000, Ionicon Analytik GmbH; Barmet et al., 2012). The total flow rate in the PAM chamber was maintained at ~ 7 L min^{-1}, which was the sum of the flow rates of the instruments and a supplementary flow, resulting in a residence time of approximately 2 minutes. The OH exposure was controlled by adjusting the UV light intensity to obtain different OH concentrations. An outer ring flow (~0.7 L min^{-1}), which was discarded, was used to minimize wall losses and the instrument sampled only from the inner flow of the PAM chamber (~6.3 L min^{-1}). The temperature in the PAM chamber was around 38 ^{o}C due to the lamps. Primary wood combustion emissions were characterized either before or after the PAM chamber when the lights were switched off. Aged emissions were characterized after the PAM chamber with lights on. All the experiments were conducted under OH exposures of (1.1-2.0)×10^8 molec cm^{-3} h which corresponds to ~ 4.5-8 days of aging in ambient by assuming a mean daily OH concentration of 1×10^6 molec cm^{-3}. The applicability of the PAM chamber to measure wood combustion emissions has been shown in a previous study (Bruns et al., 2015).

4.2.3.2   Smog chamber aging

The second set of experiments was conducted in the PSI mobile smog chamber (PSI-MSC, ~ 7 m^3) at temperatures of 263 K and 288 K, and the PSI stationary smog chamber (PSI-SSC, 27 m^3) at 295.5 K. An overview of the experimental setup is also shown in Fig. B.1. In general, three pieces of dry beech logs, four pieces of kindling, and three fire starters were combusted in LWS4 for average (2.9 ± 0.3 kg) experiments and nine pieces dry beech logs, eight pieces kindling and four fire starters were combusted

for high (5.1 kg) load experiments (details in Sect. 4.2.1). The wood moisture content was 19 ± 2 %. Only emissions during the flaming phase with a modified combustion efficiency (MCEs) in the range from 0.974 to 0.978 were sampled. Emissions were sampled for 11-21 min and injected into the PSI-MSC using an ejection diluter, yielding a total dilution factor of 100 to 200. Hydroxyl radical (OH) concentrations in the chamber are controlled by continuous injection of nitrous acid into the smog chamber (after the characterization of the primary emissions as described below in Sect. 3.1), which produces OH upon irradiation by UV lights (Platt et al., 2013). The OH exposure was estimated by monitoring the decay of d9-butanol (butanol-D9, 98%, Cambridge Isotope Laboratories) following a single injection before the UV lights were turned on. In all five experiments conducted in the PSI-MSC, the aging time lasted 4.5-6 h. The OH exposure was $2.6\text{-}4.8 \times 10^7$ molec cm^{-3} h, which corresponds to ~1-2 days of aging in ambient by assuming a mean daily OH concentration of 1×10^6 molec cm^{-3}. More details about some of the PSI-MSC experiments of this campaign can also be found in Bruns et al. (2016, 2017). One additional experiment was conducted in the PSI-SSC, with an OH exposure up to 4.0×10^8 molec cm^{-3} h, equivalent to ~17 days of aging assuming a mean daily OH concentration of 1×10^6 molec cm^{-3}, extending the aging range beyond the range achieved by the PAM chamber (~1-8.5 days).

4.2.4 Particle-phase characterization

The non-refractory particle chemical composition was measured using a high-resolution time-of-flight aerosol mass spectrometer (HR-ToF-AMS; flow rate: 0.1 L min^{-1}, Aerodyne Research Inc.; DeCarlo et al., 2006). The HR-ToF-AMS measured the total organic aerosol (OA), SO_4^{2-}, NO_3^-, NH_4^+, Cl$^-$, and the two most dominant oxygen-containing ions in the OA spectra, i.e., the mass-to-charge ratios m/z 44 (Org44, mostly CO_2^+) and m/z 43 (Org43, mainly $C_2H_3O^+$ for the oxygenated OA and $C_3H_7^+$ for the hydrocarbon-like OA; Ng et al., 2011). Equivalent black carbon (eBC) was determined using an Aethalometer (AE33, Magee Scientific; flow rate: 2 L min^{-1}, Drinovec et al., 2015).

The particle-bound ROS was characterized by an online ROS analyzer (flow rate: 1.7 L min^{-1}) (Zhou et al., 2018a). The aerosols particles were collected in a mist chamber-type aerosol collector, dissolved into water, and mixed with a 2',7'-dichlorofluorescin (DCFH)/horseradish peroxidase solution. The ROS converts DCFH to DCF, which is detected by fluorescence and quantified as nM-H_2O_2 equivalents. The time resolution of the online ROS analyzer was ~ 8 minutes, preventing resolving brief discrete combustion phases. Therefore, different methods were used to calculate the average PB-ROS emissions under different conditions:

1. average (Figure S2a): utilized when the combustion conditions were relatively stable and sufficiently long to yield a stable ROS signal;

2. integrated average (Figure S2b): in cases of variable combustion conditions, the ROS signal was integrated over the measurement period which could include one or several phases from the same burn;

3. extrapolation + integrated average (Figure S2: panels 2c_1 and c_2): when the combustion conditions were variable and the background could not be measured between two combustion conditions due to the

time resolution of the ROS instrument. We extrapolate each measurement to the background value and then make the integrated average calculation as described above.

The various definitions for PB-ROS and related aerosol characteristics are presented below:

PB-ROS emission factors *(EF_{ROS})*. PB-ROS emission factors (EF_{ROS}) were calculated as the amount of PB-ROS in nmol-H_2O_2 equivalents per kilogram wood burnt, using Eq. (4.2):

$$EF_{ROS} = \frac{n_{ROS}}{M_c} C_{wood} \cong \frac{[n_{ROS}]}{\Sigma([\rho C_{CO_2}]+[\rho C_{CO}]+[\rho C_{CH_4}]+[\rho C_{VOC}]+[\rho C_{eBC}]+[\rho C_{OC}])} C_{wood} \qquad (4.2)$$

where $[n_{ROS}]$ is the background-corrected concentration of PB-ROS (nmol m^{-3}) in the emitted particles either before (primary PB-ROS) or after aging (aged PB-ROS), $[\rho C_x]$ are the carbon mass concentrations calculated from the background-corrected, carbon-containing species where x includes CO_2, CO, CH_4, volatile organic compounds (VOC), eBC, and particulate organic carbon (OC). M_C is the carbon mass burnt and C_{wood} represents the average carbon fraction of the wood fuel, ~ 0.46, measured in this study using an elemental analyzer. OC data were obtained from AMS measurements. Similarly, the organic aerosol (OA) emission factors (EF_{OA}) were calculated by replacing the PB-ROS concentration by OA.

PB-ROS fraction. In order to study the PB-ROS formation during aging, the secondary PB-ROS fraction ($f_{ROS-SOA}$) is introduced. It expresses the amount of secondary PB-ROS (ROS_S = aged ROS – primary ROS) per amount of secondary organic aerosol (SOA) formed during aging and is calculated from Eq. (4.3)

$$f_{ROS-SOA} = \frac{ROS_S}{SOA} \qquad (4.3)$$

Secondary organic aerosol (SOA) and secondary PB-ROS (ROSs) were calculated by subtracting primary organic aerosol (POA) and primary PB-ROS (ROSp) from the total OA and aged PB-ROS, respectively, assuming ROSp and POA to only be lost to the chamber wall at the same rate as eBC but otherwise to remain constant during aging. Although both quantities may not be conserved, a decrease of both does abate their effect on the PB-ROS fraction calculation. In the SC experiments, POA is defined as the OA mass before lights on, while SOA is estimated as the difference between total OA after lights on and the time-dependent POA mass accounting for particle wall loss. Wall loss rates for POA and SOA were assumed to be the same as that of the measured eBC. In PAM aging experiments, each experiment had a certain POA (measurements before PAM or after PAM with lights off) and SOA (measurements after PAM with lights on).

$f_{44\text{-}SOA}$ and $f_{43\text{-}SOA}$. To express the degree of oxygenation of SOA, the fraction of secondary Org44 and Org43 in SOA (represented as $f_{44\text{-}SOA}$ and $f_{43\text{-}SOA}$) is introduced, which is calculated from Eq. (4.4)

$$f_{44-SOA} = \frac{Org_{44-SOA}}{SOA}; \; f_{43-SOA} = \frac{Org_{43-SOA}}{SOA} \qquad (4.4)$$

where $Org_{44\text{-}SOA}$ is the difference of total Org44 and primary Org44, $Org_{43\text{-}SOA}$ is the difference of total Org43 and primary Org43 and using the same procedure as for the SOA calculation mentioned above.

Wall loss correction. The wall loss correction in the SC was done by assuming the same losses for all particle components as for the inert tracer eBC. The wall loss-corrected concentration of OA or PB-ROS (X) can be derived using Eq. (4.5):

$$X_{WLC}(t) = X_{meas}(t) \times \frac{eBC(t0)}{eBC(t)} \tag{4.5}$$

where $X_{meas}(t)$ refers to the concentration of X measured at time t. eBC (t_0) and eBC (t) are the concentrations of eBC when lights were switched on and at time t, respectively.

4.2.5 Gas-phase characterization

During the PAM chamber experiments, total volatile organic compounds (VOC) and CH_4 (using a flame ionization detector (FID) with a non-methane cutter, model 109A, J.U.M Engineering), CO and NO (with a non-dispersive infrared analyzer, Ultramat 23 Siemens), and O_2 (using a paramagnetic oxygen analyzer, Ultramat 23 Siemens) were determined in the hot undiluted flue gas. In SC aging experiments CO was measured with a cavity ring-down spectrometer (G2401, Picarro, Inc.). In all experiments, the composition of VOCs was determined by the PTR-MS 8000 (Ionicon Analytik GmbH). For CO_2 a cavity ring-down spectrometer (G2401, Picarro, Inc.) was used in the SC aging experiments and a non-dispersive infrared (NDIR) analyzer (model LI-820, LI-COR®) in the PAM chamber aging experiments.

4.3 Results and discussion

4.3.1 Primary and aged ROS emission factors (EFROS)

The PB-ROS and OA emission factors are presented in Table 2 for all combustion conditions, together with the number of tests, the combustion efficiency (MCE), the air-to-fuel ratio (λ), and the aerosol bulk properties determined with the AMS (OM:OC, O:C and H:C ratios). The high O:C ratios observed here are in accordance with a previous study on efficient burners (Heringa et al., 2012), and may be associated with ash (dominated by carbonates and detected as CO2+) present in the emissions (this also affects the OM:OC ratios).

The given values are the 25th and 75th percentiles of averages from several experiments and the data points considered for the calculations were restricted to the time period of the PB-ROS measurements. As shown in Fig. 4.1, PB-ROS emission factors (EF_{ROS}) for primary and aged OA were highly variable depending on the combustion conditions and devices. For all devices and combustion conditions, a substantial enhancement in the EF_{ROS} is observed with aging, indicating the importance of secondary PB-ROS production. The PB-ROS enhancement factor, defined as the ratio between aged and primary EF_{ROS}, range between 4 and 20, with lower values for MGB (~ 4) and PB under λ^{opt} combustion conditions (~ 6), and higher values for PB under λ^- and λ^{++} combustion conditions (> 10). The PB-ROS enhancement factors for all log wood stoves as well as LWB are comparable, with an average value around 10.

The variability in the EF_{ROS} in primary and aged OA for one device is much higher than the variability between average emission factors for different devices, spanning almost 2 orders of

magnitudes. Despite this, EF_{ROS} from PB and MGB (80-8 890 nmol kg^{-1} wood and 2 440-1.83×10^5 nmol kg^{-1} wood for primary and aged emissions, respectively) are on average 1 order of magnitude lower than those from PS, LWB, and LWS1-4 (220-1.89 × 10^6 nmol kg^{-1} wood and 3 570-1.1×10^6 nmol kg^{-1} wood for primary and aged emissions, respectively). These results clearly indicate differences due to the combustion technology, as a general rule, EF_{ROS} were lowest for automatically operated devices and higher for manually operated devices: PB and MGB are automatically operated and the primary and secondary air supply as well as the fuel feeding is controlled permanently, while LWB and LWS1-4 are manually operated. The PS is automatically operated but is operated at high λ and exhibits similar EF_{ROS} to the manual devices. Part of the EF_{ROS} variability within each device can be ascribed to the combustion phase, with higher emission factors for the starting and burn-out phases compared to the flaming/stable phase. This is especially true for the aged emissions from the PS (EF_{ROS} of the start phases was on average 13 times higher than the flaming phase; Mann–Whitney, p value = 0.06), the LWS2 (EF_{ROS} of the start phases was on average 1.7 times higher than the flaming phase, Mann–Whitney, p value = 0.24, not significant) and the LWS3 (EF_{ROS} of the start and burn-out phases were on average 1.5 times higher than the flaming and flaming + burn out phase, Mann–Whitney, p value = 0.07).

For the automatically operated MGB, the primary EF_{ROS} did not statistically differ between partial- and full- load operation (Mann–Whitney, p value = 0.95). However, the aged EF_{ROS} was a factor of ~3 higher for partial- load than for full load (Mann–Whitney, p value = 0.23). The use of the electrostatic precipitator decreased primary and aged ROS emissions, on average by a factor of ~1.5 times, however, these differences are not statistically significant (Mann–Whitney, p value = 0.12 for both primary and aged emissions) and are within the burn-to-burn variability.

For PB, the combustion operation could be systematically varied to investigate the influence of air-to-fuel ratio on PB-ROS and OA emission factors before and after aging. The EF_{ROS} were highest under λ^{++} conditions for both primary and aged emissions, with average values of 4 100 and 5.8 × 10^4 nmol kg^{-1} wood burnt, respectively (Fig. 4.1 and Table 4.2). Primary PB-ROS emissions under λ^{opt} conditions did not statistically differ from λ^- conditions (Mann–Whitney, p value = 0.43), but were on average 7 (λ^-) and 3 (λ^{opt}) times lower than those obtained under λ^{++} conditions, respectively (Mann–Whitney, p value < 0.005 for both cases). The aged EF_{ROS} under λ^{opt} and λ^- were also quite similar (Mann–Whitney, p value = 0.20), but with average values 8 and 5.5 times lower than those obtained under λ^{++} conditions, respectively (Mann–Whitney, p value = 0.02 for both cases). This shows that the air-to-fuel ratio has a significant effect on the PB-ROS emissions, which will be investigated for all devices hereafter.

Table 4.2 Characterization of primary emissions from PAM chamber and SC aging experiments*

Devices	Test aspects		Number of tests	MCE	λ	ROS nmol kg⁻¹	Total PM mg kg-1	Org mg kg-1	OM:OC	O:C	H:C
PB	λ^-		3	[0.991, 0.992]	[1.29, 1.30]	[345, 882]	[246, 301]	[56, 62]	[2.1, 2.4]	[0.7, 0.9]	[1.3, 1.4]
	λ^{opt}		7	[0.999, 0.999]	[1.59, 1.64]	[288, 2325]	[50, 69]	[22, 29]	[2.7, 2.8]	[1.1, 1.2]	[1.3, 1.4]
	λ^{++}		15	[0.963, 0.983]	[3.02, 3.11]	[1940, 5944]	[33, 61]	[15, 26]	[2.5, 2.6]	[0.9, 1.0]	[0.9, 1.0]
MGB	Full load	Before ESP	5	[0.999, 0.999]	[1.99, 2.04]	[1758, 2034]	[65, 100]	[27, 48]	[3.1, 3.1]	[1.4, 1.4]	[1.1, 1.3]
		After ESP	3	[0.999, 0.999]	[3.91, 3.99]	[775, 1098]	[3, 4]	[1, 2]	[2.3, 2.7]	[0.7, 1.0]	[1.2, 1.4]
	Partial load	Before ESP	6	[0.999, 0.999]	[2.12, 2.30]	[780, 4083]	[19, 25]	[8, 9]	[2.1, 2.3]	[0.6, 0.8]	[1.1, 1.3]
PS	All burning phases		5	[0.989, 0.995]	[4.97, 7.59]	[5376, 36415]	[204, 625]	[60, 427]	[2.2, 2.5]	[0.8, 1.0]	[1.1, 1.3]
LWB	All burning phases		20	[0.904, 0.999]	[1.47, 2.49]	[4307, 27590]	[262, 741]	[111, 277]	[2.5, 2.9]	[1.0, 1.4]	[1.1, 1.2]
LWS1	All burning phases		6	[0.850, 0.933]	[3.57, 7.05]	[5915, 52528]	[381, 572]	[142, 379]	[2.3, 2.4]	[0.9, 1.0]	[1.2, 1.2]
LWS2	Flaming		6	[0.948, 0.976]	[3.51, 4.31]	[141457, 249755]	[49, 98]	[49, 98]	[2.3, 2.4]	[0.9, 1.0]	[1.2, 1.3]
LWS3	Flaming		19	[0.930, 0.968]	[4.61, 9.57]	[12160, 61258]	[151, 356]	[14, 55]	[1.9, 2.1]	[0.5, 0.6]	[1.4, 1.6]
LWS4	Flaming		5	[0.972, 0.975]	[3.0, 3.6]	[37766, 57403]	[171, 440]	[83, 162]	[1.6, 1.7]	[0.30, 0.45]	[1.3, 1.5]

* Values of each parameter is described as [a, b], where a and b represent the 25 percentile and 75 percentile of the averages from several experiments and the data points considered for the calculations were restricted to the time period of the PB-ROS measurements
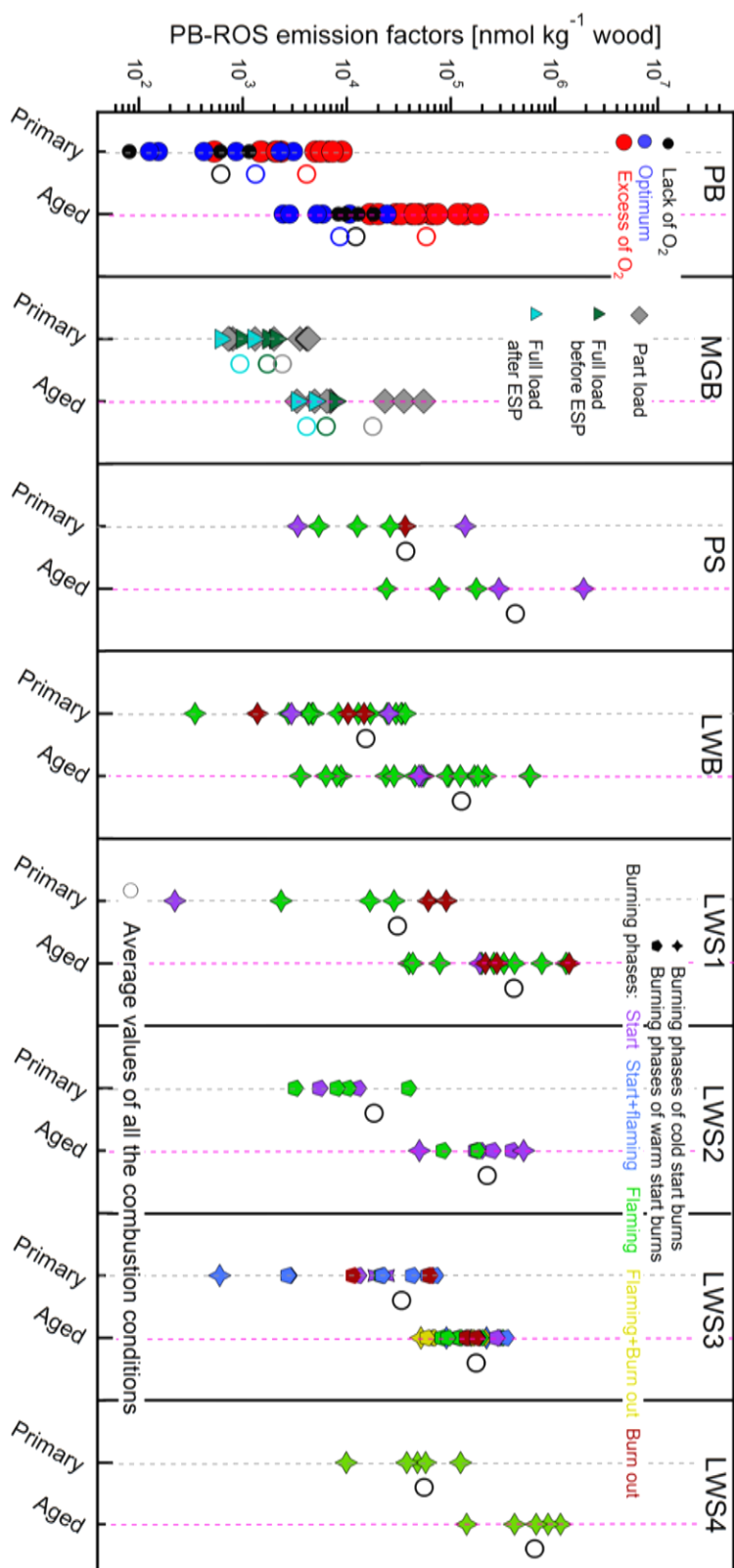
Figure 4.1 PB-ROS emission factors (EF$_{ROS}$) for all tested combustion devices under different operating and aging conditions. Open circles represent the average values of all the experimental data points for each condition. PB denotes Pellet boiler; MGB Moving grate boiler; PS Pellet stove; LWB Log wood boiler; LWSn Log wood stove n (n = 1, 2, 3, 4). Each data point represents one experiment. For each device, primary EF$_{ROS}$ appear on the left side (gray dashed line) and aged EF$_{ROS}$ on the right side (pink dashed line).

4.3.2 Aged EFROS under different combustion regimes

Fig. 4.2 shows the aged EF_{ROS} of the eight devices as a function of λ. Similar to PB, as already described above, a clear increase of EF_{ROS} in the aged aerosol can be observed with increasing λ values, with ~2-80 times higher aged EF_{ROS} values under bad combustion conditions than under optimum combustion conditions, although the extent of the increase and the overall trend were not the same for all individual devices. In the MGB all the burns occurred at $2.0 < \lambda < 2.2$, leading to aged EF_{ROS} (without ESP) in line with those from the PB between λ^{opt} ($\lambda = 1.6$) and λ^{++} (λ ranged from 2.7 to 3.4). The combustion in all stoves (PS, LWS1-4) exhibited higher λ ($\lambda > 2.2$) due to a less controlled air supply leading to less efficient combustion. In this range of oxygen excess, aged EF_{ROS} ranged between 1.68×10^4 nmol kg^{-1} wood and 1.38×10^6 nmol kg^{-1} for λ values between 2.2-17.6, where all aged EF_{ROS} were high but without any systematic trend with λ, suggesting that other parameters may influence PB-ROS emissions as well. The LWB follows a different trend, where the aged EF_{ROS} increase sharply with λ, starting at lower λ-values than the other manually operated devices. Aged EF_{ROS} for LWB ranged from 3530 to 5.79×10^5 nmol kg^{-1} wood within the λ-range of 1.5-2.6. Although trends in Fig. 4.2 show differences between devices, they highlight quite readily the important influence of the combustion conditions on aged EF_{ROS}.
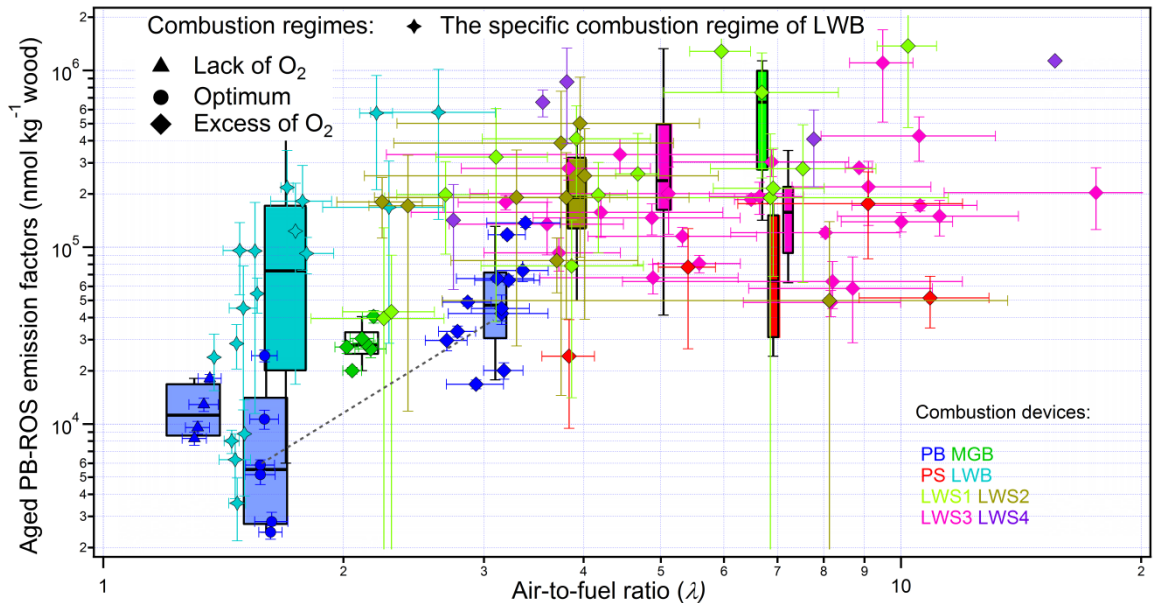
Figure 4.2 Aged ROS emission factors (EF_{ROS}) from different combustion regimes and combustion devices. The grey dashed line represents the EF_{ROS} increase with λ for the PB. The error bars of the y-axis of the data points denote the propagation of the uncertainty ($\delta = \sqrt{{\delta_1}^2 + {\delta_2}^2}$, with δ_1 and δ_2 representing the standard deviation of the averaged aged ROS and aged OA of the measurement time periods, respectively.); the error bars of the x-axis of the data points denote the standard deviation of the averaged λ of the measurement time periods.

While the combustion efficiency was found to have a strong influence on aged EF_{ROS}, the latter varies considerably, by a factor of 3-50, within the same combustion regime but for different combustion devices. In Fig. 4.3, we investigate to which extent this variability in aged EF_{ROS} is related

to the variability in the bulk OA emissions. The high correlation (Pearson's R = 0.92) observed in Fig. 4.3 suggests that changes in aged EF_{OA} explain a great fraction of the variability in aged EF_{ROS}, implying that this variation is inherent to wood combustion conditions. Nonetheless, additional unexplained variation was observed between the two variables in Fig. 4.3, with the aged PB-ROS emission factors varying by a factor of 2.6 on average for the same aged EF_{OA}. To elucidate the reasons behind this variability, we investigate in the following the parameters controlling the secondary PB-ROS formation and its content in OA upon aging.
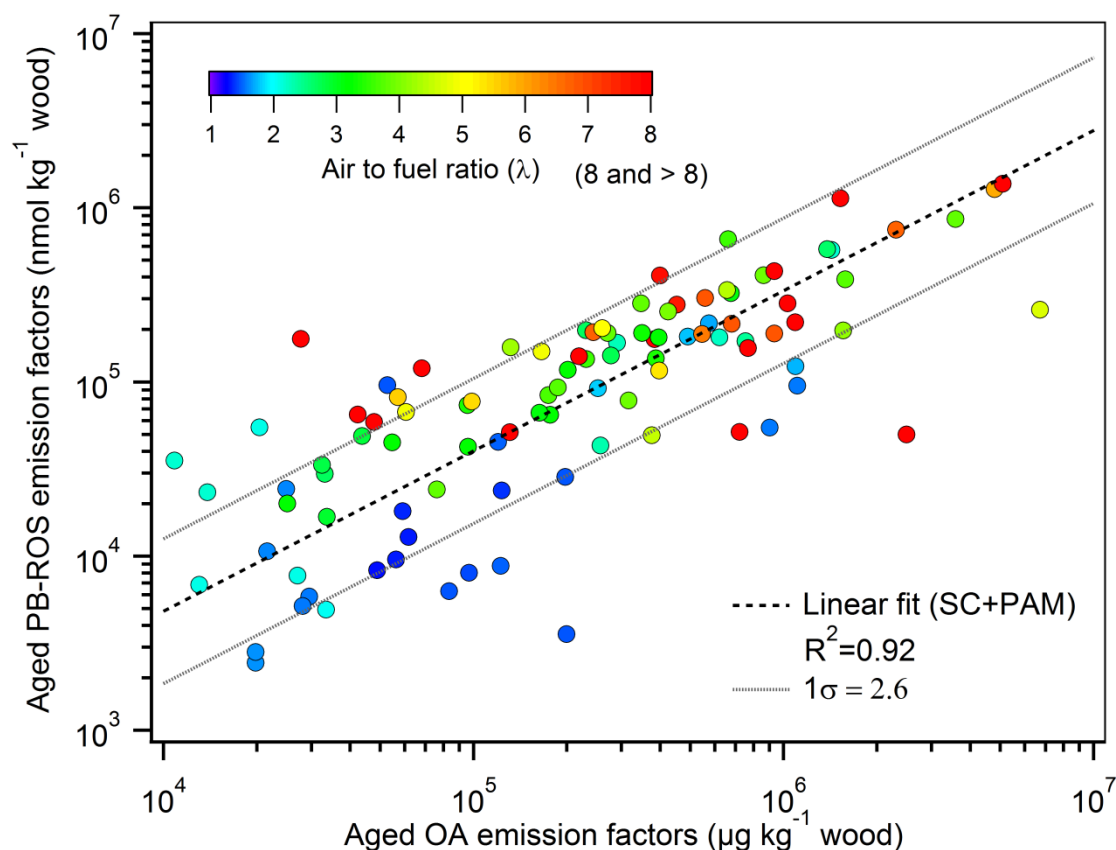
Figure 4.3 Aged ROS emission factors vs. aged OA emission factors. Marker color correspond to the air to fuel ratio (λ). The fitting equation: $\log_{10}(EF_{ROS}) = 0.92\log_{10}(EF_{OA})$ indicating that the relationship between aged ROS and aged OA is almost linear. The geometric standard deviation obtained from the fit is 2.6, suggesting that the aged ROS content of aged OA may vary significantly depending on the combustion and atmospheric aging conditions.

4.3.3   Influence of aging conditions on PB-ROS formation
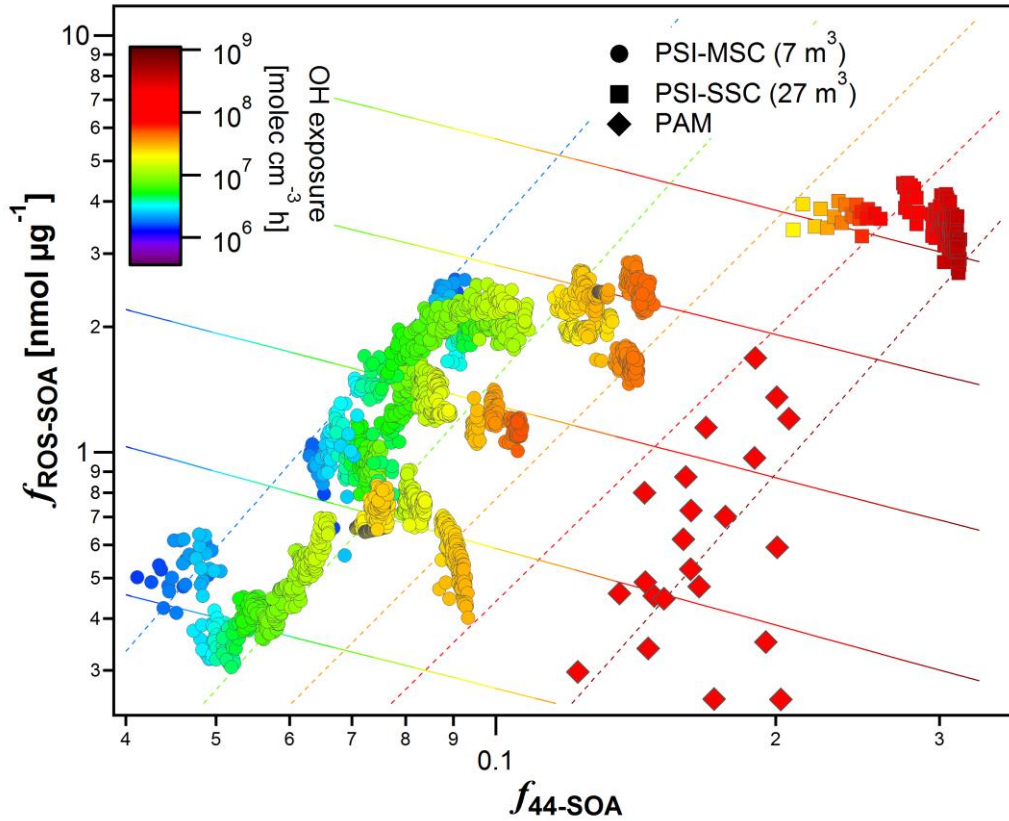
Figure 4.4 Variation of the fraction of ROS in SOA, $f_{ROS\text{-}SOA}$, with the fraction of *m/z* 44 in the total signal SOA as measured by the AMS ($f_{44\text{-}SOA}$) color coded with the OH exposure estimated from the decay of d9-butanol measured by the PTR-ToF-MS. Data are collected from two different smog chambers (SC) and from the PAM chamber. Dashed lines are isopleths of constant OH exposures, while solid lines are obtained by isolating the effect of OH exposure from other variables. To help discerning different experiments performed in SC, the same content in this figure is plotted again in Fig. B.3, where those SC experiments are labeled by different numbers.

Regression model setup and performance. In this section, we seek to evaluate the relationship between the fraction of PB-ROS in SOA, $f_{ROS\text{-}SOA}$, and parameters controlling its formation. To exclude the influence of the combustion devices, the data obtained using the LWS4 in the SC experiments and using LWS3 in the PAM chamber experiments was chosen for the analysis, as LWS3 and LWS4 are both conventional single-stage combustion devices. Four different parameters were investigated, including $f_{43\text{-}SOA}$ and $f_{44\text{-}SOA}$, the OH exposure, and the organic aerosol mass, by running the regression model as follows:

$$f_{ROS-SOA} = a \times SOA + b \times f_{44-SOA} + c \times f_{43-SOA} + d \times (OH\ exposure) + intercept \ , \qquad (4.6)$$

where $f_{43\text{-}SOA}$ and $f_{44\text{-}SOA}$ are supposed to represent the contributions of moderately oxygenated components (e.g. alcohols and carbonyls) and highly oxygenated components (e.g. carboxylic acids and peroxides), respectively. The organic aerosol mass may influence the fraction of PB-ROS in SOA, by affecting the amount of condensing semi-volatile species, which might be characterized by different $f_{ROS\text{-}SOA}$ compared to low-volatility species dominating at low organic aerosol mass. The aim of the

multiple regression analysis used here is to extract the influence of different aging factors on the observed variance in $f_{ROS-SOA}$ (the 2.6 factor variance described in Fig. 4.3), and to assess the magnitude of their influence. We do not, however, propose using the model and the model coefficients for a deterministic explanation of PB-ROS formation.

Since the dependent variable, $f_{ROS-SOA}$, and the predictors considered are log-normally distributed – typical of concentrations and contributions –, we have log-transformed the data before the multiple regression analysis. We note though that this step did not influence the conclusions of the analysis, as a multi-linear model applied to the raw data without a prior log-transformation suggests a similar relationship between $f_{ROS-SOA}$ and the predictors. Both models reasonably represented the measurements (~ 20 % error, Fig. B.4), but log-transforming the data allowed for a better capturing of lower $f_{ROS-SOA}$ and a less skewed distribution of the model residuals (Fig. B.4). We did not consider any interactions between the different regressors, as this is taken into account through the prior log-transformation of the data. For the parameterization, we only considered the SC data and will discuss whether the PAM chamber data could be satisfactorily explained by the same parameterization or whether the amount of PB-ROS formed under different conditions, with high OH concentrations in the PAM chamber, is different.

We note that the different predictors exhibit some degree of collinearity. For example, not unexpectedly, f_{44-SOA} significantly increases with aging (R^2 between f_{44-SOA} and OH exposure = 0.68), while f_{43-SOA} increases with the amount of organic aerosol in the smog chamber ($R^2 = 0.56$), possibly due to the enhanced partitioning of the moderately oxygenated organic species at higher absorptive mass (Pfaffenberger et al., 2013). Both variables, f_{44-SOA} and f_{43-SOA}, are slightly inversely correlated ($R^2 = 0.26$). Therefore, prior to the regression analysis we inspected the severity of multicollinearity by computing the variance inflation factors (VIF) for all four predictors. All VIF values were between 2.5 and 6 (highest for f_{44}-SOA and for OH exposure), indicating a moderate degree of multicollinearity (VIF values above 10 would be related to excessive multicollinearity). While a direct consequence of multicollinearity is an increased probability of erroneously rejecting the dependence of $f_{ROS-SOA}$ on one of the factors, a type two error, the regression analysis suggests that the dependence of $f_{ROS-SOA}$ on all parameters is significant ($p < 10^{-6}$).

Model results for SC data. The correlation between $f_{ROS-SOA}$ and the most important regressors is shown in Fig. 4.4. The analysis suggests that the greatest share of explained variability in $f_{ROS-SOA}$ could be attributed to f_{44-SOA}. An increase in f_{44}-SOA by 1 geometric standard deviation (a factor of 1.45) resulted in our case in a doubling of the secondary PB-ROS fraction ($f_{ROS-SOA}$). This indicates that more oxygenated compounds are preferentially PB-ROS active compared to others.

The second most important parameter controlling the secondary aerosol PB-ROS content under our conditions is found to be the OH exposure. An increase in OH exposure by 1 geometric standard deviation (a factor of 2.7) resulted in our case in a 60 % decrease of the PB-ROS fraction in SOA ($f_{ROS-SOA}$). We note that the considerable effect size of this variable stems from its large variability, spanning a dynamic range of 2.5 orders of magnitude (e.g., ~ 4 times more variation in OH exposure compared to f_{44-SOA} would be required to achieve the same effect on $f_{ROS-SOA}$). The anti-correlation between OH exposure and $f_{ROS-SOA}$ indicates that the initially formed PB-ROS are prone to further reactions,

consistent with previous observations of rapid peroxide (Krapf et al., 2016) and PB-ROS (Zhou et al., 2018a) decay. The mechanism by which PB-ROS evolves remains uncertain, but may involve the oxidation of PB-ROS-related molecules by OH as well as their photolysis and unimolecular decay reaction. We note that the OH exposure increases the oxidation state of the aerosol, here represented by $f_{44\text{-SOA}}$, thereby indirectly increasing the PB-ROS content, especially in the beginning of the experiment. Therefore, the actual effect of OH exposure on $f_{\text{ROS-SOA}}$ could only be revealed when it was isolated from the $f_{44\text{-SOA}}$ effect (see Fig. 4.4).

The analysis suggests that $f_{43\text{-SOA}}$ and the organic mass concentrations exhibit a low, but statistically significant, effect on $f_{\text{ROS-SOA}}$ (Fig. B.5). Their increase results in a decrease in the secondary PB-ROS content, consistent with the increased partitioning of moderately oxygenated components, which seem to contain less PB-ROS.

Comparison between SC and PAM chamber data. The conditions in the PAM chamber are different from those in the SC. PAM chamber experiments were conducted at high OH exposures of $\sim10^8$ molecules cm^{-3} h, where the resulting aerosol was highly oxygenated. However, the secondary PB-ROS content of the aerosol in the PAM chamber was largely within the expected range, following consistent trends with high OH exposures and high $f_{44\text{-SOA}}$ as in the SC (Fig. 4.4). We examined in more detail whether the regression model parameters obtained from the SC could faithfully represent the $f_{\text{ROS-SOA}}$ measured in the PAM chamber. Indeed, the model was capable of predicting, within uncertainties (2σ), the $f_{\text{ROS-SOA}}$ measured in the PAM chamber for low organic aerosol concentrations (average 21 µg m^{-3}), but considerably (factor of 3 on average) overestimated $f_{\text{ROS-SOA}}$ at higher concentrations (average 68 µg m^{-3}). This is because such a range of concentrations at high OH exposures and high $f_{44\text{-SOA}}$ was not included in the training dataset, and as a result the model slightly underestimated the effect of OA concentration on $f_{\text{ROS-SOA}}$ (e.g., a three-fold increase in OA concentration in the PAM chamber results in a decrease of $f_{\text{ROS-SOA}}$ by 45 %, while the model suggests that the same increase would only result in a 10 % decrease). Despite this, for similar conditions $f_{\text{ROS-SOA}}$ measured in the PAM chamber and the SC were similar within our uncertainties. We also note that this slight bias does not affect the main conclusions of the analysis: the secondary PB-ROS content seems to initially increase with the SOA oxidation state, which increases with OH exposure and decreases with the additional partitioning of semi-volatile components with lower secondary PB-ROS content at higher SOA concentrations, while further aging seems to result in a decay of PB-ROS.

4.4 Summary and Conclusions

In this study, eight wood combustion devices for log wood, pellets, and wood chips, denoted as log wood boiler (LWB), log wood stove 1 (LWS1), log wood stove 2 (LWS2), log wood stove 3 (LWS3), log wood stove 4 (LWS4), pellet boiler (PB), pellet stove (PS), and moving grate boiler (MGB), were tested. Experiments were conducted in a suite of aging tools, including the Paul Scherrer Institute mobile smog chamber (PSI-MSC, ~ 7 m^3, OH exposure: (2.6-4.8)$\times10^7$ molec cm^{-3} h), the Paul Scherrer Institute stationary smog chamber (PSI-SSC, 27 m^3, OH exposure: (0.13-40)$\times10^7$ molec cm^{-3} h), and the potential aerosol mass chamber (PAM chamber, OH exposure: (11-20)$\times10^7$ molec cm^{-3} h), to investigate

the particle-bound reactive oxygen species (PB-ROS) formation potential of primary and aged wood combustion emissions from different combustion devices and conditions. The influence of combustion technologies, wood types (wood logs, wood pellets and wood chips), operation type (e.g. with/without ESP, automatic vs. manual operation), combustion regime (different air-to fuel-ratio (λ) ranging from low (λ^-), optimum (λ^{opt}), to high values (λ^{++})), combustion phases (start, flaming, burn-out) and aging conditions (SC aging/PAM chamber aging) on PB-ROS emission factors (EF$_{ROS}$) were investigated. Results show that EF$_{ROS}$ for primary and aged OA were highly variable depending on the combustion conditions and devices. For all devices and combustion conditions, EF$_{ROS}$ substantially increased upon aging, indicating the secondary production of PB-ROS. The PB-ROS enhancement factors ranged between 4 and 20, with lower values for the MGB (~ 4) and PB under λ^{opt} combustion conditions (~ 6), and higher values for the PB under λ^- and λ^{++} combustion conditions (> 10). The PB-ROS enhancement factors for all log wood stoves and the LWB were comparable, with an average value around 10.

The variability in the EF$_{ROS}$ in primary and aged OA for a single device was much higher than the variability between emission factors from different devices. A part of this variability within each device could be ascribed to the combustion phase, with higher emission factors for the starting and burn-out phases compared to the flaming phase. This was especially true for the aged emissions from the PS, LWS2, and LWS3. Despite this, EF$_{ROS}$ values from the PB and MGB were on average 1 order of magnitude lower than those from the PS, LWB, and LWS1-4. This indicates that applying automatic combustion devices operated at optimum conditions, to achieve near-complete combustion, is most effective at minimizing PB-ROS, in addition to those of POA, SOA, and BC. Although the EF$_{ROS}$ showed somewhat different trends between devices with varying λ, a clear increase of EF$_{ROS}$ in the aged aerosol can be observed from optimal to high lambda values, emphasizing the important influence of the combustion conditions on EF$_{ROS}$. For the PB, the EF$_{ROS}$ under λ^{opt} ($\lambda = 1.6$) did not statistically differ from that under λ^- ($\lambda \approx 1.3$) conditions for both primary and secondary emissions (Mann–Whitney, p value = 0.43 and 0.20, respectively). When comparing the EF$_{ROS}$ under λ^{opt} and λ^- conditions with λ^{++} (2.7 < λ < 3.4) conditions, primary EF$_{ROS}$ values under λ^{opt} and λ^- conditions were on average 3 and 7 times lower than those obtained under λ^{++} conditions, respectively (Mann–Whitney, p value < 0.005 for both cases). Aged EF$_{ROS}$ values under λ^{opt} and λ^- conditions were on average 8 and 5.5 times lower than those obtained under λ^{++} conditions, respectively (Mann–Whitney, p value = 0.02 for both cases). In the MGB all the burns occurred at 2.0 < λ < 2.2, leading to EF$_{ROS}$ in line with those from the PB between λ^{opt} ($\lambda = 1.6$) and λ^{++} (where λ ranged from 2.7 to 3.4). The combustion in all stoves (PS, LWS1-4) exhibited higher λ (λ > 2.2) due to a less controlled air supply leading to a lower combustion temperature and increased products of incomplete combustion (less efficient combustion). In this range of oxygen excess, all aged EF$_{ROS}$ were high but without any systematic trend with λ, suggesting that other parameters also influence PB-ROS emissions. We further revealed that this variability was related to the bulk OA emissions, implying that this variation is inherent to the combustion conditions.

Nonetheless, the PB-ROS content still varied by a factor of 2.6 on average for the same OA emission factor (EF$_{OA}$). We used a regression model on the data of SC and PAM chamber aging experiments to identify the different parameters that control the PB-ROS secondary formation and content in OA upon aging. This regression model showed that the PB-ROS contents in SOA (represented as $f_{ROS\text{-}SOA}$)

depends significantly on all the aging parameters investigated, including the fractions of m/z 44 and m/z 43 in SOA, $f_{44\text{-SOA}}$ and $f_{43\text{-SOA}}$, respectively, the OH exposure and the organic aerosol mass concentration. The greatest share of explained variability in $f_{\text{ROS-SOA}}$ was attributed to $f_{44\text{-SOA}}$, which indicates that the more oxygenated compounds are preferentially PB-ROS active compared to others. The OH exposure was the second most important parameter controlling the aerosol PB-ROS content under our conditions where the anti-correlation between OH exposure and $f_{\text{ROS-SOA}}$ indicated that initially formed PB-ROS are prone to further reactions. The organic mass and $f_{43\text{-SOA}}$ exhibited a small, but statistically significant effect on $f_{\text{ROS-SOA}}$. In summary, the PB-ROS content seems to increase with the SOA oxidation state, which increases with OH exposure and decreases with the additional

partitioning of semi-volatile components with lower PB-ROS content at higher OA concentrations, while further aging seems to result in a decay of PB-ROS. The comparison and evolution of PB-ROS with different combustion and aging conditions in this study could eventually provide a speedy assessment of potential health risks of wood combustion emissions from different combustion and aging conditions. However, a link between PB-ROS as measured with the DCFH method and oxidative stress in cell cultures and health effects still needs to be established.

Acknowledgements

5

The evolution of particle-bound reactive oxygen species (PB-ROS) in the primary and aged aerosols emitted from Chinese residential coal combustion

J. Zhou[1], S.M. Pieber[1], J. G. Slowik[1], I. EI Haddad[1], G. Stefenelli[1], R. Huang[1,2], A.S.H. Prevot[1],

U. Baltensperger[1] & J. Dommen[1]

[1]Laboratory of Atmospheric Chemistry, Paul Scherrer Institute, 5232, Villigen, Switzerland

[2]Institute of Earth Environment, Chinese Academy of Sciences, Xi'an, 710061, China

Abstract: Residential heating with coal is an important source of pollution in China. Here, we investigated particle-bound reactive oxygen species (PB-ROS) emissions of five types of coal used in residual heating in China. Those coals were collected from different regions in China and combusted in a conventional Chinese household cook stove, including three types of Chinese bituminous coal and two types of Chinese anthracite coal. The atmospheric aging of the emissions was simulated in the Paul Scherrer Institute Mobile Smog Chamber (PSI-MSC). PB-ROS was quantified by an on-line ROS analyzer based on the 2',7'-dichlorofluorescin (DCFH) assay. The chemical characterization of the aerosols was done with an Aerodyne high resolution time-of-flight aerosol mass spectrometer (HR-TOF-AMS) and an Aethalometer. The primary PB-ROS emission factors (EF_{ROS}) of the three types of bituminous coal were not statistically different. Primary EF_{ROS} of the two types of anthracite coal were not detectable. The EF_{ROS} of the bituminous coals were increased upon aging, and their secondary EF_{ROS} were ~ 7 times higher than of the anthracite coal, indicating the importance of the type of coal used for the combustion. The primary EF_{ROS} from the wood combustion were significantly higher than those of the bituminous coal, while the aged EF_{ROS} from wood combustion were on average comparable to those from bituminous coal, indicating the equal or higher capacity of the particle borne components to act as ROS of wood combustions emissions compare to the coal combustion emissions, depending on the types of coal used. For all three types of bituminous coal, variable $f_{ROS-SOA}$ were observed under the same OH exposure, which is then dominated by the OA loading: $f_{ROS-SOA}$ was higher at lower SOA loading when considering each individual type of coal. Results provide the first evidence of PB-ROS emissions from residential coal combustion used in China, thus can benefit for Chinese policy making and further toxicological studies of residential coal combustion emissions.

5.1 Introduction

Particulate pollution is a serious environmental problem which influences air quality in China nowadays. Huang et al. (2014) found that severe haze pollution events in China are driven to a large extent by secondary aerosol formation, of which the organic-rich fraction correlates with the aggregate primary emissions from traffic, coal burning, biomass burning and cooking. Li et al. (2012) revealed that residential coal combustion constituents are an important source of air pollution. A relatively high contribution in Beijing and Xi'an can be attributed to coal burning due to its extensive use in residential heating in northern and western China (Elser et al., 2016). Coal combustion, as one of the most important energy source for producing electricity and heat, counts for one fourth of the total world energy consumption (IEO, 2006). In China, it accounts for about 70 % of the primary energy consumption (2003), mainly because residential heating and cooking is widely relying on coal (Geng et al., 2012). Coal combustion can result in emissions of sulfur and other toxic contaminants (WHO, 2015). Factors such as coal maturity, coal combustors or combustion conditions influence the emissions. Toxic components such as PAHs or trace metals (e.g. As, Se, Hg, Cr, Cd, Pb, Sb, Zn) are emitted from coal combustion and are usually present in the fine $PM_{2.5}$ fraction, thus making them deleterious to human health (Liu et al., 2008; Xu et al., 2011). Even with good combustion, those contaminants from coal combustion are not destroyed (WHO, 2015). Due to the very low-end technology of the coal combustion

stoves as well as the lack of treatment of the coal combustion emissions, residential coal combustion makes a large contribution to the deleterious air quality (Wu et al., 2006; Wang et al., 2009). Zhang and Tao (2009) revealed that coal combustion may contribute approximately 10.7 % of the total PAH emitted in China in 2004.

PM$_{2.5}$ emitted from coal combustion can decrease cell viability, increase global DNA methylation and cause oxidative DNA damage in human umbilical vein endothelial cells (Wang et al., 2016). As has been widely accepted, the dysfunctions of human body associated with PM exposures are due to the generation of reactive oxygen species (ROS), which will cause oxidative stress when its concentration overwhelm the antioxidants in the human body (Gurgueira et al., 2002; Nel et al., 1998; Tao et al., 2003). ROS denote chemically reactive molecules containing oxygen, e.g., OH and superoxide radicals, oxygen ions and peroxides (Sagai et al., 1993; Halliwell and Cross, 1994). In order to identify the potential adverse health effects of the coal combustion, in this study, the primary and secondary emissions from five types of Chinese residential coal were characterized by an online ROS analyzer based on the 2',7'-dichlorofluorescin (DCFH) assay coupled with an aerosol collector. The details of this method are described elsewhere (Zhou et al., 2018a).

The aim of this study is to make some fundamental experiments on the PB-ROS emissions of different types of coal that are currently used in different regions of China. Both bituminous coal and anthracite coal used in household stoves usually used by Chinese families were tested in this study. The experiments were conducted in the Paul Scherrer Institute Mobile Smog Chamber (PSI-MSC). The real-time evaluation of particle phase reactive oxygen species (ROS) emissions as well as of other chemical components from two different types of coal were conducted during simulated atmospheric aging. An inter-comparison of the PB-ROS emission factors of the different types of coal as well as of their association with the OA loading was done. Further, we investigated the influence of the different aging parameters to the PB-ROS formation upon aging, as well as the comparison of the PB-ROS emission factors of the coal and wood combustion. Results provided the first evidence of the PB-ROS emissions of the residential coal used in China. This fundamental research will be helpful for the air pollution control strategies in China.

5.2 Materials and methods

5.2.1 Experimental design and setup

A schematic drawing of the experimental system to characterize primary emissions and their ageing is shown in Fig. 5.1. We tested three types of Chinese bituminous coal (denoted B1-B3: from Ningxia (B1), Inner Mongolia (B2) and Yunnan (B3)) and two types of Chinese anthracite coal (denoted A1-A2: from Shanxi (A1) and Shaanxi (A2)), which were combusted in a conventional Chinese household cook stove. For each experiment, 100-300 g coal was pre-heated first by the hot honeycomb and anthracite coal until the temperature rose up to 200 $^{\circ}$C or 600 $^{\circ}$C, and then the emissions were injected into the Paul Scherrer Institute Mobile Smog Chamber (PSI-MSC) after dilution by a factor of 10-100 by the Dekati dilutor.
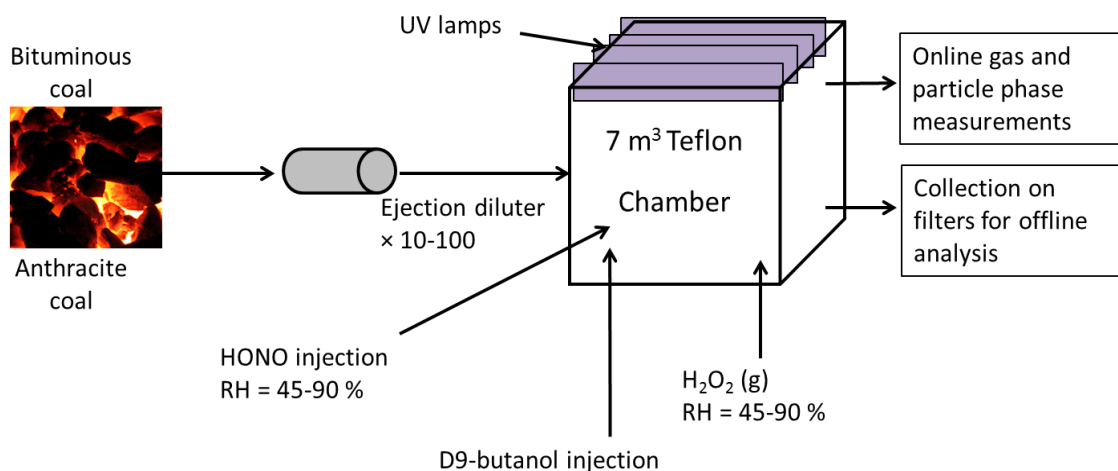
Figure 5.1 Schematic representation of the experimental setup.

The collapsible PSI mobile smog chamber (PSI-MSC) is a 7 m^3 (2.7×1.6×1.7 m, L×W×H) Teflon foil (125 μm thick, DuPont Teflon fluorocarbon film (FEP), type 500A, Foiltec GmbH, Germany). It is flanked by 4 sets of 10 UV lamps (90-100W, Cleo Performance, Philips) and is housed in a cooling trailer. The temperature can be actively controlled between -10 °C and +25 °C. Hydroxyl radicals (OH) are generated by photolysis of HONO, which is generated by the reaction of sodium nitrite and sulfuric acid (NaNO$_2$+H$_2$SO$_4$ → HONO +NaHSO$_4$) and continuously injected into the chamber. The OH exposures were estimated by monitoring the decay of d9-butanol (butanol-D9, 98%, Cambridge Isotope Laboratories) following a single injection before the UV lights were turned on. A suite of online instrumentation to characterize the chemical and physical properties was used to evaluate the oxidation processes, including the reactive oxygen species analyser (ROS), a high resolution time of flight aerosol mass spectrometer (HR-ToF-AMS), a proton transfer reaction-mass spectrometer (PTR-MS), a scanning mobility particle sizer (SMPS), a condensation particle counter (CPC) and an Aethalometer. The fuel elemental composition (C/H/N content) of the coal samples was measured by using an elemental analyzer. Pure air flushing started at the end of the experiments to minimize transport of products to the walls. Additionally, high concentrations of ozone (> 2 ppm) and humidified pure air were flushed into the chamber for at least 1 hours to facilitate cleaning of the bag walls with lights off, followed by flushing with dry, pure air for at least 10 h (Bruns et al., 2015), prior to the next experiment.

5.2.2 Instrumentation

ROS analyzer. The homemade reactive oxygen species (ROS) analyzer was employed to quantify the PB-ROS. Particles were collected at a flow rate of ~1.7 L min^{-1}, using an aerosol collector, of which the main part is the mist chamber (Takeuchi et al., 2005). Before the aerosol collector, a honeycomb charcoal denuder was installed inside a stainless steel tube to remove gas vapors. Oxygen-free ultra pure

water (OF-UPW) was used to extract the aerosol samples. This aqueous extract was then mixed with the reagent solution containing 2',7'-dichlorofluorescin (DCFH) and horseradish peroxidase (HRP). The reacted solution was then analyzed using a spectrofluorimeter with excitation and emission wavelengths of 470 nm and 520 nm, respectively. All the PB-ROS content in the particulate matters were calculated as H_2O_2 equivalents. More details are given in Zhou et al. (2018a).

HR-ToF-AMS. The non-refractory particle was quantified by a high resolution time-of-flight aerosol mass spectrometer (HR-ToF-AMS, Aerodyne) was equipped with a $PM_{2.5}$ aerodynamic inlet lens (DeCarlo et al., 2006; Williams et al., 2013).

Aethalometer. A 7-wavelength aethalometer was deployed to determine the concentration of equivalent and refractory black carbon (eBC, AE33, Magee Scientific).

Gas phase instruments. The evolution of several gas phase species was measured during the experiments. Carbon dioxide (CO_2) was measured using a differential, non-dispersive, infrared (NDIR) gas analyzer (LI-7000, Li-Cor Biosciences). Carbon monoxide (CO) was measured by an ultra-fast fluorescence analyzer (AL5002, Aero-laser GmbH).

CHNOS elemental analyzer. The elemental composition (C/H/N content) of the coal was measured by a Flash HT plus elemental analyzer (Thermo Fisher Scientific, USA).

5.2.3 Data analysis

Wall loss correction (WLC) As loss of particles to the chamber walls is one of the largest uncertainties in the simulation of atmospheric aging, it is necessary to determine the wall losses of the chemical components existing in the particle phase. The wall loss correction in the SC was done by assuming the same losses for all particle components as for the inert tracer eBC. The wall loss corrected concentration of OA or ROS (X) can be derived using Equation Eq. 5.1:

$$X_{WLC}(t) = X_{meas}(t) \times \frac{BC(t0)}{BC(t)} \tag{5.1}$$

where $X_{meas}(t)$ refers to the concentration of X measured at time t. BC (t_0) and BC (t) are the concentrations of BC when lights were switched on and at time t, respectively.

PB-ROS and OA emission factors The PB-ROS emission factors (EF_{ROS}) were calculated as the amount of ROS in mol H_2O_2-equivalents per kilogram coal burnt, using Eq. 5.2:

$$EF_{ROS} = \frac{n_{ROS}}{M_c}[C]_{coal} \cong \frac{[n_{ROS}]}{\Sigma([\rho C_{CO_2}] + [\rho C_{CO}] + [\rho C_{CH_4}] + [\rho C_{VOC}] + [\rho C_{eBC}] + [\rho C_{OC}])} C_{coal} \tag{5.2}$$

where $[n_{ROS}]$ is the wall loss and background-corrected concentration of PB-ROS (nmol m^{-3}) in the emitted particles either before (primary PB-ROS) or after aging (aged PB-ROS), $[\rho C_x]$ are the carbon mass concentrations calculated from the background-corrected, carbon-containing species where x includes CO_2, CO, CH_4, volatile organic compounds (VOC), eBC, and organic carbon (OC). M_C is the carbon mass burnt and C_{coal} represents the average carbon fraction of the coal fuel. The carbon content

(g C per g fuel) of B1-B3 and A1-A2 respectively was: B1 (0.71 ± 0.36), B2 (0.63 ± 0.10), B3 (0.72 ± 0.63) and A1 (0.78 ± 0.36), A2 (0.77 ± 0.71), measured in this study using an elemental analyzer. Similarly, the organic aerosol (OA) emission factors (EF$_{OA}$) were calculated by replacing the PB-ROS concentration by OA.

PB-ROS fraction. To study the PB-ROS formation during aging, the secondary PB-ROS fraction (ROS$_{SOA}$) is introduced. It expresses the amount of secondary PB-ROS (ROS$_S$ = aged ROS –primary ROS) per amount of secondary organic aerosol (SOA) formed during aging and as calculated from Eq. 5.3:

$$ROS_{SOA} = \frac{ROS_S}{SOA} \qquad (5.3)$$

Secondary organic aerosol (SOA) and secondary PB-ROS (ROSs) were calculated by subtracting primary organic aerosol (POA) and primary PB-ROS (ROSp) from the total OA and aged PB-ROS, respectively, assuming ROSp and POA to be only lost to the chamber wall at the same rate as eBC but otherwise to remain constant during aging. Although both quantities may not be conserved, a decrease of both does partially compensate in the PB-ROS fraction. In the SC experiments, POA is defined as the OA mass before lights on, while SOA is estimated as the difference between total OA and the time dependent POA mass accounting for particle wall loss. Wall loss rates for POA and SOA were assumed to be the same as that of the measured eBC.

$f_{44\text{-}SOA}$ and $f_{43\text{-}SOA}$. To express the degree of oxygenation of SOA, the fraction of secondary Org44 and Org43 in SOA (represented as $f_{44\text{-}SOA}$ and $f_{43\text{-}SOA}$) is introduced, which is calculated from Eq. (5.4)

$$f_{44-SOA} = \frac{Org_{44-SOA}}{SOA}; \; f_{43-SOA} = \frac{Org_{43-SOA}}{SOA} \qquad (5.4)$$

where Org_{44-SOA} is the difference of total Org44 and primary Org44, Org_{43-SOA} is the difference of total Org43 and primary Org43 and using the same procedure as for the SOA calculation mentioned above.

5.3 Results and discussion

5.3.1 PB-ROS and OA evolution during photochemical aging

The evolution of PB-ROS emitted from coal combustion upon aging is shown in Fig. 5.2 from one exemplary smog chamber aging experiment (non-wall loss corrected). Injection of the coal combustion emissions led to a primary organic aerosol (POA) concentration of 10.8 µg m^{-3} and 0.12 nmol m^{-3} of PB-ROS in the PSI-MSC. After the lights were switched on, secondary organic aerosol (SOA) was produced and total organic aerosol (OA) measured by AMS reached a maximum concentration one hour later, but then decreased because of higher wall loss than SOA production rate. The PB-ROS concentration increased concurrently with the increasing OA, indicating the formation of PB-ROS by photochemical reactions induced by OH radicals. When we sampled through a particle filter inserted upstream of the ROS online analyzer (pink areas), the ROS signal went to almost zero, which was considered as measurement base-line during aging (Fig. 5.2, Panel a).

To investigate the influence of aging on PB-ROS formation, SOA and secondary PB-ROS (ROS formed during aging, ROSs) were calculated by subtracting POA and primary PB-ROS from the total OA and total PB-ROS measured during lights on (Fig. 5.2, panel b), respectively. Here the POA and primary Pb-ROS calculation was based on the assumption that they were not further oxidized after lights on and the wall loss rate was the same as for the inert tracer black carbon (BC). $f_{ROS-SOA}$ was in the range of 0.12-0.64 nmol μg^{-1} within the oxidant OH exposure range of 0-37×10^6 molec m^{-3} h. Initially, aging resulted in an increase of the ROSs content in SOA, which then remained rather stable with increasing OH exposure (Fig. 5.2, Panel c).
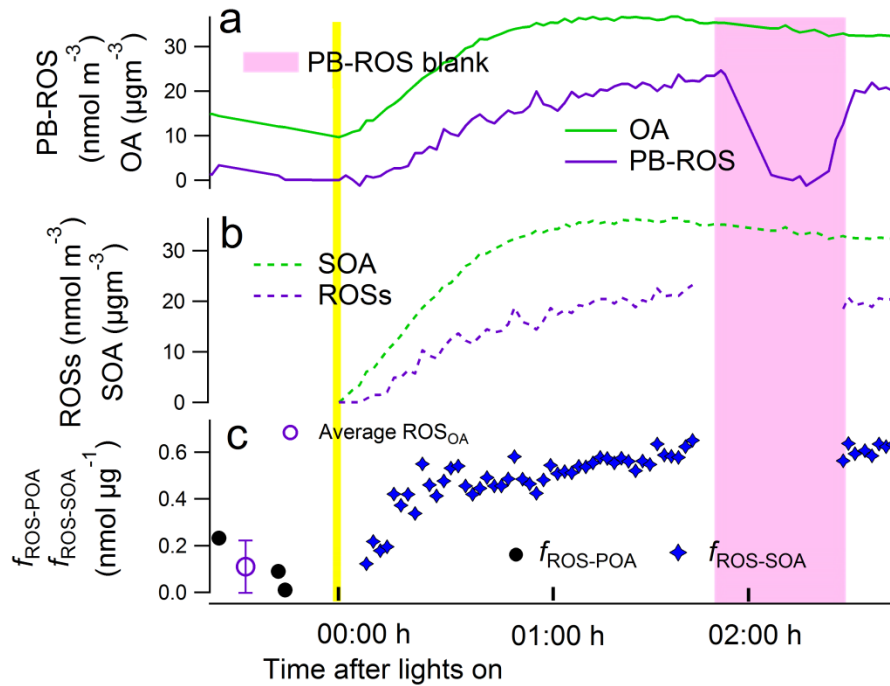
Figure 5.2 Evolution of the PB-ROS content in SOA during a coal burning smog chamber aging experiment. a) Total OA and ROS, b) SOA and ROS$_S$, c) ROS content in POA ($f_{ROS-POA}$, before lights on) and ROS$_S$ content in SOA ($f_{ROS-SOA}$, after lights on). The pink area represents the ROS blank measurement.

5.3.2 The primary and secondary PB-ROS emission factors (EF$_{ROS}$) during photochemical aging

Fig. 5.3 shows the evolution of the EF$_{ROS}$ of the different types of coal upon aging. No substantial amount of PB-ROS was measured in primary emissions from all the two types of bituminous coal. EF$_{ROS}$ for primary and aged aerosols were highly variable for different types of coal. The decrease of the primary EF$_{ROS}$ is due to the wall loss, as we applied wall loss correction only for aged EF$_{ROS}$. A substantial enhancement in the EF$_{ROS}$ was observed with aging, indicating the importance of secondary PB-ROS production. Aged EF$_{ROS}$ from the bituminous coal B1 (0.54 ± 0.46 mmol kg^{-1} coal), B2 (0.41 ± 0.38 mmol kg^{-1}) and B3 (0.45 ± 0.07 mmol kg^{-1}) were about a factor of two higher compared to the anthracite coal A1 (0.23 ± 0.14 mmol kg^{-1} coal) and A2 (0.24 ± 0.20 mmol kg^{-1} coal). Similarly, aged

organic aerosol emission factors (EF_{OA}) were on average 1115, 1610 and 1535 mg kg^{-1} for bituminous coal B1, B2 and B3, and on average 760 and 879 mg kg^{-1} for anthracite coal A1 and A2, respectively.
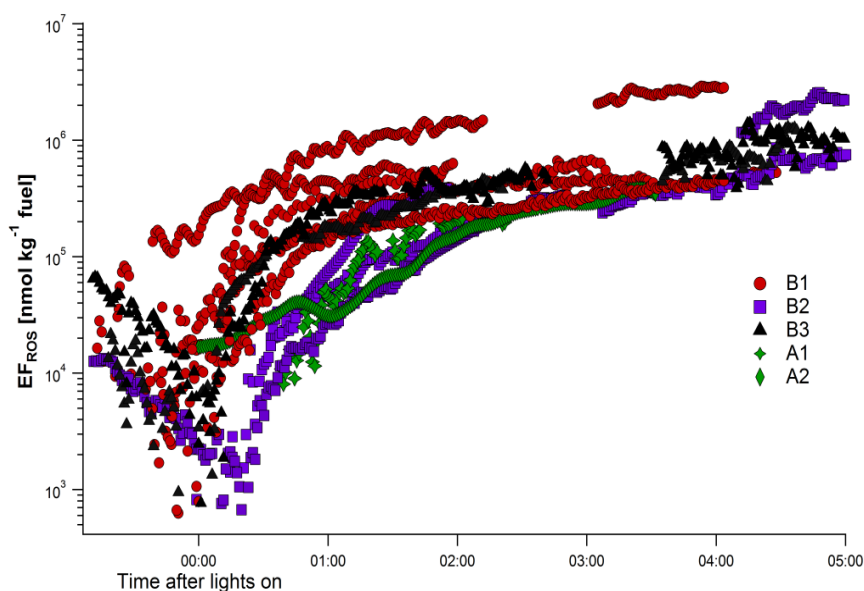
Figure 5.3 The PB-ROS emission factors of primary and aged aerosols emitted from the combustion of different types of coal.

5.3.3 Comparison of PB-ROS emission factors from coal and wood combustion

To compare the EF_{ROS} of coal combustion with those of wood combustion, we appended to the coal combustion emissions the EF_{ROS} of five wood combustion experiments which were also performed in PSI-MSC, they are presented as pink circles in Fig. 5.4. Details of those five wood combustion SC aging experiments are presented in Chapter 4 and Zhou et al. (2018b). The comparison shows that the primary EF_{ROS} from wood combustion were significantly (~ 2.5 times) higher than those from the bituminous coal (Mann-Whitney, p-value = 0.04). The secondary EF_{ROS} in wood combustion emissions on average were not statistically different from the bituminous coal (~ 1.9 times higher, but with Mann-Whitney p-value = 0.2), but ~ 7.4 times (significantly different, Mann-Whitney, p-value = 0.05) higher than anthracite coal emissions, respectively. This indicates equal or higher capability of the particle borne components to act as ROS of wood combustions compared to the coal combustion emissions, depending on the types of coal used.
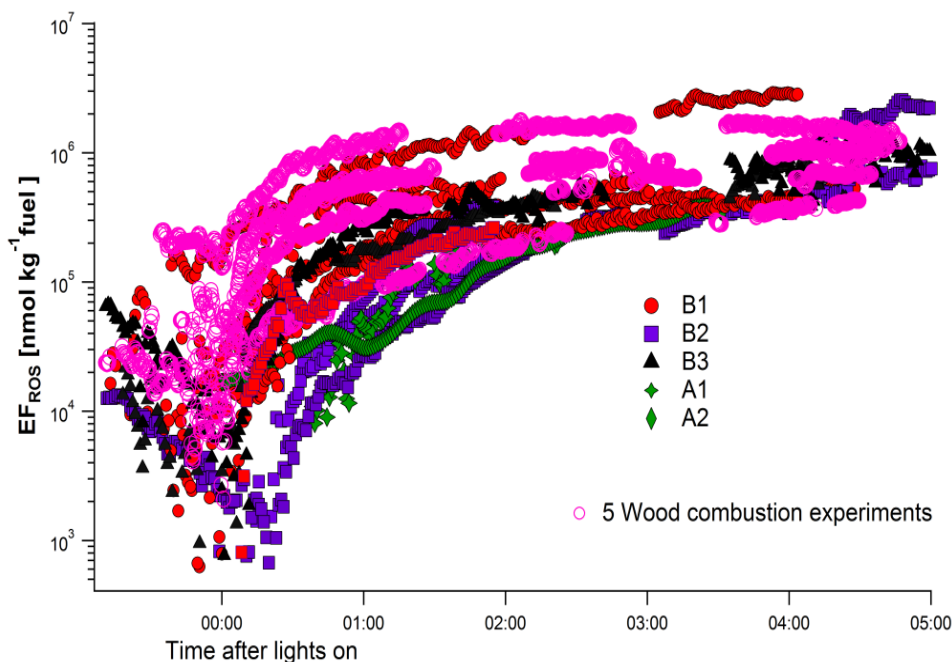
Figure 5.4 The PB-ROS emission factors (EF_{ROS}) of primary and aged aerosols (in nmol per kg of fuel) emitted from the combustion of different types of coal (solid symbols), as well as from the combustion of log wood (pink circles).

5.3.4 PB-ROS emission factors vs. OA emission factors

Further, we investigated whether the variability of emission factors from the different sources is related to the bulk OA emissions. EF_{ROS} were plotted as a function of EF_{OA} for both coal and wood combustion emissions in Fig. 5.5. Here we should note that the wood combustion data do not only include the five SC experiments described in Fig. 5.4, but also other experiments of wood combustion emissions aged in a PAM reactor, as described in Chapter 4. The dependence of PB-ROS and OA can be fitted relatively well by a linear relationships for both coal and wood combustion emissions. Linear fitting equations: wood: $\log_{10} (EF_{ROS}) = 0.92\log_{10} (EF_{OA})$; Coal: $\log_{10} (EF_{ROS}) = 0.93\log_{10} (EF_{OA})$, indicating that the relationship between PB-ROS and OA is almost linear for both coal and wood combustion. The geometric standard deviation obtained from the wood emissions fit is 2.6, for the coal emissions is 2.3, suggesting that the PB-ROS content of OA may vary significantly depending on the combustion and atmospheric aging conditions, in Chapter 4 we have investigated the reason of the variation of the wood combustion emissions. We noted that the variation of coal combustion is smaller than that of wood, may due to the smaller data set of coal combustion emissions and the use of only one aging tool (PSI-MSC) in coal combustion experiments compared to two aging tools in wood combustion experiments (PSI-MSC and PAM). To investigate the reason of the variation of the coal combustions, the influence of different parameters during aging on the PB-ROS content of OA is further investigated in the following.
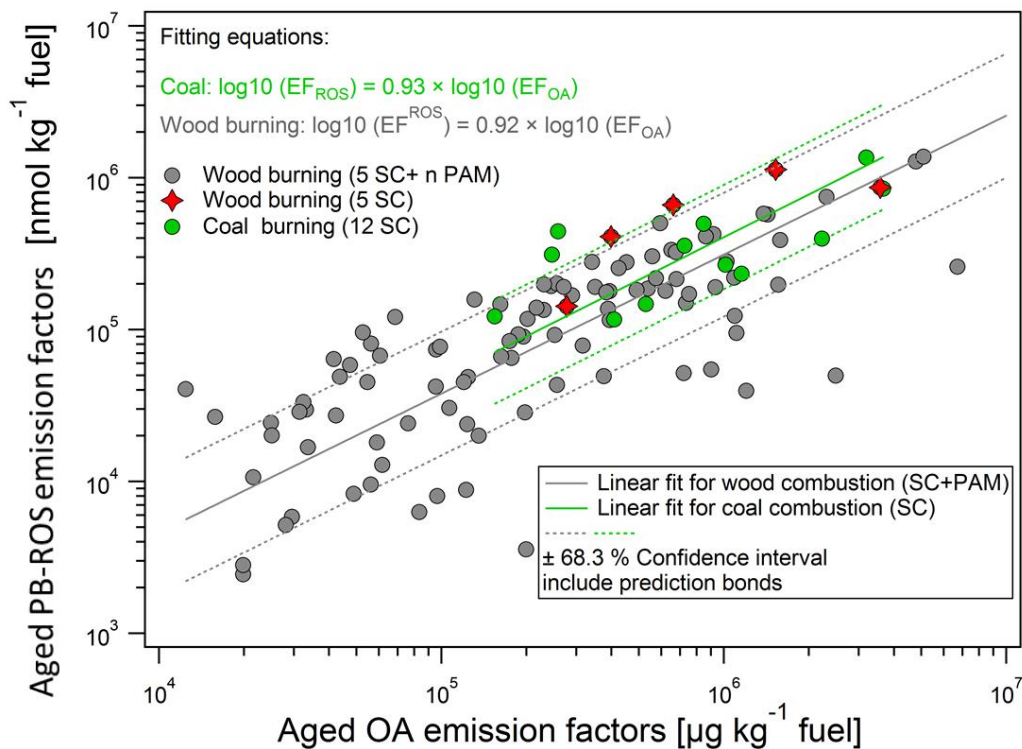
Figure 5.5 PB-ROS emission factors vs. OA emission factors of wood and coal combustions.

5.3.5 *ROS$_{SOA}$ evolution upon aging*

The evolution of $f_{ROS-SOA}$ upon aging is shown in Fig. 5.6. In general, ROS$_{SOA}$ substantially increased upon aging, after reaching its maximum it starts to decrease with even higher OH exposure. For each individual bituminous coal B1, B2 and B3, ROS$_{SOA}$ is higher with lower SOA loading. For the Anthracite coal A1 and A2, we have only 1 experiment for each, thus not possible to identify if they have the similar trend mentioned above. Under similar OH exposure, anthracite coal has a somewhat lower ROS$_{SOA}$ value for similar SOA loading of bituminous coal, indicating that the anthracite coal emitted aerosols with less ROS-containing SOA than bituminous coal upon aging.
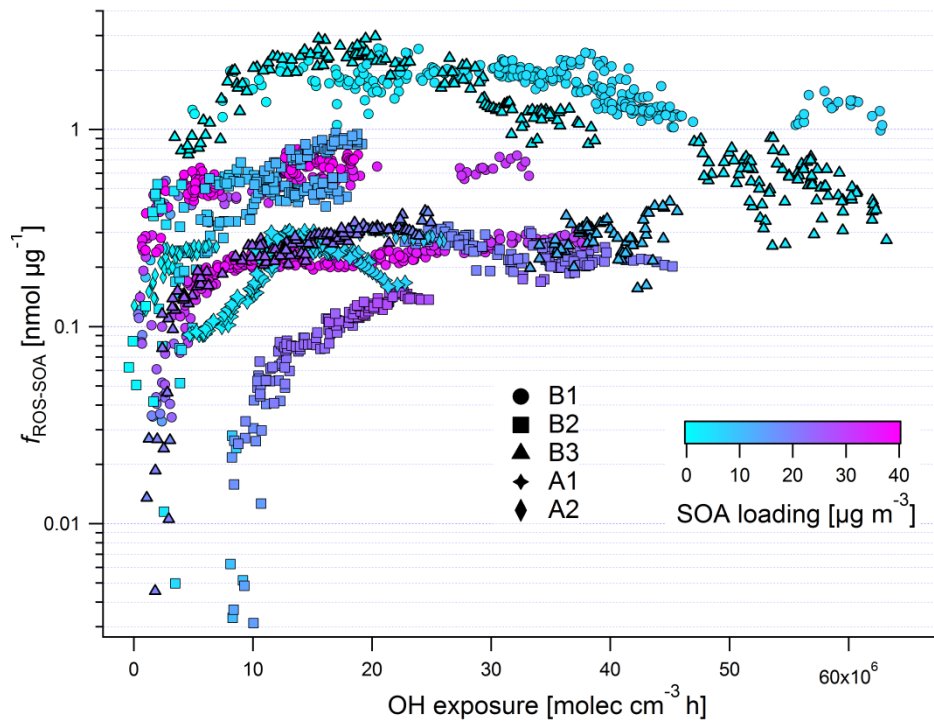
Figure 5.6 The evolution of $f_{\text{ROS-SOA}}$ upon aging, as a function of OH exposure. Symbols represent different types of coal from different places in China.

5.3.6 The influence of aging parameters to $f_{\text{ROS-SOA}}$

To elucidate the variation of the $f_{\text{ROS-SOA}}$ upon aging, we investigated the aging parameters that may influence the secondary ROS formation. We plot $f_{\text{ROS-SOA}}$ vs. $f_{\text{44-SOA}}$ v for each individual bituminous coal in Fig. 5.7a-c, and then all the types of coal together (Fig. 5.7d), and color coded with OH exposure. ROS$_{\text{SOA}}$ substantially increased upon aging. Under similar OH exposure and $f_{\text{44-SOA}}$, ROS$_{\text{SOA}}$ varies strongly able range within the same type of coal. Thus we also color coded those plots with the SOA loading (Fig. C.1), where they indicate that the variables are dominated by OA loading within one type of coal, e.g. the ROS$_{\text{SOA}}$ tend to be higher with lower OA loading.
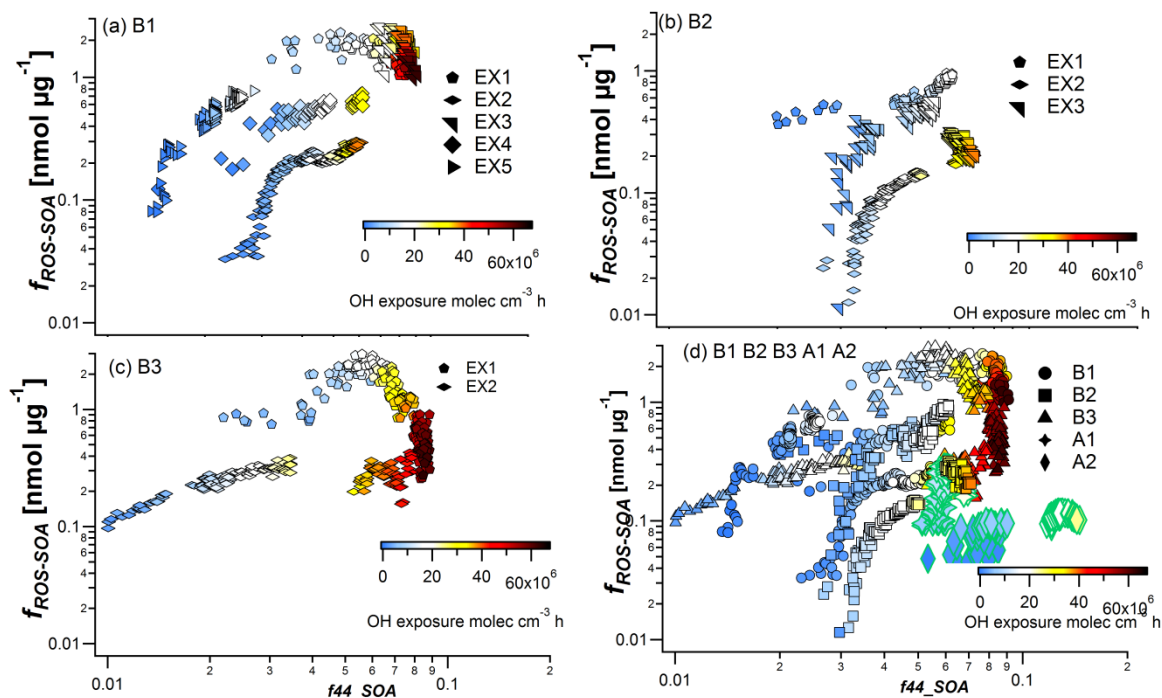
Figure 5.7 The correlation of $f_{ROS\text{-}SOA}$ with $f_{44\text{-}SOA}$ of SC aging of different types of coal. Data is color coded with OH exposure. The data points represent one minute average of the aging process.

5.4 Conclusions

The particle-bound reactive oxygen species (PB-ROS) emissions of five types of coal used in residual heating in China were investigated, including three types of Chinese bituminous coal (denoted B1-B3, from Ningxia (B1), Inner Mongolia (B2) and Yunnan (B3)) and two types of Chinese anthracite coal (denoted A1-A2, from Shanxi (A1) and Shaanxi (A2)). Notable emissions of PB-ROS of anthracite coal was only found in secondary particles. The primary EF_{ROS} of the three bituminous coal were not statistically different, while the aged EF_{ROS} of the bituminous coal were higher compared to the anthracite coal. When comparing the wood combustion emissions with coal combustion emissions, the primary EF_{ROS} of wood combustions were significantly higher than the bituminous coal. The aged EF_{ROS} in wood combustion emissions were not statistically different from bituminous coal, but much higher than in anthracite coal emissions, indicating the equal or higher particle borne components to act as ROS of wood combustions compared to the coal combustion emissions. The secondary PB-ROS fractions in secondary organic aerosol ($f_{ROS\text{-}SOA}$) were increased upon aging, after reaching the maximum, $f_{ROS\text{-}SOA}$ start to decrease with even higher OH exposure. When considering each individual type of bituminous coal, $f_{ROS\text{-}SOA}$ was higher with lower SOA loading. Under the same OH exposure, the $f_{44\text{-}SOA}$ of the coal emissions were quite similar, but with variable $f_{ROS\text{-}SOA}$, which was then dominated by the SOA loading. However, more parameters which might affect PB-ROS formation upon aging need to be investigated. Results in this study provide the first investigation of PB-ROS emissions of coal used in residential appliances in China, which can provide the evidence for the policy and facilitate toxicological studies of residential coal combustion emissions.

6

Large predominance of secondary organic aerosol to reactive oxygen species activity in fine aerosol

J. Zhou[1], M. Elser[1], R.-J. Huang[1,2], H. Ni[2], M. Krapf[1], R. Fröhlich[1], D. Bhattu[1], G. Stefenelli[1], P. Zotter[4], E. A. Bruns[1], S. M. Pieber[1], Q. Y. Wang[2], Y. Wang[2], Y. Zhou[2], C. Chen[5], M. Xiao[1], J. G. Slowik[1], S. Brown[1,6], L.-E. Cassagnes[1], K. R. Daellenbach[1], T. Nussbaumer[4], M. Geiser[3], A.S.H. Prévôt[1], I. El-Haddad[1], J.-J. Cao[2], U. Baltensperger[1] & J. Dommen[1]

[1]Laboratory of Atmospheric Chemistry, Paul Scherrer Institute, 5232, Villigen, Switzerland

[2]Institute of Earth Environment, Chinese Academy of Sciences, Xi'an, 710061, China

[3]Institute of Anatomy, University of Bern, 3012, Bern, Switzerland

[4]Bioenergy Research Group, Engineering and Architecture, Lucerne University of Applied Sciences and Arts, 6048, Horw, Switzerland

[5]CAS Key Laboratory for Biological Effects of Nanomaterials and Nanosafety, National Centre for Nanoscience and Technology, Beijing 100191, China

[6]Institute for Atmospheric and Climate Science, ETH, 8092, Zurich, Switzerland

Abstract. Reactive oxygen species (ROS) are believed to contribute to the adverse health effects of aerosols. This may happen by inhaled particle-bound (exogenic) ROS (PB-ROS) or by ROS formed within the respiratory tract by certain aerosol components (endogenic ROS). We investigated the chemical composition of aerosols and their exogenic ROS content at the two contrasting locations Beijing (China) and Bern (Switzerland). We apportioned the ambient organic aerosol to different sources and attributed the observed PB-ROS to them. The oxygenated organic aerosol (OOA, a proxy for secondary organic aerosol) explained the highest fraction of the ROS concentration variance at both locations. We also characterized primary and secondary aerosol emissions generated from different biogenic and anthropogenic sources. The PB-ROS content in the OOA from these emission sources was comparable to that in the ambient measurements, confirming the importance of the secondary organic aerosol for the PB-ROS level in the ambient atmosphere.

6.1 Introduction

Air pollution has been shown to adversely impact human health through cardiovascular and respiratory disorders, which may ultimately lead to a reduction in life expectancy (WHO, 2013a; Pope et al., 2009; Salvi, 2007; Guarnieri and Balmes, 2014; Du et al., 2016; Cohen, 2000; Johnson, 2004). Epidemiological estimates suggest more than four million premature deaths per year due to air pollution, with a significant fraction attributed to China and India (Cohen et al., 2017; Lelieveld, 2017). Such analysis is based on relations between total particulate air pollution and health effects to provide exposure-response functions. A significant correlation between fine particle mass concentration and excess mortality was reported in the nineties in the "Harvard Six-City" study (Dockery et al., 1993) and consistently confirmed later on (Laden et al., 2006; Lepeule et al., 2012; Beelen et al., 2014).

Since the composition of the atmospheric particulate matter (PM) depends on the sources and their chemical transformation in the atmosphere, an important question is which PM constituents are responsible for the adverse human health effects. Secondary sulfate, organic carbon (OC) and transition metals have been shown to be more prominently associated with adverse health outcomes than other pollutants (Lippmann et al., 2013; Adams et al., 2015; Vedal et al., 2013; Burnett et al., 2000), even though there is no toxicological evidence supporting a causal role (WHO, 2013b). It is generally anticipated that the adverse health effects caused by PM largely derive from oxidative stress induced by reactive oxygen species (ROS). The mechanism by which oxidative stress can be initiated is either through direct delivery of oxidants contained in PM (exogenous ROS) or by introduction of redox-active compounds which are able to generate ROS in lung cells (endogenous ROS). Different acellular assays have been explored to characterize the oxidant activity of PM. For instance, the 2′-7′-dichlorofluorescin (DCFH) and the p-hydroxyphenylacetic acid (POHPAA) assays respond to a range of organic peroxides (Venkatachari and Hopke, 2008; Wang et al., 2011b; King and Weber, 2013; S. J. Fuller et al., 2014; Zhou et al., 2018a; Hasson and Paulson, 2003; Venkatachari and Hopke, 2008) and are used to measure particle-bound ROS (PB-ROS). The dithiothreitol (DTT) assay is mainly sensitive to redox active components, i.e., transition metals and quinones and is considered as a good estimator of ROS generation in lung cells (Cho et al., 2005; Verma et al., 2012; Charrier and Anastasio, 2012; Fang et al.,

2016; Weber et al., 2018). The electron spin resonance (ESR) assay measures the capability of PM to induce hydroxyl radicals (Shi et al., 2003). Other assays measure the ability of PM to deplete biological antioxidants such as ascorbic acid (AA), glutathione and uric acid (Mudway et al., 2004; Fang et al., 2016). Since the different assays capture different fractions of the oxidant activity of PM, a direct comparison of measurements is challenging (Shiraiwa et al., 2017; Fang et al., 2016;Weber et al., 2018; Calas et al., 2018; Perrone et al., 2016; Yang et al., 2014; Janssen et al., 2015). Nonetheless, the ROS generation potential (referred to as oxidative potential, OP) determined using these assays was found to be more strongly associated with emergency department visits for airway and nasal inflammation, asthma, wheezing and congestive heart failure than $PM_{2.5}$ (PM with a partcle diameter smaller than 2.5 μm) (Bates et al., 2015; Fang et al., 2016; Janssen et al., 2015).

More detailed analyses revealed associations between health effects and specific sources of particulate matter , such as wildfires, traffic, shipping, construction dust, metals sources, coal and residual oil combustion (Liu et al., 2017; Ostro et al., 2011; Lippmann et al., 2013; Adam et al., 2015). To date, the emission sources governing ROS concentrations especially during haze episodes in developing and emerging countries are poorly constrained. Recent studies attributed the OP of ambient PM to different emission sources by applying source apportionment techniques like positive matrix factorization (PMF). Biomass burning and traffic contributed to the OP measured by DTT in most cases while contributions by secondary PM components like ammonium sulfate or the more-oxidized fraction of OA were only found in some studies (Verma et al., 2015; Fang et al., 2016; Bates et al., 2015; Weber et al., 2018). The OP measured by AA was found to correlate with Cu, secondary processes and traffic (Weber et al., 2018; Fang et al., 2016), but not with biomass burning. The overwhelming majority of these studies are based on offline measurements conducted in the US, which suffer from the inherent limitations related to filter sampling, including positive and negative artifacts and the loss of short-lived ROS during filter storage (Zhou et al., 2018a).

Here we systematically investigate the links between the chemical nature and sources of atmospheric aerosols and their PB-ROS content, by coupling aerosol mass spectrometry with online PB-ROS measurements and provide unprecedented insights into the sources of the reactive oxidants in PM. We cover for the first time the most important sources of $PM_{2.5}$ world-wide, by combining field data from two distinct environments, i.e., Beijing (China) and Bern (Switzerland), with results from comprehensive laboratory experiments, where we quantified the PB-ROS content in primary and secondary aerosols emitted from traffic, biomass burning, coal burning, and biogenic sources. We show that PB-ROS, a large fraction of which is not accessible by offline measurements, is generated in-situ in the atmosphere through oxidation processes.

6.2 Results

The measurements in the city of Bern were performed in November 2014 using a quadrupole aerosol chemical speciation monitor (Q-ACSM), an aethalometer, and a novel ROS analyzer. In Beijing a high-resolution time-of-flight aerosol mass spectrometer (HR-ToF-AMS), an aethalometer, and the ROS analyzer (see Methods section) were used. Visibility was determined by an Automatic Weather Station

(MAWS201, Vaisala, Vantaa, Finland) configured with a visibility sensor (Vaisala Model PWD22). Haze periods were defined by a visibility of less than 10 km while time periods with a visibility above 10 km were termed reference days (China Meteorological Administration, 2010). PB-ROS measurements were performed online with a DCFH assay at both locations.

6.2.1 Bulk chemical composition

Fig. 6.1a shows the average contributions of organic aerosol (OA), sulfate (SO4), nitrate (NO3), ammonium (NH_4), chloride (Cl), and equivalent black carbon (eBC) to $PM_{2.5}$ in Beijing in January-February 2015 (time series shown in Fig. D.1). During haze events, its sum, considered as a proxy for $PM_{2.5}$, exceeded occasionally values of 200 µg m^{-3} (average ~ 110 µg m^{-3}). On reference days the $PM_{2.5}$ concentration ranged from 4 to 140 µg m^{-3} with an average value of 28 µg m^{-3}. OA dominated in both haze and reference days, with a contribution of 49 ± 10% and 54 ± 8% to the total mass, respectively. As seen from the average diurnal patterns (Fig. D.2), OA, eBC and Cl increased during the night time of the haze days, while NO_3 exhibited a maximum in the afternoon during both haze and reference days. During reference days, OA additionally showed a significant afternoon peak concurrent with NO_3, possibly indicating additional secondary OA formation.
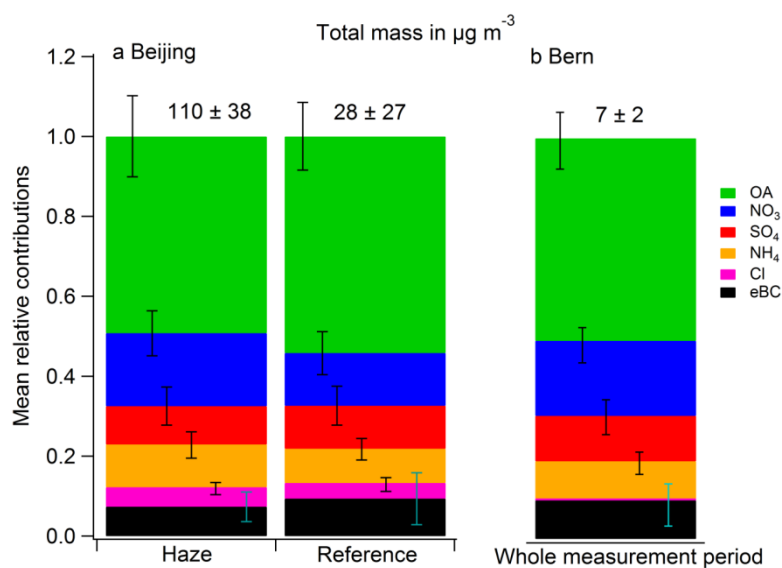
Figure 6.1 Total PM mass concentrations and relative contributions of non-refractory chemical components plus eBC in (a) Beijing ($PM_{2.5}$, January-February, 2015) and (b) Bern (PM_1, November, 2014).

The average concentrations of PM_1 in Bern were ~ 15 and ~ 4 times lower than in Beijing ($PM_{2.5}$) during haze and reference periods, respectively (Fig. 6.1b, note that PM_1 ~ 0.7 $PM_{2.5}$ in Bern). The relative contributions of the different chemical components in the aerosols from Bern were similar to those from Beijing, except for chloride which contributed much less to the total mass in Bern than in Beijing. This may be due to hydrogen chloride (HCl) and methyl chloride (CH_3Cl) emissions from combustion sources in Beijing, e.g. coal emissions, incinerators and other industrial sources (Huang et al., 2014; Elser et al., 2016; McCulloch et al., 1999; Yudovich and Ketris, 2006).

6.2.2 Reactive oxygen species & OA sources

PMF was applied to the organic aerosol mass spectra acquired by the ACSM and the AMS to extract the contributions of the different sources (see Methods). Advanced error analyses methodologies were deployed to assess the PMF model uncertainties (as shown in Elser et al. 2016). In Beijing, we identified four OA sources, including oxygenated OA (OOA), a combination of hydrocarbon-like OA from traffic and coal burning emissions (denoted HOA + CCOA), cooking OA (COA) and biomass burning OA (BBOA). In Bern, the optimal solution was a 5-factor solution, consisting of OOA, BBOA, HOA, COA and a fifth, yet unidentified factor (Fig. D.4). The time series of PB-ROS and the different identified source contributions are shown in Fig. 6. 2 while the spectral profiles of the OA components can be found in Fig. D.3.

The factors were initially identified using their mass spectral fingerprints, and their source assignments were confirmed based on the factor diurnal patterns and their correlation with corresponding marker time-series. The OOA profile was characterized by a dominant peak at m/z 44 and was associated with aged emissions and secondary organic aerosol formation. BBOA showed high contributions of m/z 29, m/z 60 ($C_2H_4O_2^+$), and m/z 73 ($C_3H_5O_2^+$), associated with cellulose pyrolysis products generated during biomass burning such as levoglucosan (Elser et al., 2016). The HOA+CCOA profile exhibited the typical fragmentation pattern of saturated and unsaturated hydrocarbons (Ng et al., 2011a). The COA profile was characterized by high signals at m/z 55 ($C_3H_3O^+$) (Crippa et al., 2013b).

The average diurnal patterns of the OA components during the measurement periods in Beijing and Bern are shown in Fig. D.5 and discussed below. To explore the correlations between the fine aerosol chemical species, OA sources, and PB-ROS (referred to as testing factors in the following), we calculated a Pearson correlation matrix from 1000 bootstrap tests of those testing factors in Beijing and Bern (see Methods section and Fig. D. 6).

Beijing. As shown in Fig. 2a, PB-ROS as well as all the other aerosol species exhibited a simultaneous increase during the haze periods. Most of the variables had a strong ($r \geq 0.7 \pm 0.04$) or moderate ($r \geq 0.5 \pm 0.05$) positive Pearson correlation (Fig. D.6a), which may be due to the influence of meteorological factors (Chen et al., 2017). HOA+CCOA correlated with eBC ($r = 0.78 \pm 0.04$), a tracer for traffic and coal combustion emissions. HOA+CCOA strongly decreased during noon, most likely due to a combined effect of decreased vehicular emissions (e.g. heavy-duty diesel vehicles are only allowed to operate from 2200 to 0600 LT) (Bureau, 2004; Lin et al., 2009) and an increase in the mixing height. COA showed clear peaks during lunch (from 1200 to 1300 LT) and dinner time (from 1800 to 2300 LT) in both haze and reference days, consistent with local emissions from cooking processes. During both episodes, BBOA contributed less than 10% to the total OA (8.9% and 6.6% during haze and reference episodes, respectively), with little diurnal variability. The secondary inorganic components of $PM_{2.5}$ (SO_4, NO_3, and NH_4, see Fig. D.2) followed the same trend as OOA, highlighting that these components were formed through atmospheric processes of precursors from the same emission regions, involving atmospheric oxidation of gaseous emissions. The PB-ROS concentration closely followed the trend of OOA with the highest average concentrations occurring during the afternoon and early night.
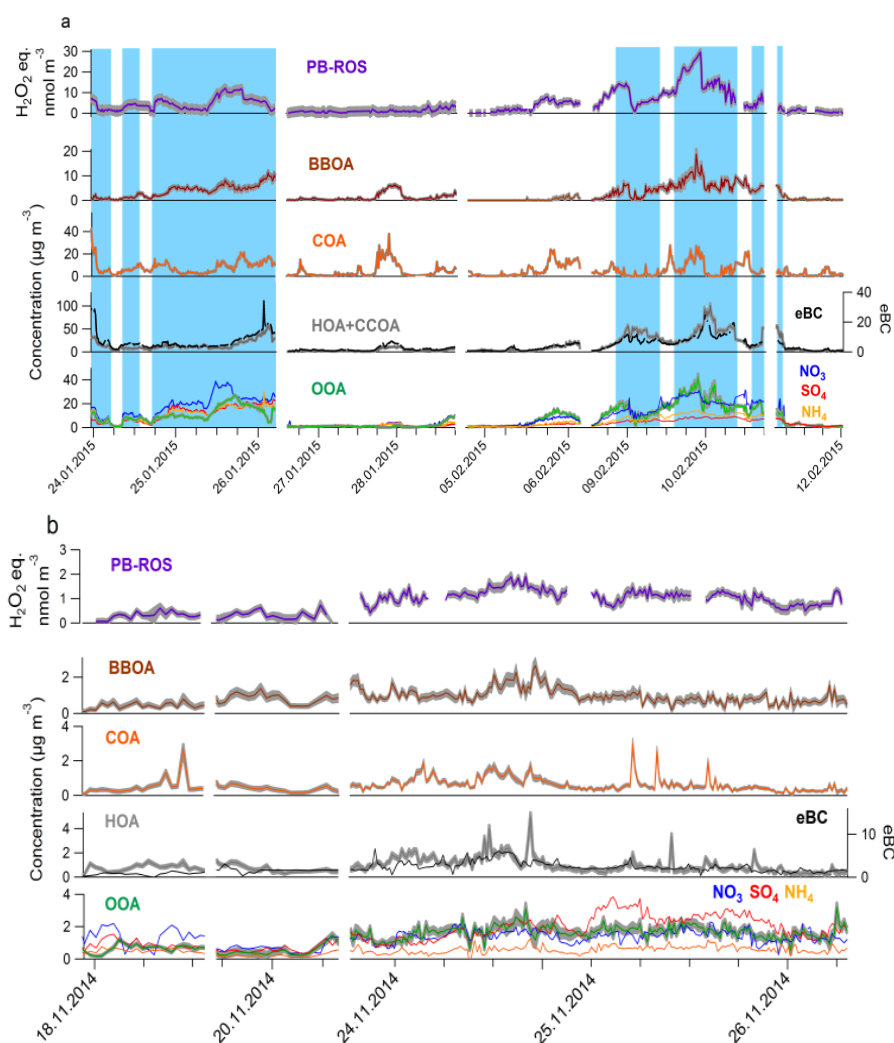
Figure 6.2 Concentrations of PB-ROS, OA components, and eBC during the measurement periods in (**a**) Beijing and (**b**) Bern. In Beijing, the periods highlighted with a blue background represent the haze periods (visibility < 10 km). The remaining periods were termed reference periods (visibility ≥ 10 km). The gray bands indicate 1σ errors of the PB-ROS measurements and of our best estimates of the factors.

Bern. In Bern, the Pearson correlation coefficients showed similar features, but were generally weaker than those in Beijing (see Methods section and Fig. D. 6b). The PB-ROS concentrations had moderate to high correlations with OA, SO_4, Cl, BBOA, eBC and OOA ($r \geq 0.5 \pm 0.04$), but weak ones with NO_3, NH_4, COA and HOA ($r \leq 0.5 \pm 0.04$). HOA increased during the day with a small peak during the morning rush hour (0800 LT), representing urban traffic behavior. COA was elevated from late morning to early afternoon and again in the evening, reflecting local cooking activities. BBOA showed a clear increase during night time, related to residential heating with wood, a well-known aerosol source in Bern (Zotter et al., 2014). We separated eBC into the fossil fuel (eBC_{TR}) and wood burning (eBC_{WB}) fractions according to the method described by Sandradewi et al. (2008) and Zotter et al. (2017). As shown in Fig. D. 5b, eBC_{WB} had the same diurnal trend as BBOA, characterized by higher night time values, while eBC_{TR} showed the opposite trend rather consistent with HOA, confirming the source

apportionment results. The secondary inorganic component SO_4 correlated with OOA similarly to Beijing (Fig. 6.2b). These secondary components dominated the PM burden, indicating the importance of atmospheric aging to the chemical composition of the aerosol. PB-ROS levels also followed OOA in Bern (Fig. D.5b), with no substantial diurnal trends, except for a slight increase during daytime.

It should be noted that these correlations are not necessarily causative relations. For example, the inorganic species NO_3, SO_4, NH_4 correlated with each other due to their photochemical production and ammonium salt formation. As we measured the water soluble PB-ROS concentration in the aerosol phase, eBC is not considered as a contributor to PB-ROS due to its water-insoluble character. Rather, the correlation of PB-ROS with eBC is a coincidence caused by the superposition of the two opposite trends of eBC_{WB} and eBC_{TR}. Also, our previous tests showed that inorganic components like NO_3 and SO_4 did not contribute to the PB-ROS signal in the DCFH assay (Zhou et al., 2018a). Thus, we conclude that the correlations of the secondary inorganics with PB-ROS are a coincidence due to the fact that both are influenced by the atmospheric aging.

6.2.3 Source contributions to PB-ROS

A multiple linear regression model (MLRM) was employed to identify the PB-ROS sources, combining the measured PB-ROS and the different OA sources determined by PMF, including HOA, COA, BBOA, and OOA in Bern and HOA+CCOA, COA, BBOA, and OOA in Beijing. The outcome of the model provides the PB-ROS content of the different OA components. The uncertainties related to the modeled PB-ROS content values and the sensitivity of the MLRM to the input data were thoroughly assessed (see Methods). The average regression coefficients obtained from MLRM associated with each independent variable are listed in Table S1. For a better overview, their distributions are illustrated as boxplots in Fig. S7.

The measured PB-ROS time series was fairly well captured by the model at both locations, with 61% of the variability explained in Bern and 77% in Beijing (Fig. 6.3 and Fig. 6.4). With OOA as the main parameter affecting ROS formation in both locations. In Beijing, the contributions of the primary OA sources to PB-ROS activity could not be retrieved within our uncertainties, when these sources were considered individually or lumped together. Additional MLRM runs were performed where the ratio between POA and OOA ROS contents was constrained based on chamber results (Fig. 6.5). Results show that the OOA ROS content is not sensitive to these constraints and suggest that the contribution of POA to the total PB-ROS activity in Beijing does not exceed 18%. OOA was also the highest contributor to the MLRM explained PB-ROS in Bern (contributing 52%), followed by contributions by BBOA (24%) and HOA (19%), and a small contribution by COA (5%). On average, OA and PB-ROS were driven by different emission sources (Fig. 6.4). For example in Beijing, even though the primary OA sources contributed ~ 70% to the total OA, their contribution to PB-ROS was much less significant.
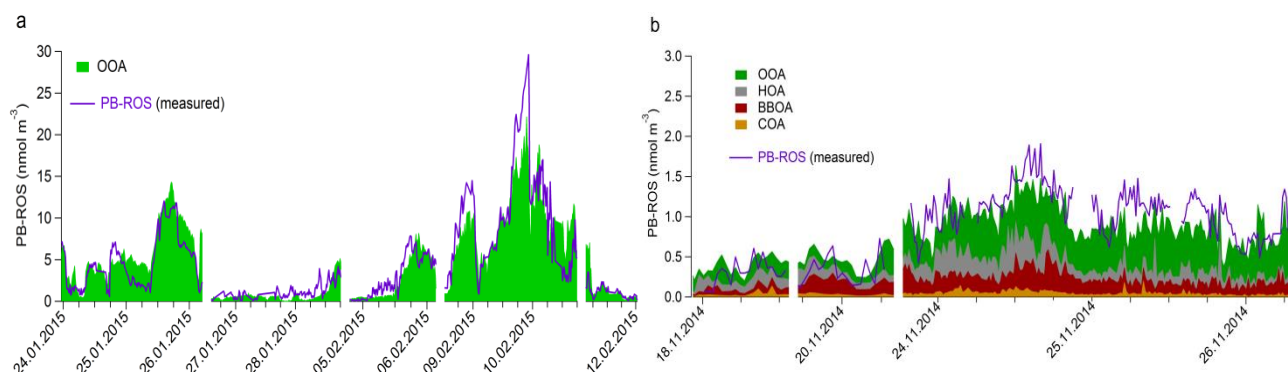
Figure 6.3 Comparison of measured and simulated ROS concentrations in (a) Beijing and (b) Bern with HOA, COA, BBOA and OOA representing their source contributions to the simulated PB-ROS activity.
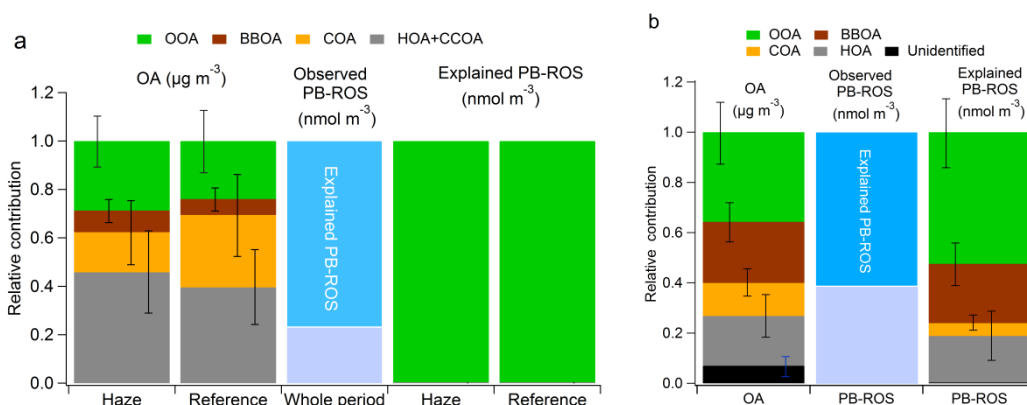
Figure 6.4 Average relative contributions of the OA sources to the observed total OA and to the explained PB-ROS by OA sources during the measurement period in (a) Beijing and (b) Bern. Data in Beijing are separated for haze and reference periods. The error bars represent the standard deviation of the mean of the whole measurement period.

6.2.4 Comparison of the ROS content of OA from different sources

Fig. 6.5 compiles online measurements of the ROS content in aerosols from various ambient and laboratory measurements performed in this study or taken from literature. Ambient measurements are presented as ROS content of the total collected aerosol mass ($PM_{2.5}$ in Beijing and PM_1 in Bern, denoted as ROS_{PMx}) or the organic aerosol (OA) fraction alone (ROS_{OA}). Our values for $ROS_{PM2.5}$ and ROS_{PM1} (0.07 ± 0.04, 0.09 ± 0.06, and 0.13 ± 0.06 nmol μg^{-1} for Beijing_Haze, Beijing_Reference, and Bern, respectively) are in line with the values reported by Huang et al. (2016) for Beijing (0.12 ± 0.05 and 0.10 ± 0.05 nmol μg^{-1} in Winter 2014 and Spring 2015, respectively). Fig. 6.5b indicates the PB-ROS contents attributed to different sources identified in Bern and Beijing, and Fig. 6.5c summarizes the PB-

ROS contents from our own laboratory measurements of different emission sources (see Methods section), complemented by literature values, i.e., 2-stroke scooter emissions (2s_scooter (Platt et al., 2014)), as well as SOA from limonene and oleic acid oxidation (Gallimore et al., 2017; S. J. Fuller et al., 2014). The PB-ROS contents in primary emissions (ROS_{POA}) from 2-stroke scooters or wood and coal burning are about 4 to 25 times lower than those in the corresponding SOA samples (ROS_{SOA}, see Methods section). Results are consistent with the field measurements, where the ROS content in OOA is 2-50 times higher than that in primary emission sources (more details are shown in Fig. D.7 and Table D1). Clearly, the PB-ROS content is enhanced by photochemical reactions, although the enhancement depends on the emitted precursors. We demonstrate that SOA from anthropogenic emissions (vehicular exhaust and coal and biomass burning) is related to at least a 10 fold higher ROS activity compared to biogenic SOA, from monoterpene precursors. Thus, despite the widespread dominance of biogenic SOA, especially during summer, SOA formed from anthropogenic precursors might dominate the PB-ROS burden in the atmosphere. Previously we have shown that the degree of oxygenation and the OA loading do influence the PB-ROS content of aerosols in a specific source (biomass burning) (Zhou et al., 2018b). However, Figure S9 shows that the averaged PB-ROS content in SOA from different emission sources does not significantly depend on these parameters in the given range but is more driven by the nature of the precursor, with aromatic VOCs yielding a much more ROS active aerosol compared to monoterpenes.
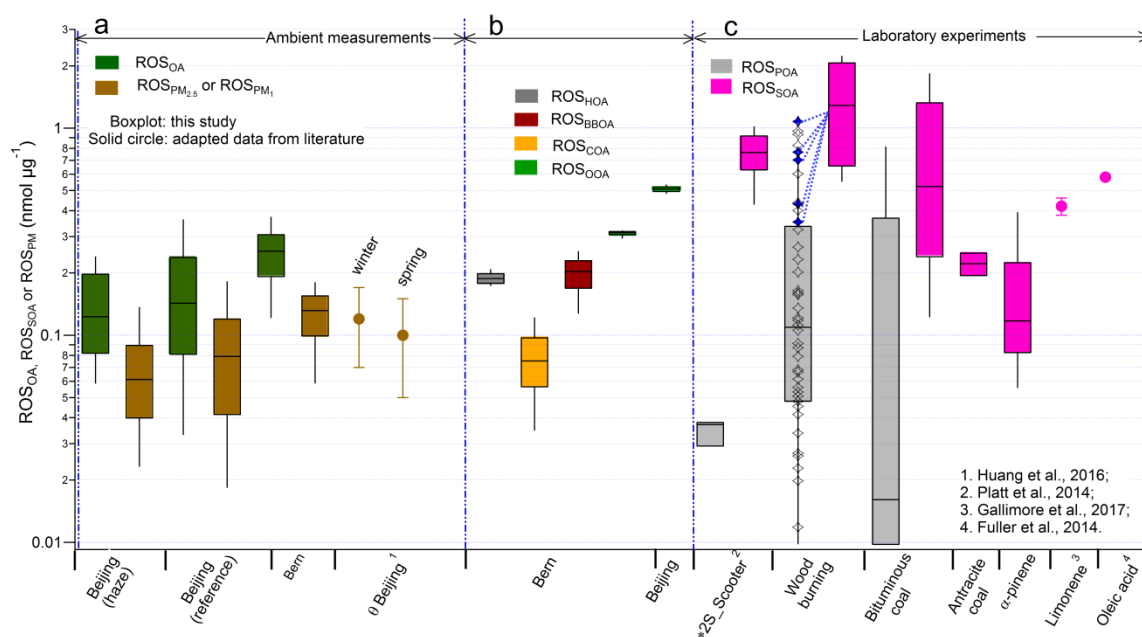
Figure 6.5 Comparison of the ROS content in aerosols from different sources (listed on the x-axis). (**a**) PB-ROS content in OA (ROS_{OA}) and PM ($ROS_{PM2.5}$ for Beijing and ROS_{PM1} for Bern) at ambient sites. For comparison, the ROS content for winter and spring in Beijing (represented as θ Beijing) is calculated from the ROS concentrations reported in the literature in equivalent nmol H_2O_2 per m^3 air and then normalized to $PM_{2.5}$ concentrations obtained from the U.S. Department of State(Embassy); (**b**) PB-ROS content of individual source factors in Bern); (**c**) PB-ROS contents in primary (ROS_{POA}) and secondary organic aerosol (ROS_{SOA}) from wood and coal burning), in SOA from α-pinene (this study, as well as literature data for 2-stroke scooters (2s_Scooter)(Platt et al., 2014), and for SOA from limonene(Gallimore et al., 2017) and oleic acid (S. J. Fuller et al., 2014). The blue points and the blue dotted lines in the wood burning experiment are used to identify the corresponding $ROSP_{OA}$ of the listed ROS_{SOA}. *For the ROS_{POA} of the 2S_Scooters (gasoline emissions) we take only the points right

before lights on from the original data as earlier data points seemed still be influenced by incomplete mixing of emissions in the chamber.

Overall, the ROS_{BBOA} derived from the Bern data was in the same range as ROS_{POA} of wood burning emissions obtained from the laboratory study. The contribution of HOA+CCOA to PB-ROS was found to be negligible for Beijing within the analysis uncertainties (see Table D1), while in laboratory experiments PB-ROS was observed in primary emissions from bituminous coal but not from anthracite coal. The fairly low and variable PB-ROS content in primary emissions from laboratory studies may explain why we could not derive its contribution to the observed PB-ROS in Beijing. ROS_{OOA} in both Beijing and Bern were about 2 to 4 times lower than ROS_{SOA} of gasoline and wood burning emissions, but equal or higher than ROS_{SOA} of coal burning, α-pinene, limonene and oleic acid. It is reasonable to assume that the ambient OOA was formed from a complex mixture of precursors from various sources like traffic, wood burning, coal burning and biogenic gases, therefore, the ambient ROS_{SOA} is expected to lie somewhere in the range of these sources.

6.3 Implications

OA, dominated by secondary aerosols, is the largest fraction of PM_1 mass worldwide. Using both field and laboratory measurements we provide compelling evidence that PB-ROS are predominantly secondary. We estimate that while less than 40% of the OA mass at the urban locations investigated is secondary, this fraction contributes more than 60% of the total PB-ROS. These findings are corroborated by chamber experiments, showing that atmospheric aging does not only enhance the OA aerosol mass by up to ~8 fold, it results in the formation of 10 times more ROS active material (in nmol μg^{-1}) compared to POA. We show that SOA from anthropogenic complex precursor mixtures are especially ROS active, implying that despite their lower overall contribution to the OA burden compared to biogenic SOA, anthropogenic emissions can be an important PB-ROS source. While results mentioned above are related to exogenous ROS, measurements of the aerosol oxidative potential (e.g. using the DDT assay) show consistent trends, with higher potential related to more oxygenated aerosols, including aerosols derived from gas phase precursors (e.g., isoprene and naphthalene (Tuet et al., 2017)), diesel emissions (Li et al., 2009), and ambient measurements (Verma et al., 2015). All these reports indicate that SOA appears to be highly relevant for promoting oxidative stress in human lungs. This hypothesis is supported by epidemiological studies, which revealed seasonal trends in health effects of PM. Studies in the US, Western Europe, Japan, South Korea including up to 112 cities and time periods up to 13 years showed a stronger effect of PM on mortality in spring, summer or fall compared to winter (Peng et al., 2005; Nawrot et al., 2007; Zanobetti and Schwartz, 2009; Franklin et al., 2008; Yi et al., 2010), while in China the effects were highest in summer and winter (Kim et al., 2015; Chen et al., 2013). Kim et al. (2015) showed the highest overall risk of PM_{10} on non-accidental or cardiovascular mortality on extremely hot days. All in all, except for locations affected by haze and specific sources of toxic components (e.g., PAHs and coal combustion in winter in China), a stronger association between PM and mortality was observed at different locations during hotter days, when SOA formation is the most active.

Further support for our findings that OOA and oxidative stress might be linked comes from laboratory experiments showing that SOA can be an efficient source of OH radicals. Tong et al. (2016) observed direct formation of OH, upon dissolution of SOA in water in the dark. Others reported that SOA dissolved in water exhibited a high OH radical or H_2O_2 generation under irradiation (Wang et al., 2011a; Lim and Turpin, 2015; Badali et al., 2015). Lakey et al. (2016) developed a model to simulate the response of air pollutants including PM on the production rates and concentrations of ROS in the epithelial lining fluid of the human respiratory tract. They found that the OH production rate from SOA in the lung could be as high as the H_2O_2 production rate from redox-active trace metals and quinones.

The PB-ROS content in OOA (nmol μg^{-1}) in Beijing, where anthropogenic emissions dominate, is slightly higher than in Bern, but still comparable within a factor of two. The results here emphasize the importance of anthropogenic combustion emissions to the particulate ROS activity and thus their general abatement could lead to a reduction of adverse health effects from air pollution. The on-line measurement of aerosols ensures that the attribution of PB-ROS to its sources can be made with less uncertainty arising from possible sampling artefacts and rapid ROS decay during filter storage. Future research should provide deeper links between PB-ROS quantified by the DCFH assay and adverse biological effects of PM determined by toxicological and epidemiological studies. Specifically, the health relevance of short-lived versus long-lived ROS should be evaluated, in order to assess the suitability of off-line versus on-line ROS determination methods. Since the DCFH assay does not capture the oxidant activity from redox-cycling, a combination with complementary assays might also be needed.

6.4 Methods

6.4.1 Measurement campaigns

We combined the results from two field campaigns and three laboratory studies. One field campaign was conducted in November 2014 at the Institute of Anatomy of the University of Bern, Switzerland, and the other from January to February 2015 at the National Center for Nanoscience and Technology, Beijing, China. For the laboratory studies two Atmospheric Chemistry Simulation Chambers of the Paul Scherrer Institute (PSI) were used, i.e., the 27-m^3 stationary smog chamber (PSI-SSC) and the 7-m^3 mobile smog chamber (PSI-MSC). The PSI-SSC is a flexible bag made of fluorinated ethylene propylene (FEP) suspended in a temperature-controlled enclosure, where four xenon arc lamps (4 kW rated power, 1.55 × 10^5 lumen each, XBO 4000 W/HS, OSRAM) are used to simulate the solar light spectrum and to mimic natural photochemistry(Paulsen et al., 2005). Before each experiment, high concentrations of ozone (> 2 ppm) and humidified pure air were flushed into the chamber for at least 1 hour to clean the bag walls with lights on, followed by flushing with dry, pure air for at least 10 h. The PSI-MSC is located inside a temperature-controlled housing flanked by 4 sets of 10 UV-lights (90–100 W, Cleo Performance, Philips)(Platt et al., 2013). In both chambers, OH was formed to a large degree from the photolysis of HONO and its concentration was evaluated by the decay of the marker compound d9-butanol (butanol-D9, 98%, Sigma-Aldrich) measured by a proton transfer reaction-mass spectrometer (PTR-MS, Ionicon

Analytik GmbH)(Barmet et al., 2012). The gas- and particle-phase primary products that were injected into the chambers were first thoroughly studied before the lights were switched on. Photochemical gas-phase reactions and formation of secondary organic aerosol were then initiated by turning on the lights in the smog chambers. The following precursor emission sources were tested in laboratory in this study:

Wood combustion emissions: In total, we investigated eight combustion devices with different technologies and combustion conditions, including a two-stage combustion updraft pellet boiler, a moving grate boiler equipped with an electrostatic precipitator, a pellet stove, a two-stage combustion downdraft log wood boiler, two advanced two-stage combustion log wood stoves, and two conventional single-stage combustion log wood stoves. Primary emission measurements from all these devices are reported here. For the secondary wood burning emissions, only the experiments conducted with one of the conventional single-stage combustion log wood stove and aged in the PSI-MSC are presented here, as it is more representative for the genuine atmospheric aging (with OH exposure ranged from 2.6 - 4.8 $\times 10^7$ molec cm^{-3} h), compared to the emissions from the other burning devices that were aged in the potential aerosol mass (PAM) chamber (with OH exposure ranged from 1.1 - 2.0 $\times 10^8$ molec cm^{-3} h). More details of the experimental method as well as the evolution of PB-ROS formation during the aging can be found in our previous publication (Zhou et al., 2018b).

Coal combustion emissions: We combusted three types of Chinese bituminous coal and two types of Chinese anthracite coal, in a conventional Chinese household cook stove. For each experiment, 100-300 g coal was pre-heated first by a hot honeycomb and anthracite coal until the temperature rose up to ~ 600 ^{o}C, and then emissions were sampled, diluted 100-fold and injected into the PSI-MSC. One exemplary experiment showing the evolution of ROS and OA formation during the aging of the bituminous coal combustion emissions is presented in Fig. D.10. Aging resulted in a strong increase of the total OA and of ROS reaching a relatively stable ROS content in the SOA for the rest of the measurement period.

α-pinene: α-pinene (40 ppbv) was injected into the PSI-SSC containing O$_3$ (~ 500 ppbv) resulting in rapid formation of SOA. More details about the experimental procedure can be found elsewhere (Krapf et al., 2016). As seen in Fig. D.11, the injection of α-pinene resulted in a fast production of OA and ROS, where ROS decreased strongly with time when α-pinene had reacted away, similar to the observed decay of peroxides by (Krapf et al., 2016).

6.4.2 Instrumentation

A suite of online instrumentation were deployed to characterize the chemical and physical properties of gas and particle phase emissions in all the above mentioned campaigns.

Reactive oxygen species (ROS) analyzer: An on-line ROS analyzer based on the 2',7'-dichlorofluorescin (DCFH) assay was used for the quantification of monitoring the water-soluble particle-bound components acting as ROS (PB-ROS). A detailed description of the ROS analyzer is given in our previous publication (Zhou et al., 2018a). Particles were collected using an aerosol collector, of which the main part is a mist chamber. Before the aerosol collector, a honeycomb charcoal denuder was installed in a stainless steel tube to remove interfering gas phase compounds. The oxygen-

free ultra-pure water (OF-OPW) was continuously sprayed into the mist chamber and incorporated the collected aerosol particles. The sample extracts were then mixed with the working solution (the DCFH solution) for analysis. The PB-ROS concentration was measured continuously and was calculated as H_2O_2 equivalents.

Aerosol mass spectrometer (AMS): A field-deployable high-resolution time-of-flight aerosol mass spectrometer (HR-ToF-AMS, Aerodyne Research Inc.) DeCarlo et al.(2006) was used for the characterization of the non-refractory aerosol mass in Beijing. Ambient air was sampled through a critical orifice into a recently developed aerodynamic lens which efficiently transmitted particles between 80 nm and up to at least 3 μm (Williams et al., 2013). Particles were flash-vaporized by impaction on a resistively heated surface (~ 600 ^{o}C) and ionized by electron ionization (70 eV). The mass-to-charge ratios (*m/z*) of the resulting fragments were determined by a ToF mass spectrometer. Data were analyzed with the ToF-AMS softwares SQUIRREL and PIKA. Data was not corrected for lens transmission efficiency. For ambient data, standard relative ionization efficiencies (RIE) were used for organics (RIE=1.4), nitrate (RIE=1.1) and chloride (RIE=1.3). RIE for sulfate and ammonium were experimentally determined to be 1.12 and 3.58, respectively. The composition-dependent collection efficiency (CDCE) was evaluated using the algorithm by Middlebrook et al. (2012). For laboratory experiments, RIE of 1.4, 1.3, 1.1, and 1.2 were used for organics, chloride, nitrate, and sulfate, respectively, and experimentally determined 3.83 for ammonium. In line with past laboratory biomass burning experiments, a CDCE of 1 was used in all wood burning tests.

Aerosol chemical speciation monitor (ACSM): A quadrupole aerosol chemical speciation monitor (Q-ACSM, Aerodyne Research Inc.) was employed to monitor the composition and mass concentration of non-refractory submicron PM in Bern (Ng et al., 2011b). The Q-ACSM is built upon the same sampling and detection technology as the AMS described above, but with reduced complexity (e.g. no particle size measurement), resolution and performance(Fröhlich et al., 2013). Data was not corrected for lens transmission efficiency. Standard RIE were used for organics (1.4), nitrate (1.1) and chloride (1.3). RIE for sulfate and ammonium were experimentally determined to be 0.58 and 4.6, respectively. The CDCE was corrected based on the methodology described by Middlebrook et al. (2012).

Aethalometer: Real-time measurement of the optical absorption (b_{abs}) was performed by an aethalometer at 7 different wavelengths. A "next generation" aethalometer was used (AE33, Magee Scientific, Berkeley, CA, USA), which performed an online correction for possible scattering artefacts of the measured b_{abs} (Drinovec et al., 2015). The b_{abs} was then converted to an equivalent black carbon (eBC) concentration using the nominal mass absorption cross section (MAC) values (Zotter et al., 2017).

Gas phase instrumentation: In the wood combustion PAM chamber experiments, total volatile organic compounds (VOCs) and CH_4 were measured with a flame ionization detector (FID) with a non-methane cutter (model 109A, J.U.M Engineering), CO and NO with a non-dispersive infrared analyzer (Ultramat 23 Siemens), O_2 with a paramagnetic oxygen analyzer (Ultramat 23 Siemens) and CO_2 with a non-dispersive infrared (NDIR) analyzer (model LI-820, LI-COR®). In the smog chamber (SC) aging experiments CO, CO_2, and CH_4 were measured with a cavity ring-down spectrometer (G2401, Picarro,

Inc.). In all experiments, the composition of non-methane VOCs was determined by a high resolution proton transfer reaction–mass spectrometer (HR-PTR-MS 8000, Ionicon Analytik GmbH).

VACES: A versatile aerosol concentration enrichment system (VACES) was used to enrich the Bern ambient aerosol to increase the ROS concentration above the instrument detection limit. More detailed information on the VACES can be found in Künzi et al. (2015). The aerosol sample was drawn into the VACES at a flow rate of ~ 100 L min^{-1} into a tank with water heated up to ~ 30 °C. The water vapor saturated air stream was then cooled down in a condenser (-2 °C) where water droplets with diameter > 2 µm formed on the collected aerosol particles. The droplets were then enriched in concentration with a virtual impactor and dried by passing through a diffusion dryer. The concentration enrichment factor CE was calculated as:

$$CE = Q_{tot}/q_{min}(1 - WL) \times \eta_{vi} \tag{6.1}$$

where Q_{tot} and q_{min} are the intake and minor flows of the impactor, respectively, and η_{vi} and WL the collection efficiency and fractional loss of the impactor (Sioutas et al., 1999).

6.4.3 Statistical analysis

Positive matrix factorization (PMF) & **Multilinear engine (ME-2)**

Source apportionment was performed on the organic AMS and ACSM data using PMF as implemented by the multilinear engine (ME-2; Paatero, 1997) and controlled via the interface SoFi coded in Igor Wavemetrics (Source Finder(Canonaco et al., 2013)). PMF was developed by Paatero and Tapper (1993, 1994) as a receptor model to apportion the sources on the basis of observations (internal correlations) at the receptor site alone (Viana et al., 2008), as represented by Eq. 2.

$$x_{ij} = \sum_{k=1}^{p}(g_{ik} \times f_{kj}) + e_{ij} \tag{6.2}$$

Here x_{ij}, g_{ik}, f_{kj} and e_{ij} are matrix elements of the measurements, factor time series, factor profiles and residual matrices, respectively, where $f_{ik} \geq 0$, $g_{ik} \geq 0$. The indices *i*, *j*, *k* correspond to time, *m/z* and a discrete factor, respectively. *p* denotes the number of factors in the PMF solution determined by the user. The factor profiles remain constant, while their contributions to the matrix elements of the measurements are allowed to vary with time (concentration time series). In PMF, an "objective function" Q as defined in Eq. 3 is iteratively minimized:

$$Q(E) = \sum_{i=1}^{m}\sum_{j=1}^{n}[\frac{e_{ij}}{s_{ij}}]^2 \tag{6.3}$$

where e_{ij} is the residual in the ith variable measured in the jth sample and s_{ij} represents the corresponding "uncertainty" of e_{ij}. The main theoretical limitations of PMF are: 1) Source interpretation is relatively subjective; 2) Inability to clearly separate covariant sources (Viana et al., 2008) with similar chemical composition, e.g. cooking and traffic.

ME-2 provides a more flexible framework for controlling the solutions of the factor analysis where it permits the imposition of explicit external constraints (Ramadan et al., 2003). Within the *a*-value approach, *a priori* information (factor profiles or factor time series) of one or more sources can be used as an additional input into the model, using the scalar *a* to regulate the strength of the constraints:

$$f_{j,solution} = f_j \pm a \times f_j \tag{6.4}$$

$$g_{i,solution} = g_i \pm a \times g_i \tag{6.5}$$

Here $0 \leq a \leq 1$, and f_j, g_i are the input profiles and the time series, which can either entirely or partially be constrained by a.

The mass spectra of the identified OA factors in both Beijing and Bern are presented in Fig. D.3. In Beijing, the result representing our data best was a 4-factor solution with three unconstrained factors, including oxygenated OA (OOA), combined hydrocarbon like OA and coal combustion OA (HOA + CCOA), and cooking OA (COA), and a constrained biomass burning OA (BBOA) factor. The BBOA factor profile obtained in previous ambient measurements in China by Elser et al. (2016) was constrained varying the a-value between 0 and 0.3 in steps of 0.1. Several tests were performed in the attempt to separate the HOA and CCOA factors, including the constraint of the factor profiles obtained in Elser et al. (2016). However, none of the tested approaches provided a satisfactory separation of these two sources, which were therefore recombined in the final solution. In Bern, the solution that represented our data best was a 5-factor solution, with the four unconstrained factors OOA, BBOA, HOA, COA and a constrained fifth factor that could not be attributed to any specific source, but is required to properly extract COA in Bern, and is referred to as unidentified factor. In order to extract a clean profile of the unidentified factor (to be constrained in the final solution), we studied the changes in the mass spectra of the unidentified factor for an increasing number of factors (Fig. D.4). Based on these changes we constrained the unidentified mass spectra obtained in the 9-, 10-, and 11-factor solutions with a-values between 0 and 1 in steps of 0.1.

Aethalometer model: The Aethalometer-based source apportionment model developed by Sandradewi et al. (2008) was used to separate the contributions of traffic (TR) and wood burning (WB) to the measured eBC in Bern. The equation used for the model is:

$$b_{abs,total}(\lambda) = b_{abs,tr}(\lambda) + b_{abs,wb}(\lambda) \tag{6.6}$$

Using the power law of the spectral dependence of the absorption, the measured b_{abs} at two different wavelengths, and Eq. 6, TR and WB can be apportioned in the following way:

$$\frac{b_{abs,TR}(\lambda_1)}{b_{abs,TR}(\lambda_2)} = \left(\frac{\lambda_1}{\lambda_2}\right)^{-\alpha TR} \tag{6.7}$$

$$\frac{b_{abs,WB}(\lambda_1)}{b_{abs,WB}(\lambda_2)} = \left(\frac{\lambda_1}{\lambda_2}\right)^{-\alpha WB} \tag{6.8}$$

$$b_{abs,WB(\lambda_2)} = \frac{b_{abs}\lambda_1 - b_{abs}\lambda_2 \times \left(\frac{\lambda_1}{\lambda_2}\right)^{-\alpha TR}}{\left(\frac{\lambda_1}{\lambda_2}\right)^{-\alpha WB} - \frac{\lambda_1}{\lambda_2}^{-\alpha TR}} \tag{6.9}$$

$$b_{abs,TR(\lambda_2)} = \frac{b_{abs}\lambda_1 - b_{abs}\lambda_2 \times \left(\frac{\lambda_1}{\lambda_2}\right)^{-\alpha WB}}{\left(\frac{\lambda_1}{\lambda_2}\right)^{-\alpha TR} - \frac{\lambda_1}{\lambda_2}^{-\alpha WB}} \tag{6.10}$$

In Eqs. 7-10, α is the absorption Ångström exponent for traffic and wood combustion emissions (α_{TR} and α_{WB}, respectively), which have to be assumed a priori. Similar to Fröhlich et al. (2015) and Sciare et al. (2011), α_{TR}=1 and α_{WB}= 2 were used, and b_{abs} (λ_1) and b_{abs} (λ_2), were at 470 nm and 950 nm as respectively. The b_{abs} values attributed to each source was then converted to eBC using nominal mass absorption cross section (MAC) values from the instrument manufacturer. In this study, the model was

only applied to the Bern data, where the contributions of other combustion emissions to eBC were negligible (Zotter et al., 2017), but not in Beijing, as the contribution of coal combustion is substantial there (Liu et al., 2016; Elser et al., 2016) and large uncertainties regarding the optical properties of eBC emitted from coal combustion still exist.

Multiple linear regression model (MLRM): A multiple linear regression model (MLRM) was used to identify the dependence of the PB-ROS concentration on the different organic aerosol (OA) sources. By deploying the Matlab software (R2016b), we put the observed ROS data as input y, coupled with the ROS measurement error and the different OA sources obtained from source apportionment as the predictors. First, we used the Function D1 to fit the data in Beijing and Bern, as described in Table D.1. Further, to exclude any influence of the separation of the individual primary sources, we tested the contribution of the total primary emission sources (here combined as primary organic aerosol, POA = (HOA + CCOA) + COA + BBOA) to the ROS activity in Beijing by running the MLRM with only two variables, POA and OOA (using Function D2 in Table D.1). To assess the uncertainties related to the modeled PB-ROS content values, we performed in total 40 and 315 MLRM fits according to the PMF solutions obtained in Beijing and Bern, respectively. In each MLRM fit, we used one set of PMF solutions, coupled with one set of PB-ROS concentrations generated by varying the observed PB-ROS within the measurement uncertainties determined by the instrument precision and the background subtraction (uniformly distributed random number with the constraint of the observed ROS and its measurement error), as described in our previous publication (Zhou et al., 2018a). Finally, we performed 1000 bootstrap runs on the final PMF solution (the average PMF results of all the solutions) to test the sensitivity of the MLRM to the input data, especially in Beijing where model results were potentially driven by the haze periods.

The MLRM explained 61% of the variability of water soluble PB-ROS in Bern and 77% in Beijing (see Fig. D.8 for the normalized frequency distributions of R^2). For Beijing, the unexplained variance could be related to the measurement uncertainties, while for Bern, the model did not explain the entire variance in the data (22% of the remaining variability could be related to uncertainty and 17% remain unexplained). This unexplained part may be related to the variability of the composition/precursors of the OA factors or to components not considered in this analysis (e.g. metals).

Bootstrap tests: The bootstrap method, which is an effective approach to partially explore the influence of abnormal experimental conditions (i.e., the haze and reference episodes in Beijing, the presence of outliers, etc.) is employed in this study to: 1) calculate a Pearson correlation matrix of all the testing factors in Beijing and Bern (Fig. D.6); 2) test the sensitivity of the MLRM to the input data as described above. This statistical method is based on the creation of replicate inputs perturbing the original data by resampling. This was done by randomly reorganizing the rows of the original time series, so that some rows of the original data were present several times, while other rows were removed. Both of the analyses 1) and 2) were obtained by running the data for 1000 bootstrap replicates.

6.4.4 Definitions

ROS fraction: In order to study the ROS formation during aging, the secondary ROS content (ROS$_{SOA}$) was introduced. It describes the number of moles of secondary ROS (ROS$_S$ = aged ROS–primary ROS) per mass of secondary organic aerosol (SOA) formed during aging and was calculated as:

$$ROS_{SOA} = \frac{ROS_S}{SOA} \tag{6.11}$$

Secondary organic aerosol (SOA) and secondary ROS (ROS$_S$) were calculated by subtracting primary organic aerosol (POA) and primary ROS (ROSp) from the total OA and aged ROS, respectively, assuming ROS$_P$ and POA to be lost to the chamber walls at the same rate as eBC but otherwise to remain constant during aging. Although both quantities may not be conserved, a decrease of both did abate their effect on the PB-ROS fraction. In the SC experiments, POA was defined as the OA mass before lights on, while SOA was estimated as the difference between total OA and the time dependent POA mass accounting for particle wall loss. Wall loss rates for POA and SOA were assumed to be the same as that of the measured eBC.

f$_{44-SOA}$: To express the degree of oxygenation of SOA, the fraction of secondary *Org44* (corresponding to *m/z* 44) in SOA (represented as $f_{44\text{-}SOA}$) is introduced, which was calculated as:

$$f_{44-SOA} = \frac{Org_{44-SOA}}{SOA} \tag{6.12}$$

where Org_{44-SOA} is the difference of total Org_{44} and primary Org_{44} and using the same procedure as for the SOA calculation mentioned above.

7
Conclusions and outlook

Human health is adversely influenced by the severe air pollution worldwide, especially in the developing countries. The oxidative stress aroused by an imbalance between the reactive oxygen species (ROS) and the antioxidants in the human body is regarded as the main reason for the adverse human health outcomes. Particulate matter (PM) is of utmost importance to take this responsibility when people are exposed to polluted air as it can penetrate deeply into human lungs and induce ROS through three modes: 1) carry the particle-bound ROS (PB-ROS) into the human body; 2) generate ROS through redox cycling reactions with the antioxidants *in vivo*; 3) irritating the biological system generates ROS. Therefore, in order to assess the health effects of the PM, it is important to understand the capacity of the PM emitted from different biogenic and anthropogenic sources to increase the ROS burden in the respiratory tract.

Although the cellular response to the oxidative stress may represent the *in vivo* situation better than an acellular assay, it is usually time consuming and expensive, thus hard to be applied in field studies and routine analysis. For the work presented in this thesis, we used the acellular 2',7'-dichlorofluorescin (DCFH) based assay to achieve the following goals: a fast screening of the capability of the particle-borne components to act as ROS (PB-ROS); understanding the routes of PB-ROS formation of different emission sources upon aging; a real-time evaluation of PB-ROS at contrasting sites, as well as the investigation of the relationship between laboratory and ambient studies. An on-line reactive oxygen species (ROS) analyzer was developed, characterized and successfully deployed for the quantification of PB-ROS of different emissions sources including wood and coal combustion, of SOA from α-pinene (performed in laboratory studies), as well as of the ambient air in Beijing (China) and Bern (Switzerland) (performed in-situ). The main parameters affecting PB-ROS formation in wood and coal

combustion emissions upon aging were identified, and the PB-ROS content in primary and secondary emissions of different sources was then compared with that derived from ambient studies.

The results presented in this work demonstrate that the sensitivity of the DCFH assay to oxidants/peroxides varies substantially due to their chemical structure and bulky functional groups (i.e., tert-butyl and phenyl) that may sterically hinder the interaction between the enzyme and the peroxides. Components known to induce redox cycling (e.g. trace metals like iron, anthraquinone, etc.) do not seem to react with DCFH, thus we conclude that the DCFH assay measures the capacity of particle-borne components to act as ROS rather than to mediate the ROS formation. No potential interference from gas phase O_3 and NO_2, as well as matrix effects of particulate SO_4^{2-} and NO_3^- to DCFH assay were observed. Fe^{3+} showed no influence on the ROS signal while soluble Fe^{2+} can reduce it if present at high concentrations in the extracts.

We found that a large fraction of PB-ROS decomposes rapidly with a half-life of 1.7 ± 0.4 h and that on average 60 ± 20 % of the ROS decayed during filter storage time. This emphasizes the importance of a fast online measurement of PB-ROS as developed in this work. Wood combustion for residential heating has been recognized as a large source of air pollution. Here we achieved a profound understanding of the ROS-generating potential of wood combustion emissions from different combustion devices and technologies, different fuel types, operation methods, combustion regimes and phases, as well as aging conditions. The ROS emission factors in primary and aged OA are highly variable spanning almost two orders of magnitudes. Still, the emission factors from the automatically operated devices are on average one order of magnitude lower than those from the manually operated devices. These observations indicate that the ROS emissions of wood combustion could be significantly lowered by promoting the use of automated devices, which operate mostly under optimal conditions. A clear increase of PB-ROS emissions could be observed when the burning conditions were changed from optimal to high air to fuel ratio conditions. For all eight tested devices the PB-ROS emission factors were substantially increased upon aging. The enhancement factors varied from 4-6 for automatically operated devices to larger than 10 for the manually operated devices. Altogether, these results provide important information to state authorities dealing with air pollution issues. Besides the implications different burning technologies can have they also show that it is important to include the atmospheric processing of the emissions into the evaluation of their impact on the environment.

Furthermore, coal combustion, one of the main sources for the energy supply and residential heating in worldwide, was also tested in this study. Specifically, the emissions of five types of Chinese coal used in residential heating, three types of bituminous coal and two anthracite coal, were measured. While primary PB-ROS emissions was detected from bituminous coal combustion none was measured in anthracite coal. Interestingly, primary PB-ROS emissions of wood combustion are significantly higher than from bituminous coal, while aged PB-ROS emissions from wood combustion emissions are not statistically different from bituminous coal combustion emissions, but ~ 7.4 times higher than the anthracite coal emissions. This indicates equal or higher toxicity of wood combustions compare to the coal combustion emissions, depending on the types of coal used.

The OA sources in Beijing and Bern were successfully identified from the ambient high resolution time of flight aerosol mass spectrometer (HR-ToF-AMS) data and the aerosol chemical speciation monitor (ACSM), using the positive matrix factorization (PMF) coupled with the Multilinear Engine (ME-2). Using the multiple linear regression model (MLRM), the contribution of OA sources to the observed ROS in both locations was determined.

In Beijing, we have captured two different air conditions: a haze period with a visibility smaller than 10 km, and a relatively clean reference period. OA dominated in both haze and reference episodes with a contribution of 49 ± 10 % and 54 ± 8 % to total mass, respectively. The OA was attributed to oxygenated OA (OOA), combined hydrocarbon like OA and coal combustion OA (HOA+CCOA), cooking OA (COA) and biomass burning OA (BBOA). In Bern, the air condition was fairly stable during the whole measurement period. OA contributed 50 ± 7 % to the total mass and could be apportioned to OOA, HOA, COA and BBOA. The ROS content in different emission sources obtained from the MLRM revealed that the main parameter affecting ROS formation was OOA in both locations. However, HOA, COA and BBOA also have a small but non-negligible contribution to PB-ROS in Bern.

The PB-ROS contents in the primary organic aerosol (POA) and secondary organic aerosol (SOA) (represented as $f_{ROS-POA}$ and $f_{ROS-SOA}$, respectively) of different emission are highly variable and have a large source-to-source variability. The higher $f_{ROS-SOA}$ than $f_{ROS-POA}$ may be due to the higher oxygenation of the SOA compared to POA. However, we could not attribute the source-to-source variability of $f_{ROS-SOA}$ to differences in the degree of oxygenation. This indicates that the $f_{ROS-SOA}$ of different emission sources are highly dependent on the molecular composition, which is determined by the SOA precursors. For example, the $f_{ROS-SOA}$ of the wood combustion emissions showed higher median values than the gasoline and coal combustion emissions. Nevertheless, the tested anthropogenic emissions (except the anthracite coal) possess relatively higher $f_{ROS-SOA}$ than that of the biogenic emissions, including the Olic acid, Limone and α-pinene. The $f_{ROS-POA}$ obtained from the laboratory are comparable to those derived from ambient studies, and the elevated $f_{ROS-SOA}$ is in line with the increased PB-ROS content in OOA.

In this thesis, we provide the first comparison and evolution of PB-ROS content in the emissions of different wood combustion appliances and after aging, as well as of the PB-ROS emissions of residential coal used in China. This may help to guide the policy and facilitate following toxicological studies of the biomass combustion emissions. The combination of in-situ and laboratory studies provided reliable evidence to infer adverse health impacts of aerosols at different ambient locations. The acellular DCFH assay used in our study targets mostly the capacity of the particle-borne components to act as ROS (i.e. the intrinsic PB-ROS), and the efficiency of the reaction of DCFH to oxidants/peroxides varies substantially. The chemical composition of the PM emitted from varying emission sources strongly affects the capacity to act as ROS (i.e. non-catalytic organic hydroperoxides) or the capacity to induce redox cycling yielding ROS (i.e. catalytic transition metals, quinones). This will largely affects the result of the ROS quantified by different assays and its generation potential *in vivo*. To obtain the overall intrinsic redox activity of PM, the inclusion of different acellular ROS quantification assays that are sensitive to different compounds, coupled with the identification of the different chemical components contained in the PM, should be considered. Furthermore, investigations on the association between PB-

ROS quantified by the DCFH assay and adverse biological effects induced by the particles *in vivo* is scarce. Thus, the extent the acellular ROS assessed in this study predict the cellular PM toxicity needs to be further investigated. To achieve this, a stronger collaboration between the disciplines of aerosol science, chemistry and toxicology is advantageous.

A

Supplement material of

Chapter 3: Development, characterization and first deployment of an improved online reactive oxygen species analyzer

J. Zhou[1], E. A. Bruns[1], P. Zotter[2], G. Stefenelli[1], A. S. H. Prévôt[1], U. Baltensperger[1], I. El-Haddad[1], and J. Dommen[1]

[1] Paul Scherrer Institute, Laboratory of Atmospheric Chemistry, 5232 Villigen PSI, Switzerland

[2] Lucerne University of Applied Sciences and Arts, School of Engineering and Architecture, CC Thermal Energy Systems & Technology, Bioenergy Research, 6048 Horw, Switzerland

Figure A.1 The reaction scheme of the DCFH assay (Miljevic et al., 2014).
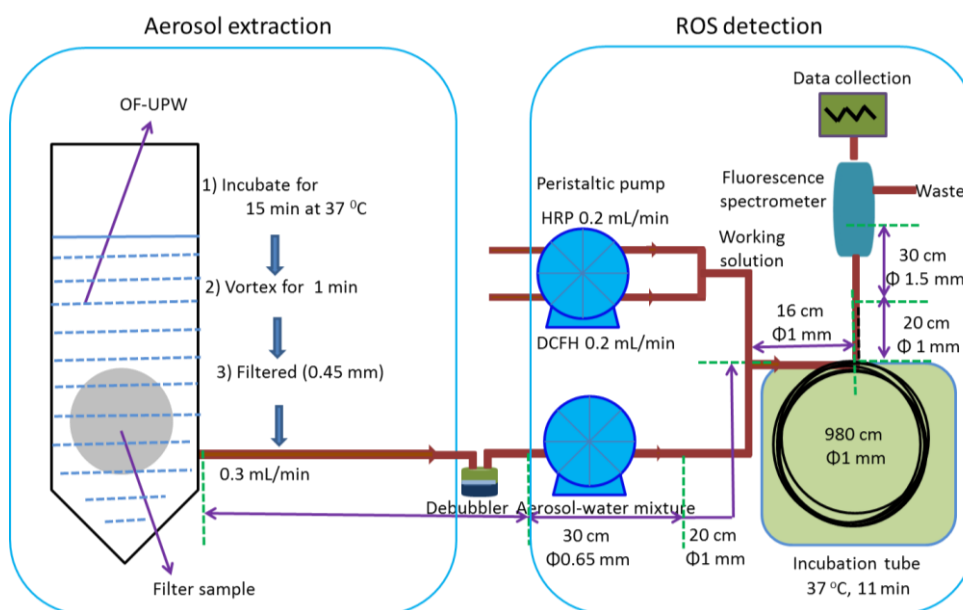
Figure A.2 Overview of the offline ROS analyzer.
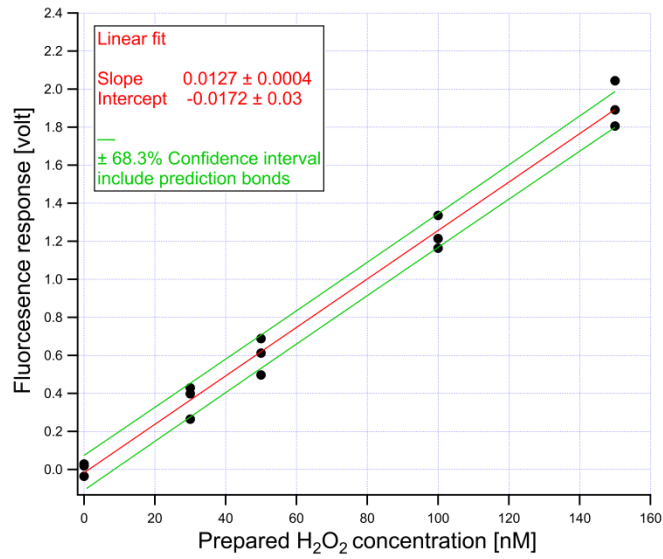
Figure A.3 Average of calibrations of the ROS analyzer with different H2O2 concentrations which were repeated three times.
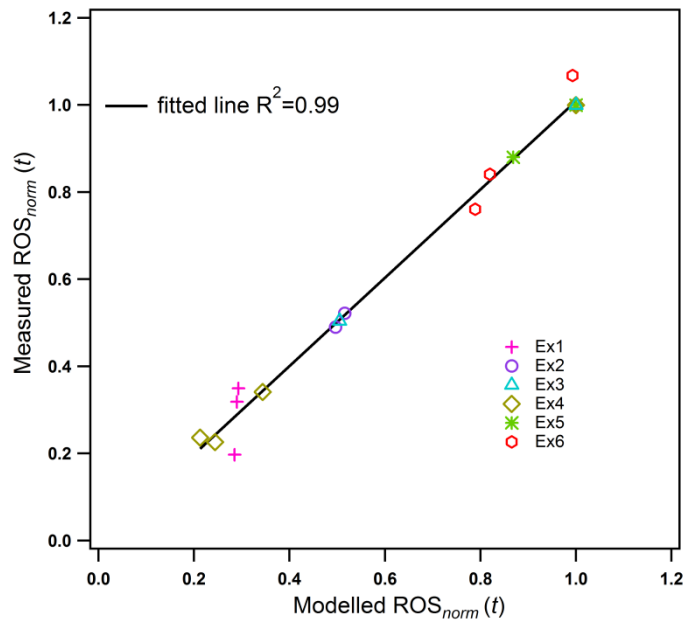
Figure A.4 Comparison of measured ROS_{norm}(t) and modeled ROS_{norm}(t). ROS_{norm}(t) is the ROS measured at time t normalized to the ROS measured the first time (t1).
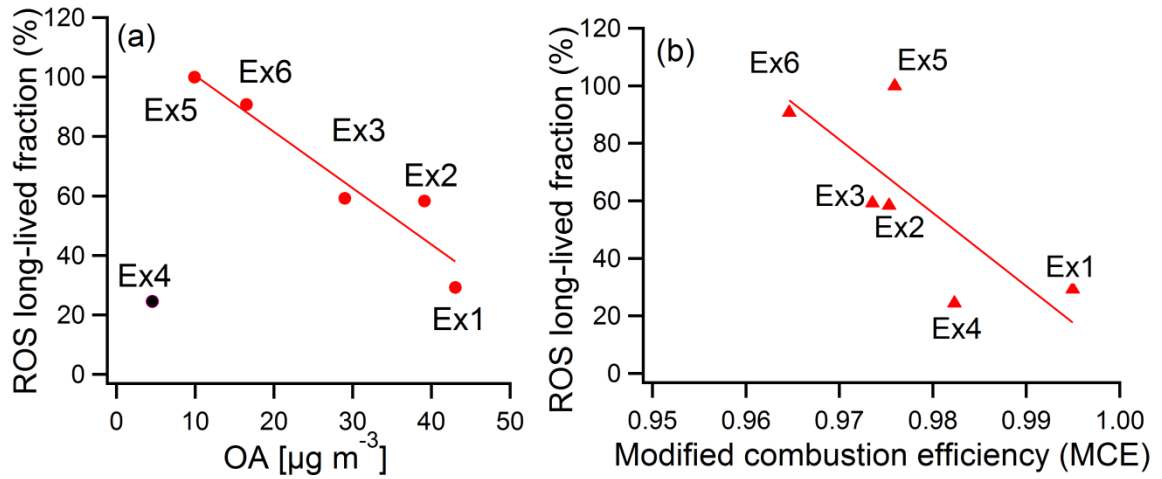
Figure A.5 Long-lived ROS fraction as a function of OA loading (a) and modified combustion efficiency (MCE) (b). Markers indicate the modelled long-lived-ROS fraction (see section 3.4.2) and the solid lines a linear least-square fit.
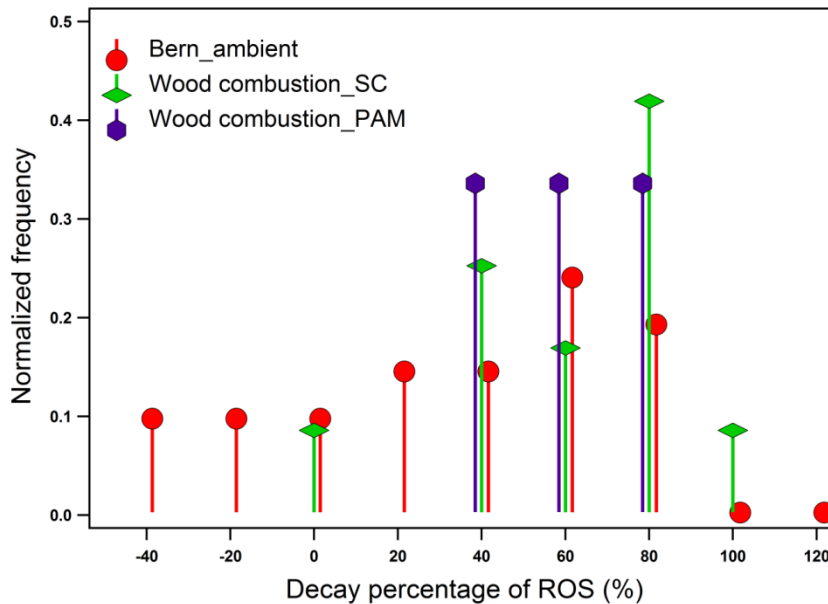
Figure A.6 Normalized frequency of ROS decay percentages. "Bern_ambient" and "wood combustion_SC" represent the results from Bern ambient air (filter storage time: 1 year) and wood combustion smog chamber aging (filter storage time: 2 years), respectively; "Wood combustion_PAM" represents the estimated results from wood combustion potential aerosol mass chamber aging using the biexponential decay model described in section 3.4.2 (filter storage time: 1 year).

B

Supplement material of

Chapter 4: Particle-bound reactive oxygen species (PB-ROS) emissions and formation pathways in residential wood smoke under different combustion and aging conditions

J. Zhou[1], P. Zotter[2], E. A. Bruns[1], G. Stefenelli[1], D. Bhattu[1], S. Brown[1,3], A. Bertrand[4], N. Marchand[4], H. Lamkaddam[1], J. G. Slowik[1], A. S. H. Prévôt[1], U. Baltensperger[1], T. Nussbaumer[2], I. El-Haddad[1], and J. Dommen[1]

[1]Laboratory of Atmospheric Chemistry, Paul Scherrer Institute, 5232 Villigen PSI, Switzerland

[2]Lucerne University of Applied Sciences and Arts, School of Engineering and Architecture, Bioenergy Research, 6048 Horw, Switzerland

[3]Institute for Atmospheric and Climate Science, ETH, Zurich, Switzerland

[4]Aix Marseille Univ, CNRS, LCE, Marseille, France

Figure B.1 Schematic of wood combustion emissions aged by a) smog chamber (SC) and b) and potential aerosol mass (PAM) chamber.
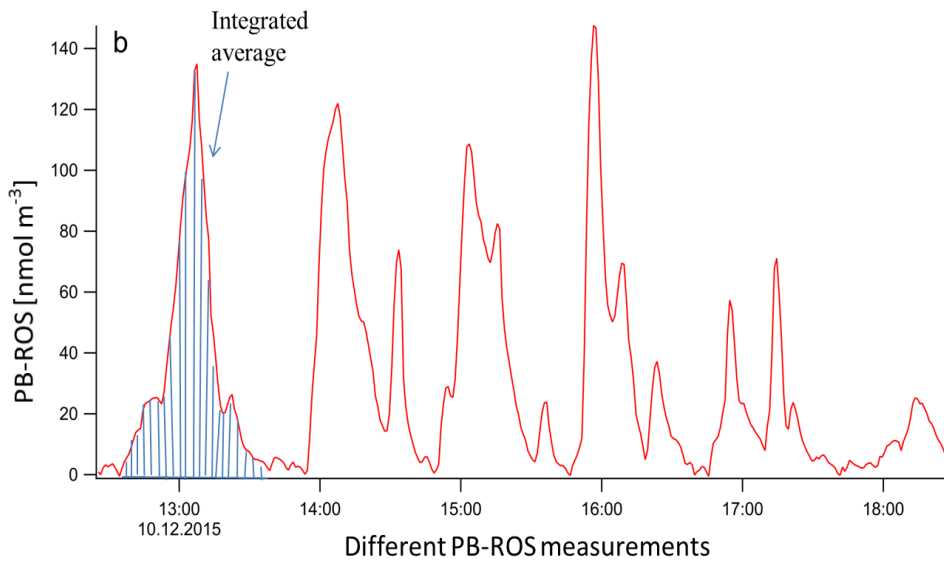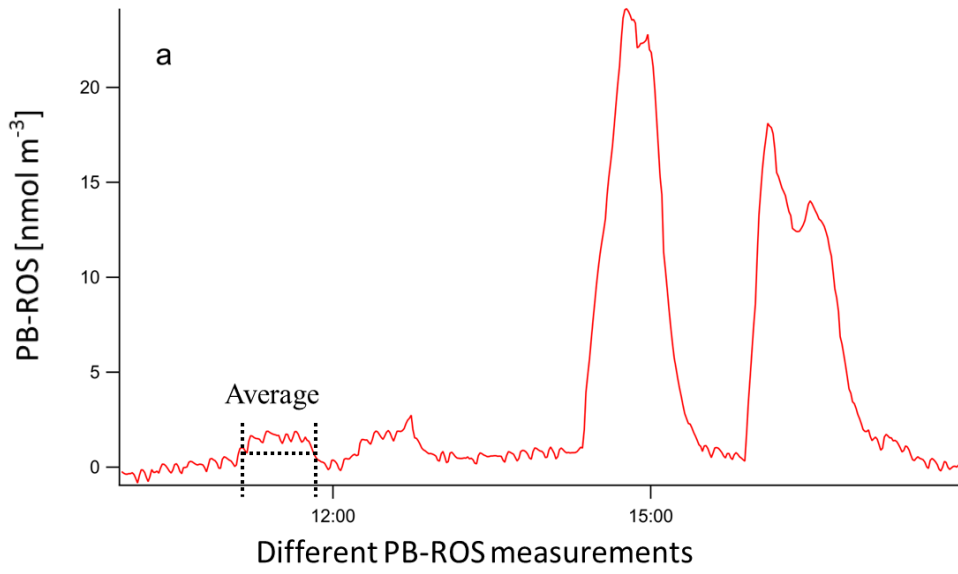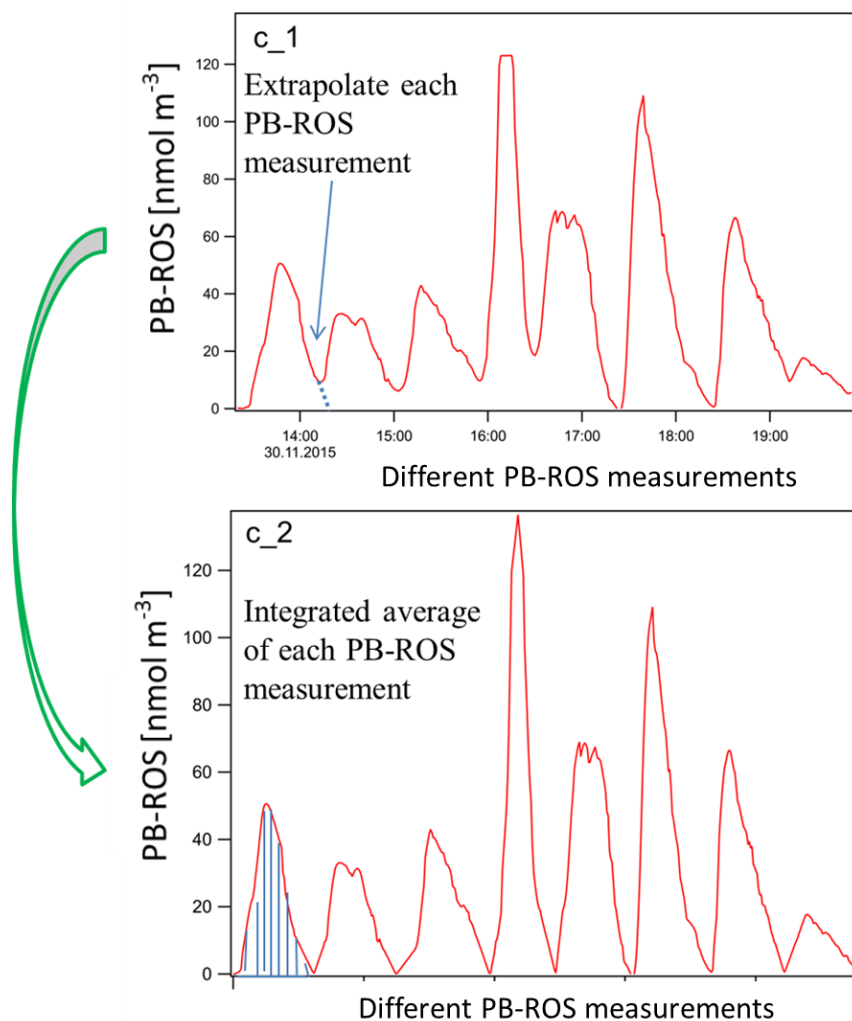
Figure B.2 PB-ROS content calculation methods during different combustion conditions, a) average b) integrated average c) extrapolated for the experiments with no background measurements (c_1) and the integrated average (c_2) of those experiments.
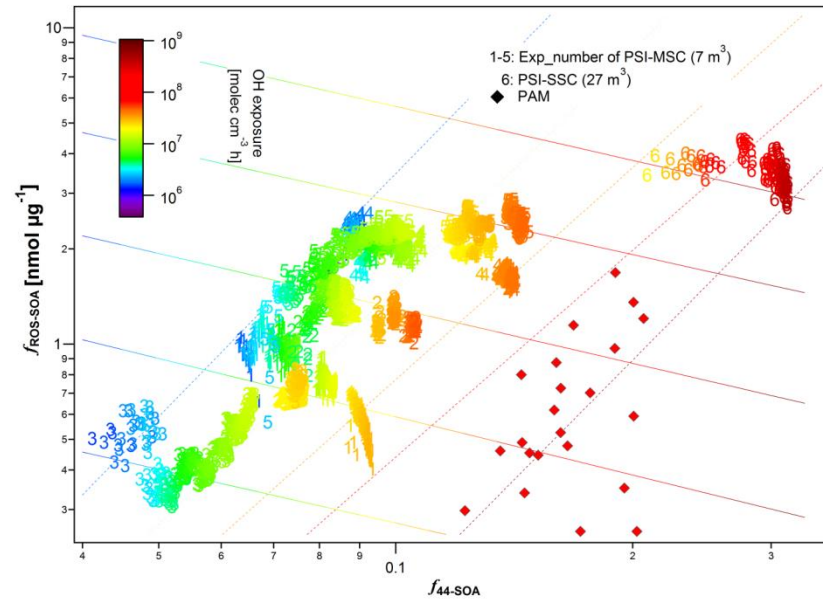
Figure B.3 Variation of the fraction of ROS in SOA, fROS-SOA, with the fraction of m/z44 in the secondary organic aerosol measured by the AMS (f44-SOA, x-axis) and the OH exposure estimated from the decay of d9-butanol measured by the PTR-ToF-MS (color code). Data are collected from two different smog chambers (SC) and from the PAM chamber. Dashed lines are isopleths of constant OH exposures, while solid lines are obtained by isolating the effect of OH exposure from the other variables. Numbers 1-5 represent the sequence of the five 7-m^3 SC experiments, Number 6 represents a single 27-m^3 SC experiment.
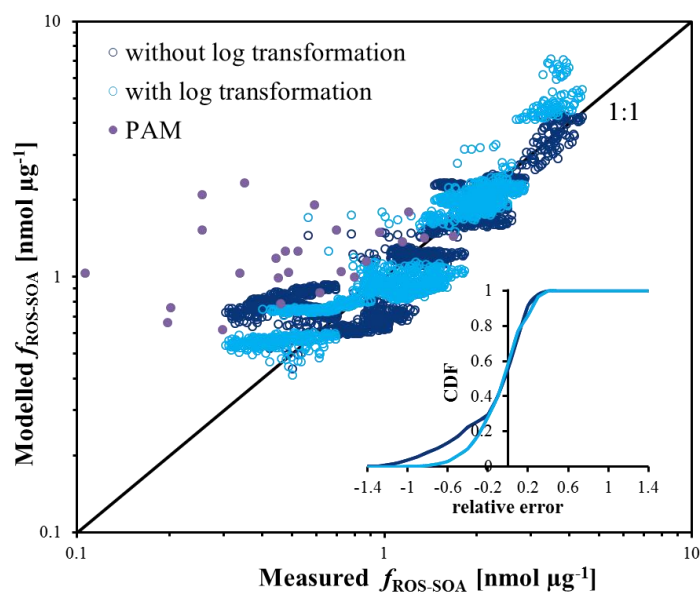
Figure B.4 Comparison of the performance of two multiple regression models, with and without log-transformation of the data. The *f*ROS-SOA measured in the PAM is predicted using the same parameterization and results are displayed for comparison. The inset shows the cumulative density function (CDF) of the relative model residuals (measurements-model).
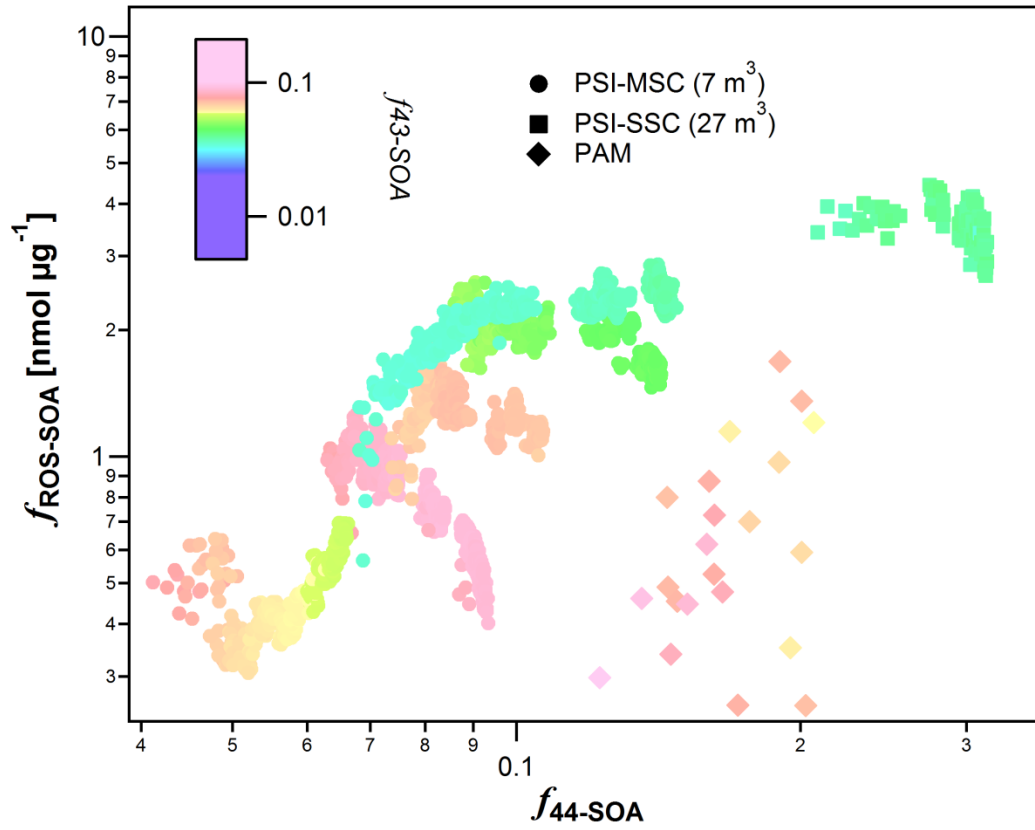
Figure B.5 Variation of the fraction of ROS in SOA, fROS-SOA, with the fractions of m/z 44 and m/z 43 in the secondary organic aerosol measured by the AMS (f44-SOA, x-axis and f43-SOA color code).

C

Supplement material of

Chapter 5: The evolution of particle-bound reactive oxygen species (PB-ROS) in the primary and aged aerosols emitted from Chinese residential coal combustion

J. Zhou[1], S.M. Pieber[1], J. G. Slowik[1], I. EI Haddad[1], G. Stefenelli[1], R. Huang[1,2], A.S.H. Prevot[1], U. Baltensperger[1] & J. Dommen[1]

[1]Laboratory of Atmospheric Chemistry, Paul Scherrer Institute, 5232, Villigen, Switzerland

[2]Institute of Earth Environment, Chinese Academy of Sciences, Xi'an, 710061, China
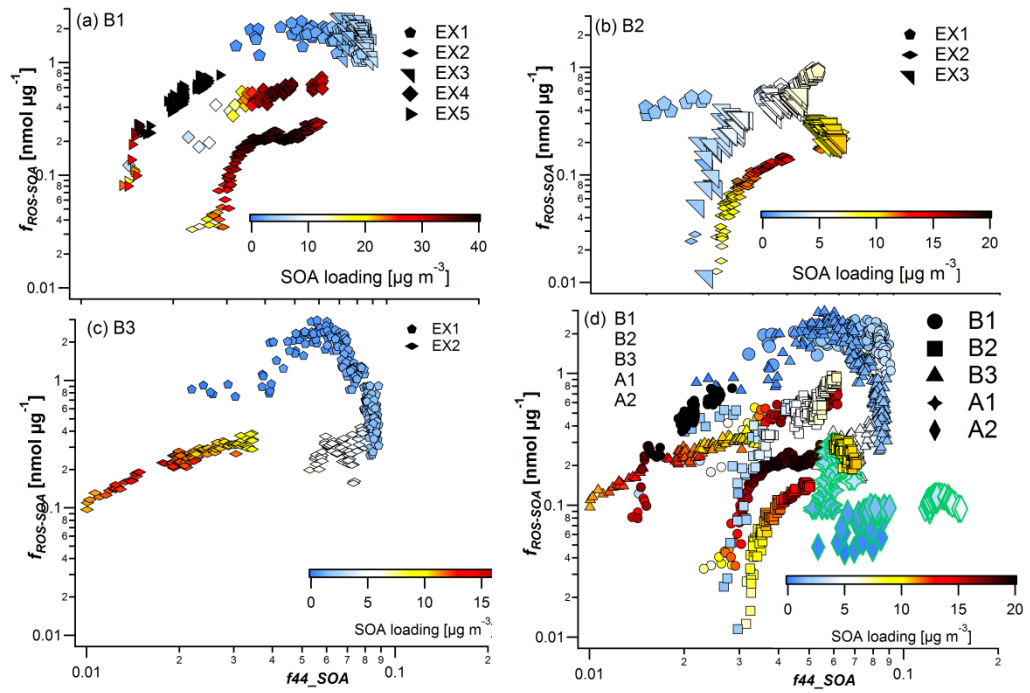
Figure C.1 The correlation of $f_{\text{ROS-SOA}}$ with $f_{\text{44-SOA}}$ of SC aging of different types of coal. Data is color coded with OA loading. The data points represent one minute average of the aging process.

D

Supplement material of

Chapter 6: Large predominance of secondary organic aerosol to particle-bound reactive oxygen species activity in fine aerosol

J. Zhou[1], M. Elser[1], R.-J. Huang[1,2], H. Ni[2], M. Krapf[1], R. Fröhlich[1], D. Bhattu[1], G. Stefenelli[1], P. Zotter[4], E. A. Bruns[1], S. M. Pieber[1], Q. Y. Wang[2], Y. Wang[2], Y. Zhou[2], C. Chen[5], M. Xiao[1], J. G. Slowik[1], S. Brown[1,6], L.-E. Cassagnes[1], K. R. Daellenbach[1], T. Nussbaumer[4], M. Geiser[3], A.S.H. Prévôt[1], I. El-Haddad[1], J.-J. Cao[2], U. Baltensperger[1] & J. Dommen[1]

[1]Laboratory of Atmospheric Chemistry, Paul Scherrer Institute, 5232, Villigen, Switzerland

[2]Institute of Earth Environment, Chinese Academy of Sciences, Xi'an, 710061, China

[3]Institute of Anatomy, University of Bern, 3012, Bern, Switzerland

[4]Bioenergy Research Group, Engineering and Architecture, Lucerne University of Applied Sciences and Arts, 6048, Horw, Switzerland

[5]CAS Key Laboratory for Biological Effects of Nanomaterials and Nanosafety, National Centre for Nanoscience and Technology, Beijing 100191, China

[6]Institute for Atmospheric and Climate Science, ETH, 8092, Zurich, Switzerland

Fig. D.1a and Fig. D.1b show temporal variations of the non-refractory chemical components (including organic aerosol (OA), SO4, NO3, NH4, Cl) concentrations and equivalent black carbon (eBC) measured by either an AMS or an ACSM, and aethalometer, during the measurement periods January-February 2015 in Beijing and November 2014 in Bern. In Beijing, the periods highlighted with a blue background represent the haze periods, which were defined by a visibility of less than 10 km. The remaining periods are classified as reference periods (with a visibility above 10 km).
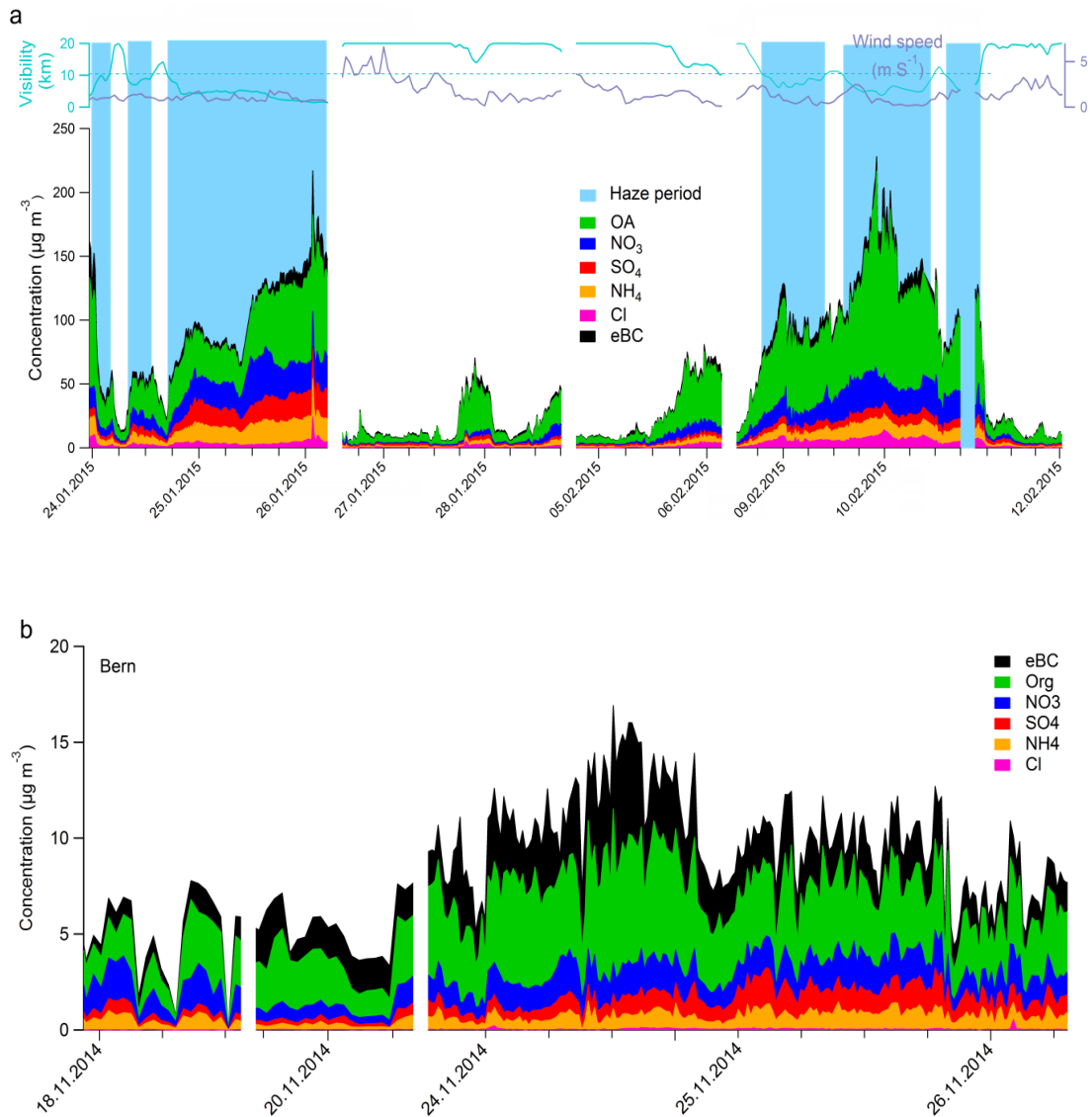
Figure D.1 Time series of non-refractory chemical components and eBC in (a) Beijing and (b) Bern during the measurement periods.
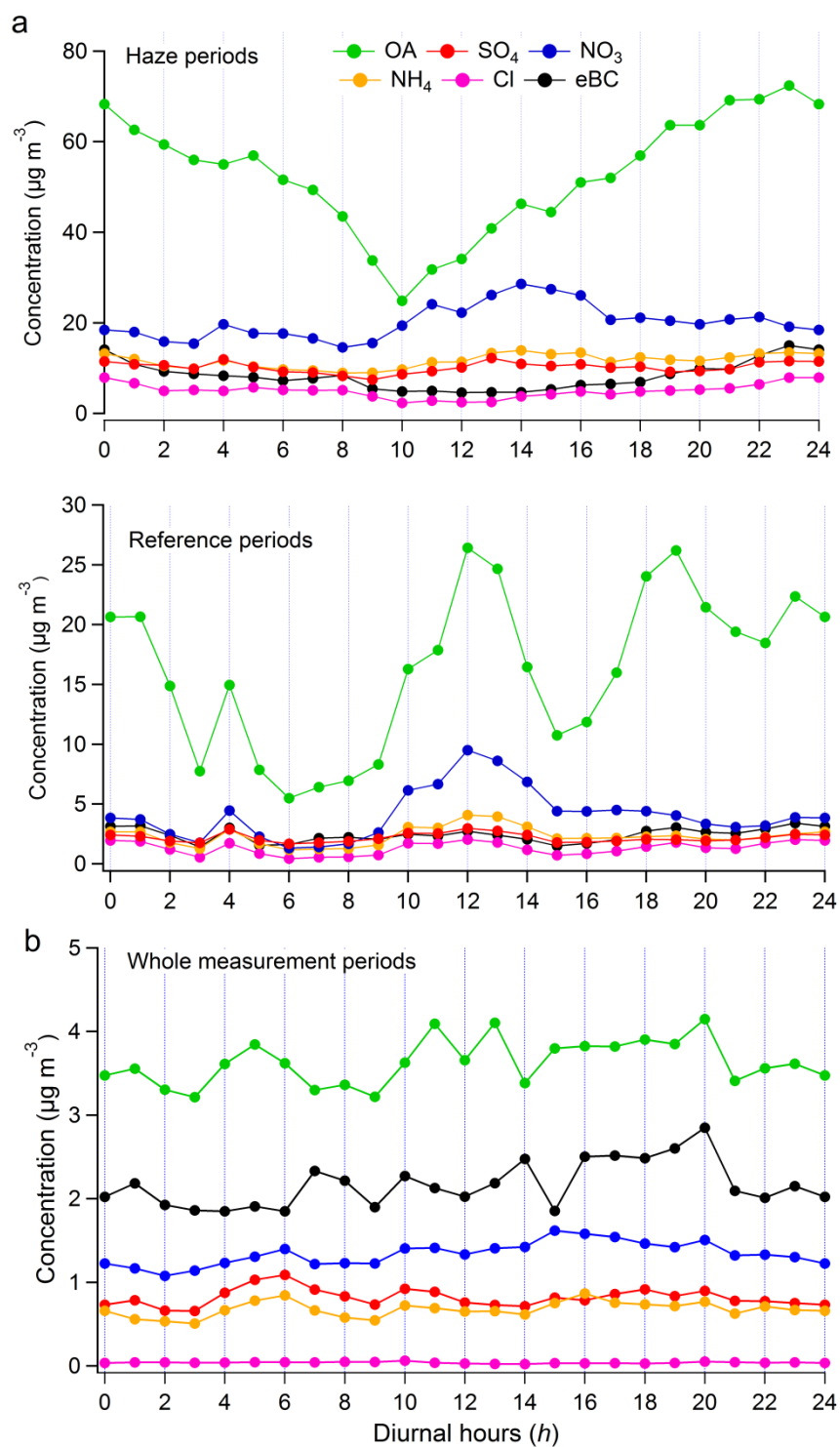
Figure D.2 Average diurnal trends of mass concentrations of all chemical components measured during the campaigns in (a) Beijing and (b) Bern.
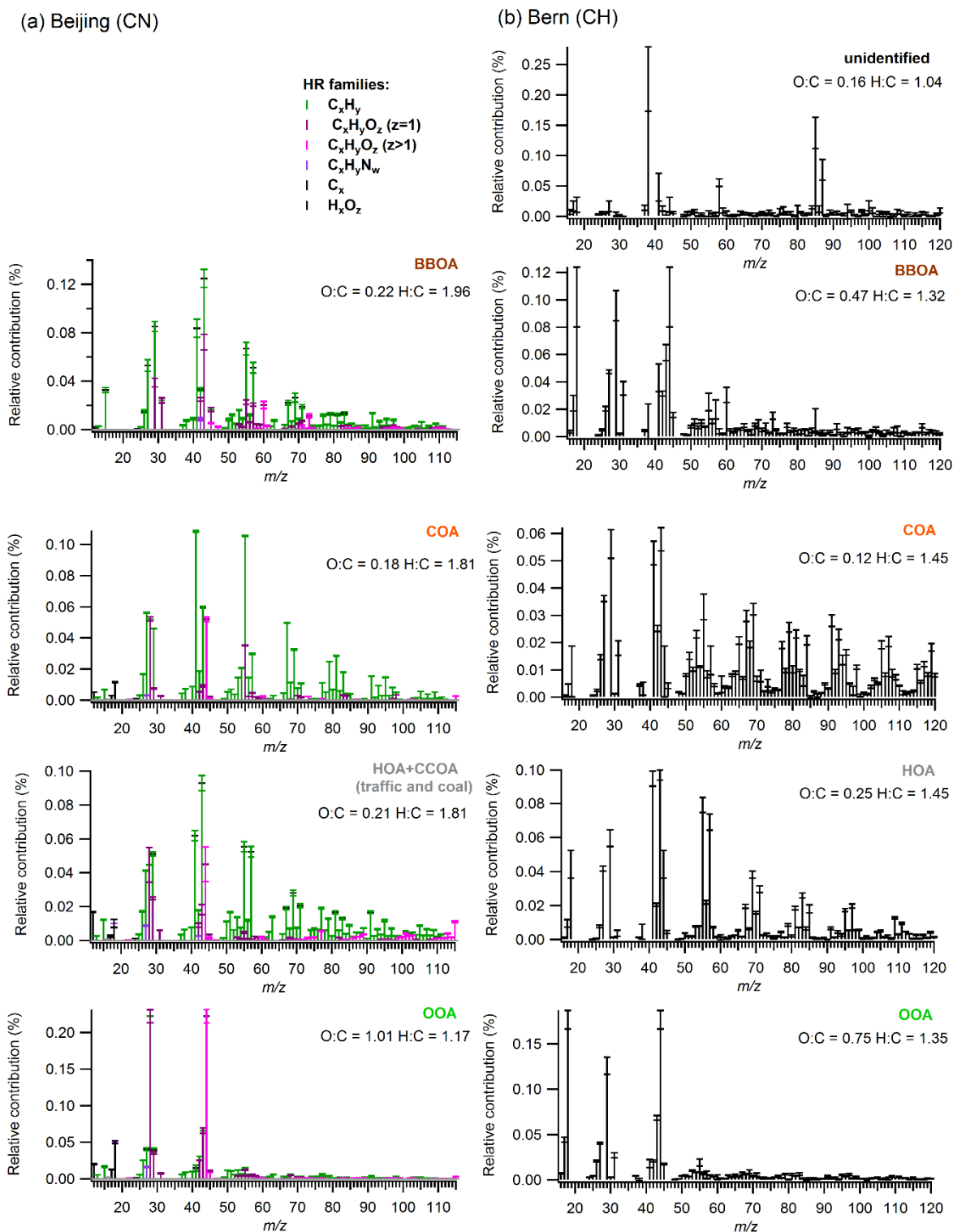
Figure D.3 Mass spectra of the identified OA factors for (**a**) Beijing and (**b**) Bern, color-coded with the chemical families. Spectra are averaged over all good a-value combinations (see Methods section). Error bars represent one standard deviation of each *m/z* over all the accepted solutions. In Bern, the mass spectra were obtained from the unit mass resolution-ACSM. O:C was calculated according to Aiken et al. (2008), and H:C was estimated according to Ng et al. (2011a).
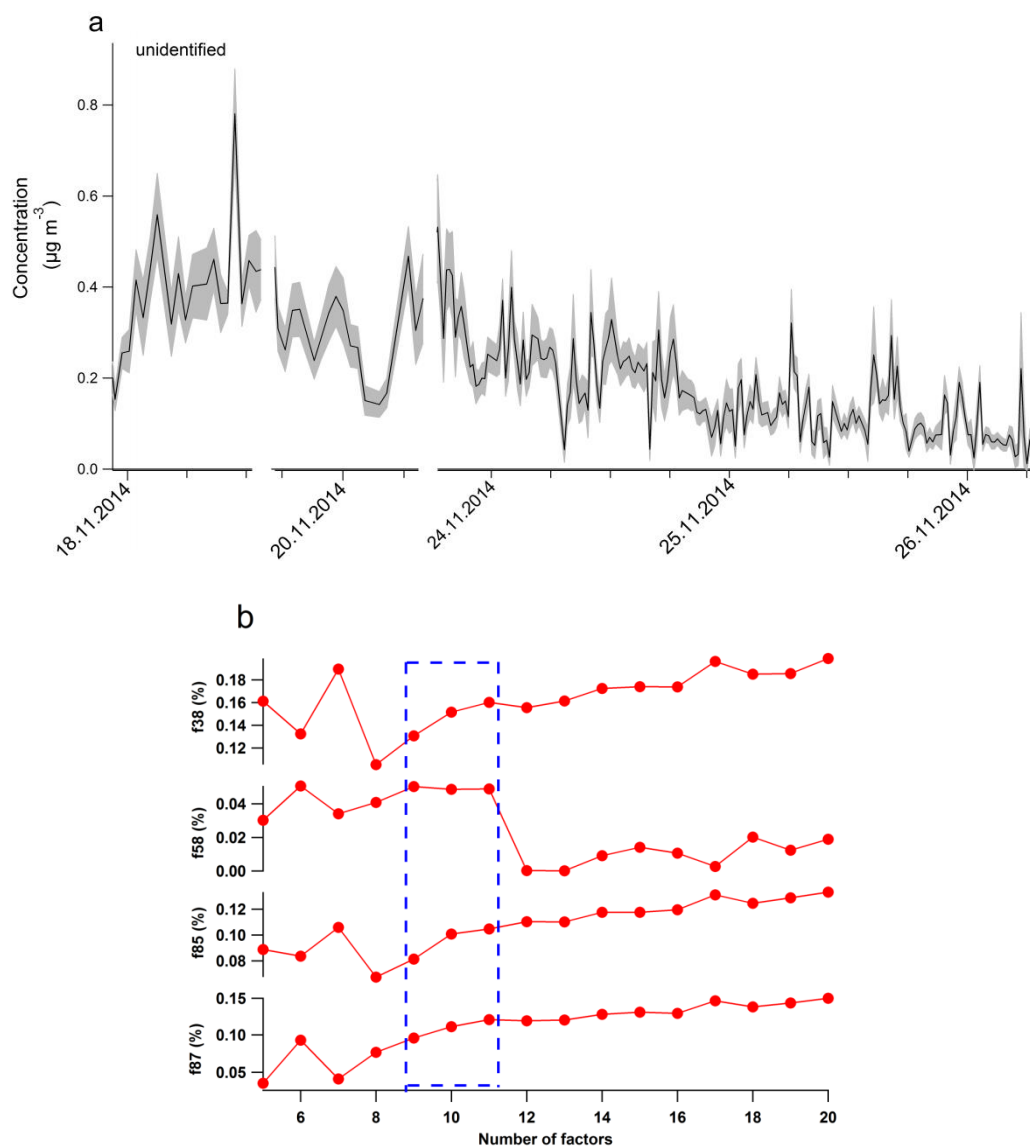
Figure D.4 Evaluation of the unidentified factor. (a) time series of the unidentified factor in Bern and (b) changes in the most important m/z-fractions of this factor for an increasing number of factors. The unidentified mass spectra obtained from the 9-, 10-, and 11-factor solutions labeled in the blue rectangle were used in the source apportionment analysis.

.
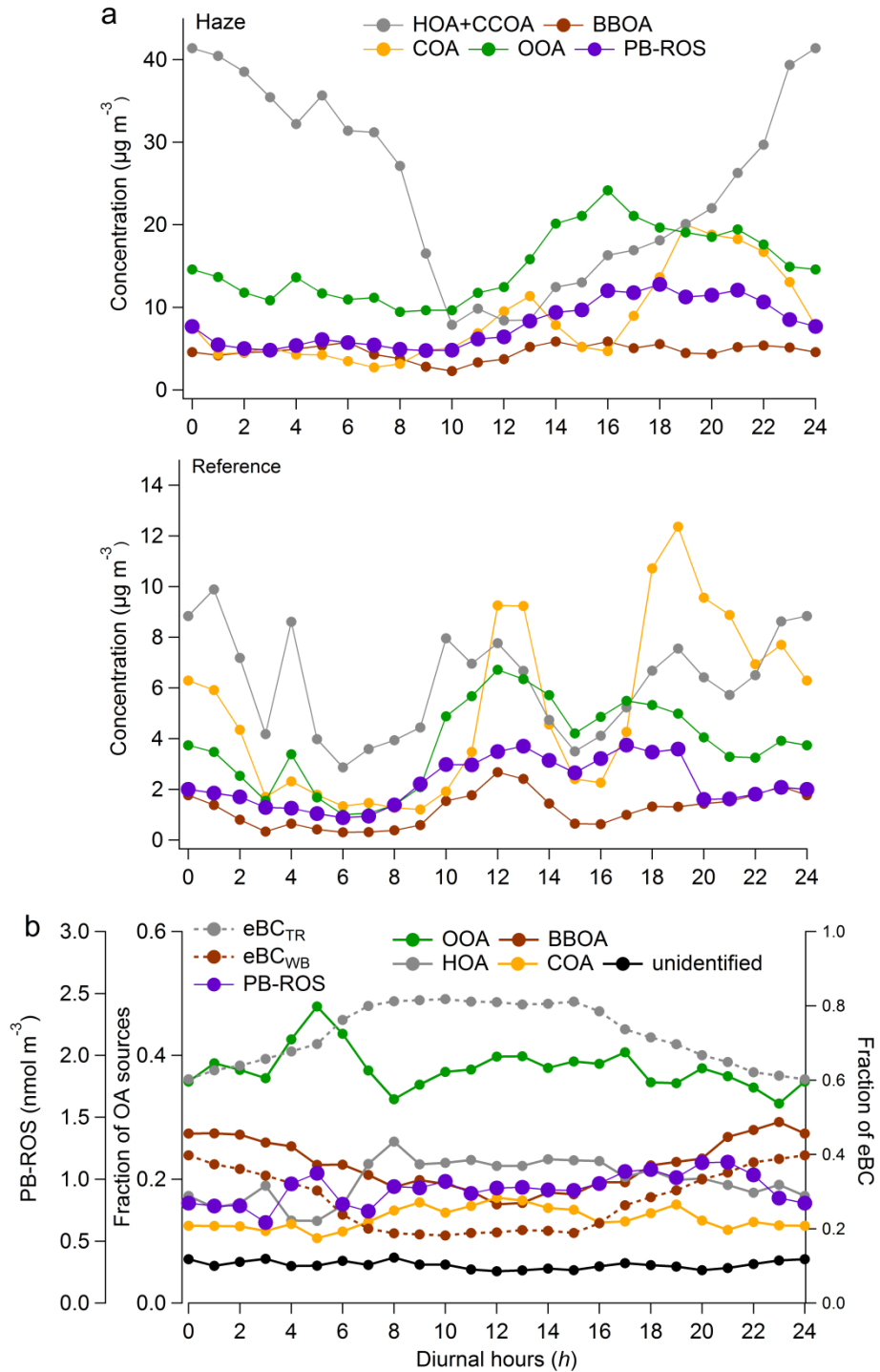
Figure D.5: Average diurnal patterns of the concentrations of OA components during the measurement periods in (a) Beijing and (b) Bern. In Bern, the diurnal variation of ROS, the PMF factors: OOA, BBOA, HOA, COA, and unidentified are shown as fraction of OA sources, and the eBC fractions from traffic (eBC$_{TR}$) and wood combustion (eBC$_{WB}$) are shown as fraction of eBC.
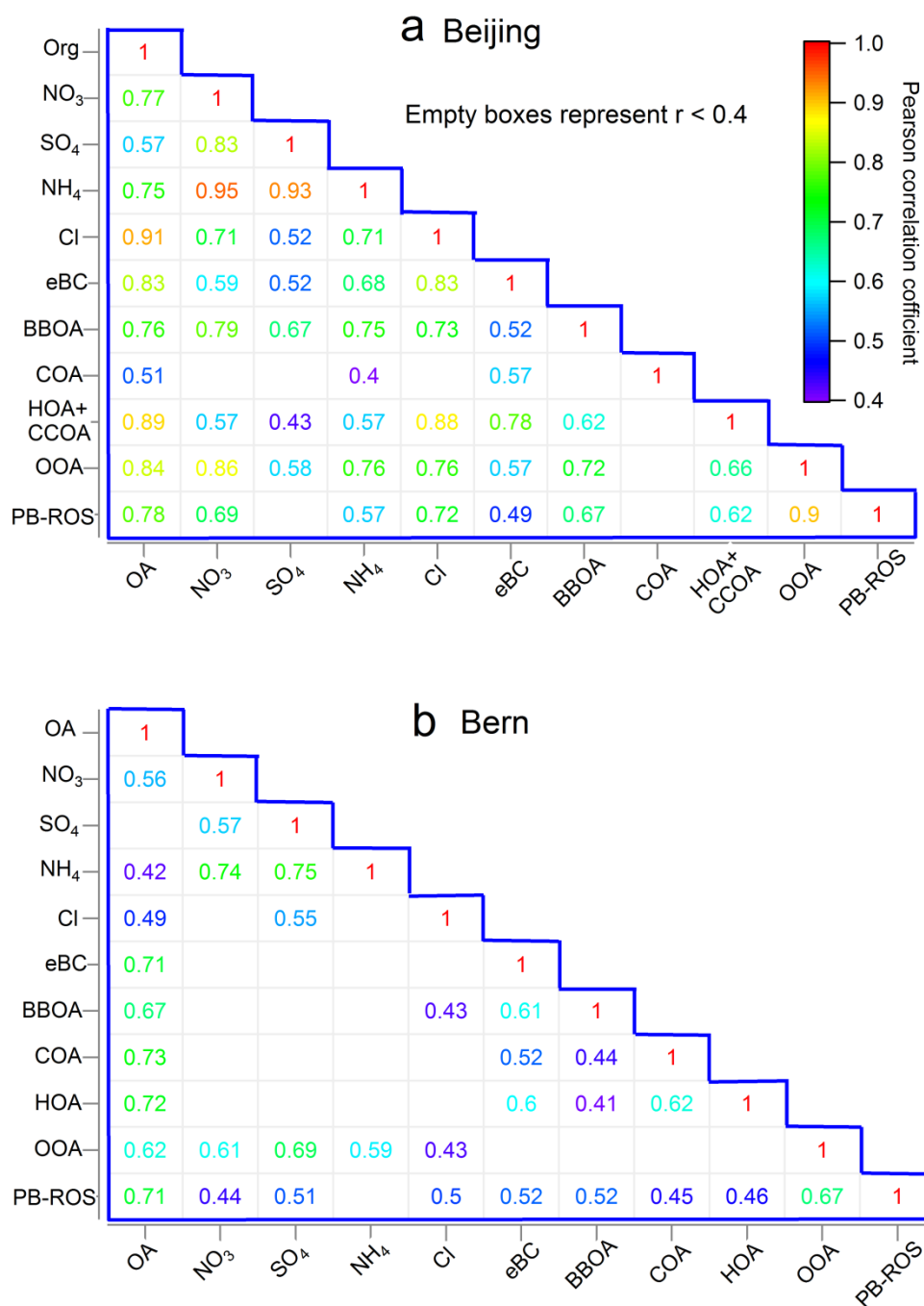
Figure D.6 Correlation matrix showing Pearson's r for the chemical composition and OA components in (a) Beijing and (b) Bern during the corresponding measurement periods.
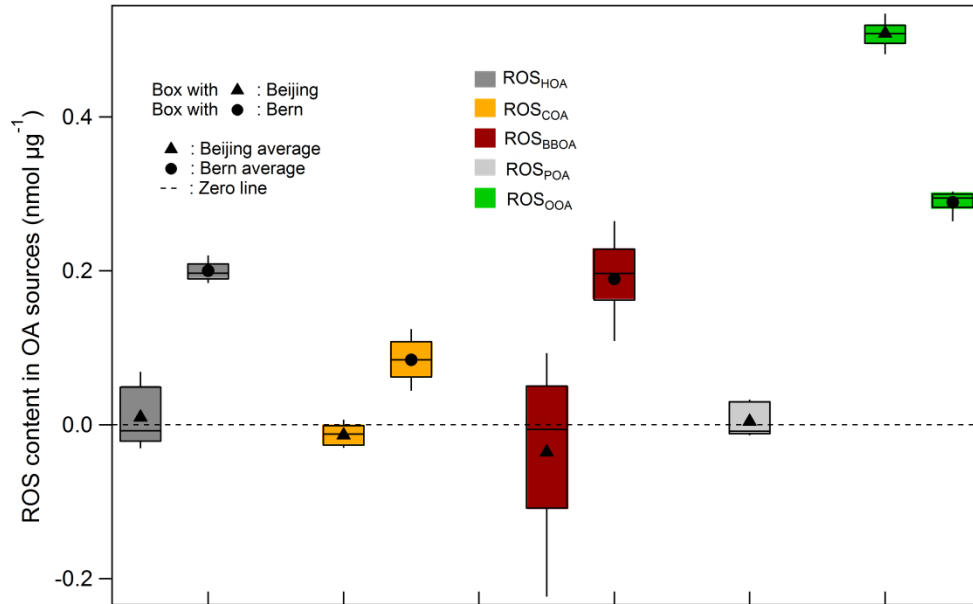
Figure D.7 Box plot of the regression coefficients of ROS with different OA sources obtained from the multiple linear regression model (MLRM) of the ambient data of Beijing (triangle) and Bern (solid circle). The bottom and the top of the box are the first and third quartiles. The band inside the box is the second quartile of the data. The vertical line through the box connects the data from minimum to maximum.

Table D.1 The average regression coefficients and their standard deviation (1 σ) for MLRM with function D1 and D2. These values are also illustrated as box plots in Fig. D.7.

Function D1		ROS = a × (HOA or HOA+CCOA)+ b × COA + c × BBOA + d × OOA+ intercept				
Parameter		a (HOA)	b (COA)	c (BBOA)	d (OOA)	intercept
Beijing	40 fits	0.01±0.04	-0.01±0.01	-0.04±0.11	0.51±0.02	0.07±2.00
	1000 bootstraps	0.01±0.01	0.00±0.01	-0.01±0.06	0.53±0.19	-0.00±0.00
Bern		a (HOA+CCOA)	b (COA)	c (BBOA)	d (OOA)	intercept
	315 fits	0.19±0.02	0.08±0.03	0.20±0.06	0.31±0.02	0.11±0.12
	1000 bootstraps	0.21±0.03	0.08±0.05	0.18±0.04	0.34±0.03	0.00±0.00
Function D2		ROS = e × (HOA+CCOA + COA + BBOA)+ f × OOA+ intercept				
Beijing		e (HOA+CCOA+COA+BBOA)			f (OOA)	intercept
	40 fits	0.00±0.02			0.51±0.02	0.7±2.00

± represents one standard deviation (1 σ) of the average coefficients of all the MLRM fittings; 40 and 315 fits represent the source parameters obtained by using 40 and 315 PMF solutions for Beijing and Bern, respectively, to assess the uncertainties related to the modeled ROS content values. In addition, the PB-ROS concentration used in each fit was generated varying the measured PB-ROS within the measurement uncertainties. 1000 bootstrap runs were performed on the final PMF solution (the average PMF results of all the solutions) to test the sensitivity of the MLRM to the input data, especially in Beijing where model results might be driven by the haze periods.
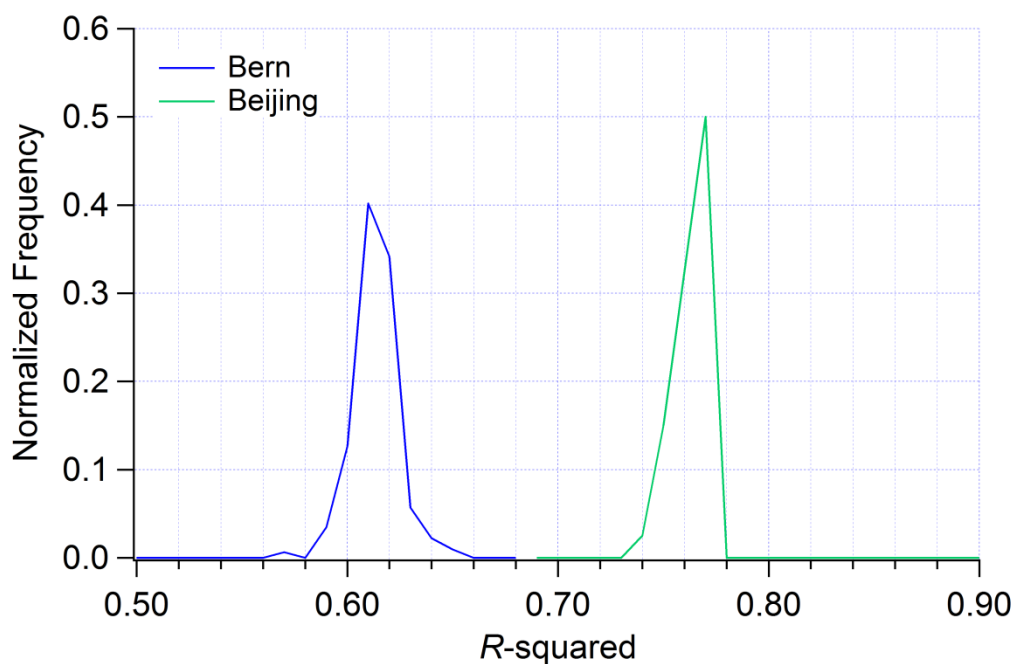
Figure D.8 Normalized frequency distributions of adjusted *R*-squared obtained from the MLRM in Beijing and Bern.
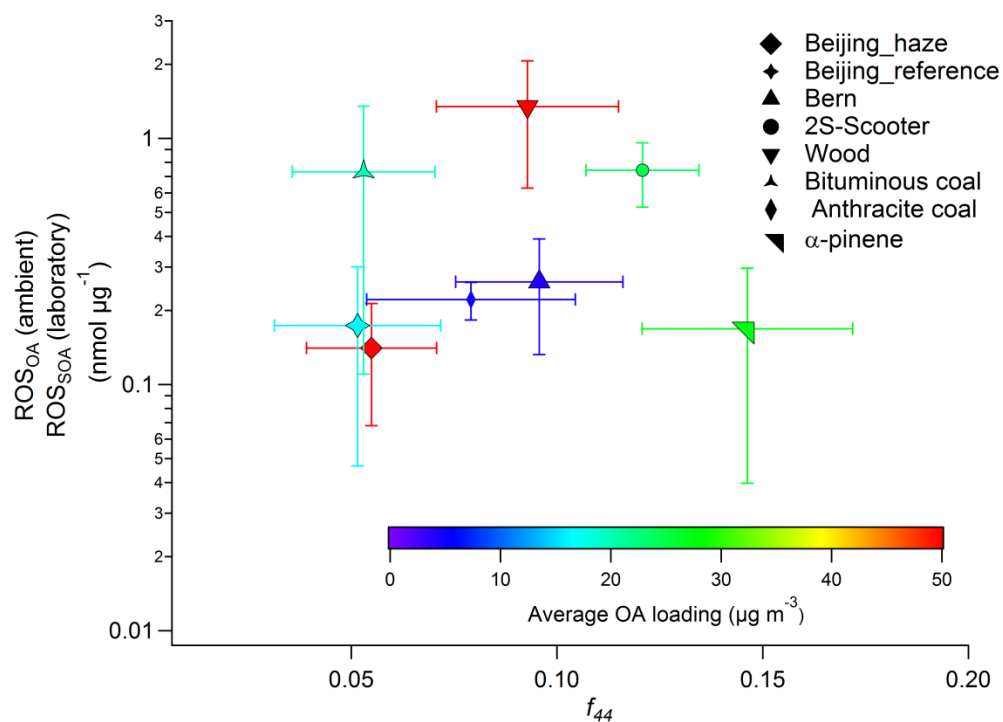
Figure D.9 The ROS$_{OA}$ and ROS$_{SOA}$ vs. f_{44} color coded by the average OA loading. Symbols represent different emission sources, including ambient aerosols in Beijing and Bern, as well as different emission sources investigated in the laboratory experiments. Error bars represent the standard deviations of the average of all experiments.
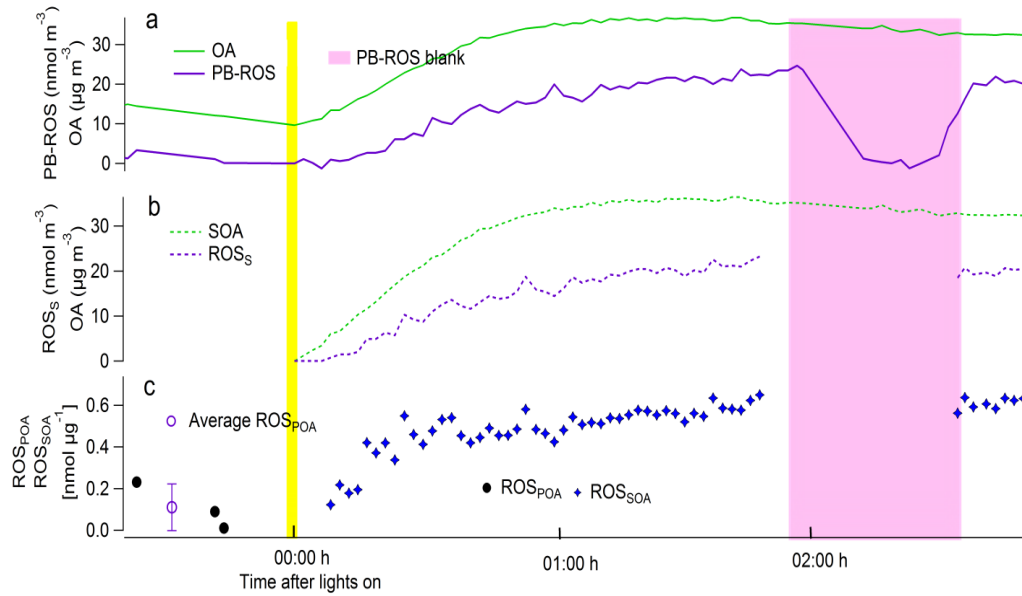
Figure S10 Evolution of the ROS content in SOA during a coal burning smog chamber aging experiment. a) Total OA and ROS, b) SOA and ROS_S, c) ROS content in POA (ROS_{POA}, before lights on) and ROSS content in SOA (ROS_{SOA}, after lights on). The pink area represents the ROS blank measurement.
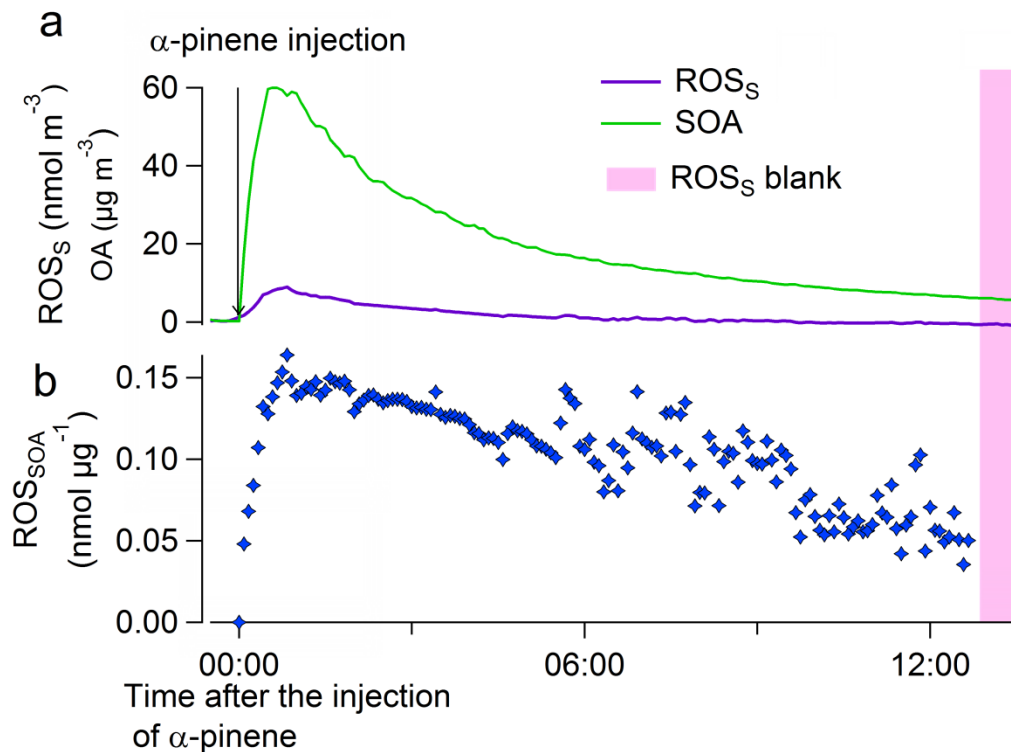
Figure D.11 Evolution of (a) SOA and ROSs, and (b) ROSs content in the SOA (ROS_{SOA} = ROSs/SOA) concentrations measured during an α-pinene ozonolysis experiment in the smog chamber. The pink area represents the ROS blank measurement.

Bibliography

Adam, M., Schikowski, T., Carsin, A. E., Cai, Y., Jacquemin, B., Sanchez, M., Vierkötter, A., Marcon, A., Keidel, D., Sugiri, D., Al Kanani, Z., Nadif, R., Siroux, V., Hardy, R., Kuh, D., Rochat, T., Bridevaux, P.-O., Eeftens, M., Tsai, M.-Y., Villani, S., Phuleria, H. C., Birk, M., Cyrys, J., Cirach, M., de Nazelle, A., Nieuwenhuijsen, M. J., Forsberg, B., de Hoogh, K., Declerq, C., Bono, R., Piccioni, P., Quass, U., Heinrich, J., Jarvis, D., Pin, I., Beelen, R., Hoek, G., Brunekreef, B., Schindler, C., Sunyer, J., Krämer, U., Kauffmann, F., Hansell, A. L., Künzli, N., and Probst-Hensch, N.: Adult lung function and long-term air pollution exposure. ESCAPE: a multicentre cohort study and meta-analysis, Eur. Respir. J., 45, 38-50, 2015.

Adams, K., Greenbaum, D. S., Shaikh, R., van Erp A. M., Russell, A. G. Particulate matter components, sources, and health: Systematic approaches to testing effects. J. Air Waste Manag, Association, 65, 544-558 2015.

Aiken, A. C., DeCarlo, P. F., Kroll, J. H., Worsnop, D. R., Huffman, J. A., Docherty, K. S., Ulbrich, I. M., Mohr, C., Kimmel, J. R., Sueper, D., Sun, Y., Zhang, Q., Trimborn, A., Northway, M., Ziemann, P. J., Canagaratna, M. R., Onasch, T. B., Alfarra, M. R., Prevot, A. S. H., Dommen, J., Duplissy, J., Metzger, A., Baltensperger, U., and Jimenez, J. L.: O/C and OM/OC Ratios of primary, secondary, and ambient organic aerosols with High-Resolution Time-of-Flight Aerosol Mass Spectrometry, Environ. Sci. Technol., 42, 4478-4485, 2008.

Allan, J. D., Jimenez, J. L., Williams, P. I., Alfarra, M. R., Bower, K. N., Jayne, J. T., Coe, H., and Worsnop, D. R.: Quantitative sampling using an Aerodyne aerosol mass spectrometer 1. Techniques of data interpretation and error analysis, Journal of Geophysical Research: Atmospheres, 108, n/a-n/a, 2003.

Antonini, J. M., Clarke, R. W., Krishna Murthy, G. G., Sreekanthan, P., Jenkins, N., Eagar, T. W., and Brain, J. D.: Freshly generated stainless steel welding fume induces greater lung inflammation in rats as compared to aged fume, Toxicol. Letters, 98, 77-86, 1998.

Arellanes, C., Paulson, S. E., Fine, P. M., and Sioutas, C.: Exceeding of Henry's law by hydrogen peroxide associated with urban aerosols, Environ. Sci. Technol., 40, 4859-4866, 2006.

Baltensperger, U., Dommen, J., Alfarra M. R., Duplissy J., Gaeggeler K., Metzger A., Facchini M. C., Decesari S., Finessi E., Reinnig C., Schott M., Warnke J., Hoffmann T., Klatzer B., Puxbaum H., Geiser M., Savi M., Lang D., Kalberer M., and Geiser T.: Combined determination of the chemical composition and of health effects of secondary organic aerosols: The POLYSOA Project, J. Aerosol Med. Pulm. Drug Deliv., 21, 145-154, 2008.

Barmet, P., Dommen, J., DeCarlo, P. F., Tritscher, T., Praplan, A. P., Platt, S. M., Prévôt, A. S. H., Donahue, N. M., and Baltensperger, U.: OH clock determination by proton transfer reaction mass spectrometry at an environmental chamber, Atmos. Meas. Tech., 5, 647-656, 2012.

Barregard, L., Sallsten, G., Gustafson, P., Andersson, L., Johansson, L., and Basu, S.: Experimental exposure to wood-smoke particles in healthy humans: effects on markers of inflammation, coagulation, and lipid peroxidation, Inhal. Toxicol., 18, 2006.

Bates, J. T., Weber, R. J., Abrams, J., Verma, V., Fang, T., Klein, M., Strickland, M. J., Sarnat, S. E., Chang, H. H., Mulholland, J. A., Tolbert, P. E., and Russell, A. G.: Reactive oxygen species generation linked to sources of atmospheric particulate matter and cardiorespiratory effects, Environ. Sci. Technol., 49, 13605-13612, 2015.

Beelen, R., Raaschou-Nielsen, O., Stafoggia, M., Andersen, Z. J., Weinmayr, G., Hoffmann, B., Wolf, K., Samoli, E., Fischer, P., Nieuwenhuijsen, M., Vineis, P., Xun, W. W., Katsouyanni, K., Dimakopoulou, K., Oudin, A., Forsberg, B., Modig, L., Havulinna, A. S., Lanki, T., Turunen, A., Oftedal, B., Nystad, W., Nafstad, P., De Faire, U., Pedersen, N. L., Östenson, C.-G., Fratiglioni, L., Penell, J., Korek, M., Pershagen, G., Eriksen, K. T., Overvad, K., Ellermann, T., Eeftens, M., Peeters, P. H., Meliefste, K., Wang, M., Bueno-de-Mesquita, B., Sugiri, D., Krämer, U., Heinrich, J., de Hoogh, K., Key, T., Peters, A., Hampel, R., Concin, H., Nagel, G., Ineichen, A., Schaffner, E., Probst-Hensch, N., Künzli, N., Schindler, C., Schikowski, T., Adam, M., Phuleria, H., Vilier, A., Clavel-Chapelon, F., Declercq, C., Grioni, S., Krogh, V., Tsai, M.-Y., Ricceri, F., Sacerdote, C., Galassi, C., Migliore, E., Ranzi, A., Cesaroni, G., Badaloni, C., Forastiere, F., Tamayo, I., Amiano, P., Dorronsoro, M., Katsoulis, M., Trichopoulou, A., Brunekreef, B., and Hoek, G.: Effects of long-term exposure to air pollution on natural-cause mortality: an analysis of 22 European cohorts within the multicentre ESCAPE project, The Lancet, 383, 785-795, 2013.

Beelen, R., Raaschou-Nielsen, O., Stafoggia, M., Andersen, Z. J., Weinmayr, G., Hoffmann, B., Wolf, K., Samoli, E., Fischer, P., Nieuwenhuijsen, M., Vineis, P., Xun, W. W., Katsouyanni, K., Dimakopoulou, K., Oudin, A., Forsberg, B., Modig, L., Havulinna, A. S., Lanki, T., Turunen, A., Oftedal, B., Nystad, W., Nafstad, P., De Faire, U., Pedersen, N. L., Östenson, C.-G., Fratiglioni, L., Penell, J., Korek, M., Pershagen, G., Eriksen, K. T., Overvad, K., Ellermann, T., Eeftens, M., Peeters, P. H., Meliefste, K., Wang, M., Bueno-de-Mesquita, B., Sugiri, D., Krämer, U., Heinrich, J., de Hoogh, K., Key, T., Peters, A., Hampel, R., Concin, H., Nagel, G., Ineichen, A., Schaffner, E., Probst-Hensch, N., Künzli, N., Schindler, C., Schikowski, T., Adam, M., Phuleria, H., Vilier, A., Clavel-Chapelon, F., Declercq, C., Grioni, S., Krogh, V., Tsai, M.-Y., Ricceri, F., Sacerdote, C., Galassi, C., Migliore, E., Ranzi, A., Cesaroni, G., Badaloni, C., Forastiere, F., Tamayo, I., Amiano, P., Dorronsoro, M., Katsoulis, M., Trichopoulou, A., Brunekreef, B., and Hoek, G.: Effects of long-term exposure to air pollution on natural-cause mortality: an analysis of 22 European cohorts within the multicentre ESCAPE project, The Lancet, 383, 785-795, 2014.

Berglund, G. I., Carlsson, G. H., Smith, A. T., Szoke, H., Henriksen, A., and Hajdu, J.: The catalytic pathway of horseradish peroxidase at high resolution, Nature, 417, 463-468, 2002.

Bologa, A., Paur, H.-R., and Woletz, K.: Development and study of an electrostatic precipitator for small scale wood combustion, Environ. Sci. Technol., 5, 168-173, 2011.

Boman, B. C., Forsberg, A. B., and Järvholm, B. G.: Adverse health effects from ambient air pollution in relation to residential wood combustion in modern society, Scandinavian Journal of Work, Environ. & Health, 251-260, 2003.

Bond, T. C., and Bergstrom, R. W.: Light Absorption by Carbonaceous Particles: An investigative review,   Aerosol Sci. Technol., 40, 27-67, 2006.

Bruns, E. A., El Haddad, I., Keller, A., Klein, F., Kumar, N. K., Pieber, S. M., Corbin, J. C., Slowik, J. G., Brune, W. H., Baltensperger, U., and Prévôt, A. S. H.: Inter-comparison of laboratory smog chamber and flow reactor systems on organic aerosol yield and composition, Atmos. Meas. Tech., 8, 2315-2332, 2015.

Bruns, E. A., El Haddad, I., Slowik, J. G., Kilic, D., Klein, F., Baltensperger, U., and Prévôt, A. S. H.: Identification of significant precursor gases of secondary organic aerosols from residential wood combustion, Sci. Rep., 6, 27881, 2016.

Bruns, E. A., Slowik, J. G., El Haddad, I., Kilic, D., Klein, F., Dommen, J., Temime-Roussel, B., Marchand, N., Baltensperger, U., and Prévôt, A. S. H.: Characterization of gas-phase organics using proton transfer reaction time-of-flight mass spectrometry: fresh and aged residential wood combustion emissions, Atmos. Chem. Phys., 17, 705-720, 2017.

Bureau, B. T. M.: Current measures on traffic management in Beijing (in Chinese), 2004.

Burnett, R. T., Brook, J., Dann, T., Delocla, C., Philips, O., Cakmak, S., Vincent, R., Goldberg, M. S., and Krewski, D.: Association between particulate- and gas-phase components of urban air pollution and daily mortality in eight Canadian cities. Inhal. Toxicol., 12 Suppl 4, 15-39, 2000.

Buseck, P. R. , Adachi, K., Nanoparticles in the atmoshpere, Elements, 4, 389-394, 2008.

Buseck, P. R., Pósfai, M.: Airborne minerals and related aerosol particles: Effects on climate and the environment, Proc. Natl. Acad. Sci. U. S. A., 96, 3372-3379, 1999.

Calas, A., Uzu, G., Kelly, F. J., Houdier, S., Martins, J. M. F., Thomas, F., Molton, F., Charron, A., Dunster, C., Oliete, A., Jacob, V., Besombes, J. L., Chevrier, F., and Jaffrezo, J. L.: Comparison between five acellular oxidative potential measurement assays performed with detailed chemistry on PM_{10} samples from the city of Chamonix (France), Atmos. Chem. Phys., 18, 7863-7875, 2018.

Canada, E. P. B. E.: Impact of Residential Wood Stove Replacement on Air Emissions in Canada, in: Environmental Protection Branch Environment Canada, Montréal, 2005.

Canonaco, F., Crippa, M., Slowik, J. G., Baltensperger, U., Prévôt, A.S.H.: SoFi, an IGOR-based interface for the efficient use of the generalized multilinear engine (ME-2) for the source apportionment: ME-2 application to aerosol mass spectrometer data, Atmos. Meas. Tech., 6, 3649-3661, 2013.

Charrier, J. G., and Anastasio, C.: Impacts of antioxidants on hydroxyl radical production from individual and mixed transition metals in a surrogate lung fluid, Atmos. Environ. (Oxford, England : 1994), 45, 7555-7562, 2011.

Charrier, J. G., and Anastasio, C.: On dithiothreitol (DTT) as a measure of oxidative potential for ambient particles: evidence for the importance of soluble transition metals, Atmos. Chem. Phys., 12, 9321-9333, 2012.

Chen, R., Peng, R. D., Meng, X., Zhou, Z., Chen, B., Kan, H. Seasonal variation in the acute effect of particulate air pollution on mortality in the China Air Pollution and Health Effects Study (CAPES), Sci. Total Environ., 450-451, 259-265, 2013.

Chen, X., Hopke, P. K., and Carter, W. P. L.: Secondary organic aerosol from ozonolysis of biogenic volatile organic compounds: Chamber studies of particle and reactive oxygen species formation, Environ. Sci. Technol., 45, 276-282, 2011.

Chen, Z., Cai, J., Gao, B., Xu, B., Dai, S., He, B., and Xie, X.: Detecting the causality influence of individual meteorological factors on local PM (2.5) concentration in the Jing-Jin-Ji region, Sci. Rep., 7, 40735, 2017.

China Meteorological Administration (2010). Observation and Forecasting Levels of Haze. QX/T 113-2010.

Cho, A. K., Sioutas, C., Miguel, A. H., Kumagai, Y., Schmitz, D. A., Singh, M., Eiguren-Fernandez, A., and Froines, J. R.: Redox activity of airborne particulate matter at different sites in the Los Angeles Basin, Environ. Res., 99, 40-47, 2005.

Ciarelli, G., Aksoyoglu, S., El Haddad, I., Bruns, E. A., Crippa, M., Poulain, L., Äijälä, M., Carbone, S., Freney, E., O'Dowd, C., Baltensperger, U., and Prévôt, A. S. H.: Modelling winter organic aerosol at the European scale with CAMx: evaluation and source apportionment with a VBS parameterization based on novel wood burning smog chamber experiments, Atmos. Chem. Phys., 17, 7653-7669, 2017.

Cohen, A. J., Brauer, M., Burnett, R., Anderson, H. R., Frostad, J., Estep, K., Balakrishnan, K., Brunekreef, B., Dandona, L., Dandona, R., Feigin, V., Freedman, G., Hubbell, B., Jobling, A., Kan, H., Knibbs, L., Liu, Y., Martin, R., Morawska, L., Pope, C. A., 3rd, Shin, H., Straif, K., Shaddick, G., Thomas, M., van Dingenen, R., van Donkelaar, A., Vos, T., Murray, C. J. L., and Forouzanfar, M. H.: Estimates and 25-year trends of the global burden of disease attributable to ambient air pollution: an analysis of data from the Global Burden of Diseases Study 2015, Lancet, 389, 1907-1918, 2017.

Cohen, A. J.: Outdoor air pollution and lung cancer, Environ. Health Perspect., 108, 743-750, 2000.

Crippa, M., DeCarlo, P. F., Slowik, J. G., Mohr, C., Heringa, M. F., Chirico, R., Poulain, L., Freutel, F., Sciare, J., Cozic, J., Di Marco, C. F., Elsasser, M., Nicolas, J. B., Marchand, N., Abidi, E., Wiedensohler, A., Drewnick, F., Schneider, J., Borrmann, S., Nemitz, E., Zimmermann, R., Jaffrezo, J. L., Prevot, A. S. H., and Baltensperger, U.: Wintertime aerosol chemical composition and source apportionment of the organic fraction in the metropolitan area of Paris, Atmos. Chem. Phys., 13, 961-981, 2013a.

Crippa, M., El Haddad, I., Slowik, J. G., DeCarlo, P. F., Mohr, C., Heringa, M. F., Chirico, R., Marchand, N., Sciare, J., Baltensperger, U., and Prévôt, A. S. H.: Identification of marine and continental aerosol sources in Paris using high resolution aerosol mass spectrometry, J. Geophy. Res.: Atmospheres, 118, 1950-1963, 2013b.

Cross, C. E., van der Vliet, A., Louie, S., Thiele, J. J., and Halliwell, B.: Oxidative stress and antioxidants at biosurfaces: plants, skin, and respiratory tract surfaces, Environ. Health Perspect., 106, 1241-1251, 1998.

Daellenbach, K. R., Stefenelli, G., Bozzetti, C., Vlachou, A., Fermo, P., Gonzalez, R., Piazzalunga, A., Colombi, C., Canonaco, F., Hueglin, C., Kasper-Giebl, A., Jaffrezo, J. L., Bianchi, F., Slowik, J. G., Baltensperger, U., El Haddad, I., and Prévôt, A. S. H.: Long-term chemical analysis and organic aerosol source apportionment at 9 sites in Central Europe: Source identification and uncertainty assessment, Atmos. Chem. Phys. Discuss., 2017, 1-36, 2017.

Daher, N., Ning, Z., Cho, A. K., Shafer, M., Schauer, J. J., and Sioutas, C.: Comparison of the chemical and oxidative characteristics of particulate matter (PM) collected by different methods: filters, impactors, and biosamplers, Aerosol Sci. Technol., 45, 1294-1304, 2011.

Dall'Osto, M., Beddows, D. C. S., Harrison, R. M., and Onat, B.: Fine iron aerosols are internally mixed with nitrate in the urban European atmosphere, Environ. Sci. Technol. 50, 4212-4220, 2016.

Dall'Osto, M., Ovadnevaite, J., Ceburnis, D., Martin, D., Healy, R. M., O'Connor, I. P., Kourtchev, I., Sodeau, J. R., Wenger, J. C., and O'Dowd, C.: Characterization of urban aerosol in Cork city (Ireland) using aerosol mass spectrometry, Atmos. Chem. Phys., 13, 4997-5015, 2013.

DeCarlo, P. F., Kimmel, J. R., Trimborn, A., Northway, M. J., Jayne, J. T., Aiken, A. C., Gonin, M., Fuhrer, K., Horvath, T., Docherty, K. S., Worsnop, D. R., and Jimenez, J. L.: Field-deployable, high-resolution, time-of-flight aerosol mass spectrometer, Anal. Chem., 78, 8281-8289, 2006.

Delfino, R. J., Sioutas, C., and Malik, S.: Potential role of ultrafine particles in associations between airborne particle mass and cardiovascular health, Environ. Health Perspect., 113, 934-946, 2005.

Delfino, R. J., Staimer, N., Tjoa, T., Arhami, M., Polidori, A., Gillen, D. L., George, S. C., Shafer, M. M., Schauer, J. J., and Sioutas, C.: Associations of primary and secondary organic aerosols with airway and systemic inflammation in an elderly panel cohort, Epidemiology, 21, 892-902, 2010.

Delfino, R. J., Staimer, N., Tjoa, T., Gillen, D. L., Schauer, J. J., and Shafer, M. M.: Airway inflammation and oxidative potential of air pollutant particles in a pediatric asthma panel, J. Expo. Sci. Environ. Epidemiol., 23, 466-473, 2013.

Deneke, S. M., Baxter, D. F., Phelps, D. T., and Fanburg, B. L.: Increase in endothelial cell glutathione and precursor amino acid uptake by diethyl maleate and hyperoxia, Am. J. Physiol., 257, 1989.

Devasagayam, T. P., Tilak, J. C., Boloor, K. K., Sane, K. S., Ghaskadbi, S. S., and Lele, R. D.: Free radicals and antioxidants in human health: current status and future prospects, J. Assoc. Physicians India, 52, 794-804, 2004.

DiStefano, E., Eiguren-Fernandez, A., Delfino, R. J., Sioutas, C., Froines, J. R., and Cho, A. K.: Determination of metal-based hydroxyl radical generating capacity of ambient and diesel exhaust particles, Inhal. Toxicol., 21, 731-738, 2009.

Dockery, D. W., Pope , C. A., Xu , X., Spengler , J. D., Ware , J. H., Fay , M. E., Ferris , B. G. J., and Speizer , F. E.: An Association between air pollution and mortality in six U.S. cities, N. Engl. J. Med., 329, 1753-1759, 1993.

Donahue, N. M., Robinson, A. L., Stanier, C. O., and Pandis, S. N.: Coupled partitioning, dilution, and chemical aging of semivolatile organics, Environ. Sci. Technol., 40, 2635-2643, 2006.

Donaldson, K., Brown, D., Clouter, A., Duffin, R., MacNee, W., Renwick, L., Tran, L., and Stone, V.: The pulmonary toxicology of ultrafine particles, J. Aerosol Med., 15, 213-220, 2002.

Drinovec, L., Močnik, G., Zotter, P., Prévôt, A. S. H., Ruckstuhl, C., Coz, E., Rupakheti, M., Sciare, J., Müller, T., Wiedensohler, A., and Hansen, A. D. A.: The "dual-spot" Aethalometer: an improved measurement of aerosol black carbon with real-time loading compensation, Atmos. Meas. Tech., 8, 1965-1979, 2015.

Drinovec, L., Močnik, G., Zotter, P., Prevot, A., Ruckstuhl, C., Coz, E., Rupakheti, M., Sciare, J., Müller, T., Wiedensohler, A., and Hansen, A.: The "dual-spot" Aethalometer: 2014.

Du, Y., Xu, X., Chu, M., Guo, Y., and Wang, J.: Air particulate matter and cardiovascular disease: the epidemiological, biomedical and clinical evidence, J. Thoracic Dis., 8, E8-E19, 2016.

Dusek, U., Frank, G. P., Hildebrandt, L., Curtius, J., Schneider, J., Walter, S., Chand, D., Drewnick, F., Hings, S., Jung, D., Borrmann, S., and Andreae, M. O.: Size matters more than chemistry for Cloud-Nucleating ability of aerosol particles, Science, 312, 1375-1378, 2006.

Ebi, K., and McGregor, G.: Climate change, tropospheric ozone and particulate matter, and health impacts, Ciência & Saúde Coletiva, 14, 2281-2293, 2009.

EEA: European Union emission inventory report 1990-2011 under the UNECE Convention on Long-range Transboundary Air Pollution (LRTAP), in: EEA Technical report, EEA (European Environment Agency), Copenhagen, 2013.

Elser, M., Huang, R. J., Wolf, R., Slowik, J. G., Wang, Q., Canonaco, F., Li, G., Bozzetti, C., Daellenbach, K. R., Huang, Y., Zhang, R., Li, Z., Cao, J., Baltensperger, U., El-Haddad, I., and Prévôt, A. S. H.: New insights into $PM_{2.5}$ chemical composition and sources in two major cities in China during extreme haze events using aerosol mass spectrometry, Atmos. Chem. Phys., 16, 3207-3225, 2016.

EPBE: Impact of Residential Wood Stove Replacement on Air Emissions in Canada, in, Environmental Protection Branch Environment Canada, Montréal, 2005.

Fang, T., Verma, V., Bates, J. T., Abrams, J., Klein, M., Strickland, M. J., Sarnat, S. E., Chang, H. H., Mulholland, J. A., Tolbert, P. E., Russell, A. G., and Weber, R. J.: Oxidative potential of ambient water-soluble $PM_{2.5}$ in the southeastern United States: contrasts in sources and health associations between ascorbic acid (AA) and dithiothreitol (DTT) assays, Atmos. Chem. Phys., 16, 3865-3879, 2016.

Fang, T., Verma, V., Guo, H., King, L. E., Edgerton, E. S., and Weber, R. J.: A semi-automated system for quantifying the oxidative potential of ambient particles in aqueous extracts using the dithiothreitol (DTT) assay: results from the Southeastern Center for Air Pollution and Epidemiology (SCAPE), Atmos. Meas. Tech., 8, 471-482, 2015.

Fantechi, G., Jensen, N. R., Saastad, O., Hjorth, J., and Peeters, J.: Reactions of Cl Atoms with Selected VOCs: Kinetics, Products and Mechanisms, J. Atmos. Chem., 31, 247-267, 1998.

Fitzpatrick, E. M., Ross, A. B., Bates, J., Andrews, G., Jones, J. M., Phylaktou, H., Pourkashanian, M., and Williams, A.: Emission of oxygenated species from the combustion of pine wood and its relation to soot formation, Process Saf. Environ. Prot., 85, 430-440, 2007.

Franklin, M., Koutrakis, P., Schwartz, P., The role of particle composition on the association between $PM_{2.5}$ and mortality. Epidemiology, 19, 680-689, 2008.

Friedlander, S. K., and Yeh, E. K.: The submicron atmospheric aerosol as a carrier of reactive chemical species: case of peroxides, Appl. Occup. Environ. Hyg., 13, 416-420, 1998.

Fröhlich, R., Crenn, V., Setyan, A., Belis, C., Canonaco, F., Favez, O., Riffault, V., G. Slowik, J., Aas, W., Aijälä, M., Alastuey, A., Artíñano, B., Bonnaire, N., Bozzetti, C., Bressi, M., Carbone, C., Coz, E., L. Croteau, P., J. Cubison, M., and Prevot, A.: ACTRIS ACSM intercomparison – Part 2: Intercomparison of ME-2 organic source apportionment results from 15 individual, co-located aerosol mass spectrometers, 2555-2576, 2015.

Fröhlich, R., Cubison, M. J., Slowik, J. G., Bukowiecki, N., Prévôt, A. S. H., Baltensperger, U., Schneider, J., Kimmel, J. R., Gonin, M., Rohner, U., Worsnop, D. R., and Jayne, J. T.: The ToF-ACSM: a portable aerosol chemical speciation monitor with TOFMS detection, Atmos. Meas. Tech., 6, 3225-3241, 2013.

Fuller, G. W., Tremper, A. H., Baker, T. D., Yttri, K. E., and Butterfield, D.: Contribution of wood burning to PM10 in London, Atmospheric Environ., 87, 87-94, 2014.

Fuller, S. J., Wragg, F. P. H., Nutter, J., and Kalberer, M.: Comparison of on-line and off-line methods to quantify reactive oxygen species (ROS) in atmospheric aerosols, Atmos. Environ., 92, 97-103, 2014.

Fullerton D. G., Semple A. S., S., Kalambo F., Malamba R., White S., Jack S., Calverley P. M., Gordon S. B.: Wood smoke exposure, poverty and impaired lung function in Malawian adults, Int. J. Tuberc. Lung Dis., 15, 391-398, 2011.

Gallimore, P. J., Mahon, B. M., Wragg, F. P. H., Fuller, S. J., Giorio, C., Kourtchev, I., and Kalberer, M.: Multiphase composition changes and reactive oxygen species formation during limonene oxidation in the new Cambridge Atmospheric Simulation Chamber (CASC), Atmos. Chem. Phys. Discuss., 2017, 1-30, 2017.

Gaschen, A., Lang, D., Kalberer, M., Savi, M., Geiser, T., Gazdhar, A., Lehr, C.-M., Bur, M., Dommen, J., Baltensperger, U., and Geiser, M.: Cellular responses after exposure of lung cell cultures to secondary organic aerosol particles, Environ. Sci. Technol., 44, 1424-1430, 2010.

Geng, C., Wang, K., Wang, W., Chen, J., Liu, X., and Liu, H.: Smog chamber study on the evolution of fume from residential coal combustion, J. Environ. Sci. (China), 24, 169-176, 2012.

Germain, A.: Impact of residential wood stove replacement on air emissions in Canada, Environmental Protection Branch Environment, Canada, Montréal, 19 pp., 2005.

Godri, K. J., Harrison, R. M., Evans, T., Baker, T., Dunster, C., Mudway, I. S., and Kelly, F. J.: Increased oxidative burden associated with traffic component of ambient particulate matter at roadside and urban background schools sites in London, PLoS One, 6, e21961, 2011.

Guarnieri, M., and Balmes, J. R.: Outdoor air pollution and asthma, Lancet, 383, 1581-1592, 2014.

Gundel, L. A., R.L., D., H., R., and T., N.: The relationship between Optical Attenuation and Black Carbon concentration for ambient and source particles, Sci. Total Environ., 36, 191-196, 1984.

Gurgueira, S. A., Lawrence, J., Coull, B., Murthy, G. G., and Gonzalez-Flecha, B.: Rapid increases in the steady-state concentration of reactive oxygen species in the lungs and heart after particulate air pollution inhalation, Environ. Health Perspect., 110, 749-755, 2002.

Gysel, M., Crosier, J., Topping, D. O., Whitehead, J. D., Bower, K. N., Cubison, M. J., Williams, P. I., Flynn, M. J., McFiggans, G. B., and Coe, H.: Closure study between chemical composition and hygroscopic growth of aerosol particles during TORCH2, Atmos. Chem. Phys., 7, 6131-6144, 2007.

Halliwell, B., and Cross, C. E.: Oxygen-derived species: their relation to human disease and environmental stress, Environ. Health Perspect., 102, 5-12, 1994.

Hallquist, M., Wenger, J. C., Baltensperger, U., Rudich, Y., Simpson, D., Claeys, M., Dommen, J., Donahue, N. M., George, C., Goldstein, A. H., Hamilton, J. F., Herrmann, H., Hoffmann, T., Iinuma, Y., Jang, M., Jenkin, M. E., Jimenez, J. L., Kiendler-Scharr, A., Maenhaut, W., McFiggans, G., Mentel, T. F., Monod, A., Prévôt, A. S. H., Seinfeld, J. H., Surratt, J. D., Szmigielski, R., and Wildt, J.: The formation, properties and impact of secondary organic aerosol: current and emerging issues, Atmos. Chem. Phys., 9, 5155-5236, 2009.

Hammond, D. M., Dvonch, J. T., Keeler, G. J., Parker, E. A., Kamal, A. S., Barres, J. A., Yip, F. Y., and Brakefield-Caldwell, W.: Sources of ambient fine particulate matter at two community sites in Detroit, Michigan, Atmospheric Environ., 42, 720-732, 2008.

Hansen, A. D. A., Rosen, H., and Novakov, T.: The aethalometer – an instrument for the real-time measurement of optical absorption by aerosol particles, Sci. Total Environ., 191-196, 1984.

Hari, P., and Kulmala L., Boreal forest and chlimate change, Springer Netherlands, 2008.

Hasson, A. S., and Paulson, S. E.: An investigation of the relationship between gas-phase and aerosol-borne hydroperoxides in urban air, J. Aerosol Sci., 34, 459-468, 2003.

Hausmann, M., Brandenburger, U., Brauers, T., and Dorn, H.-P.: Detection of tropospheric OH radicals by long-path differential-optical-absorption spectroscopy: Experimental setup, accuracy, and precision, Journal of Geophysical Research: Atmospheres, 102, 16011-16022, 1997.

He, T., Yang, Z., Liu, T., Shen, Y., Fu, X., Qian, X., Zhang, Y., Wang, Y., Xu, Z., Zhu, S., Mao, C., Xu, G., and Tang, J.: Ambient air pollution and years of life lost in Ningbo, China, 6, 22485, 2016.

HEI: Panel on the Health Effects of Traffic-Related Air Pollution. Traffic-related air Pollution: a critical review of the literature on emissions, exposure, and health effects, MA: Health Effects Institute, 2009.

Heringa, M. F., DeCarlo, P. F., Chirico, R., Lauber, A., Doberer, A., Good, J., Nussbaumer, T., Keller, A., Burtscher, H., Richard, A., Miljevic, B., Prevot, A. S. H., and Baltensperger, U.: Time resolved

characterization of primary emissions from residential wood combustion appliances, Environ. Sci. Technol., 46, 11418–11425, 2012.

Heringa, M. F., DeCarlo, P. F., Chirico, R., Tritscher, T., Dommen, J., Weingartner, E., Richter, R., Wehrle, G., Prévôt, A. S. H., and Baltensperger, U.: Investigations of primary and secondary particulate matter of different wood combustion appliances with a high-resolution time-of-flight aerosol mass spectrometer, Atmos. Chem. Phys., 11, 5945-5957, 2011.

Hopke, P. K.: Review of receptor modeling methods for source apportionment, Journal of the Air & Waste Management Association, 66, 237-259, 2016.

Hsiao, I. L., Hsieh, Y. K., Wang, C. F., Chen, I. C., and Huang, Y. J.: Trojan-horse mechanism in the cellular uptake of silver nanoparticles verified by direct intra- and extracellular silver speciation analysis, Environ. Sci. Technol., 49, 2015.

Huang, R.-J., Zhang, Y., Bozzetti, C., Ho, K.-F., Cao, J.-J., Han, Y., Daellenbach, K. R., Slowik, J. G., Platt, S. M., Canonaco, F., Zotter, P., Wolf, R., Pieber, S. M., Bruns, E. A., Crippa, M., Ciarelli, G., Piazzalunga, A., Schwikowski, M., Abbaszade, G., Schnelle-Kreis, J., Zimmermann, R., An, Z., Szidat, S., Baltensperger, U., Haddad, I. E., and Prevot, A. S. H.: High secondary aerosol contribution to particulate pollution during haze events in China, Nature, 514, 218-222, 2014.

Huang, W., Zhang, Y., Zhang, Y., Fang, D., and Schauer, J. J.: Optimization of the measurement of particle-bound reactive oxygen species with 2′,7′-dichlorofluorescin (DCFH), Water Air Soil Pollut., 227, 2016.

Hung, H.-F., and Wang, C.-S.: Experimental determination of reactive oxygen species in Taipei aerosols, J. Aerosol Sci., 32, 1201-1211, 2001.

Hwang, B.-F., Chen, Y.-H., Lin, Y.-T., Wu, X.-T., and Leo Lee, Y.: Relationship between exposure to fine particulates and ozone and reduced lung function in children, Environ. Res., 137, 382-390, 2015. /syr/en/mains1.html#1-1, last assessed: 09 November 2017.

ICRP: International Commission on Radiological Protection: Human respiratory model for radiological protection, 1-300, 1994.

IEO: International energy outlook 2006, June 2006; U.S. Department of Energy: Washington, DC, 2006.

Ingham, D. B.: Diffusion of aerosols from a stream flowing through a cylindrical tube, J. Aerosol Sci., 6, 125-132, 1975.

IPCC, Myhre, G., Shindell, D., Bréon, F.-M., Fuglestvedt W. C., Huang, J., Koch, D., Lamarque, J.-F., Lee, D., Nakajima, B. M., T., Robock, A., Stephens, G., Takemura, T., and Zhang, H.: Anthropogenic and Natural Radiative Forcing. In: Climate Change 2013: The Physical Science Basis. Contribution of Working Group I to the Fifth Assessment Report of the Intergovernmental Panel on Climate Change [Stocker, T.F., Qin D., Plattner G.-K., Tignor M., Allen S.K., Boschung, J., Nauels A., Xia, Y., Bex V. and Midgley, P.M. (eds.)]. Cambridge University Press, Cambridge, United Kingdom and New York, NY, USA, 2013.

IPCC: Fifth assessment report, summary for policymakers, Synthesis Report, Climate Change 2014.

IPCC: Fourth assessment report: Climate Change 2007. https://www.ipcc.ch/publications_and_data/ar4, last assessed: 10th, November 2017.

Jackson, A. V., and Hewitt, C. N.: Atmosphere hydrogen peroxide and Oorganic hydroperoxides: a review, Crit. Rev. Environ. Sci. Technol., 29, 175-228, 1999.

Janssen, N. A. H., Strak, M., Yang, A., Hellack, B., Kelly, F. J., Kuhlbusch, T. A. J., Harrison, R. M., runekreef, B., Cassee, F. R., Steenhof, M., and Hoek, G.: Associations between three specific a-cellular measures of the oxidative potential of particulate matter and markers of acute airway and nasal inflammation in healthy volunteers, Occup. Environ. Med., 72, 49–56, 2015.

Jayne, J. T., Leard, D. C., Zhang, X., Davidovits, P., Smith, K. A., Kolb, C. E., and Worsnop, D. R.: Development of an aerosol mass spectrometer for size and composition analysis of submicron particles, Aerosol Sci.Technol., 33, 49-70, 2000.

Jimenez, J. L., Canagaratna, M. R., Donahue, N. M., Prevot, A. S. H., Zhang, Q., Kroll, J. H., DeCarlo, P. F., Allan, J. D., Coe, H., Ng, N. L., Aiken, A. C., Docherty, K. S., Ulbrich, I. M., Grieshop, A. P., Robinson, A. L., Duplissy, J., Smith, J. D., Wilson, K. R., Lanz, V. A., Hueglin, C., Sun, Y. L., Tian, J., Laaksonen, A., Raatikainen, T., Rautiainen, J., Vaattovaara, P., Ehn, M., Kulmala, M., Tomlinson, J. M., Collins, D. R., Cubison, M. J., Dunlea, J., Huffman, J. A., Onasch, T. B., Alfarra, M. R., Williams, P. I., Bower, K., Kondo, Y., Schneider, J., Drewnick, F., Borrmann, S., Weimer, S., Demerjian, K., Salcedo, D., Cottrell, L., Griffin, R., Takami, A., Miyoshi, T., Hatakeyama, S., Shimono, A., Sun, J. Y., Zhang, Y. M., Dzepina, K., Kimmel, J. R., Sueper, D., Jayne, J. T., Herndon, S. C., Trimborn, A. M., Williams, L. R., Wood, E. C., Middlebrook, A. M., Kolb, C. E., Baltensperger, U., and Worsnop, D. R.: Evolution of organic aerosols in the atmosphere, Science, 326, 1525-1529, 2009.

Jimenez, J. L., Jayne, J. T., Shi, Q., Kolb, C. E., Worsnop, D. R., Yourshaw, I., Seinfeld, J. H., Flagan, R. C., Zhang, X., Smith, K. A., Morris, J. W., and Davidovits, P.: Ambient aerosol sampling using the Aerodyne Aerosol Mass Spectrometer, J. Geophys. Res. Atmos., 108, n/a-n/a, 2003.

Johansson, L. S., Leckner, B., Gustavsson, L., Cooper, D., Tullin, C., and Potter, A.: Emission characteristics of modern and old-type residential boilers fired with wood logs and wood pellets, Atmos. Environ., 38, 4183-4195, 2004.

Johnson, R. L.: Relative effects of air pollution on lungs and heart, Circulation, 109, 5-7, 2004.

Johnston, F. H., Henderson, S. B., Chen, Y., Randerson, J. T., Marlier, M., Defries, R. S., Kinney, P., Bowman, D. M., and Brauer, M.: Estimated global mortality attributable to smoke from landscape fires, Environ. Health Perspect., 120, 695-701, 2012.

Judith C. Chow, Nanoparticles and the Environment, J. the Air & Waste Manag. Assoc., 55, 706-707, 2005.

Kaiser, J.: Air pollution. Evidence mounts that tiny particles can kill, Science, 289, 22-23, 2000.

Kang, E., Root, M. J., Toohey, D. W., and Brune, W. H.: Introducing the concept of Potential Aerosol Mass (PAM), Atmos. Chem. Phys., 7, 5727-5744, 2007.

Kao, M. C., and Wang, C. S.: Reactive oxygen species in intense smoke, in: Aerosol Air Qual. Res., 2002/06 ed., 2, 61-69, 2002.

Keenan, C. R., Goth-Goldstein, R., Lucas, D., and Sedlak, D. L.: Oxidative stress induced by zero-valent iron nanoparticles and Fe(II) in human bronchial epithelial cells. Environ. Sci. Technol., 43, 4555-4560, 2009.

Kelly, F. J., and Fussell, J. C.: Size, source and chemical composition as determinants of toxicity attributable to ambient particulate matter, Atmos. Environ., 60, 504-526, 2012.

Khurshid, S. S., Siegel, J. A., and Kinney, K. A.: Technical Note: Particulate reactive oxygen species concentrations and their association with environmental conditions in an urban, subtropical climate, Atmos. Chem. Phys., 14, 6777-6784, 2014.

Kim, S. E., Lim, Y. H, Kim, H.: Temperature modifies the association between particulate air pollution and mortality: A multi-city study in South Korea., Sci. Total Environ., 524-525, 376-383, 2015.

Kim, S., Jaques, P. A., Chang, M., Froines, J. R., and Sioutas, C.: Versatile aerosol concentration enrichment system (VACES) for simultaneous in vivo and in vitro evaluation of toxic effects of ultrafine, fine and coarse ambient particles Part I: Development and laboratory characterization, J. Aerosol Sci., 32, 1281-1297, 2001.

King, L. E. and Weber, R. J.: Development and testing of an online method to measure ambient fine particulate reactive oxygen species (ROS) based on the 2',7'-dichlorofluorescin (DCFH) assay, Atmos. Meas. Tech., 6, 1647-1658, 2013.

Kolthoff, I. M. and Medalia, A. I.: The reaction between ferrous iron and peroxides. I. reaction with hydrogen peroxide in the absence of oxygen, J. Am. Chem. Soc., 71, 3777-3783, 1949.

Krapf, M., Haddad, I. E., Bruns, E. A., Molteni, U., Daellenbach, K. R., Prévôt, A. S. H., Baltensperger, U., and Dommen, J.: Labile peroxides in secondary organic aerosol, Chem, 603-616, 2016.

Krapf, M., Kunzi, L., Allenbach, S., Bruns, E. A., Gavarini, I., El-Haddad, I., Slowik, J. G., Prevot, A. S. H., Drinovec, L., Mocnik, G., Dumbgen, L., Salathe, M., Baumlin, N., Sioutas, C., Baltensperger, U., Dommen, J., and Geiser, M.: Wood combustion particles induce adverse effects to normal and diseased airway epithelia, Env. Sci. Processes. Impact, 19, 538-548, 2017.

Künzi, L., Krapf, M., Daher, N., Dommen, J., Jeannet, N., Schneider, S., Platt, S., Slowik, J. G., Baumlin, N., Salathe, M., Prévôt, A. S. H., Kalberer, M., Strähl, C., Dümbgen, L., Sioutas, C., Baltensperger, U., and Geiser, M.: Toxicity of aged gasoline exhaust particles to normal and diseased airway epithelia, Sci. Rep., 5, 11801, 2015.

Laden, F., Schwartz, J., Speizer, F.E., Dockery, D.W. Reduction in fine particulate air pollution and mortality: Extended follow-up of the Harvard Six Cities study, Am. J. Respir. Crit. Care Med., 173, 667-672, 2006.

Lagzi I, Mészáros R, Gelybó G, Leelőssy Á. Atmospheric Chemistry. Eötvös Loránd University, 2013.

Lakey, P. S. J., Berkemeier, T., Tong, H., Arangio, A. M., Lucas, K., Pöschl, U., and Shiraiwa, M.: Chemical exposure-response relationship between air pollutants and reactive oxygen species in the human respiratory tract, Sci. Rep., 6, 32916, 2016.

Landreman, A. P., Shafer, M. M., Hemming, J. C., Hannigan, M. P., and Schauer, J. J.: A Macrophage-Based Method for the Assessment of the Reactive Oxygen Species (ROS) Activity of atmospheric particulate matter (PM) and application to routine (Daily-24 h) aerosol monitoring studies, Aerosol Sci. Technol., 42, 946-957, 2008.

LeBel, C. P., Ischiropoulos, H., and Bondy, S. C.: Evaluation of the probe 2',7'-dichlorofluorescin as an indicator of reactive oxygen species formation and oxidative stress, Chem. Res. Toxicol., 5, 227-231, 1992.

Lee, S., Liu, W., Wang, Y., Russell, A. G., and Edgerton, E. S.: Source apportionment of PM2.5: Comparing PMF and CMB results for four ambient monitoring sites in the southeastern United States, Atmospheric Environ., 42, 4126-4137, 2008.

Lee, Y. L., Wang, W.-H., Lu, C.-W., Lin, Y.-H., and Hwang, B.-F.: Effects of ambient air pollution on pulmonary function among schoolchildren, Int. J. Hyg. and Environ. Health, 214, 369-375, 2011.

Lelieveld, J.: Clean air in the Anthropocene, Faraday discussions, 200, 693-703, 2017.

Lepeule, J., Laden, F., Dockery, D., Schwartz, J. Chronic exposure to fine particles and mortality: an extended follow-up of the Harvard Six Cities study from 1974 to 2009, Environ. Health Perspect., 120, 965-970 2012.

Li, N., Sioutas, C., Cho, A., Schmitz, D., Misra, C., Sempf, J., Wang, M., Oberley, T., Froines, J., and Nel, A.: Ultrafine particulate pollutants induce oxidative stress and mitochondrial damage, Environ. Health Perspect., 111, 455-460, 2003.

Li, Q., Wyatt, A., Kamens, R.M.: Oxidant generation and toxicity enhancement of aged-diesel exhaust. Atmos. Environ., 43, 1037-1042, 2009.

Li, W., Shi, Z., Zhang, D., Zhang, X., Li, P., Feng, Q., Yuan, Q., and Wang, W.: Haze particles over a coal-burning region in the China Loess Plateau in winter: Three flight missions in December 2010, Journal of Geophysical Research: Atmospheres, 117, n/a-n/a, 2012.

Lim, Y. B., Turpin, B. J., Laboratory evidence of organic peroxide and peroxyhemiacetal formation in the aqueous phase and implications for aqueous OH, Atmos. Chem. Phys., 15, 12867-12877, 2015.

Limbach, L. K., Wick, P., Manser, P., Grass, R. N., Bruinink, A., and Stark, W. J.: Exposure of engineered nanoparticles to human lung epithelial cells: influence of chemical composition and catalytic activity on oxidative stress, Environ. Sci. Technol, 41, 4158-4163, 2007.

Lin, P., Hu, M., Deng, Z., Slanina, J., Han, S., Kondo, Y., Takegawa, N., Miyazaki, Y., Zhao, Y., and Sugimoto, N.: Seasonal and diurnal variations of organic carbon in $PM_{2.5}$ in Beijing and the estimation of secondary organic carbon, Journal of Geophysical Research: Atmospheres, 114, n/a-n/a, 2009.

Lippmann, M., Chen, L. C., Gordon, T., Ito, K., Thurston G. D. National Particle Component Toxicity (NPACT) initiative: integrated epidemiologic and toxicologic studies of the health effects of particulate matter components, Res. Rep. Health eff. Inst. 177, 5-13, 2013.

Liu J. C., Wilson A., Mickley L. J., Dominici F., Ebisu K., Wang Y., Sulprizio M. P., Peng R. D., Yue X., Son J. Y., Anderson G. B., and Bell, a. M. L.: Wildfire-specific fine particulate matter and risk of hospital admissions in urban and rural counties, Epidemiology, 28, 77-85, 2017.

Liu, G., Niu, Z., Van Niekerk, D., Xue, J., and Zheng, L.: Polycyclic aromatic hydrocarbons (PAHs) from coal combustion: emissions, analysis, and toxicology, Rev. Environ. Contam. Toxicol., 192, 1-28, 2008.

Liu, J. C., Wilson A., Mickley L. J., Dominici F., Ebisu K., Wang Y., Sulprizio M. P., Peng R. D., Yue X., Son J. Y., Anderson G. B., and Bell, M. L.: Wildfire-specific fine particulate matter and risk of hospital admissions in urban and rural counties, Epidemiology, 28, 77-85, 2017.

Liu, J., Han, Y., Tang, X., Zhu, J., Zhu, T. Estimating adult mortality attributable to $PM_{2.5}$ exposure in China with assimilated $PM_{2.5}$ concentrations based on a ground monitoring network. Sci. Total Environ., 568, 1253-1262, 2016.

Lobo, V., Patil, A., Phatak, A., and Chandra, N.: Free radicals, antioxidants and functional foods: Impact on human health, Pharmacogn. Rev., 4, 118-126, 2010.

Long, G. L. and Winefordner, J. D.: Limit of detection a closer look at the IUPAC definition, Anal. Chem., 55, 712A-724A, 1983.

Marabini, L., Ozgen, S., Turacchi, S., Aminti, S., Arnaboldi, F., Lonati, G., Fermo, P., Corbella, L., Valli, G., Bernardoni, V., Dell'Acqua, M., Vecchi, R., Becagli, S., Caruso, D., Corrado, G. L., and Marinovich, M.: Ultrafine particles (UFPs) from domestic wood stoves: genotoxicity in human lung carcinoma A549 cells, Mutat. Res., 820, 39-46, 2017.

Mark, G., Tauber, A., Laupert, R., Schuchmann, H.-P., Schulz, D., Mues, A., and von Sonntag, C.: OH-radical formation by ultrasound in aqueous solution – Part II: Terephthalate and Fricke dosimetry and the influence of various conditions on the sonolytic yield, Ultrason. Sonochem., 5, 41-52, 1998.

McCulloch, A., Aucott, M. L., Benkovitz, C. M., Graedel, T. E., Kleiman, G., Midgley, P. M., and Li, Y.-F.: Global emissions of hydrogen chloride and chloromethane from coal combustion, incineration and industrial activities: Reactive Chlorine Emissions Inventory, J. Geophys. Res. Atmos., 104, 8391-8403, 1999.

Middlebrook, A. M., Bahreini, R., Jimenez, J. L., Canagaratna, M. R., Evaluation of composition-dependent collection efficiencies for the Aerodyne Aerosol Mass Spectrometer using field data. Aerosol Sci. Technol., 46, 258-271, 2012.

Miljevic, B., Hedayat, F., Stevanovic, S., Fairfull-Smith, K. E., Bottle, S. E., and Ristovski, Z. D.: To sonicate or not to sonicate PM filters: Reactive oxygen species generation upon ultrasonic irradiation, Aerosol Sci. Technol., 48, 1276-1284, 2014.

Miljevic, B., Heringa, M. F., Keller, A., Meyer, N. K., Good, J., Lauber, A., DeCarlo, P. F., Fairfull-Smith, K. E., Nussbaumer, T., Burtscher, H., Prevot, A. S. H., Baltensperger, U., Bottle, S. E., and Ristovski, Z. D.: Oxidative potential of logwood and pellet burning particles assessed by a novel profluorescent nitroxide probe, Environ. Sci. Technol., 44, 6601-6607, 2010.

Mohr, C., DeCarlo, P. F., Heringa, M. F., Chirico, R., Slowik, J. G., Richter, R., Reche, C., Alastuey, A., Querol, X., Seco, R., Peñuelas, J., Jiménez, J. L., Crippa, M., Zimmermann, R., Baltensperger, U., and Prévôt, A. S. H.: Identification and quantification of organic aerosol from cooking and other sources in Barcelona using aerosol mass spectrometer data, Atmos. Chem. Phys., 12, 1649-1665, 2012.

Muala, A., Rankin, G., Sehlstedt, M., Unosson, J., Bosson, J. A., Behndig, A., Pourazar, J., Nyström, R., Pettersson, E., Bergvall, C., Westerholm, R., Jalava, P. I., Happo, M. S., Uski, O., Hirvonen, M.-R., Kelly, F. J., Mudway, I. S., Blomberg, A., Boman, C., and Sandström, T.: Acute exposure to wood smoke from incomplete combustion - indications of cytotoxicity, Part. Fibre Toxicol., 12, 33, 2015.

Mudway, I. S., and Kelly, F. J.: Ozone and the lung: a sensitive issue, Mol. Aspects of Med., 21, 1-48, 2000.

Mudway, I. S., Stenfors, N., Duggan, S. T., Roxborough, H., Zielinski, H., Marklund, S. L., Blomberg, A., Frew, A. J., Sandstrom, T., and Kelly, F. J.: An in vitro and in vivo investigation of the effects of diesel exhaust on human airway lining fluid antioxidants, Archives of biochemistry and biophysics, 423, 200-212, 2004.

Naeher, L. P., Brauer, M., Lipsett, M., Zelikoff, J. T., Simpson, C. D., Koenig, J. Q., and Smith, K. R.: Woodsmoke health effects: a review, Inhal Toxicol, 19, 67-106, 2007.

Nawrot, T. S., Torfs, R., Fierens, F., De Henauw, S., Hoet, P. H., Van Kersschaever, G., De Backer, G., and Nemery, B.: Stronger associations between daily mortality and fine particulate air pollution in summer than in winter: evidence from a heavily polluted region in western Europe, J. epidemiol. community health, 61, 146-149, 2007.

Nel, A. E., Diaz-Sanchez, D., Ng, D., Hiura, T., and Saxon, A.: Enhancement of allergic inflammation by the interaction between diesel exhaust particles and the immune system, J. Allergy Clin. Immun., 102, 539-554, 1998.

Ng, N. L., Canagaratna, M. R., Jimenez, J. L., Chhabra, P. S., Seinfeld, J. H., and Worsnop, D. R.: Changes in organic aerosol composition with aging inferred from aerosol mass spectra, Atmos. Chem. Phys., 11, 6465-6474, 2011a.

Ng, N. L., Herndon, S. C., Trimborn, A., Canagaratna, M. R., Croteau, P. L., Onasch, T. B., Sueper, D., Worsnop, D. R., Zhang, Q., Sun, Y. L., and Jayne, J. T.: An Aerosol Chemical Speciation Monitor (ACSM) for routine monitoring of the composition and mass concentrations of ambient aerosol, Aerosol Sci. Technol., 45, 780-794, 2011b.

Nussbaumer T. and Kaltschmitt M.: 8.1 Begriffsdefinitionen, in M. Kaltschmitt and H. Hartmann (Eds.), Energie aus Biomasse: Springer, Berlin, Heidelberg, 239–247, 2000.

Nussbaumer, T., and Lauber, A.: Formation mechanisms and physical properties of particles from wood combustion for design and operation of electrostatic precipitators, 18th European Biomass Conference and Exhibition, Lyon, ETA-Florence, 3–7 May 2010, 2010.

Oakes, M., Weber, R. J., Lai, B., Russell, A., and Ingall, E. D.: Characterization of iron speciation in urban and rural single particles using XANES spectroscopy and micro X-ray fluorescence measurements: investigating the relationship between speciation and fractional iron solubility, Atmos. Chem. Phys., 12, 745-756, 2012.

Oberdorster, G., Oberdorster, E., and Oberdorster, J.: Nanotoxicology: an emerging discipline evolving from studies of ultrafine particles, Environ. Health Perspect., 113, 823-839, 2005.

Ochs, M., Nyengaard, J. R., Jung, A., Knudsen, L., Voigt, M., Wahlers, T., Richter, J., and Gundersen, H. J.: The number of alveoli in the human lung, Am. J. Respir. Crit. Care Med., 169, 120-124, 2004.

Ostro, B., Tobias, A., Querol, X., Alastuey, A., Amato, F., Pey, J., Pérez, N., and Sunyer, J.: The effects of particulate matter sources on daily mortality: A case-crossover study of Barcelona, Spain, Environ. Health Perspect., 119, 1781-1787, 2011.

Paatero, P., and Tapper, U.: Analysis of different modes of factor analysis as least squares fit problems, Chemom. Intell. Lab. Syst., 18, 183-194, 1993.

Paatero, P., and Tapper, U.: Positive matrix factorization: A non-negative factor model with optimal utilization of error estimates of data values, Environmetrics, 5, 111-126, 1994.

Paatero, P.: Least squares formulation of robust non-negative factor analysis, Chemometrics and intelligent laboratory systems, 37, 23-35, 1997.

Paulsen, D., Dommen, J., Kalberer, M., Prevot, A. S. H., Richter, R., Sax, M., Steinbacher, M., Weingartner, E., and Baltensperger, U.: Secondary organic aerosol formation by irradiation of 1,3,5-trimethylbenzene-NO_x-H_2O in a new reaction chamber for atmospheric chemistry and physics, Environ. Sci. Technol., 39, 2668-2678, 2005.

Peng, R. D., Dominici, F., Pastor-Barriuso, R., Zeger, S. L., and Samet, J. M.: Seasonal analyses of air pollution and mortality in 100 US cities, Am. J. epidemiol., 161, 585-594, 2005.

Perrone, M. G., Zhou, J., Malandrino, M., Sangiorgi, G., Rizzi, C., Ferrero, L., Dommen, J., and Bolzacchini, E.: PM chemical composition and oxidative potential of the soluble fraction of particles at two sites in the urban area of Milan, Northern Italy, Atmos. Environ., 128, 104-113, 2016.

Pfaffenberger, L., Barmet, P., Slowik, J. G., Praplan, A. P., Dommen, J., Prévôt, A. S. H., and Baltensperger, U.: The link between organic aerosol mass loading and degree of oxygenation: an α-pinene photooxidation study, Atmos. Chem. Phys., 13, 6493-6506, 2013.

Pham-Huy, L. A., He, H., and Pham-Huy, C.: Free Radicals, Antioxidants in disease and health, Int. J. Biomed. Sci., 4, 89-96, 2008.

Platt, S. M., El Haddad, I., Zardini, A. A., Clairotte, M., Astorga, C., Wolf, R., Slowik, J. G., Temime-Roussel, B., Marchand, N., Ježek, I., Drinovec, L., Močnik, G., Möhler, O., Richter, R., Barmet, P., Bianchi, F., Baltensperger, U., and Prévôt, A. S. H.: Secondary organic aerosol formation from gasoline vehicle emissions in a new mobile environmental reaction chamber, Atmos. Chem. Phys., 13, 9141-9158, 2013.

Platt, S. M., Haddad, I. E., Pieber, S. M., Huang, R. J., Zardini, A. A., Clairotte, M., Suarez-Bertoa, R., Barmet, P., Pfaffenberger, L., Wolf, R., Slowik, J. G., Fuller, S. J., Kalberer, M., Chirico, R., Dommen, J., Astorga, C., Zimmermann, R., Marchand, N., Hellebust, S., Temime-Roussel, B., Baltensperger, U., and Prévôt, A. S. H.: Two-stroke scooters are a dominant source of air pollution in many cities, Nat. commun., 5, 3749, 2014.

Pope, C. A. and Dockery, D. W.: Health effects of fine particulate air pollution: lines that connect, J. Air Waste Manage.Assoc., 56, 709-742, 2006.

Pope, C. A. I., Ezzati, M., Dockery, D. W.: Fine-particulate air pollution and life expectancy in the United States. N. Engl. J. Med., 360, 376-386, 2009.

Pope, I. C., Burnett, R. T., Thun, M. J., and et al.: Lung cancer, cardiopulmonary mortality, and long-term exposure to fine particulate air pollution, JAMA, 287, 1132-1141, 2002.

Pourazar, J., Mudway, I. S., Samet, J. M., Helleday, R., Blomberg, A., Wilson, S. J., Frew, A. J., Kelly, F. J., and Sandström, T.: Diesel exhaust activates redox-sensitive transcription factors and kinases in human airways, Am. J. Physiol. Lung Cellular Mol. Physiol., 289, L724-L730, 2005.

Pourkhesalian, A. M., Stevanovic, S., Rahman, M. M., Faghihi, E. M., Bottle, S. E., Masri, A. R., Brown, R. J., and Ristovski, Z. D.: Effect of atmospheric aging on volatility and reactive oxygen species of biodiesel exhaust nano-particles, Atmos. Chem. Phys., 15, 9099-9108, 2015.

Pyka, I., and Wierzchowski, K.: Estimated mercury emissions from coal combustion in the households sector in Poland, J. Sust. Min., 15, 66-72, 2016.

Ramadan, Z., Eickhout, B., Song, X.-H., Buydens, L. M. C., and Hopke, P. K.: Comparison of Positive Matrix Factorization and Multilinear Engine for the source apportionment of particulate pollutants, Chemometr. Intell. Lab. Syst., 66, 15-28, 2003.

Reiss, R., Anderson, E. L., Cross, C. E., Hidy, G., Hoel, D., McClellan, R., and Moolgavkar, S.: Evidence of health impacts of sulfate-and nitrate-containing particles in ambient air, Inhal. Toxicol., 19, 419-449, 2007.

Ren, Y., Qu, Z., Du, Y., Xu, R., Ma, D., Yang, G., Shi, Y., Fan, X., Tani, A., Guo, P., Ge, Y., and Chang, J.: Air quality and health effects of biogenic volatile organic compounds emissions from urban green spaces and the mitigation strategies, Environ. pollut. (Barking, Essex : 1987), 230, 849-861, 2017.

Robinson, A. L., Donahue, N. M., Shrivastava, M. K., Weitkamp, E. A., Sage, A. M., Grieshop, A. P., Lane, T. E., Pierce, J. R., and Pandis, S. N.: Rethinking organic aerosols: semivolatile emissions and photochemical aging, Science, 315, 1259-1262, 2007.

Rodvold, K. A., George, J. M., and Yoo, L.: Penetration of anti-infective agents into pulmonary epithelial lining fluid: focus on antibacterial agents, Clinical pharmacokinetics, 50, 637-664, 2011.

Rota, C., Chignell, C. F., and Mason, R. P.: Evidence for free radical formation during the oxidation of 2′-7′-dichlorofluorescin to the fluorescent dye 2′-7′-dichlorofluorescein by horseradish peroxidase:: Possible implications for oxidative stress measurements, Free Radical Biol. Med., 27, 873-881, 1999a.

Rota, C., Fann, Y. C., and Mason, R. P.: Phenoxyl free radical formation during the oxidation of the fluorescent dye 2′,7′-dichlorofluorescein by horseradish peroxidase: possible consequences for oxidative stress measurements, J. Biol. Chem., 274, 28161-28168, 1999b.

Ruusunen, J., Tapanainen, M., Sippula, O., Jalava, P. I., Lamberg, H., and Nuutinen, K.: A novel particle sampling system for physico-chemical and toxicological characterization of emissions, Anal. Bioanal. Chem., 401, 2011.

Sagai, M., Saito, H., Ichinose, T., Kodama, M., and Mori, Y.: Biological effects of diesel exhaust particles. I. In vitro production of superoxide and in vivo toxicity in mouse, Free Radical Biol. Med., 14, 37-47, 1993.

Salvi, S.: Health effects of ambient air pollution in children, Paediatr. Respir. Rev., 8, 275-280, 2007.

Sandradewi, J., Prévôt, A. S. H., Szidat, S., Perron, N., Alfarra, M. R., Lanz, V. A., Weingartner, E., and Baltensperger, U.: Using aerosol light absorption measurements for the quantitative determination of wood burning and traffic emission contributions to particulate matter, Environ. Sci. Technol., 42, 3316-3323, 2008.

Sauvain, J.-J., Rossi, M. J., and Riediker, M.: Comparison of three acellular tests for assessing the oxidation potential of nanomaterials, Aerosol Sci. Technol., 47, 218-227, 2013.

Schlesinger, R. B., and Cassee, F.: Atmospheric secondary inorganic particulate matter: the toxicological perspective as a basis for health effects risk assessment, Inhal. Toxicol., 15, 197-235, 2003.

Schmidl, C., Luisser, M., Padouvas, E., Lasselsberger, L., Rzaca, M., Ramirez-Santa Cruz, C., Handler, M., Peng, G., Bauer, H., and Puxbaum, H.: Particulate and gaseous emissions from manually and automatically fired small scale combustion systems, Atmos. Environ., 45, 7443-7454, 2011.

Sciare, J., d'Argouges, O., Sarda-Estève, R., Gaimoz, C., Dolgorouky, C., Bonnaire, N., Favez, O., Bonsang, B., and Gros, V.: Large contribution of water-insoluble secondary organic aerosols in the region of Paris (France) during wintertime, J. Geophys. Res. Atmos., 116, n/a-n/a, 2011.

Seinfeld, J. H., and Pandis, S. N., Atmospheric chemistry and physics: from air pollution to climate change, edited by: 3, John Wiley, New York, USA, 2016.

Shen, G., Wang, W., Yang, Y., Zhu, C., Min, Y., Xue, M., Ding, J., Li, W., Wang, B., Shen, H., Wang, R., Wang, X., and Tao, S.: Emission factors and particulate matter size distribution of polycyclic aromatic hydrocarbons from residential coal combustions in rural Northern China, Atmos. Environ., 44, 5237-5243, 2010.

Shi, T., Schins, R. P., Knaapen, A. M., Kuhlbusch, T., Pitz, M., Heinrich, J., and Borm, P. J.: Hydroxyl radical generation by electron paramagnetic resonance as a new method to monitor ambient particulate matter composition, Journal of environmental monitoring : JEM, 5, 550-556, 2003.

Shiraiwa, M., Ueda, K., Pozzer, A., Lammel, G., Kampf, C. J., Fushimi, A., Enami, S., Arangio, A. M., Fröhlich-Nowoisky, J., Fujitani, Y., Furuyama, A., Lakey, P. S. J., Lelieveld, J., Lucas, K., Morino, Y., Pöschl, U., Takahama, S., Takami, A., Tong, H., Weber, B., Yoshino, A., and Sato, K.: Aerosol health effects from molecular to global scales, Environ. Sci. Technol., 51, 13545-13567, 2017.

Sioutas, C., Kim, S., and Chang, M.: Development and evalution of a prototype ultrafine particle concentrator, J. Aerosol Sci., 30, 1001-1017, 1999.

Slama, R., Morgenstern, V., Cyrys, J., Zutavern, A., Herbarth, O., Wichmann, H. E., and Heinrich, J.: Traffic-related atmospheric pollutants levels during pregnancy and offspring's term birth weight: a study relying on a land-use regression exposure model, Environ. Health Perspect., 115, 1283-1292, 2007.

Squadrito, G. L., Cueto, R., Dellinger, B., and Pryor, W. A.: Quinoid redox cycling as a mechanism for sustained free radical generation by inhaled airborne particulate matter, Free Radic. Biol. Med., 31, 1132-1138, 2001.

Staehelin, J., Prévôt, A. S. H., and Barnes, J.: Photochemie der Troposphäre, Handbuch der Umweltveränderungen und Ökotoxikologie, 2000th edition ed., Band IA; Band IA: Atmosphäre,, edited by: Guderian, R., Springer Verlag, 207-341, 2000.

Sun, Y., Jiang, Q., Wang, Z., Fu, P., Li, J., Yang, T., and Yin, Y.: Investigation of the sources and evolution processes of severe haze pollution in Beijing in January 2013, J. Geophys. Res. Atmos., 119, 4380-4398, 2014.

Takeuchi, M., Ullah, S. M. R., Dasgupta, P. K., Collins, D. R., and Williams, A.: Continuous collection of soluble atmospheric particles with a wetted hydrophilic Filter, Anal. Chem., 77, 8031-8040, 2005.

Tao, F., Gonzalez-Flecha, B., and Kobzik, L.: Reactive oxygen species in pulmonary inflammation by ambient particulates, Free Radic. Biol. Med., 35, 327-340, 2003.

Tapanainen, M., Jalava, P. I., Mäki-Paakkanen, J., Hakulinen, P., Lamberg, H., Ruusunen, J., Tissari, J., Jokiniemi, J., and Hirvonen, M.-R.: Efficiency of log wood combustion affects the toxicological and chemical properties of emission particles, Inhalation Toxicol., 24, 343-355, 2012.

Tong, H., Arangio, A. M., Lakey, P. S. J., Berkemeier, T., Liu, F., Kampf, C. J., Brune, W. H., Pöschl, U., and Shiraiwa, M.: Hydroxyl radicals from secondary organic aerosol decomposition in water, Atmos. Chem. Phys., 16, 1761-1771, 2016.

Tuet, W. Y., Chen, Y., Fok, S., Champion, J. A., and Ng, N. L.: Inflammatory responses to secondary organic aerosols (SOA) generated from biogenic and anthropogenic precursors, Atmos. Chem. Phys., 17, 11423-11440, 2017.

Tuet, W. Y., Chen, Y., Xu, L., Fok, S., Gao, D., Weber, R. J., and Ng, N. L.: Chemical oxidative potential of secondary organic aerosol (SOA) generated from the photooxidation of biogenic and anthropogenic volatile organic compounds, Atmos. Chem. Phys., 17, 839-853, 2017.

U.S. Department of State, http://www.stateair.net/web/historical/1/1.html, last assessed: 01 October 2017.

U.S. Environmental Protection Administration (USEPA): National emission trends (NET) database, Emission Factor and Inventory Group, Office of Air Quality Planning and Standards, in, Research Triangle Park, N.C., 2000.

Valko, M., Morris, H., and Cronin, M. T. D.: Metals, Toxicity and oxidative stress, Curr. Med. Chem., 12, 1161-1208, 2005.

Van der Vliet, A., O'Neill, C. A., Cross, C. E., Koostra, J. M., Volz, W. G., Halliwell, B., and Louie, S.: Determination of low-molecular-mass antioxidant concentrations in human respiratory tract lining fluids, Am. J. Physiol., 276, L289-296, 1999.

Vanda, V., Boris, T., Franc, B., and Zsolt, C.: air Pollution, Ozone pollution and its bioindication, edited by: Villanyi, V., 2010.

Vedal, S., Kim S. Y., Miller K. A., Fox, J. R., Bergen, S., Gould, T., Kaufman J. D., Larson, T.V., Sampson P. D., Sheppard, L., Simpson, C. D., and Szpiro, A. A. Section 1. NPACT epidemiologic study of components of fine particulate matter and cardiovascular disease in the MESA and WHI-OS cohorts. In national particle component toxicity (NPACT) initiative report on cardiovascular effects, Res. Rep. 178, Health Effects Institute, Boston, Massachusetts, U.S.A., 9–128, 2013.

Venkatachari, P., and Hopke, P. K.: Development and laboratory testing of an automated monitor for the measurement of atmospheric particle-bound reactive oxygen species (ROS), Aerosol Sci. Technol., 42, 629-635, 2008.

Venkatachari, P., Hopke, P. K., Brune, W. H., Ren, X., Lesher, R., Mao, J., and Mitchell, M.: Characterization of wintertime reactive oxygen species concentrations in flushing, New York, Aerosol Sci. Technol., 41, 97-111, 2007.

Venkatachari, P., Hopke, P. K., Grover, B. D., and Eatough, D. J.: Measurement of particle-bound reactive oxygen species in rubidoux aerosols, J. Atmos. Chem., 50, 49-58, 2005.

Verma, V., Fang, T., Xu, L., Peltier, R. E., Russell, A. G., Ng, N. L., and Weber, R. J.: Organic aerosols associated with the generation of reactive oxygen species (ROS) by water-soluble $PM_{2.5}$, Environ. Sci. Technol., 49, 4646-4656, 2015.

Verma, V., Rico-Martinez, R., Kotra, N., King, L., Liu, J., Snell, T. W., and Weber, R. J.: Contribution of water-soluble and insoluble components and their hydrophobic/hydrophilic subfractions to the reactive oxygen species-generating potential of fine ambient aerosols, Environ. Sci. Technol., 46, 11384–11392, 2012.

Viana, M., Kuhlbusch, T. A. J., Querol, X., Alastuey, A., Harrison, R. M., Hopke, P. K., Winiwarter, W., Vallius, M., Szidat, S., Prévôt, A. S. H., Hueglin, C., Bloemen, H., Wåhlin, P., Vecchi, R., Miranda, A. I., Kasper-Giebl, A., Maenhaut, W., and Hitzenberger, R.: Source apportionment of particulate matter in Europe: A review of methods and results, J. Aerosol Sci., 39, 827-849, 2008.

Visser, S., Slowik, J. G., Furger, M., Zotter, P., Bukowiecki, N., Canonaco, F., Flechsig, U., Appel, K., Green, D. C., Tremper, A. H., Young, D. E., Williams, P. I., Allan, J. D., Coe, H., Williams, L. R., Mohr, C., Xu, L., Ng, N. L., Nemitz, E., Barlow, J. F., Halios, C. H., Fleming, Z. L., Baltensperger, U., and Prévôt, A. S. H.: Advanced source apportionment of size-resolved trace elements at multiple sites in London during winter, Atmos. Chem. Phys., 15, 11291-11309, 2015.

Wang, D., Kam, W., Cheung, K., Pakbin, P., and Sioutas, C.: Development of a two-stage virtual impactor system for high concentration enrichment of ultrafine, $PM_{2.5}$, and coarse particulate matter, Aerosol Sci. Technol., 47, 231-238, 2012.

Wang, F. F., Geng, C. M., Hao, W. D., Zhao, Y. D., Li, Q., Wang, H. M., and Qian, Y.: The cellular toxicity of $PM_{2.5}$ emitted from coal combustion in human umbilical vein endothelial cells, Biomed. Environ. Sci. : BES, 29, 107-116, 2016.

Wang, G., Zhang, R., Gomez, M. E., Yang, L., Levy Zamora, M., Hu, M., Lin, Y., Peng, J., Guo, S., Meng, J., Li, J., Cheng, C., Hu, T., Ren, Y., Wang, Y., Gao, J., Cao, J., An, Z., Zhou, W., Li, G., Wang, J., Tian, P., Marrero-Ortiz, W., Secrest, J., Du, Z., Zheng, J., Shang, D., Zeng, L., Shao, M., Wang, W., Huang, Y., Wang, Y., Zhu, Y., Li, Y., Hu, J., Pan, B., Cai, L., Cheng, Y., Ji, Y., Zhang, F., Rosenfeld,

D., Liss, P. S., Duce, R. A., Kolb, C. E., and Molina, M. J.: Persistent sulfate formation from London Fog to Chinese haze, Proc. Natl. Acad. Sci., 113, 13630-13635, 2016.

Wang, L., Arey, J., and Atkinson, R.: Reactions of chlorine atoms with a series of aromatic hydrocarbons, Environ. Sci. Technol., 39, 5302-5310, 2005.

Wang, W., Tao, S., Wang, W., Shen, G., Zhao, J., Lam, K.: Airborne particulates and polycyclic aromatic hydrocarbons (PAHs) in ambient air in Donghe, Northern China. J. Environ. Sci. Health A Toxic Hazard Subst. Environ. Eng., 4, 854–860, 2009.

Wang, Y., Hopke, P. K., Sun, L., Chalupa, D. C., and Utell, M. J.: Laboratory and field testing of an automated atmospheric particle-bound reactive oxygen species sampling-analysis system, J. Toxicol., 419–476, 2011a.

Wang, Y., Kim, H., and Paulson, S.: Hydrogen peroxide generation from α- and β-pinene and toluene secondary organic aerosols, Atmos. Environ., 45, 3149–3156, 2011b.

Ward, D. E. and Radke, L. F.: Emission measurements from vegetation fires: A comparative evalution of methods and results. In: Fire in the Environment: The ecological, atmospheric and climatic importance of vegetation fires, Crutzen, P. J. and Goldammer, J. G. (Eds.), John Wiley, Chichester UK, 1993.

Weber, S., Gaëlle, U., Calas, A., Chevrier, F., Besombes, J. L., Charron, A., Salameh, D., Ježek, I., Močnik, G., and Jaffrezo, J. L.: An apportionment method for the oxydative potential to the atmospheric PM sources: application to a one-year study in Chamonix, France, Atmos. Chem. Phys. Discuss., 2018, 1-19, 2018.

Wheeler, A., Zanobetti, A., Gold, D. R., Schwartz, J., Stone, P., and Suh, H. H.: The relationship between ambient air pollution and heart rate variability differs for individuals with heart and pulmonary disease, Environ. Health Perspect., 114, 560-566, 2006.

Whitby, K.T., Physical characteristics of sulfur aerosols. Atmos. Environ., 12: 135-159. 1987.

WHO. Review of evidence on health effects of air pollution-REVIHAAP Project, Technical Report. (2013b).

WHO: Ambient air pollution: A global assessment of exposure and burden of disease, World Health Organization, 2016.

WHO: Health effects of particulate matter: policy implications for countries in eastern Europe, Caucasus and central Asia, the original office for Europe of the World Health Organization, 2013a.

WHO: Residential heating with wood and coal: health impacts and policy options in Europe and North america, World Health Organization (WHO), 2015.

WHO: Tackling the Global Clean Air Challenge. World Health Organization News Release, 26 September, World Health Organization, 2011.

Wilkins, E. T.: Air pollution and the London fog of December, 1952, Journal. Royal Sanitary Institute (Great Britain), 74, 1-15; discussion, 15-21, 1954.

Williams, L. R., Gonzalez, L. A., Peck, J., Trimborn, D., McInnis, J., Farrar, M. R., Moore, K. D., Jayne, J. T., Robinson, W. A., Lewis, D. K., Onasch, T. B., Canagaratna, M. R., Trimborn, A., Timko,

M. T., Magoon, G., Deng, R., Tang, D., de la Rosa Blanco, E., Prévôt, A. S. H., Smith, K. A., and Worsnop, D. R.: Characterization of an aerodynamic lens for transmitting particles greater than 1 micrometer in diameter into the Aerodyne aerosol mass spectrometer, Atmos. Meas. Tech., 6, 3271-3280, 2013.

Wilson, D. W., Aung, H. H., Lame, M. W., Plummer, L., Pinkerton, K. E., Ham, W., Kleeman, M., Norris, J. W., and Tablin, F.: Exposure of mice to concentrated ambient particulate matter results in platelet and systemic cytokine activation, Inhal. Toxicol., 22, 267-276, 2010.

Winterbourn, C. C.: Reconciling the chemistry and biology of reactive oxygen species, Nat. Chem. Biol., 4, 278-286, 2008.

Wragg, F. P. H., Fuller, S. J., Freshwater, R., Green, D. C., Kelly, F. J., and Kalberer, M.: An automated online instrument to quantify aerosol-bound reactive oxygen species (ROS) for ambient measurement and health-relevant aerosol studies, Atmos. Meas. Tech., 9, 4891-4900, 2016.

Wu, S. P., Tao, S., Liu, W. X.: Particle size distributions of polycyclic aromatic hydrocarbons in rural and urban atmosphere of Tianjin, China, Chemosphere, 62, 357-367. 2006.

Xu, M., Yu, D., Yao, H., Liu, X., and Qiao, Y.: Coal combustion-generated aerosols: Formation and properties, Proc. Combust. Inst., 33, 1681-1697, 2011.

Yang, A., Jedynska, A., Hellack, B., Kooter, I., Hoek, G., Brunekreef, B., Kuhlbusch, T. A. J., Cassee, F. R., and Janssen, N. A. H.: Measurement of the oxidative potential of $PM_{2.5}$ and its constituents: The effect of extraction solvent and filter type, Atmos. Environ., 83, 35-42, 2014.

Yap, S. G. P.: The potential impact of residential wood burning regulations in a California Region: Concurrent Wintertime reductions in ambient pollution and cardiovascular mortality, ISEE 20th Annual Conference, 12-16 October, Pasadena, California, USA, 2008.

Yearbook, C. S.: China Statistical Yearbook: China Statistics Press: Beijing, China, 2003.

Yi, O., Hong, Y. C., Kim, H. Seasonal effect of PM(10) concentrations on mortality and morbidity in Seoul, Korea: a temperature-matched case-crossover analysis., Environ. Res., 110, 89-95, 2010.

Yudovich, Y., and P. Ketris, M.: Chlorine in coal: A review, 127-144 pp., 2006.

Zanatta, M., Gysel, M., Bukowiecki, N., Müller, T., Weingartner, E., Areskoug, H., Fiebig, M., Yttri, K. E., Mihalopoulos, N., Kouvarakis, G., Beddows, D., Harrison, R. M., Cavalli, F., Putaud, J. P., Spindler, G., Wiedensohler, A., Alastuey, A., Pandolfi, M., Sellegri, K., Swietlicki, E., Jaffrezo, J. L., Baltensperger, U., and Laj, P.: A European aerosol phenomenology-5: Climatology of black carbon optical properties at 9 regional background sites across Europe, Atmos. Environ., 145, 346-364, 2016.

Zanobetti, A., Schwartz, J. The effect of fine and coarse particulate air pollution on mortality: a national analysis. Environ, Health Perspect., 117, 898-903, 2009.

Zhang, X., Hecobian, A., Zheng, M., Frank, N. H., and Weber, R. J.: Biomass burning impact on $PM_{2.5}$ over the southeastern US during 2007: integrating chemically speciated FRM filter measurements, MODIS fire counts and PMF analysis, Atmos. Chem. Phys., 10, 6839-6853, 2010.

Zhang, X., Staimer, N., Tjoa, T., Gillen, D. L., Schauer, J. J., Shafer, M. M., Hasheminassab, S., Pakbin, P., Longhurst, J., Sioutas, C., and Delfino, R. J.: Associations between microvascular function

and short-term exposure to traffic-related air pollution and particulate matter oxidative potential, Environmental health : a global access science source, 15, 81, 2016.

Zhang, Y., Tao, S., Shen, H., Ma, J.: Inhalation exposure to ambient polycyclic aromatic hydrocarbons and lung cancer risk of Chinese population. Proc. Natl. Acad. Sci. U. S. A., 106:21063–21067, 2009.

Zhao, J. and Riediker, M.: Detecting the oxidative reactivity of nanoparticles: a new protocol for reducing artifacts, J. Nanopart. Res., 16, 2493, 2014.

Zhao, J., and Hopke, P. K.: Concentration of Reactive Oxygen Species (ROS) in Mainstream and Sidestream Cigarette Smoke, Aerosol Sci. Technol. 46, 191-197, 2012.

Zhou, J., Bruns, E. A., Zotter, P., Stefenelli, G., Prévôt, A. S. H., Baltensperger, U., El-Haddad, I., and Dommen, J.: Development, characterization and first deployment of an improved online reactive oxygen species analyzer, Atmos. Meas. Tech., 11, 65–80, 2018a.

Zhou, J., Zotter, P., Bruns, E. A., Stefenelli, G., Bhattu, D., Brown, S., Bertrand, A., Marchand, N., Lamkaddam, H., Slowik, J. G., Prévôt, A. S. H., Baltensperger, U., Nussbaumer, T., El Haddad, I., and Dommen, J.: Particle bound reactive oxygen species (PB-ROS) emissions and formation pathways in residential wood smoke under different combustion and aging conditions, Atmos. Chem. Phys., 18, 6985–7000, 2018b.

Zhou, M., Diwu, Z., Panchuk-Voloshina, N., and Haugland, R. P.: A stable nonfluorescent derivative of resorufin for the fluorometric determination of trace hydrogen peroxide: applications in detecting the activity of phagocyte NADPH oxidase and other oxidases, Anal. Biochem., 253, 162-168, 1997.

Zotter, P., Ciobanu, V. G., Zhang, Y. L., El-Haddad, I., Macchia, M., Daellenbach, K. R., Salazar, G. A., Huang, R. J., Wacker, L., Hueglin, C., Piazzalunga, A., Fermo, P., Schwikowski, M., Baltensperger, U., Szidat, S., and Prévôt, A. S. H.: Radiocarbon analysis of elemental and organic carbon in Switzerland during winter-smog episodes from 2008 to 2012 – Part 1: Source apportionment and spatial variability, Atmos. Chem. Phys., 14, 13551-13570, 2014.

Zotter, P., Herich, H., Gysel, M., El-Haddad, I., Zhang, Y., Močnik, G., Hüglin, C., Baltensperger, U., Szidat, S., and Prévôt, A. S. H.: Evaluation of the absorption Ångström exponents for traffic and wood burning in the Aethalometer-based source apportionment using radiocarbon measurements of ambient aerosol, Atmos. Chem. Phys., 17, 4229-4249, 2017.

List of Figures

List of Tables

Acknowledgements

I would like to thank

--- Dr. Josef Dommen, my advisor, for always being available for his scientific support to me. I am really grateful for his concerned help, his exacting attitude to the scientific work, and providing the inspiration and strength to me to cope with the challenges of my research work. His guidance and the insightful discussions during my Ph. D., have improved a lot of the quality of my research work and granted the success of this thesis.

--- Prof. Dr. Urs Baltensperger, my doctor advisor, for his careful supervision of my Ph. D. work and the positive support. He has been very patient and taught me how to become a better scientist. He was closely following my research work and gave lots of constructive scientific inputs, which helped to make the thesis meet a much better quality.

My sincerely thank to both of them for providing me the opportunity to work here on a project which have a lot of prospects.

I would also like to thank

--- My Ph.D. supervisor Prof. McNeill for kindly accepting me as his student and being my co-referent and taking the time to revise my thesis. Thanks for all your essential supports to me during my Ph. D. periods.

--- Prof. Dr. Markus Kalberer for accepting to be my external co-examiner, spending time to review my thesis and travelling to Switzerland for the defense, it is my honor to have you as the co-examiner of my defense.

I would like to give very special thanks to:

--- Dr. Imad El Haddad, for his always be ready to help, his novel and interesting suggestions, and tried to make the papers meet a better quality. Dr. André S. H. Prévôt for all his scientific input and very helpful feedbacks to my research work.

--- René Richter and Günther Wehrle for all their competent technical advices and the pleasant discussions as well as Thomas Attinger for his IT support, Hannelore for her assistant in travelling. And Dr. Michel J. Rossi for many interesting discussions.

--- All the co-authors listed in each chapter for their contributions and helpful comments on the manuscripts, also for their contributions in different field and laboratory studies.

--- My thanks also go to all current and former LAC members, especially Dr. Carla Frege, thanks for her always being together with me, inspiring me whenever I am feeling down, Mao Xiao for the interesting discussions about science. And all those I shared time with at PSI (random sequence): Dosh, Miriam, Ghislain, Yandong, Laure-Estelle, Samuel, Andrea, Robin, Giulia, Deepika, Nassia, Manolis, Galina, Jay, Joel, Claudia, Jnfeng, Veronika, Manu, Carlo, Giancarlo, Felix, Robert, Kasper, Pragati, Janhui, Liwei, Lu, Meng, Yang, Bing, Ugo, Anna, Michele, Rosaria, David and all the other LAC new members I didn't have time to be familiar with yet.

--- Finally and importantly, I would like to thank my families, who have always encouraged me to pursue whatever I like, and provided priceless supporting all the time, which has contributed greatly to the success of my Ph.D. study.